

# Renormalized Fermi hypernetted chain approach in medium-heavy nuclei

F. Arias de Saavedra<sup>1</sup>, C. Bisconti<sup>2</sup>, G. Co' <sup>2</sup>, and A. Fabrocini<sup>3</sup>

<sup>1)</sup> Departamento de Física Atómica, Molecular y Nuclear,  
Universidad de Granada, E-18071 Granada, Spain

<sup>2)</sup> Dipartimento di Fisica, Università del Salento  
and Istituto Nazionale di Fisica Nucleare sez. di Lecce,  
I-73100 Lecce, Italy

<sup>3)</sup> Dipartimento di Fisica, Università di Pisa  
and Istituto Nazionale di Fisica Nucleare sez. di Pisa,  
I-73100 Pisa, Italy

## Abstract

The application of the Correlated basis function theory and of the Fermi hypernetted chain technique, to the description of the ground state of medium-heavy nuclei is reviewed. We discuss how the formalism, originally developed for symmetric nuclear matter, should be changed in order to describe finite nuclear systems, with different number of protons and neutrons. This approach allows us to describe doubly closed shell nuclei by using microscopic nucleon-nucleon interactions. We presents results of numerical calculations done with two-nucleon interactions of Argonne type, implemented with three-body forces of Urbana type. Our results regard ground-state energies, matter, charge and momentum distributions, natural orbits, occupation numbers, quasi-hole wave functions and spectroscopic factors of  $^{12}\text{C}$ ,  $^{16}\text{O}$ ,  $^{40}\text{Ca}$ ,  $^{48}\text{Ca}$  and  $^{208}\text{Pb}$  nuclei.

PACS: 21.60.-n; 21.10.Dr; 21.10.Ft; 21.10.Gv; 21.10.Jx; 21.90+f

# 1 Introduction

Aim of the many-body theories is the description of composite systems in terms of their elementary components. In our present understanding of nature, only leptons, quarks, and gauge bosons are considered to be elementary. In principle, any composite system should be described in terms of these entities. In reality, pragmatical difficulties hinder the accomplishment of such an ambitious program. For example, the difficulties in dealing with the non perturbative features of Quantum Chromodynamics (QCD) complicates the description even of the individual hadrons. The description of even more complex systems in terms of quarks and gluons is evidently not practicable, at least at present.

A more pragmatical, and fruitful, approach for the study of composite systems abandons quarks and leptons and uses effective degrees of freedom and interactions. For nuclear systems, the most convenient choice is to consider the nucleon as the basic degree of freedom. The nucleon-nucleon (NN) interaction, even if modeled in various manners, is always fixed to reproduce the NN elastic scattering data and the deuteron properties [1, 2, 3, 4, 5].

After choosing the basic degrees of freedom and their interaction it is necessary to define the theoretical framework to use. In the case of nuclear systems, if one is interested in the ground state properties and in low energy phenomenology (we mean here energies well below a GeV) the role of antiparticles can be neglected. Therefore a good description of these systems can be provided by the Schrödinger equation.

In the last decade the Schrödinger equation has been solved without approximations by using Green function Montecarlo (GFMC) techniques, for several light nuclei up to  $A=12$  [6, 7, 8, 9]. In these calculations the two-body interaction has been implemented with a three-body force chosen to reproduce the triton binding energy. The great success in describing binding energies and low-lying spectrum of these nuclei, is the pragmatical demonstration of the validity of the non relativistic many-body approach.

Various techniques to solve the many-body Schrödinger equation without approximations have been developed. Some of them are tailored to describe only few-body systems [10]. Others, formulated to handle any number of nucleons, like the GFMC, are limited for computational reasons to deal with light nuclei. Recently, a new Montecarlo approach, called Auxiliary Field Diffusion Montecarlo (AFDMC) [11], has been developed and it shows potentialities to be applied to the description of medium-heavy nuclear systems.

The many-body theories try to overcome the difficulties in solving the many-body Schrödinger equation by using approximations which simplify the problem, but still provide a proper description of the relevant physics effects. Because of the strong repulsion in the scalar channel of the NN interaction at short internucleonic distances the use of the most traditional, and simplest, approximations, such as the mean-field approximation, fails badly. For example, the use of microscopic interactions in Hartee-Fock (HF) calculations leads to unbound nuclei [12]. Dealing with the strong repulsion at short distances is the major issue of the nuclear many-body theories.

Loosely speaking the various nuclear many-body theories can be classified in two categories depending upon how they treat the short-range repulsion problem. There are theories acting on the interaction, and others working on the trial many-body wave function. The Brueckner theory, and all the theories constructing effective interactions from microscopic ones, belong to the first category. One of the theories belonging to the second category is the Correlated Basis Function (CBF) theory whose most recent extensions and applications to medium-heavy nuclei will be presented in this report. Strictly speaking, our approach is the lowest order

approximation of the CBF theory [13].

The starting point of the CBF approach is the solution of the many-body Schrödinger equation by means of the variational principle:

$$\delta E[\Psi] = \delta \frac{\langle \Psi | H | \Psi \rangle}{\langle \Psi | \Psi \rangle} = 0. \quad (1)$$

The search for the minimum is done by using trial wave functions of the form:

$$\Psi(1, \dots, A) = F(1, \dots, A) \Phi(1, \dots, A). \quad (2)$$

In the above equation  $\Phi$  describes the system as a set of  $A$  particles moving independently from each other. We call Independent Particles Model (IPM) this picture, which, in our calculations, is modified by the correlation function  $F$ . In its easiest form, we use for  $F$  the expression [14]:

$$F(1, \dots, A) = \prod_{j>i=1}^A f(r_{ij}), \quad (3)$$

where  $f(r_{ij})$  is a scalar function of the distance between two particles of the system.

The peculiarity of our approach consists in the technique used to calculate the expectation values of Eq. (1). This technique is inspired by the cluster expansion method used in statistical mechanics to describe liquids [15]. The particles, correlated by the function  $f$ , form clusters. A topological study of the various clusters shows that it is possible to construct a set of integral equations which allows one to sum in a closed form the contributions of all the clusters with some specific topological properties. This set of integral equations, called HyperNetted Chain (HNC) equations, can be used to describe both classical and bosonic systems [16].

In the mid 1970's, the cluster expansion techniques were extended to include also the Pauli exclusion principle, and the Fermi HyperNetted Chain (FHNC) equations were formulated [17, 18, 19]. The complexity of the NN interactions requires the use of correlation functions that are more complex than those of Eq. (3). These new correlations contain operator dependent terms which commute neither with the nuclear hamiltonian, nor among them. Also for this reason it became necessary to extend the FHNC equations to deal with this new type of correlations [20]. The computational difficulties require the use of an approximation called Single Operator Chain (SOC). The resulting set of equations is called FHNC/SOC [21], and it has been successfully applied to describe infinite systems [22, 23, 24, 25].

In this review, we are concerned about the application of the FHNC/SOC computational scheme to medium-heavy nuclei. The extension of the FHNC theory to finite Fermi systems was introduced by Fantoni and Rosati in the late 1970s [26]. In their works they have shown that a cluster expansion with an infinite numbers of terms can be formulated even for finite systems. Consequently, the basic set of FHNC equations, can be used also for finite systems. However, one has to consider that the loss of translational invariance in these systems produces the so-called vertex corrections. We shall refer to the new set of equations as Renormalized Fermi HyperNetted Chain (RFHNC) equations.

The results of the first numerical application of the RFHNC equations to finite nuclear systems were presented in Ref. [27]. In that article, model nuclei were described. Protons and neutrons wave functions were produced by a unique mean field potential, and in a  $ls$  coupling scheme. The NN interactions considered had only central terms, and the correlations were scalar

functions. This simplified situation was used to test the theoretical, and numerical, feasibility of the approach. Results for binding energies of  $^{16}\text{O}$  and  $^{40}\text{Ca}$  model nuclei were presented in [27] while the momentum distributions were shown in a following article [28].

A more realistic description of doubly closed shell nuclei was given in [29], where proton and neutrons were separately treated, and the single particle wave functions were expressed in a  $jj$  coupling scheme. The RFHNC equations required a non trivial reformulation. Binding energies, matter densities and momentum distributions, have been calculated for various doubly magic nuclei up to  $^{208}\text{Pb}$ . However, also in this case, simple central interactions and scalar correlations were used.

In a following step, the RFHNC equations were extended to treat the correlation terms commuting neither with the hamiltonian, nor among themselves. This involved the extension of the SOC approximation. Because of the technical difficulties the RFHNC/SOC equations have been first formulated to deal with spin and isospin saturated nuclei, and with single particle wave functions in a  $ls$  coupling scheme. Again only  $^{16}\text{O}$  and  $^{40}\text{Ca}$  nuclei could be treated. The results of these calculations have been presented in Refs. [30, 31, 32].

A formulation of the RFHNC/SOC equations general enough to handle separately protons and neutrons in the more realistic  $jj$  coupling scheme was finally done. Binding energies and density distributions have been shown in Ref. [33] for the  $^{12}\text{C}$ ,  $^{16}\text{O}$ ,  $^{40}\text{Ca}$ ,  $^{48}\text{Ca}$  and also  $^{208}\text{Pb}$  nuclei. Here fully realistic microscopic interactions, with tensor and spin-orbit terms were used. The hamiltonian included also three-body interactions.

In the literature, there are various reviews regarding the FHNC/SOC formalism applied to infinite nuclear systems [21, 34, 35, 36, 37], but there is a void regarding finite nuclei. For the sake of brevity in writing journal articles, the formalism presented in the papers quoted above is incomplete. The aim of the present article is to provide a complete, coherent, and self-contained presentation of the FHNC/SOC formalism for finite nuclear systems, and to review the most recent results.

We recall in Sect. 2 the HNC, FHNC and FHNC/SOC equations for infinite systems. They are important, not only because we want to give a self-contained presentation, but especially because the RFHNC/SOC formulation for the finite systems is constructed by modifying that of infinite systems. The RFHNC/SOC set of equations will be presented in Sect. 3, and it will be applied in Sect. 4 to evaluate the energy of the system. A selected, but significant, set of recent numerical results will be presented, and discussed, in Sect. 5. In Sect. 6 we provide a short overview of the possible extensions of the formalism. Conclusions are presented in Sect. 7.

To improve the readability of the paper we present many technical details of the derivation of the various expressions in the Appendices. Furthermore, because of the large use of acronyms and symbols, we list them in the Appendices G and H, respectively.

## 2 Infinite systems

In this section we present the HNC and FHNC equations for infinite systems. This presentation does not aim to substitute, or update, the excellent review articles describing in detail the derivations of the various expressions, see for example Refs. [21, 34, 35, 36, 37]. Our purpose is to recall the main ideas and to emphasize those details which should be reconsidered in the description of finite systems.

### 2.1 Bosons

We start to present the CBF approach by describing a system composed of  $A$  bosons contained in a volume,  $V$ . We are interested in getting an infinite system by using the thermodynamic limit, i.e.  $A$  and  $V$  go to infinity keeping the density,  $\rho = A/V$ , constant. We consider a homogeneous and translationally invariant system, with a constant density,  $\rho$ . The wave function describing the system when the interaction between the particles is switched off is:

$$\Phi(x_1, x_2, \dots, x_A) = \mathcal{S}(\phi_1(x_1) \cdots \phi_A(x_A)) , \quad (4)$$

where we have indicated with  $\mathcal{S}$  the symmetrization operator, with  $\phi_i(x_i)$  the single particle wave functions, and with  $x_i$  the generalized coordinate of the  $i$ -th particle.

In this IPM description of the ground state of the system, all the bosons occupy the lowest single particles state. We consider spin zero bosons, and because of the translational invariance of the system, the single particle wave functions are eigenfunctions of the momentum  $\mathbf{k}$ , and they can be expressed as:

$$\phi_j(x_j) = \frac{1}{\sqrt{V}} e^{i\mathbf{k}_j \cdot \mathbf{r}_j} . \quad (5)$$

In this case, the generalized coordinate  $x$  corresponds to  $\mathbf{r}$ .

The density of the system can be obtained by using Eqs. (4) and (5),

$$\rho_0(x) = A\phi^*(x)\phi(x) = \frac{A}{V} = \rho , \quad (6)$$

which is constant, as expected.

As we have already discussed in the introduction, the idea is to solve the Schrödinger equation by means of the variational principle by using a trial wave function of the form:

$$\Psi(x_1, \dots, x_A) = F(x_1, \dots, x_A)\Phi(x_1, \dots, x_A) , \quad (7)$$

where, in this case, the expression of  $\Phi$  is that of Eq. (4).

For this specific bosonic case we describe the many-body correlation function  $F(x_1, \dots, x_A)$  by using the so called Jastrow ansatz [38, 14]:

$$F(x_1, \dots, x_A) = \prod_{j>i=1}^A f(r_{ij}) , \quad (8)$$

where the two-body correlation function (TBCF),  $f(r_{ij})$ , is a scalar function of the distance between the  $i$ -th and  $j$ -th particles.

In the calculation of the energy functional

$$E[\Psi] = \frac{\langle \Psi | H | \Psi \rangle}{\langle \Psi | \Psi \rangle} , \quad (9)$$

it is very useful to employ the two-body distribution function (TBDF) defined as:

$$g(x_1, x_2) = \frac{A(A-1) \int dx_3 \dots dx_A \Psi^*(x_1, \dots, x_A) \Psi(x_1, \dots, x_A)}{\rho^2 \int dx_1 dx_2 \dots dx_A \Psi^*(x_1, \dots, x_A) \Psi(x_1, \dots, x_A)} . \quad (10)$$

The expectation value of any two-body operator, such as the two-body interaction, is obtained by integrating the TBDF on the two coordinates  $x_1$  and  $x_2$ :

$$\langle O \rangle = \frac{1}{2} \rho^2 \int dx_1 dx_2 g(x_1, x_2) O(x_1, x_2) . \quad (11)$$

The evaluation of the TBDF allows the calculation of the many-body effects independently from the explicit expression of the operator.

By using Eqs. (4), (5), (6) and the expressions (7) and (8) the numerator and the denominator of Eq. (10) can be written respectively as:

$$\mathcal{N} = (A-1) \frac{\rho^{A-2}}{A^{A-1}} \int dx_3 dx_4 \dots dx_A \prod_{i < j} f^2(r_{ij}) , \quad (12)$$

and

$$\mathcal{D} = \frac{\rho^A}{A^A} \int dx_1 dx_2 \dots dx_A \prod_{i < j} f^2(r_{ij}) . \quad (13)$$

The cluster expansion is done by defining a new function  $h(r_{ij})$  such as:

$$f^2(r_{ij}) = 1 + h(r_{ij}) . \quad (14)$$

The product of  $f^2$  factors can be rewritten by collecting all the terms with the same number of  $h$ -functions. Let's first consider the denominator  $\mathcal{D}$ , Eq. (13), which can be written as:

$$\begin{aligned} \mathcal{D} = \frac{\rho^A}{A^A} \int dx_1 dx_2 \dots dx_A & \left[ 1 + \sum_{i < j} h(r_{ij}) + 3 \sum_{i < j < k} h(r_{ik}) h(r_{kj}) \right. \\ & \left. + \sum_{i < j < k < l} h(r_{ij}) h(r_{kl}) + \dots \right] . \end{aligned} \quad (15)$$

A convenient way of investigating the structure of the various terms of Eq. (15) is to use the graphical representation introduced by Yvon and Mayer [15]. In this formalism the integrated points  $x_i \equiv \mathbf{r}_i$ , which are called *internal* points, are represented by solid circles, and the  $h$ -functions by dashed lines. The expression of Eq. (15) is obtained by associating to each integrated point the contribution of the density. In the present case the density is constant, therefore its contributions can be factorized out of the integral. This will not be the case for finite systems.

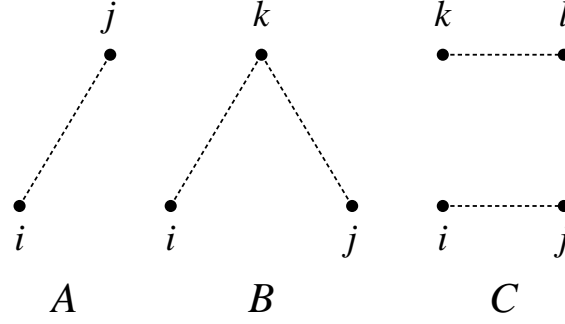


Figure 1: Graphical representation of some terms contributing to Eq.(15). The dashed line represents the correlation function  $h$ . The black dots represents the integration points.

The first sum of Eq. (15) is represented by the diagram A of Fig. 1. The second sum of Eq. (15) is represented by the diagram B. In this case, the point  $k$  is in common with the two  $h$ -functions of the sum. The total contribution of this type of term is:

$$\frac{1}{2} \frac{(A-1)(A-2)}{A^2} \rho^3 \int dx_i dx_j dx_k h(r_{ik}) h(r_{kj}) , \quad (16)$$

where the  $(A-1)(A-2)$  factor is due to the fact that the sums on the  $i, j$  and  $k$  indexes are limited to  $i < j < k$ .

In the third sum the two  $h$ -functions involves four different points. Its contribution is represented by the diagram C of Fig. 1, and it is given by:

$$\frac{A!}{4!(A-4)!} \frac{\rho^4}{A^4} \int dx_i dx_j dx_k dx_l h(r_{ij}) h(r_{kl}) , \quad (17)$$

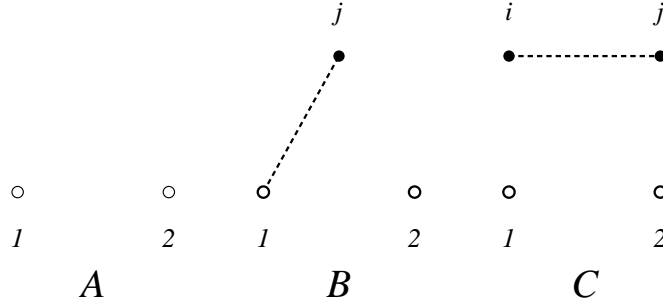


Figure 2: Graphical representation of some terms contributing to Eq. (18).

The use of Eq. (14) in the numerator of Eq. (10), allows us to obtain the expression:

$$\begin{aligned} \mathcal{N} = & f^2(r_{12}) \frac{(A-1)}{A} \left[ 1 + 2 \frac{\rho}{A} (A-2) \sum_{j>2} \int dx_j h(r_{1j}) \right. \\ & \left. + \frac{(A-2)(A-3)}{2} \frac{\rho^2}{A^2} \sum_{j>i>2} \int dx_i dx_j h(r_{ij}) + \dots \right]. \end{aligned} \quad (18)$$

A new symbol is required for the graphical representation of the numerator, since it is necessary to indicate the two coordinates which are not integrated. These coordinates are called *external* points, and we have labeled them 1 and 2. The external points are indicated by white circles as it is shown in Fig. 2, where we represent the lowest order terms of Eq. (18). The uncorrelated term is represented by the A diagram. The B diagram represents the terms of the first sum of Eq. (18), where the  $h$ -function connects an external and an internal point. Also the second sum of Eq. (18) contains only a single  $h$ -function but it connects, in this case, only internal points. The contribution of this sum is represented by the diagram C of Fig. 2.

The numerator and the denominator of the TBDF (10) are expressed by Eqs. (15) and (18) as sums of terms characterized by the number of the  $h$ -functions, and by that of the external, and internal points. Each term of these sums forms a cluster of particles, and can be described by a diagram. We proceed now by doing a topological classification of the various diagrams.

The C diagrams of Fig. 1 can be written by factorizing the non connected terms:

$$\begin{aligned} \frac{A!}{4!(A-4)!} \frac{\rho^4}{A^4} \int \int dr_i dr_j dr_k dr_l h(r_{ij}) h(r_{kl}) = \\ \frac{1}{4!} \left( 1 - \frac{6}{A} + \frac{11}{A^2} - \frac{6}{A^3} \right) \rho^2 \int dr_i dr_j h(r_{ij}) \cdot \rho^2 \int dr_k dr_l h(r_{kl}) \quad . \end{aligned}$$

Any diagram that can be factorized in two or more independent pieces is called *unlinked*. Also the C diagram of Fig. 2 is unlinked. The diagrams that cannot be expressed as a product of independent parts as the diagram B of Fig. 1, are called *linked*.

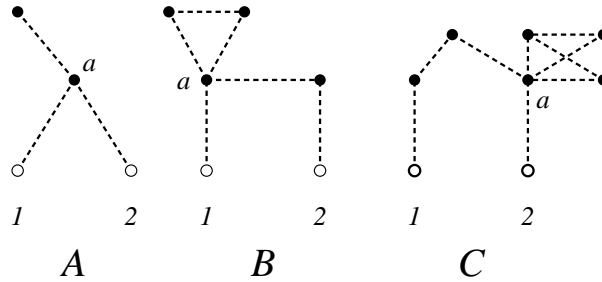


Figure 3: Examples of reducible diagrams in the numerator of the TBDF, Eq. (18).

The linked diagrams of Fig. 3, have the properties of being *reducible*. From the graphical point of view the reducible diagrams are characterized by the presence of, at least, one point



linking a part of the diagram containing the external point, and another part containing internal points only. Because of the translational invariance of the system, the contributions of these two parts can be factorized. In general, every linked diagram whose contribution to the TBDF can be expressed as a product of independent integrals is called *reducible*. In bosonic systems both reducible and unlinked diagrams are factorizable. These factorizable diagrams of the numerator simplify, up to the  $1/A$  order, all the diagrams of the denominator. The rigorous proof of this property is given in Ref. [18].

So, in the expression (10) of the TBDF, the denominator diagrams compensate the contribution of the unlinked and of the reducible diagrams of the numerator. Therefore, the TBDF can be expressed as the sum of all the irreducible linked diagrams containing the two external points 1 and 2:

$$g(r_{12}) = f^2(r_{12}) \sum_{all\ orders} Y_{irr}(r_{12}) = f^2(r_{12}) (1 + S(r_{12}) + C(r_{12})) . \quad (19)$$

The translational invariance of the infinite system makes the TBDF dependent only on the relative distance between the external points,  $r_{12}$ . A further topological classification of these irreducible diagrams, divides them into *simple* and *composite*, and in the above equation we have called  $S(r_{12})$  and  $C(r_{12})$  the corresponding contributions to the TBDF (19).

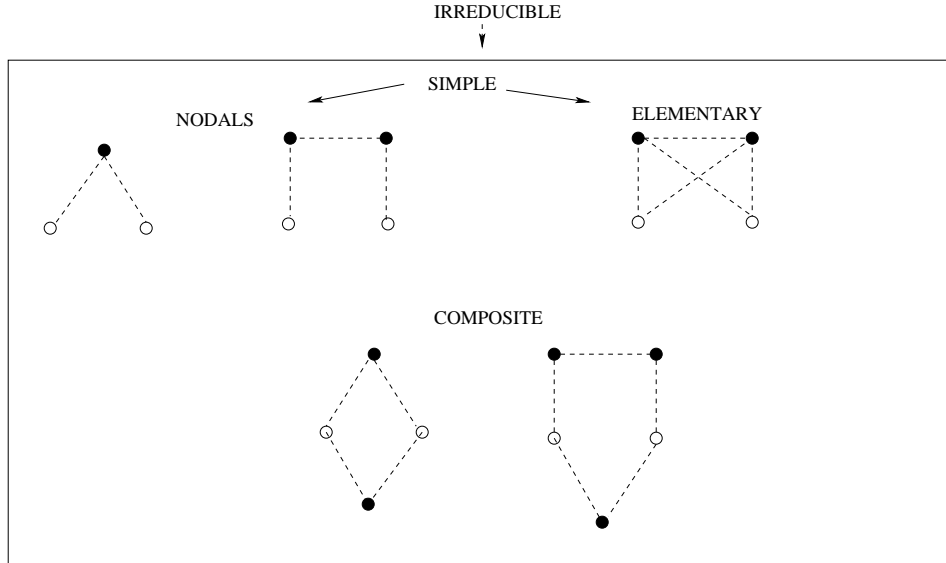


Figure 4: Example of irreducible diagrams, classified as composite and simple. This latter type of diagrams is sub-divided into nodal and elementary ones.

The composite diagrams are those composed by parts that are connected only through the two external points 1 and 2, see Fig. 4. They can be expressed in terms of simple diagrams. Since there is no integration on the external points, the contribution of a composite diagram is given by the product of the simple diagrams connected to the external points. For example, the contribution of all the composite diagrams which are formed by two simple diagrams only,

is  $S^2(r_{12})$ . Since the exchange of all the particles of one subdiagrams with those of the other one, produces the same composite diagram, we have to divide by 2 to avoid double counting. Repeating the same procedure we find that the contribution of the composite diagrams formed by three simple diagrams is  $S^3(r_{12})/3!$ , and so on. The total sum of composite diagrams can be written as:

$$C(r_{12}) = \frac{S^2(r_{12})}{2!} + \frac{S^3(r_{12})}{3!} + \frac{S^4(r_{12})}{4!} + \dots \quad (20)$$

The TBDF, (19), can be rewritten as:

$$\begin{aligned} g(r_{12}) &= f^2(r_{12}) \left[ 1 + S(r_{12}) + \frac{S^2(r_{12})}{2!} + \frac{S^3(r_{12})}{3!} + \dots \right] \\ &= f^2(r_{12}) \exp[S(r_{12})] , \end{aligned} \quad (21)$$

where the last equality appears because our system has an infinite number of particles and is called hypernetted connection.

The above equation expresses the TBDF in terms of simple diagrams only, which are further classified as *nodal* and *elementary* ones. In a nodal diagram there is at least one point where all the paths going from one external point to the other one have to pass. This point is called a node. In the literature, the diagrams without nodes are called *elementary* or *bridge* diagrams. We shall always use the adjective *elementary*. Some examples of the type of diagrams we have just defined can be found in Fig. 4.

If we call  $N$  the contribution of all the nodal diagrams, and  $E$  that of the elementary ones, we can write the TBDF as:

$$g(r_{12}) = f^2(r_{12}) \exp[N(r_{12}) + E(r_{12})] \quad (22)$$

$$\begin{aligned} &= [1 + h(r_{12})] [1 + N(r_{12}) + E(r_{12}) + \dots] \\ &= 1 + N(r_{12}) + X(r_{12}) . \end{aligned} \quad (23)$$

The above equation defines the diagrams contained in  $X(r_{12})$ , which are usually named *non-nodal* diagrams since they have no nodes.

A nodal diagram can be considered composed by parts which are linked at the nodal point. Every nodal diagrams can be obtained by integrating on the node the two functions representing the parts of the diagram. Let us consider, for example, the nodal diagram of Fig. 5 having  $i$  and  $j$  as external points and  $k$  as node. If we call  $a(r_{ik})$  and  $b(r_{kj})$  the two functions describing the two parts of the diagrams, the contribution of this diagram to the TBDF (19) is:

$$\int d\mathbf{r}_k a(r_{ik}) b(r_{kj}) \rho(r_k) = \rho \int d\mathbf{r}_k a(r_{ik}) b(r_{kj}) \equiv \left( a(r_{ik}) \middle| \rho(\mathbf{r}_k) b(r_{kj}) \right) , \quad (24)$$

where a density function  $\rho(\mathbf{r}_k)$  has been associated to the  $\mathbf{r}_k$  integration point in order to recover the proper normalization, and since the density is constant in this case, it has been factorized out of the integral. The last term defines the symbol  $\left( \middle| \right)$  we shall use henceforth to indicate the folding product or chain connection.

By using the above considerations we can write a closed expression which allows the evaluation of all the nodal diagrams. The global contribution  $N(r_{ij})$  of all the nodal diagrams between

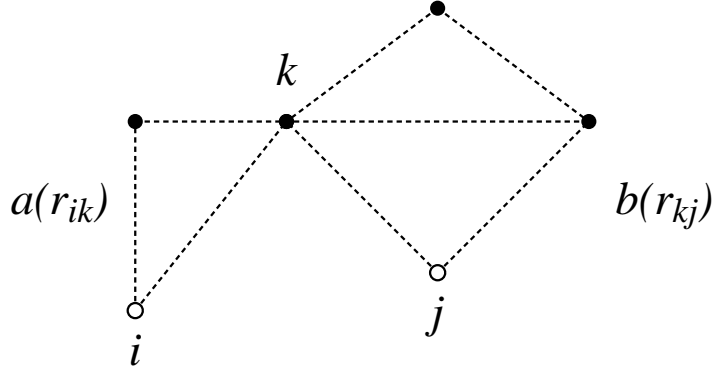


Figure 5: Example of nodal diagram. We indicate with  $a(r_{ik})$  the contribution of the part of diagram to the left of the nodal point  $k$ , and with  $b(r_{kj})$  the contribution of the right part.

the two points  $i$  and  $j$  can be obtained as a folding product at the node  $\mathbf{r}_k$  of all the irreducible diagrams which can be constructed between  $i$  and  $k$  and  $k$  and  $j$ :

$$N(r_{ij}) = \left( X(r_{ik}) \middle| \rho(\mathbf{r}_k) [N(r_{kj}) + X(r_{kj})] \right). \quad (25)$$

Every nodal diagram has at least one node and any path between its external points  $i$  and  $j$  must pass through all the nodes. The above equation tells us that the part of the diagram between  $i$  and the first node  $k$ , which is a non-nodal diagram, has to be folded to: i) the non-nodal diagrams producing in this case nodal diagrams with only one node and, ii) the nodal diagrams producing nodal diagrams with more than one node. The folding of two nodal diagrams at the  $\mathbf{r}_k$  point is forbidden since it would produce many times the same diagram.

The set of Eqs. (22), (23) and (25) are known as HyperNetted Chain (HNC) equations. Equation (22) allows one to express the TBDF in terms of the simple diagrams after summing in a closed form the composite diagrams and (25) allows the evaluation of the contribution of all the nodal diagrams in a closed form. However, there is no closed expression to evaluate the contribution of the elementary diagrams which must be calculated one by one. Calculations of the TBDM without the contribution of the elementary diagrams are labelled as HNC/0. When the contribution of the first elementary diagram is included the calculation of the TBDF is called HNC/4, since this diagram, shown in Fig. 4, has four particles. These equations are usually solved with an iterative procedure starting from the ansatz  $N(r_{12}) = E(r_{12}) = 0$ , then  $X(r_{12}) = f^2(r_{12}) - 1$  and we can get new nodals using (25).

## 2.2 Fermions

In the description of a system of fermions we have to deal with the Pauli exclusion principle. The IPM wave function  $\Phi$  to be used in the trial wave function (2), is now a Slater determinant

of single particle wave functions  $\phi$ :

$$\Phi(x_1, \dots, x_A) = \frac{1}{\sqrt{A!}} \begin{vmatrix} \phi_1(x_1) & \phi_1(x_2) & \dots & \phi_1(x_A) \\ \phi_2(x_1) & \phi_2(x_2) & \dots & \phi_2(x_A) \\ \vdots & \vdots & \ddots & \vdots \\ \phi_A(x_1) & \phi_A(x_2) & \dots & \phi_A(x_A) \end{vmatrix}, \quad (26)$$

For an infinite system we can write the single particle wave functions as:

$$\phi_a(x_j) = \frac{1}{\sqrt{V}} e^{i\mathbf{k}_a \cdot \mathbf{r}_j} \chi_{s_a}(j) \chi_{t_a}(j). \quad (27)$$

where we have indicated with  $s$  and  $t$  the projections on the  $z$  axis of the spin and isospin and with  $\chi_s$  and  $\chi_t$  the Pauli spinors. In the fermions case, the generalized coordinate  $x$  indicates position  $\mathbf{r}$ , spin and isospin third components, in addition to the total spin and isospin values.

Before attacking the problem of the calculation of the TBDF (10) we discuss some property of  $|\Phi|^2$  which we write as:

$$|\Phi(1, 2, \dots, A)|^2 = \begin{vmatrix} \rho_0(x_1, x_1) & \rho_0(x_1, x_2) & \dots & \rho_0(x_1, x_A) \\ \rho_0(x_2, x_1) & \rho_0(x_2, x_2) & \dots & \rho_0(x_2, x_A) \\ \vdots & \vdots & \ddots & \vdots \\ \rho_0(x_A, x_1) & \rho_0(x_A, x_2) & \dots & \rho_0(x_A, x_A) \end{vmatrix}, \quad (28)$$

where we have defined the various elements of the above determinant as:

$$\rho_0(x_i, x_j) = \sum_a \phi_a^*(x_i) \phi_a(x_j). \quad (29)$$

In the above expression the sum runs over all the occupied single particle states of the system. We have defined in Eq. (29) the uncorrelated One-Body Density Matrix (OBDM) which is the basic ingredient of the calculation of the TBDF in the fermion case. A fundamental property of the uncorrelated OBDM, due to the orthonormality of the single particle wave functions, is:

$$\int dx_j \rho_0(x_i, x_j) \rho_0(x_j, x_k) = \rho_0(x_i, x_k), \quad (30)$$

where in the above integral sign we include both the space integration and the sum on the spin and isospin third components, their *trace*.

We define the sub-determinant as:

$$\Delta_p(1, \dots, p) = \begin{vmatrix} \rho_0(x_1, x_1) & \rho_0(x_1, x_2) & \dots & \rho_0(x_1, x_p) \\ \rho_0(x_2, x_1) & \rho_0(x_2, x_2) & \dots & \rho_0(x_2, x_p) \\ \vdots & \vdots & \ddots & \vdots \\ \rho_0(x_p, x_1) & \rho_0(x_p, x_2) & \dots & \rho_0(x_p, x_p) \end{vmatrix}, \quad p \leq A. \quad (31)$$

Because of the property (30) of the uncorrelated OBDM the sub-determinants have the property:

$$\int dx_{p+1} \Delta_{p+1}(1, \dots, p+1) = (A-p) \Delta_p(1, \dots, p), \quad (32)$$

and, by iterating it, we obtain:

$$\int dx_{p+1} \dots dx_A \Delta_A(1, \dots, A) = (A-p)! \Delta_p(1, \dots, p) . \quad (33)$$

The above expression implies that:

$$\Delta_p = 0 , \quad p > A . \quad (34)$$

The property (34) will be extremely useful in the application of the cluster expansion technique to both finite and infinite fermion systems.

The properties of the uncorrelated OBDM and of the sub-determinants we have just presented, depend only on the orthonormality of the single particle wave functions, and not on their explicit expressions. For this reason, they will remain valid also in the case of finite fermions systems. The expression (27) of the single particle wave functions has been chosen to describe a infinite and homogeneous system. In this case, we obtain for the uncorrelated OBDM the expression:

$$\rho_0(x_i, x_j) = \frac{\rho}{\nu} \ell(k_F r_{ij}) \sum_{s,t} \chi_s^+(i) \chi_t^+(i) \chi_s(j) \chi_t(j) . \quad (35)$$

In the above equation we have indicated with  $\nu$  the spin-isospin degeneration of the system, 4 in the nuclear matter case, and with  $k_F = (6\pi^2 \rho / \nu)^{1/3}$  the Fermi momentum. In the literature the function  $\ell(x)$  is called Slater function [39], and has the following explicit expression:

$$\ell(x) = \frac{3}{x^3} (\sin x - x \cos x) . \quad (36)$$

In the description of fermion systems, it is necessary to include in the Mayer diagrams a new graphical symbol identifying the presence, and the role, of  $\rho_0(x_i, x_j)$ , which, in the calculation of the TBDF, forms closed non overlapping loops. This is an oriented line connecting the two points  $x_i$  and  $x_j$ . These lines are called *statistical* correlations to distinguish them from the *dynamical* correlations,  $f(r_{ij})$ . In the calculation of the TBDF for the infinite system a term  $-\ell(k_F r_{ij})/\nu$  should be considered for each statistical line joining the  $i$  and  $j$  points, and a factor  $-\nu$  for every closed statistical loop which is related to the spin and isospin trace [35].

There is a basic difference between dynamical and statistical correlations. While any number of dynamical lines may arrive at a given point only none or two statistical lines may arrive at that point.

By using the trial wave function (2) with the Jastrow ansatz (3) and the definition (14) of the  $h$ -function we write the TBDF (10) as:

$$\begin{aligned} & g(x_1, x_2) \\ &= \frac{A(A-1) \int dx_3 \dots dx_A (1 + \sum_{i < j} h_{ij} + \sum_{i < j < k} h_{ij} h_{jk} + \dots) |\Phi(x_1, \dots, x_A)|^2}{\rho^2 \int dx_1 \dots dx_A (1 + \sum_{i < j} h_{ij} + \sum_{i < j < k} h_{ij} h_{jk} + \dots) |\Phi(x_1, \dots, x_A)|^2} , \end{aligned}$$

with  $h_{ij} \equiv h(r_{ij})$ . By using the definition of sub-determinant (31) the numerator and the denominator of the above equation can be expressed as sums of terms identified by the number of

$h$ -functions:

$$\mathcal{N} = \frac{A(A-1)}{\rho^2} f^2(r_{12}) \int dx_3 \dots dx_A \left( 1 + \sum_{i < j} h_{ij} + \sum_{i < j < k} h_{ij} h_{jk} + \dots \right) \Delta_A , \quad (37)$$

$$\mathcal{D} = \int dx_1 \dots dx_A \left( 1 + \sum_{i < j} h_{ij} + \sum_{i < j < k} h_{ij} h_{jk} + \dots \right) \Delta_A . \quad (38)$$

We rewrite the expressions of  $\mathcal{N}$  and  $\mathcal{D}$  by grouping the terms with the same number of points,  $p$ , and we indicate them as  $X^{(p)}(1, 2, 3, \dots, p)$ . For example

$$X^{(3)}(1, 2; i) = h_{1i} + h_{2i} + h_{1i} h_{2i} .$$

The expression of the TBDF we obtain is:

$$g(x_1, x_2) = \frac{A(A-1)}{\rho^2} f^2(r_{12}) \int dx_3 \dots dx_A \Delta_A \left[ 1 + \sum_{p=3}^A \frac{(A-2)!}{(p-2)!(A-p)!} X^{(p)}(1, 2; \dots, p) \right] \left[ \int dx_1 \dots dx_A \Delta_A \left( 1 + \sum_{p=2}^A \frac{A!}{p!(A-p)!} X^{(p)}(1, \dots, p) \right) \right]^{-1} .$$

The factorial factors which multiply the  $X^{(p)}$  functions, take into account the fact that permutations of the  $p$  internal points do not change the value of the diagram.

By using the property (33) of the sub-determinants, we can integrate the above expression of the TBDM on all the coordinates not involved by the correlations, i. e. not present in the  $X^{(p)}$  functions. So we obtain for the numerator and the denominator of the TBDF, the expressions:

$$\mathcal{N} = A! \frac{f^2(r_{12})}{\rho^2} \sum_{p=2}^A \frac{1}{(p-2)!} \int dx_3 \dots dx_p X^{(p)}(1, 2; \dots, p) \Delta_p(1, \dots, p) , \quad (39)$$

$$\mathcal{D} = A! \sum_{p=0}^A \frac{1}{p!} \int dx_1 \dots dx_p X^{(p)}(1, \dots, p) \Delta_p(1, \dots, p) . \quad (40)$$

We extend up to infinity the upper limits of all the sums of the above expression by using the property (34) of the sub-determinants. Each cluster term (diagram) can be divided in linked and unlinked parts. Let us call  $\mathcal{L}_n(1, 2, i_3, \dots, i_n)$  the linked parts of the various cluster terms containing the external points 1 and 2. In these diagrams each internal point  $i_3, \dots, i_n$  is connected to the points 1 and 2 by at least one continuous path of dynamical and/or statistical correlations. We call  $\mathcal{U}_{p-n}(i_{n+1}, \dots, i_p)$  the unlinked parts of the cluster terms. In this case none of the  $p-n$  points is connected to 1 and 2, or to another point of  $\mathcal{L}_n$ . The contribution of  $\mathcal{L}_n$  does not change for a permutation of some of its internal points. The same property holds for  $\mathcal{U}_{p-n}$  and

its internal points. For this reason every diagram of  $\mathcal{N}$  separated in  $\mathcal{L}_n$  and  $\mathcal{U}_{p-n}$  parts, give  $(p-2)!/(n-2)!(p-n)!$  times the same contribution. We can then express the numerator if we define  $q = p - n$  as:

$$\begin{aligned} \mathcal{N} = & A! \frac{f^2(r_{12})}{\rho^2} \sum_{n=2}^{\infty} \frac{1}{(n-2)!} \int dx_3 \dots dx_n \mathcal{L}_n(1, 2; \dots, n) \\ & \left[ \sum_{q=0}^{\infty} \frac{1}{q!} \int dx_1 \dots dx_q \mathcal{U}_q(1, \dots, q) \right]. \end{aligned} \quad (41)$$

We extend the above considerations to the denominator (40). Since in this case there are no external points, the diagrams we have defined as linked ones, are not present. Only the  $\mathcal{U}_n$  diagrams contribute to the denominator:

$$\mathcal{D} = A! \left[ \sum_{n=0}^{\infty} \frac{1}{n!} \int dx_1 \dots dx_n \mathcal{U}_n(1, \dots, n) \right]. \quad (42)$$

This expression is identical to that giving the contribution of the unlinked terms of the numerator. In the calculation of the TBDF the denominator compensates all the unlinked diagrams of the numerator, and we can write:

$$\begin{aligned} g(x_1, x_2) &= g(r_{12}) \\ &= \frac{f^2(r_{12})}{\rho^2} \left[ \Delta_2(1, 2) + \sum_{p=3}^{\infty} \frac{1}{(p-2)!} \int dx_3 \dots dx_p \mathcal{L}_p(1, 2; \dots, p) \right]. \end{aligned} \quad (43)$$

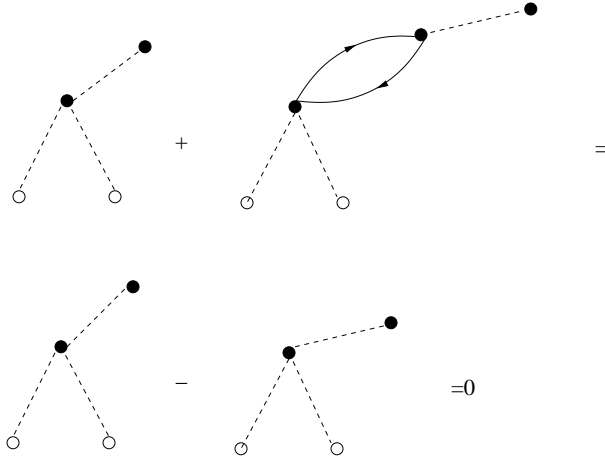


Figure 6: Example of cancelation between two FHNC diagrams. The statistical loop in the upper part produces a minus sign, and therefore the total contribution is zero.

The above result shows that the TBDF can be obtained by calculating linked cluster terms, only. As in the case of bosons, we define the reducible diagrams as those linked diagrams containing a point, the articulation point, which allows us to write the total contribution in two or more separated contributions. An example of reducible diagrams is given in Fig. 6. Like in

the bosonic case, the factorization of the reducible diagrams in two or more subdiagrams is due to the translational invariance of the system. Also in the fermionic case it is possible to show that the reducible diagrams do not contribute to the calculation of the TBDF [18]. However, in the fermionic case, the mechanism which allows the elimination of the contribution of the reducible diagrams, is very different from that of the boson case. Furthermore, the cancellation of the reducible diagrams is exact, not limited to  $1/A$  power terms. The rigorous proof of this cancellation is given in [18], and we present here only the basic idea of how the cancellation mechanism works. This discussion will become useful to present the vertex corrections in the finite fermion systems case. Let us consider, as example, the case of the diagrams shown in the upper part of Fig. 6. These diagrams differ only because the second diagram has an additional statistical loop. Because the system is translationally invariant, and for the properties of the Slater function (36), the contribution of the the two diagrams is identical but with different sign. Therefore, as is shown in the lower part of the figure, the global contribution of the two diagrams is zero.

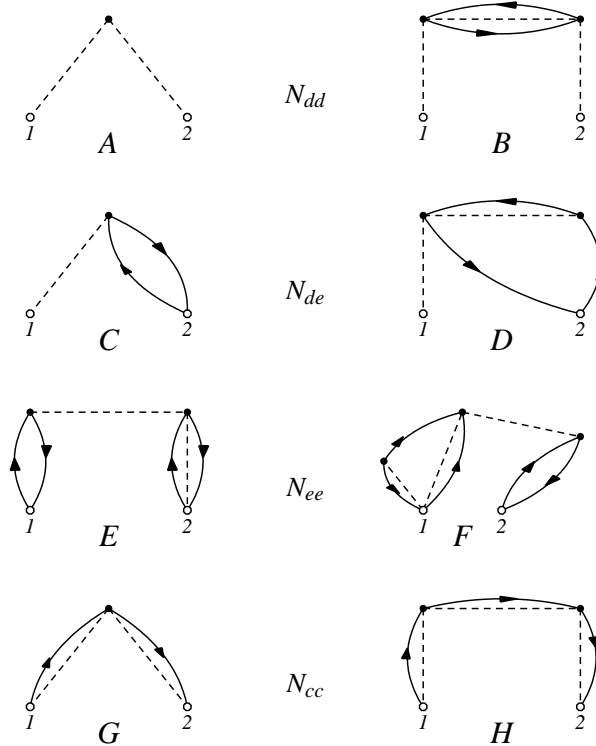


Figure 7: The various types of nodal diagrams required by the FHNC equations. The subindexes classify the diagrams with respect to the type of correlations reaching the external points 1 and 2.

The fermionic TBDF (43) can be calculated by considering the contribution of the irreducible diagrams only, in analogy to Eq. (19) for the bosons. Again in strict analogy with what has been done for the bosonic case, see Eqs.(19 - 21), it is possible to show that the contribution of all the composite diagrams can be obtained by considering simple diagrams only, which are classified in nodal and elementary ones. The elementary, and nodal, diagrams in the fermionic case are defined in analogy to those of the bosonic case, but both statistical and dynamical



correlations should be considered. The presence of the statistical correlations hinders the possibility of writing a single integral equation which allows the evaluation in closed form of the contribution of all the nodal diagrams, as Eq. (25) is doing. However, it is possible to find a set of integral equations relating the contribution of the nodal diagrams characterized by the type of correlations reaching the external points 1 and 2 [18, 39].

Graphical examples of the type of diagrams required to obtain the various integral equations of interest are given in Fig. 7. In the A and B diagrams only dynamical correlations reach the external points. These diagrams are labeled with the *dd* (dynamical-dynamical) subscripts ( $N_{dd}$ ). The C and D diagrams have only dynamical correlations reaching the external point 1 and two statistical correlation lines reaching the external point 2. In this case, we label the nodal diagram with a *de* (dynamical-exchange) subscript ( $N_{de}$ ). The E and F diagrams are labelled with a *ee* (exchange-exchange) subscript since to both external points arrive two statistical lines. Up to build those *ee* diagrams with the external points in the same statistical loop, it is convenient to define diagrams where a statistical correlation starts from the external point 1 and arrives to the external point 2, forming an open loop. We label these diagrams with the *cc* (cyclic-cyclic) subscript and we remark that they do not contribute directly to the TBDF.

As discussed in the bosonic case for Eq. (25), also in this case the total contribution of the nodal diagrams can be obtained by doing the folding product of various parts of the diagrams at the nodal point. However, the Pauli exclusion principle, prohibits some of the possible folding products. It is not possible to fold *cc* diagrams with diagrams of different type and if one of the diagrams to fold has the *e* type at the nodal point the other one has to be *d* type at this point. This restriction is caused by the afore mentioned fact that only two statistical lines may arrive at a point, in this case the nodal point.

In analogy to the bosonic case, we call  $N$  the sum of all the nodal diagrams and  $X$  the sum of all the irreducible non-nodal diagrams. Of course now  $N$  and  $X$  are classified by the subindexes *dd*, *de*, *ee* and *cc*, and, for the nodal diagrams, we obtain the following set of equations [18, 39]:

$$\begin{aligned}
N_{dd}(r_{12}) &= \left( X_{dd}(r_{13}) + X_{de}(r_{13}) \right) \rho(\mathbf{r}_3) [N_{dd}(r_{32}) + X_{dd}(r_{32})] \\
&\quad + \left( X_{dd}(r_{13}) \right) \rho(\mathbf{r}_3) [N_{ed}(r_{32}) + X_{ed}(r_{32})] , \\
N_{de}(r_{12}) &= \left( X_{dd}(r_{13}) + X_{de}(r_{13}) \right) \rho(\mathbf{r}_3) [N_{de}(r_{32}) + X_{de}(r_{32})] \\
&\quad + \left( X_{dd}(r_{13}) \right) \rho(\mathbf{r}_3) [N_{ee}(r_{32}) + X_{ee}(r_{32})] , \\
N_{ee}(r_{12}) &= \left( X_{ed}(r_{13}) + X_{ee}(r_{13}) \right) \rho(\mathbf{r}_3) [N_{de}(r_{32}) + X_{de}(r_{32})] \\
&\quad + \left( X_{ed}(r_{13}) \right) \rho(\mathbf{r}_3) [N_{ee}(r_{32}) + X_{ee}(r_{32})] , \\
N_{cc}(r_{12}) &= \left( X_{cc}(r_{13}) \right) \rho(\mathbf{r}_3) [N_{cc}(r_{32}) + X_{cc}(r_{32}) - \ell(k_F r_{32})/\nu] . \tag{44}
\end{aligned}$$

The equations for the non-nodal diagrams are:

$$\begin{aligned}
X_{dd}(r_{12}) &= g_{dd}(r_{12}) - N_{dd}(r_{12}) - 1 , \\
X_{de}(r_{12}) &= g_{dd}(r_{12}) [N_{de}(r_{12}) + E_{de}(r_{12})] - N_{de}(r_{12}) , \\
X_{ee}(r_{12}) &= g_{dd}(r_{12}) \{ N_{ee}(r_{12}) + E_{ee}(r_{12}) + [N_{de}(r_{12}) + E_{de}(r_{12})]^2 \\
&\quad - \nu [N_{cc}(r_{12}) + E_{cc}(r_{12}) - \frac{1}{\nu} \ell(k_F r_{12})]^2 \} - N_{ee}(r_{12}) ,
\end{aligned}$$

$$\begin{aligned}
X_{cc}(r_{12}) &= g_{dd}(r_{12})[N_{cc}(r_{12}) + E_{cc}(r_{12}) - \frac{1}{\nu}\ell(k_F r_{12})] \\
&- N_{cc}(r_{12}) + \frac{1}{\nu}\ell(k_F r_{12}) .
\end{aligned} \tag{45}$$

Finally, the partial TBDF are defined as:

$$\begin{aligned}
g_{dd}(r_{12}) &= f^2(r_{12}) \exp[N_{dd}(r_{12}) + E_{dd}(r_{12})] , \\
g_{de}(r_{12}) &= N_{de}(r_{12}) + X_{de}(r_{12}) , \\
g_{ed}(r_{12}) &= g_{de}(r_{12}) , \\
g_{ee}(r_{12}) &= N_{ee}(r_{12}) + X_{ee}(r_{12}) , \\
g_{cc}(r_{12}) &= N_{cc}(r_{12}) + X_{cc}(r_{12}) - \frac{1}{\nu}\ell(k_F r_{12}) .
\end{aligned} \tag{46}$$

The total TBDF can be written in terms of the partial ones as:

$$g(r_{12}) = g_{dd}(r_{12}) + g_{ed}(r_{12}) + g_{de}(r_{12}) + g_{ee}(r_{12}) \tag{47}$$

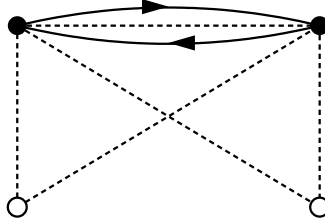


Figure 8: Graphical representation of an elementary diagram.

The set of Eqs. (44), (45), (46) and (47) forms the Fermi HyperNetted Chain (FHNC) equations. As we have already mentioned in the case of bosons, also the FHNC equations allow the evaluation of the contribution of all the composite and nodal diagrams in a closed form. Again, the contributions of the elementary diagrams, such as that shown in Fig. 8, should be included by calculating them one by one. In analogy to the HNC case, it is common practice to use the nomenclature FHNC/0, FHNC/4 etc. to indicate the elementary diagrams included in the calculations.

### 2.3 The operator dependent correlations

The use of purely scalar correlations, as it is done in the Jastrow ansatz (3), is not adequate to deal with the complicated structure of the nucleon-nucleon interaction. For example, the tensor terms of the interaction do not contribute to the energy expectation value if only scalar correlations are used. For this reason the Jastrow ansatz has been extended by introducing correlations which have the same operator structure of the NN interaction, and are called in the

literature [21] state-dependent correlations. The general expression of these type of correlations is:

$$\mathcal{F}(1, \dots, A) = \mathcal{S} \left( \prod_{j>i=1}^A F_{ij} \right) = \mathcal{S} \left( \prod_{j>i=1}^A \sum_{p=1}^6 f_p(r_{ij}) O_{ij}^p \right). \quad (48)$$

The operators  $O_{ij}^p$  are defined as:

$$O_{ij}^{p=1,6} = 1, \boldsymbol{\tau}_i \cdot \boldsymbol{\tau}_j, \boldsymbol{\sigma}_i \cdot \boldsymbol{\sigma}_j, (\boldsymbol{\sigma}_i \cdot \boldsymbol{\sigma}_j)(\boldsymbol{\tau}_i \cdot \boldsymbol{\tau}_j), S_{ij}, S_{ij}(\boldsymbol{\tau}_i \cdot \boldsymbol{\tau}_j), \quad (49)$$

where

$$S_{ij} \equiv 3(\boldsymbol{\sigma}_i \cdot \hat{\mathbf{r}}_{ij})(\boldsymbol{\sigma}_j \cdot \hat{\mathbf{r}}_{ij}) - \boldsymbol{\sigma}_i \cdot \boldsymbol{\sigma}_j, \quad (50)$$

is the tensor operator. The symmetry operator  $\mathcal{S}$  is required to guarantee the antisymmetrization of the wave function  $\Psi(1, \dots, A)$  since, in general, the operators do not commute. In Eq. (49) we have indicated only the channels up to  $p = 6$  since this is the correlation we have used in our numerical calculations. State-dependent correlations constructed by considering a larger number of channels have been used in nuclear matter [40] and in variational Monte Carlo calculations [41].

The order that we have introduced in the operators will be useful for the finite system since we can write:

$$O_{ij}^{2k-1+l} = P_{ij}^k (\boldsymbol{\tau}_i \cdot \boldsymbol{\tau}_j)^l, \quad (51)$$

with  $l = 0, 1$ ,  $k = 1, 2, 3$  and  $P_{ij}^k = 1, \boldsymbol{\sigma}_i \cdot \boldsymbol{\sigma}_j, S_{ij}$ . This allows us to separate clearly the spin and isospin parts of the operators.

The evaluation of the energy functional (9) requires the calculation of the expectation value of two-body operators related to the NN interaction which are written in terms of the operators (49). In general, these operators can be expressed as:

$$B(1, \dots, A) = \sum_{j>i=1}^A \left( \sum_{p=1}^6 B^p(r_{ij}) O_{ij}^p \right), \quad (52)$$

and this suggest to define state-dependent TBDFs as:

$$g_p(\mathbf{r}_1, \mathbf{r}_2) = \frac{A(A-1) \int dx_3 \dots dx_A \Psi^*(1, \dots, A) O_{12}^p \Psi(1, \dots, A)}{\rho^2 \int dx_1 dx_2 \dots dx_A \Psi^*(1, \dots, A) \Psi(1, \dots, A)}, \quad (53)$$

where we understand that all the spin and isospin traces are done, including those of the external points 1 and 2. With the above definition, the expectation value of  $B$  can be calculated as:

$$\langle B \rangle = \frac{1}{2} \rho^2 \sum_{p=1}^6 \int d\mathbf{r}_1 d\mathbf{r}_2 B^p(r_{12}) g_p(\mathbf{r}_1, \mathbf{r}_2). \quad (54)$$

With the help of the sub-determinants (31) we express the state-dependent TBDF as:

$$g_p(\mathbf{r}_1, \mathbf{r}_2) =$$

$$\frac{A(A-1) \int dx_3 \dots dx_A \mathcal{S} \left( \prod_{j>i=1}^A F_{ij} \right) O_{12}^p \mathcal{S} \left( \prod_{j>i=1}^A F_{ij} \right) \Delta_A(1, \dots, A)}{\rho^2 \int dx_1 dx_2 \dots dx_A \mathcal{S} \left( \prod_{j>i=1}^A F_{ij} \right) \mathcal{S} \left( \prod_{j>i=1}^A F_{ij} \right) \Delta_A(1, \dots, A)} . \quad (55)$$

In the calculation of the TBDF, we find it convenient to rewrite the correlation function as:

$$F_{ij} = \sum_{p=1}^6 f_p(r_{ij}) O_{ij}^p = f_1(r_{ij}) \left( 1 + \sum_{p=2}^6 \frac{f_p(r_{ij})}{f_1(r_{ij})} O_{ij}^p \right) = f_1(r_{ij}) (1 + H_{ij}) . \quad (56)$$

Because of the non commutativity of the operator dependent terms, in the cluster expansion we have to consider also the ordering of the various terms. Only the scalar term  $p = 1$ , which commutes with all the other ones, can be treated as we have indicated in the previous section. By using the commutativity property of the scalar term we can rewrite the correlation function as:

$$\mathcal{F}(1, \dots, A) = \mathcal{S} \left( \prod_{j>i=1}^A F_{ij} \right) = \left( \prod_{j>i=1}^A f_1(r_{ij}) \right) \mathcal{S} \left[ \prod_{j>i=1}^A (1 + H_{ij}) \right] . \quad (57)$$

This expression shows that each operator dependent term  $H_{ij}$  can be multiplied by any contribution from the central correlation functions,  $f_1$ , without changing the operator structure of the correlation. In the many-body jargon when we incorporate into the operator terms all the contributions from the central correlation, we say that the Jastrow correlations dress the operator terms.

The general treatment of the state dependent correlations for nuclear matter was first proposed in [21]. This is the basic reference for the interested reader. In the following we shall recall the basic steps of the procedure, and we point out the features of interest for the treatment of finite nuclear systems.

Although the notation in the demonstration would be more involved than in the purely Jastrow case, it is still possible to show that the compensation between the unlinked diagrams of the numerator and all the diagrams of the denominator holds for the state-dependent correlations.

We have shown in the previous section that the second step in obtaining the FHNC equations consisted in eliminating the contribution of the reducible diagrams. In the present case, this is no longer possible. We explain the problem by using the example of Fig. 9 which is analogous to Fig. 6 but with the scalar correlations substituted by state dependent correlations, indicated by the wavy lines. We should remark that in the graphical representation, the wavy lines indicate a generic operator dependent term of the correlation. Diagrams with various wavy lines, consider all the possible combinations and ordering of operators. Back to the case of Fig. 9, we should consider that all the statistical lines in a closed loop, but one, carry a spin-isospin exchange operator:

$$\Pi^{\sigma, \tau}(i, j) \equiv \frac{1}{4} (1 + \boldsymbol{\sigma}_i \cdot \boldsymbol{\sigma}_j) (1 + \boldsymbol{\tau}_i \cdot \boldsymbol{\tau}_j) = \frac{1}{4} \sum_{p=1}^6 \Gamma^p O_{ij}^p , \quad (58)$$

on the corresponding pair of particles [21] and with  $\Gamma^p$  given in Tab. 9 of Appendix A. The spin and isospin dependent part of this operator is linear in  $\boldsymbol{\sigma}$  and/or  $\boldsymbol{\tau}$ , therefore its trace is zero when only scalar correlations are used, as in the case of Fig. 6. In that case, the contributions

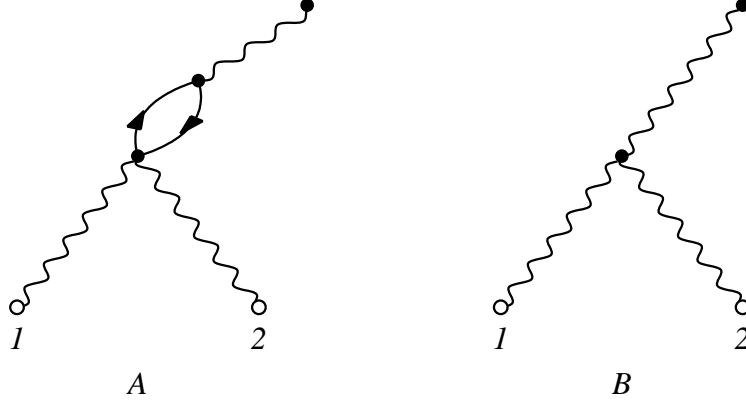


Figure 9: Diagrams analogous to those of Fig. 6 with state dependent correlations.

of the two diagrams were identical, with a sign difference, therefore, the global result was zero. In the present case, the trace of the operator dependent part of the exchange term is not always zero, but its value depends on the type of operators linked to the points at the edges of the exchange loop. For this reason, the traces of the A and B diagrams of Fig. 9 are in general different, therefore the global result is, in general, different from zero.

This loss of irreducibility in the expansion of the TBDF joined to the non commutativity among the operators makes it not possible to calculate all the contributions of state-dependent correlations. This obliges us to use approximations. The difficulty in eliminating the reducible diagrams is overcome by using an approximation, consisting in considering operator dependent diagrams with specific topological properties. These diagrams are classified as Single Operator Chain diagrams. Since the calculations of these diagrams requires the evaluation of traces of non commuting operators, we present first the technique used to calculate these traces, and then the FHNC equations in the SOC approximation.

### 2.3.1 Traces

In the calculation of the TBDF, or of the energy functional, we have to calculate expectation values of operators between the trial wave functions (2). These calculations require the integration on the space coordinates and the sum on the spin and isospin coordinates. We have called trace this last operation. There are no specific strategies for evaluating the space integrals, which are done numerically. On the contrary, there are strategies to obtain the spin and isospin traces. Here we shall present them for the specific case of the infinite symmetric nuclear matter, and, later, we shall generalize them for finite nuclei. We have emphasized the characteristics of the system under discussion, because we want to point out that it is a spin and isospin saturated system, therefore the traces of terms linear in  $\sigma$  and/or  $\tau$  operators are zero.

We start our discussion with the simplest possible case, the matrix element between two points only, 1 and 2, having a single operator  $O_{12}^p$  acting between them. Because of the Pauli principle we have direct and exchange terms. The direct term is:

$$O_{12}^p \rho_0(1,1) \rho_0(2,2) =$$

$$\begin{aligned} & \rho^2 \frac{1}{\nu^2} \sum_{s_1, s_2, t_1, t_2} \chi_{s_1}^+(1) \chi_{s_2}^+(2) \chi_{t_1}^+(1) \chi_{t_2}^+(2) O_{12}^p \chi_{t_1}(1) \chi_{t_2}(2) \chi_{s_1}(1) \chi_{s_2}(2) \\ &= \rho^2 C(O_{12}^p) , \end{aligned}$$

where we have used the expression (35) for  $\rho_0$  and the fact that the limit of the Slater function (36) when its argument goes to zero, is one. In the above expression we have indicated with  $C(O_{12}^p)$  the value of spin and isospin trace relative to the operator  $O_{12}^p$  divided by the number of states,  $\nu^2$  in this case. We call it the  $C$ -trace. The exchange term for the case under study is:

$$\begin{aligned} O_{12}^p \rho_0(1, 2) \rho_0(2, 1) &= \rho^2 \frac{\ell^2(k_F r_{12})}{\nu^2} \\ &\sum_{s_1, s_2, t_1, t_2} \chi_{s_2}^+(1) \chi_{s_1}^+(2) \chi_{t_2}^+(1) \chi_{t_1}^+(2) O_{12}^p \chi_{t_1}(1) \chi_{t_2}(2) \chi_{s_1}(1) \chi_{s_2}(2) \\ &= \rho^2 \ell^2(k_F r_{12}) C \left( \frac{1}{4} (1 + \boldsymbol{\sigma}_1 \cdot \boldsymbol{\sigma}_2) (1 + \boldsymbol{\tau}_1 \cdot \boldsymbol{\tau}_2) O_{12}^p \right) , \end{aligned}$$

where the term multiplying  $O_{12}^p$  in the  $C$ -trace is the spin and isospin exchange operator which has to be on the left of the rest of the operators.

The operators (49) are built to be scalar in the Fock space formed by the product of configuration and spin, and isospin, spaces, therefore they are constructed as scalar product of spin, coordinates and isospin operators. For this reason, their contributions can be evaluated by using the Pauli identity:

$$(\boldsymbol{\alpha}_1 \cdot \mathbf{A})(\boldsymbol{\alpha}_1 \cdot \mathbf{B}) = \mathbf{A} \cdot \mathbf{B} + i \boldsymbol{\alpha}_1 \cdot (\mathbf{A} \times \mathbf{B}) , \quad (59)$$

where  $\boldsymbol{\alpha} = \boldsymbol{\sigma}, \boldsymbol{\tau}$  and  $\mathbf{A}$  and  $\mathbf{B}$  are generic vector operators. By using this identity, we can isolate the terms linear in  $\boldsymbol{\tau}$  or  $\boldsymbol{\sigma}$  which do not contribute in infinite and symmetric nuclear matter, as we have already stated.

The two examples we have discussed are the easieast ones to calculate. In evaluation of the TBDF, or of the energy functional, we have to deal with more complicated situations. Following Ref. [21] we consider three type of situations.

- a) Products of operators acting on the same pair, such as:

$$O_{ij}^{p>1} O_{ij}^{q>1} \dots O_{ij}^{r>1} ,$$

- b) Products of operators acting on different connected points forming a ring, such as:

$$O_{12}^{p>1} O_{23}^{q>1} \dots O_{n-1n}^{r>1} O_{n1}^{s>1} .$$

We call this situation Single-Operator Ring (SOR)

- c) The situation when more than two operators act on an internal point. These are multipole operators terms.

### 2.3.1.a Products of operators

We analyze the trace algebra of the products of operators  $O_{12}^p$  acting on the same pair of coordinates 1 and 2.

The  $C$ -trace of a single operator is:

$$C(O_{12}^p) = \delta_{p,1} \quad (60)$$

since all operator linear in  $\sigma$  and/or  $\tau$  have zero  $C$ -trace in a spin and isospin saturated system, as we have already mentioned.

The  $C$ -traces of the product of two operators  $O_{12}^{p>1} O_{12}^{q>1}$  are obtained by using the relations

$$\begin{aligned} (\alpha_1 \cdot \alpha_2)^2 &= 3 - 2\alpha_1 \cdot \alpha_2 , \\ S_{12} \sigma_1 \cdot \sigma_2 &= S_{12} , \\ S_{12}^2 &= 6 + 2\sigma_1 \cdot \sigma_2 - 2S_{12} , \end{aligned} \quad (61)$$

calculated by using the Pauli identity (59) and with  $\alpha = \sigma, \tau$ . The values of the  $C$ -traces in this case can be summarized as:

$$C\left(O_{12}^p O_{12}^q\right) = B^p \delta_{pq} , \quad (62)$$

where the values of  $B^p$  are given in Tab. 10 of Appendix A. In [21], these are called  $A^p$  but we shall use this name for their spin parts.

The knowledge of the values of the  $C$ -traces of one operator and of the product of two operators is enough to calculate the values of the  $C$ -traces for the product of any number of operator. The relations (61) indicate that the product of two operators  $O_{12}^{p>1} O_{12}^{q>1}$  can be written as sum of operators  $O_{12}^r$  multiplied by a coefficient. We can write:

$$O_{12}^p O_{12}^q = \sum_{r=1}^6 K^{pqr} O_{12}^r , \quad (63)$$

where the values of the matrix  $K^{pqr}$  are given in Tab. 11 of Appendix A. For example for three operators we have:

$$C\left(O_{12}^p O_{12}^q O_{12}^r\right) = \sum_{m=1}^6 K^{pqm} C\left(O_{12}^m O_{12}^r\right) = K^{pqr} B^r .$$

We would like to point out that since the operators  $O^{p=1,6}$  acting on the same points commute, their ordering does not matter in the calculation of the  $C$ -trace. This means that:

$$K^{pqr} B^r = K^{prq} B^q = K^{qrp} B^p \dots .$$

### 2.3.1.b Single operator rings

In Fig. 10 we show an example of Single Operator Ring (SOR). In the SOR diagram each point is reached by two operators only. The ordering of these operators does not change the value of the  $C$ -trace of the SOR. This is because, due to the Pauli identity (59), the non commuting terms are linear in  $\sigma$  or  $\tau$ , therefore their trace is zero.

The basic step to evaluate of the  $C$ -trace of a SOR it is to calculate the  $C$ -trace of two operators acting on a common point. We call  $O_{12}^p$  and  $O_{23}^q$  the two operators, and 2 is the common point. All the variables relative to the common point 2 should be summed or integrated. We sum on all the spin and isospin third components and integrate on the azimuthal angle  $\phi$ :

$$\sum_{\sigma_2 \tau_2} \int d\phi_2 O_{12}^p O_{23}^q = \sum_{r=1}^6 \int d\phi_2 \xi_{123}^{pqr} O_{13}^r . \quad (64)$$

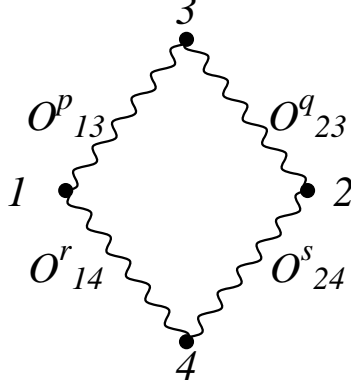


Figure 10: Example of Single Operator Ring (SOR).

The  $\xi_{123}^{pqr}$  functions depend on the angles of the triangle formed by the 1, 2 and 3 points, and have the following properties:

$$\begin{aligned}
& \xi_{123}^{2k_1-1+l_1 \ 2k_2-1+l_2 \ 2k_3-1+l_3} = \zeta_{123}^{k_1 k_2 k_3} \delta_{l_1 l_2} \delta_{l_1 l_3} , \\
\zeta_{123}^{k_1 k_2 k_3} &= \delta_{k_1 1} \delta_{k_2 1} \delta_{k_3 1} + \delta_{k_1 2} \delta_{k_2 2} \delta_{k_3 2} \\
&+ P_2(\hat{r}_{13} \cdot \hat{r}_{23})(\delta_{k_1 2} - \delta_{k_1 3}) \delta_{k_2 3} \delta_{k_3 3} \\
&+ P_2(\hat{r}_{12} \cdot \hat{r}_{13}) \delta_{k_1 3} (\delta_{k_2 2} - \delta_{k_2 3}) \delta_{k_3 3} \\
&+ P_2(\hat{r}_{12} \cdot \hat{r}_{23}) \delta_{k_1 3} \delta_{k_2 3} (2\delta_{k_3 2} - \delta_{k_3 3}) \\
&- \frac{1}{2} \left( 9(\hat{r}_{13} \cdot \hat{r}_{23})(\hat{r}_{12} \cdot \hat{r}_{13})(\hat{r}_{12} \cdot \hat{r}_{23}) + 1 \right) \delta_{k_1 3} \delta_{k_2 3} \delta_{k_3 3} , \tag{65}
\end{aligned}$$

with  $P_2(x) = (3x^2 - 1)/2$  the Legendre polynomial of second degree and we have used the separation in spin and isospin parts of the operators presented in Eq. (51). The global contribution of the SOR is calculated by using Eqs. (64) and (65) for all the points of the ring.

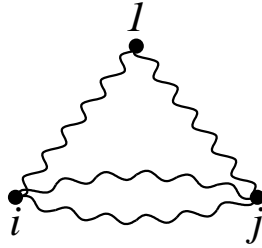


Figure 11: Example of a multipole operator diagram where more than one operator acts on the same two points.

### 2.3.1.c Multiple-operators diagrams

The last type of diagrams we discuss is represented by the diagram of Fig. 11. In this diagram two operators act on the same points  $i$  and  $j$ . The diagram of the figure represents the product



of the operators:  $O_{ij}^p$ ,  $O_{ij}^q$ ,  $O_{1i}^r$  and  $O_{1j}^s$ . In this case, the value of the  $C$ -trace depends on the ordering of the operators. It is possible to prove that this value is unchanged by a cyclic permutation of the operators of the same type [21]. That is:

$$C\left(O_{kl}^p(O_{ij}^q O_{ij}^r \dots)\right) = C\left((O_{ij}^q O_{ij}^r \dots) O_{kl}^p\right) .$$

As a consequence, for the evaluation of the  $C$ -trace we have to consider only two different orderings of operators. A first one where  $O_{ij}^p$  and  $O_{ij}^q$  are close to each other, and a second one, where these two operators are separated by another operators of the type  $O_{i1}^r$  or  $O_{1j}^s$ . In the first case, by using Eqs. (63) and (65) we obtain:

$$\int d\phi_1 C\left(O_{ij}^p O_{ij}^q O_{1i}^r O_{1j}^s\right) = \sum_{t=1}^6 K^{pqt} B^t \int d\phi_1 \xi_{i1j}^{rst} . \quad (66)$$

For the second case we have:

$$\int d\phi_1 C\left(O_{ij}^p O_{1i}^r O_{ij}^q O_{1j}^s\right) = \sum_{t=1}^6 L^{pqt} \int d\phi_1 \xi_{i1j}^{rst} , \quad (67)$$

where we have defined:

$$L^{pqt} = \pm K^{pqt} B^t . \quad (68)$$

The + sign is assigned if

$$C\left(O_{ij}^p [O_{ij}^q, O_{1i}^r] O_{1j}^s\right) = 0 ,$$

and the - sign if

$$C\left(O_{ij}^p \{O_{ij}^q, O_{1i}^r\} O_{1j}^s\right) = 0 ,$$

where we have indicated with the symbols  $[,]$  and  $\{, \}$  the commutator and anticommutator respectively. The values of matrix  $L^{pqr}$  are given in Tab. 12 of Appendix A.

Another important trace is that of

$$C\left(O_{1i}^s O_{1i}^r O_{ij}^p O_{ij}^q\right) ,$$

which represents two SOR's linked at the point  $i$ . Also in this case the result depends on the ordering of the operators and we distinguish the case when  $O_{ij}^p$  and  $O_{ij}^q$  are close together or not. In the first case, we obtain:

$$C\left(O_{ij}^p O_{ij}^q O_{1i}^s O_{1i}^r\right) = B^p \delta_{p,q} B^s \delta_{s,r} .$$

To evaluate the  $C$ -trace of the second case we consider the fact that:

$$\sum_{\sigma_j \tau_j} O_{ij}^p O_{1i}^s O_{ij}^q = \delta_{p,q} B^p (1 + E_{ps}) O_{1i}^s , \quad (69)$$

where, in the case of tensor operators, the above equation assumes an integration over the angle between  $\mathbf{r}_{ij}$  and  $\mathbf{r}_{1i}$  [21]. Then we obtain:

$$C\left(O_{ij}^p O_{1i}^s O_{ij}^q O_{1i}^r\right) = B^p \delta_{p,q} (1 + E_{ps}) B^s \delta_{s,r} , \quad (70)$$

with the values of  $E$ , given in Tab. 13 of Appendix A. In [21] these are called  $D$  but we shall use this name for their spin parts.

## 2.4 The Single Operator Chain (SOC) equations

The strategy to attack the problems arising when state-dependent correlations are used, consists in separating the purely scalar, Jastrow, terms from those depending on the operators  $O^p$  for  $p > 1$ . The Jastrow part is treated by using the set of FHNC equations (44), (45) and (46). With respect to the operator dependent part, we have learnt that we need at least two operators arriving at a given point to get a  $C$ -part different from zero. As the operators are dynamical correlations, there is no limitation in the number of them that can arrive at every point. An increasing number of operators makes more complicated the evaluation of the traces so the Single Operator Chain (SOC) approximation is adopted. This supposes that only a pair of operators arrive at every internal point of the diagrams, this makes the operators form closed single chains and it allows the formulation of closed expressions to calculate all the nodal operators and those composite ones within the approximation. The reliability of the SOC approximation is tested afterwards, by controlling the validity of sum rules exhaustion. Examples of SOC diagrams, of nodal type, are given in Fig. 12.

The SOC diagrams do not have limitations in the number of particles. The discussion made in Sect. 2.3.1 has clarified that the contribution of the SOC diagrams to the TBDF's and/or to the energy, is independent of the ordering of the operators. The single operator between two points of the SOC diagram, can come from the correlation, from the hamiltonian, or from an exchange line, whose contribution is considered by inserting the spin-isospin exchange operator (58).

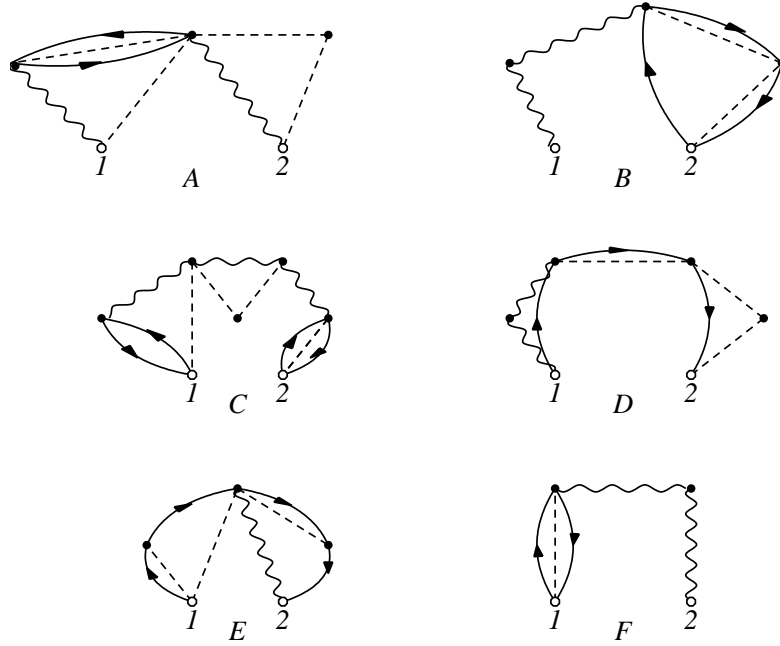


Figure 12: Some nodal diagrams considered in the FHNC/SOC computational scheme.

The choice of considering SOC diagrams only, eliminates the problem of the reducible dia-

grams, since all the SOC diagrams are irreducible. The equations we should consider contain only irreducible diagrams. Also in this case it is possible to show [21] that the composite diagrams can be obtained in terms of simple diagrams classified again in nodal and elementary ones.

As in the FHNC case, the contribution of a nodal diagram  $N_{mn,p}(r_{ij})$ , can be obtained by doing the folding product of diagrams at the nodal point, as can be deduced by observing the examples given in Fig.12. Here we used  $mn$  to indicate the type of diagram  $mn = dd, de, ed, ee, cc$ . As already discussed, the folding product in the  $\mathbf{r}_k$  point should be done between the irreducible non nodal diagrams  $X_{mn,p}(r_{ik})$  and  $X_{mn,q}(r_{kj}) + N_{mn,q}(r_{kj})$ . From the discussion made in the previous section, it appears clear that not all the possible combinations of operators acting on the integration point provide contributions different from zero. The allowed combinations are ruled by the values of  $\xi^{pqr}$  given in Eqs.(65).

The sequence of Eqs.(44) giving the nodal diagrams, is generalized for the state-dependent terms as:

$$N_{mn,r}(r_{12}) = \sum_{m',n'} \sum_{p,q=1}^6 \left( X_{mm',p}(r_{13}) \xi_{132}^{pqr} \left| \rho(\mathbf{r}_3) [X_{n'n,q}(r_{23}) + N_{n'n,q}(r_{23})] \right. \right), \quad (71)$$

for  $m, n = d, e$  and with  $m'n' = dd, ed, de$ . If we neglect the contribution of the elementary diagrams, i.e. in approximation FHNC/0, we obtain the following expressions for the TBDFs for  $p > 1$ :

$$g_p(r_{12}) = g_{dd,p}(r_{12}) + 2g_{de,p}(r_{12}) + g_{ee,p}(r_{12}), \quad (72)$$

$$g_{dd,p}(r_{12}) = h_p(r_{12})h_c(r_{12}) = X_{dd,p}(r_{12}) + N_{dd,p}(r_{12}), \quad (73)$$

$$\begin{aligned} g_{de,p}(r_{12}) &= \left( h_p(r_{12})N_{de}(r_{12}) + f_1^2(r_{12})N_{de,p}(r_{12}) \right) h_c(r_{12}) \\ &= X_{de,p}(r_{12}) + N_{de,p}(r_{12}), \end{aligned} \quad (74)$$

$$\begin{aligned} g_{ee,p}(r_{12}) &= \left[ h_p(r_{12}) \left( N_{de}(r_{12})N_{ed}(r_{12}) + N_{ee}(r_{12}) \right) \right. \\ &\quad \left. + f_1^2(r_{12}) \left( -\nu L^2(r_{12})\Gamma^p + N_{ee,p}(r_{12}) \right) \right. \\ &\quad \left. + 2N_{de,p}(r_{12})N_{de}(r_{12}) \right] h_c(r_{12}) \\ &= X_{ee,p}(r_{12}) + N_{ee,p}(r_{12}), \end{aligned} \quad (75)$$

where the  $N$  and  $X$  factor without index of the operator channel indicate the scalar  $p = 1$  term,  $\Gamma^p$  is given by Eq. (58), and we have defined:

$$h_p(r_{12}) = 2f_p(r_{12})f_1(r_{12}) + f_1^2(r_{12})N_{dd,p}(r_{12}), \quad (76)$$

$$h_c(r_{12}) = \exp[N_{dd}(r_{12})], \quad (77)$$

$$L(r_{12}) = N_{cc}(r_{12}) - \ell(k_F r_{12})/\nu, \quad (78)$$

For the calculation of the cyclic nodal diagrams within the SOC approximation, it is convenient to distinguish two cases [21]. Since all statistical lines but one carry one spin-isospin exchange operator, we have to add a dynamical operator to complete the operator chain. This no exchange operator may be added to the left or to right of the chain. Example of these two cases is given by the D and E diagrams of Fig. 12. In the D diagram the point 1 is connected

with an operator dependent correlation while the point 2 is connected by the spin-isospin exchange operator. We label  $L$  this case. The situation is reversed in the case of the E diagram, and we call  $R$  this case. By using this classification we define for the cyclic case the quantities:

$$X_{c,p}^{L,R}(r_{12}) = [h_p(r_{12})L(r_{12}) + f_1^2(r_{12})N_{c,p}^{L,R}(r_{12})] h_c(r_{12}) - N_{c,p}^{L,R}(r_{12}) , \quad (79)$$

$$X_{cc}(r_{12}) = [f_1^2(r_{12})h_c(r_{12}) - 1] L(r_{12}) , \quad (80)$$

$$N_{cc,r}(r_{12}) = N_{c,r}^L(r_{12}) + N_{c,r}^R(r_{12}) , \quad (81)$$

$$N_{c,r}^L(r_{12}) = \sum_{p,q=1}^6 \left( X_{c,p}^L(r_{13}) \xi_{132}^{pqr} \Gamma^q \Big| \rho(\mathbf{r}_3) [X_{cc}(r_{23}) + L(r_{23})] \right) , \quad (82)$$

$$N_{c,r}^R(r_{12}) = \sum_{p,q=1}^6 \left( \Gamma^p X_{cc}(r_{13}) \xi_{132}^{pqr} \Big| \rho(\mathbf{r}_3) [X_{c,q}^R(r_{23}) + N_{c,q}^R(r_{23})] \right) . \quad (83)$$

The set of equations we have presented is called FHNC/SOC. In this case the contribution of the elementary diagrams is neglected. Some example of diagrams considered by these equations is given in Fig. 12. The diagram A is a  $N_{dd,p}(r_{12})$  nodal diagram; the diagrams B and F are examples of  $N_{de,p}(r_{12})$  diagrams and the diagram C of the  $N_{ee,p}(r_{12})$  diagram. Finally, the diagrams D and E are of  $N_{cc,p}(r_{12})$  type.

### 3 Finite nuclear systems

Two of the basic hypotheses done in the previous section, infinite number of particles and translational invariance, are no longer valid in the description of finite nuclei. In the literature the extension of the FHNC theory to finite nuclear systems was first done by considering systems with equal number of protons and neutrons with single particle wave functions produced by a unique Mean-Field (MF) potential, within the  $ls$  coupling scheme [27, 28, 30, 31]. This situation allowed a straightforward use of the spin and isospin trace techniques developed to describe symmetric nuclear matter [21]. The treatment of nuclei not saturated in isospin and described in the  $jj$  coupling scheme, was done in following works [29, 33]. Here we do not follow the historical development of the theory but we present directly the formulation of the FHNC theory for double closed shell nuclei not saturated in isospin and in the  $jj$  coupling scheme.

The changes of the OBDM expression, due to the loss of the translational invariance, are presented in Sect. 3.1. We should point out that we consider doubly magic nuclei only, which are spherically symmetric. In Sect. 3.2 we present the calculation of the TBDF and we introduce vertex corrections and the Renormalized FHNC (RFHNC) equations, for purely scalar correlations. The extension of the theory when state dependent correlations are used, is presented in Sect. 3.3.

#### 3.1 The single particle basis

The nuclear system under study has  $Z$  protons,  $N$  neutrons and, therefore,  $A = Z + N$  nucleons. The set of single particles wave functions used to describe this system is produced by solving the one-body Schrödinger equation:

$$h_i^t \phi_i^t(x_i) = \epsilon_i^t \phi_i^t(x_i) , \quad (84)$$

where the one-body hamiltonian is composed by the kinetic energy term and a spherical mean-field potentials different for protons ( $t = 1/2$ ) and neutrons ( $t = -1/2$ ):

$$h_i^{t=\pm 1/2} = -\frac{\hbar^2}{2m_t} \nabla_i^2 + U^t(r_i) . \quad (85)$$

where we have indicated with  $m_t$  the nucleon mass. Our calculations have been done with single particle wave functions generated by a Wood-Saxon potential of the form:

$$\begin{aligned} U^t(r) = & \frac{V_0^t}{1 + \exp \left[ \left( r - R_0^t \right) / a_0^t \right]} \\ & + \left[ \frac{\hbar c}{m_\pi c^2} \right]^2 V_{ls}^t \frac{\exp \left[ \left( r - R_{ls}^t \right) / a_{ls}^t \right]}{\left\{ 1 + \exp \left[ \left( r - R_{ls}^t \right) / a_{ls}^t \right] \right\}^2} \mathbf{1} \cdot \boldsymbol{\sigma} - V_C^t(r) , \end{aligned} \quad (86)$$

where  $m_\pi$  is the pion mass and the Coulomb term  $V_C^t(r)$ , active only for protons, is that produced by a homogeneous charge distribution.

$$V_C^{t=1/2}(r) = \begin{cases} (Z-1)e^2/r & r \geq R_C \\ \frac{(Z-1)e^2}{2R_C} \left[ 3 - \frac{r^2}{R_C^2} \right] & r \leq R_C \end{cases} . \quad (87)$$

The values of the parameters  $V_0^t$ ,  $V_{ls}^t$ ,  $a_0^t$ ,  $a_{ls}^t$ ,  $R_0^t$ ,  $R_{ls}^t$  and  $R_C$  are fixed by the variational principle (1). In an infinite system, the variational parameter related to the single particle basis is the density of the system.

The eigenfunctions of the hamiltonian (85) are also eigenfunction of  $\mathbf{j}^2$  and  $j_z$  operators, where we have indicated with  $\mathbf{j}$  the total angular momentum of the single nucleon. The single particle wave functions are conveniently expressed as:

$$\begin{aligned}\phi_{nljm}^t(x_i) &= R_{nlj}^t(r_i) \sum_{\mu,s} \langle l\mu \frac{1}{2}s | jm \rangle Y_{l\mu}(\Omega_i) \chi_s(i) \chi_t(i) \\ &= \phi_{nljm}^t(\mathbf{r}_i) \chi_t(i) = R_{nlj}^t(r_i) \mathbf{Y}_{lj}^m(\Omega_i) \chi_t(i) ,\end{aligned}\quad (88)$$

where we have indicated with the symbol  $\langle | \rangle$  the Clebsh-Gordan coefficients, and with  $Y_{l\mu}(\Omega_i)$  the spherical harmonics. Here we used the symbol  $\Omega_i$  to indicate both polar angles  $\theta_i$  and  $\varphi_i$ , characterizing the position of the nucleon with respect to a fixed center of coordinates chosen to be the center of the spherical nucleus. We have also defined the spin spherical harmonics  $\mathbf{Y}_{lj}^m(\Omega_i)$  [42].

The uncorrelated OBDM (29) can be written as:

$$\rho_0(x_i, x_j) = \sum_{s,s',t} \rho_0^{ss't}(\mathbf{r}_i, \mathbf{r}_j) \chi_s^+(i) \chi_{s'}(j) \chi_t^+(i) \chi_t(j) , \quad (89)$$

where the spatial part is defined as:

$$\begin{aligned}\rho_0^{ss't}(\mathbf{r}_i, \mathbf{r}_j) &= \sum_{nlj} R_{nlj}^t(r_i) R_{nlj}^t(r_j) \\ &\quad \sum_{\mu\mu'm} \langle l\mu \frac{1}{2}s | jm \rangle \langle l\mu' \frac{1}{2}s' | jm \rangle Y_{l\mu}^*(\Omega_i) Y_{l\mu'}(\Omega_j) .\end{aligned}\quad (90)$$

We find it useful to consider separately the uncorrelated OBDMs of pairs of particles with parallel or antiparallel third components of their spins. For these OBDMs we obtain respectively the expressions:

$$\begin{aligned}\rho_0^{\frac{1}{2}\frac{1}{2}t}(\mathbf{r}_i, \mathbf{r}_j) &\equiv \rho_0^t(\mathbf{r}_i, \mathbf{r}_j) \\ &= \frac{1}{8\pi} \sum_{nlj} (2j+1) R_{nlj}^t(r_i) R_{nlj}^t(r_j) P_l(\cos \theta_{ij}) ,\end{aligned}\quad (91)$$

$$\begin{aligned}\rho_0^{\frac{1}{2}-\frac{1}{2}t}(\mathbf{r}_i, \mathbf{r}_j) &\equiv \rho_{0j}^t(\mathbf{r}_i, \mathbf{r}_j) \\ &= \frac{1}{4\pi} \sum_{nlj} (-1)^{j-l-1/2} R_{nlj}^t(r_i) R_{nlj}^t(r_j) \sin \theta_{ij} P'_l(\cos \theta_{ij}) ,\end{aligned}\quad (92)$$

where we have called  $\theta_{ij}$  the angle between  $\mathbf{r}_i$  and  $\mathbf{r}_j$ , and we have indicated with  $P_l(x)$  the Legendre polynomial of  $l$ th degree, and with  $P'_l(x)$  its first derivative with respect to  $x$ . Some useful symmetry properties of these OBDMs are:

$$\rho_0^t(\mathbf{r}_i, \mathbf{r}_j) = \rho_0^{\frac{1}{2}\frac{1}{2}t}(\mathbf{r}_i, \mathbf{r}_j) = \rho_0^{-\frac{1}{2}-\frac{1}{2}t}(\mathbf{r}_i, \mathbf{r}_j) , \quad (93)$$

$$\rho_{0j}^t(\mathbf{r}_i, \mathbf{r}_j) = \rho_0^{\frac{1}{2}-\frac{1}{2}t}(\mathbf{r}_i, \mathbf{r}_j) = -\rho_0^{-\frac{1}{2}\frac{1}{2}t}(\mathbf{r}_i, \mathbf{r}_j) , \quad (94)$$

$$\rho_0^t(\mathbf{r}_i, \mathbf{r}_j) = \rho_0^t(\mathbf{r}_j, \mathbf{r}_i) , \quad (95)$$

$$\rho_{0j}^t(\mathbf{r}_i, \mathbf{r}_j) = -\rho_{0j}^t(\mathbf{r}_j, \mathbf{r}_i) . \quad (96)$$

The uncorrelated OBDM's describing finite nuclei do not depend only on  $r_{ij} = |\mathbf{r}_i - \mathbf{r}_j|$ , as in the infinite systems case. However, the properties (30), (32) and (33), relevant for the construction of the FHNC equations, remain valid.

The  $ls$  coupling can be recovered by switching off the spin-orbit term  $V_{ls}^t = 0$  in Eq. (86). In this case, the single particle energies,  $\epsilon_i$ , and the radial functions do not depend on  $j$ , therefore the OBDM can be expressed as:

$$\rho_0(x_i, x_j) = \sum_{s,t} \rho_0^t(\mathbf{r}_i, \mathbf{r}_j) \chi_s^+(i) \chi_s(j) \chi_t^+(i) \chi_t(j) , \quad (97)$$

with

$$\rho_0^t(\mathbf{r}_1, \mathbf{r}_2) = \frac{1}{4\pi} \sum_{nl} (2l+1) R_{nl}^t(r_1) R_{nl}^t(r_2) P_l(\cos \theta_{12}) , \quad (98)$$

showing that only the parallel spin OBDM survives. The calculations of Refs. [27, 28, 30, 31] have been done by using an  $ls$  coupling scheme and by assuming equal number of protons and neutrons moving in a unique MF potential. With these assumptions the expression of the OBDM can be further simplified as:

$$\rho_0^{\frac{1}{2}}(\mathbf{r}_1, \mathbf{r}_2) = \rho_0^{-\frac{1}{2}}(\mathbf{r}_1, \mathbf{r}_2) = \frac{1}{4\pi} \sum_{nl} (2l+1) R_{nl}(r_1) R_{nl}(r_2) P_l(\cos \theta_{12}) , \quad (99)$$

i.e. the spatial part of the uncorrelated OBDM is also independent of the value of the isospin.

### 3.2 The vertex corrections

The construction of the FHNC equations for the finite systems follows the steps used for the infinite systems. The minimization of the energy functional, Eq. (1), with the ansatz (2) on the wave function and (3) on the correlation, leads to the requirement of evaluating the TBDF (10). The loss of translational invariance obliges us to calculate also the One-Body Distribution Function (OBDF), which, in the present case, depends on the isospin third component:

$$\rho^{t_1}(\mathbf{r}_1) = \frac{\mathcal{N}_{t_1}}{\langle \Psi | \Psi \rangle} \int dx_2 \dots dx_A \Psi^*(x_1, x_2, \dots, x_A) P_1^{t_1} \Psi(x_1, x_2, \dots, x_A) , \quad (100)$$

where  $\mathcal{N}_t$  indicates the number of protons ( $t = 1/2$ ) or of neutrons ( $t = -1/2$ ), and the projector operator  $P^t$  selects the particle with isospin third component  $t$ . By using the above definitions, we can express the operator dependent TBDF as:

$$\begin{aligned} \rho^2 g_q^{t_1 t_2}(\mathbf{r}_1, \mathbf{r}_2) &\equiv \rho_2^{q, t_1 t_2}(\mathbf{r}_1, \mathbf{r}_2) = \frac{\mathcal{N}_{t_1} (\mathcal{N}_{t_2} - \delta_{t_1 t_2})}{\langle \Psi | \Psi \rangle} \\ &\times \int dx_3 \dots dx_A \Psi^*(x_1, x_2, \dots, x_A) P_1^{t_1} O_{12}^q P_2^{t_2} \Psi(x_1, x_2, \dots, x_A), \end{aligned} \quad (101)$$

where the  $O^q$  operators have been defined in Eq. (49). In the remaining part of this section we shall be concerned only with the calculation of the scalar TBDF,  $q = 1$ . The evaluation of the other operator dependent TBDFs is treated in Sect. 3.3.

The first steps to be done to calculate the one- and two-body density functions defined above, are analogous to those used in the infinite systems case. We start by defining an  $h$ -function as in

Eq. (14) and we use it to make the cluster expansion of the numerator and the denominator of both OBDF and TBDF. The various terms of the cluster expansions can be analyzed by using Mayer diagrams. The topological analysis of these diagrams is done in analogy to what we have discussed in the case of infinite systems.

The arguments used in Sects. 2.1 and 2.2 to show that the contributions of the unlinked diagrams of the numerator are simplified by the denominator, can be repeated also in the finite systems case [26]. The demonstration is done by formally extending up to infinity all the sums of the various cluster terms, since the property (33) of the sub-determinant  $\Delta_p$  ensures that diagrams containing a number of particles greater than the number of particles forming the system, do not contribute.

In the infinite systems case, the next step was the elimination of the reducible diagrams. We have already said that this elimination is only approximated for boson systems, up the  $1/A$  order, but it is exact for infinite fermion systems. The basic point of the demonstration for this latter case, was the possibility to associate to each reducible diagram, another diagram containing only one additional exchange loop. The contributions of these two diagrams to the TBDF differ only by a sign, therefore they cancel each other. This cancellation mechanism is produced by two specific characteristics of the infinite system. The fact that for a given reducible diagram it is always possible to find another diagram having one additional particle, and one additional exchange loop, is ensured by the presence of an infinite number of particles. The translational invariance is instead responsible for the fact that the additional exchange loop contributes only an overall minus sign. In the finite nuclei the number of particles is limited, and the translational invariance is lost, therefore there is no cancellation of the reducible diagrams.

However, even in finite systems it is possible to recover the irreducibility of the expansion by introducing the so-called vertex corrections [43, 26]. A graphical representation of this idea is given in Fig. 13. Every reducible diagram can be thought as composed by two parts, as indicated by the diagrams A and B of the figure. A first part contains the external points and is the irreducible part of the diagram. A second, reducible, part contains only internal points, and it is linked to the irreducible part through the articulation point  $a$ . The total contribution of these connected, and reducible, diagrams to the TBDF can be written as the folding integral of the irreducible part with a function taking into account the contribution of all the diagrams connected to the articulation point and it is directly related to the OBDF (100).

It is necessary to distinguish the case where the irreducible part is linked to the articulation point only by dynamical correlations, as in the A diagram of the figure, from the case when there are statistical correlations joining the articulation point, as in the diagram B. To simplify the drawing, we show in the A diagram only a single dynamical correlation line connecting the irreducible part to the articulation point. In reality, there are no limitations on the number of dynamical correlations. In the case of the B diagram we show only the statistical lines connecting the articulation point, but also dynamical correlations may be present.

The fact to be considered is that the Pauli principle allows each point to be reached by no more than two exchange lines. When the articulation point is of type  $d$ , i.e. linked to the irreducible part of the diagram only by dynamical correlations, the Pauli principle is not active. In this case, the reducible part of the diagram can reach the articulation point with both dynamical and statistical correlations. We call  $C^t(a) \equiv \rho^t(a)$  the sum of all the possible linked diagrams containing the articulation point  $a$  which has isospin third component  $t$ . This is really the OBDF (100) of the nucleons with isospin third component  $t$ .

The situation changes when the articulation point is of type  $e$ , i.e. linked to the irreducible



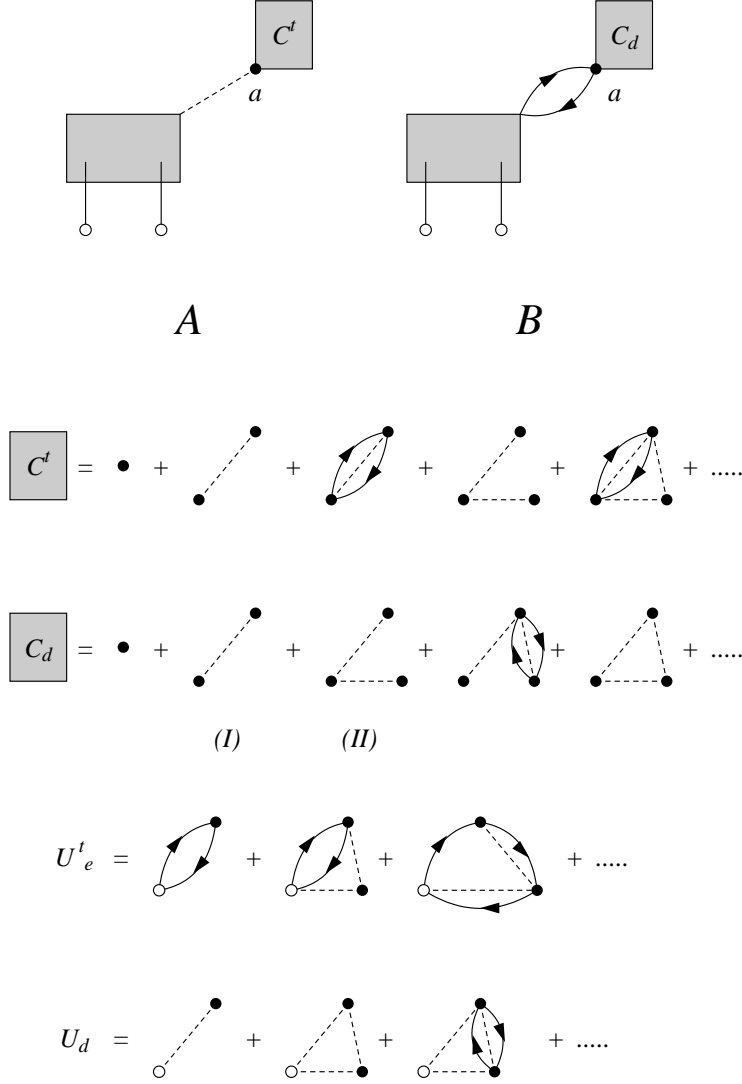


Figure 13: Graphical illustration of the vertex corrections. Since the Pauli exclusion principle allows each point to be reached by no more than two exchange lines, we have to distinguish the reducible parts of the diagrams. In  $C_d$  the articulation point  $a$  can be reached only by dynamical correlations, while in  $C^t$  also by statistical correlations.

part of the diagram also by statistical correlations. In this case, because of the Pauli principle, the reducible part of the diagram can reach the articulation point exclusively with dynamical correlations. We call  $C_d(a)$  the sum of the diagrams reaching the articulation point  $a$  with dynamical correlations only.

The evaluation of  $C_d(a)$  can be performed by extending the diagrams classification done in Sect. 2.1 to the case of a single external point. All the linked diagrams, both simple and composite ones, contribute to  $C_d(a)$ . As an example, the contribution of the  $(II)$  diagram of Fig. 13 is obtained by squaring the contribution of the  $(I)$  diagrams and dividing by two, in order to avoid double counting. The procedure used in Sect. 2.1 to calculate the contribution of the composite diagrams can be applied also in this case. If we call  $U_d(a)$  the sum of all the simple irreducible diagrams connected to the point  $a$  by dynamical correlations only, we can write:

$$C_d(a) = 1 + U_d(a) + \frac{1}{2!}U_d^2(a) + \frac{1}{3!}U_d^3(a) + \dots = \exp[U_d(a)] \quad (102)$$

It is understood that all the diagrams contained in  $U_d(a)$  are renormalized by the vertex corrections, therefore they must be irreducible in each internal point.

For the calculation of  $C^t(a)$  we have to consider also the diagrams linked to the articulation point  $a$  with statistical correlations. We call  $U_e^t(a)$  the sum of all these simple irreducible diagrams. Because of the Pauli principle, one can construct composite diagrams with  $U_e^t(a)$  combining it only with any number of  $U_d(a)$  that produces  $C_d(a)$ . By definition,  $C^t(a)$  is given by all the diagrams contributing to  $C_d(a)$ , i.e. all those reaching  $a$  with dynamical correlations, plus the diagrams constructed by associating those with  $U_e^t(a)$ :

$$C^t(a) = C_d(a) [\rho_0^t(a) + U_e^t(a)] = \rho^t(a), \quad (103)$$

where  $\rho_0^t(a)$  indicates the uncorrelated one-body density for nucleons with isospin  $t$ , and  $\rho^t(a)$  is the corresponding OBDF. In the absence of correlations,  $U_d$  and  $U_e^t$  are zero, therefore  $C^t$  is equal to the uncorrelated density, as is expected. The construction of the functions  $U_{d,e}(1)$  is done by integrating the composite diagrams over the coordinate 2. This procedure requires a careful attention to avoid the possible overcounting problems [43]. The explicit expressions of  $U_{d,e}(1)$  are given in Appendix B.

By introducing the vertex corrections idea, we recover the irreducibility of the cluster expansion. Obviously the evaluation of the nodal diagrams is more involved than in the case of infinite systems. However, the basic ideas used to calculate the nodal diagrams in the infinite system, are still valid in the present case, and the expressions of the  $N_{dd}(\mathbf{r}_1, \mathbf{r}_2)$ ,  $N_{de}^{t_2}(\mathbf{r}_1, \mathbf{r}_2)$ ,  $N_{ee}^{t_1 t_2}(\mathbf{r}_1, \mathbf{r}_2)$  diagrams, given in Appendix B, are a rather straightforward extension of those presented for the infinite systems. We have shown the dependence on isospin associated to the exchange. The only relevant differences are related to the cyclic-cyclic  $N_{cc}^{t_1}(\mathbf{r}_1, \mathbf{r}_2)$  diagrams and they are worthy of a short discussion.

In analogy to the infinite system case, the nodal  $N_{cc}^{t_1}(\mathbf{r}_1, \mathbf{r}_2)$  diagrams are generated by the folding products of  $X_{cc}^{t_1}(\mathbf{r}_1, \mathbf{r}_2)$  or of  $\rho_0^{t_1}(\mathbf{r}_1, \mathbf{r}_2)$ . In the finite system case, the presence of the vertex corrections generates the possibility of having nodal diagrams where there are two consecutive statistical correlations  $\rho_0^{t_1}(\mathbf{r}_i, \mathbf{r}_j)$ . We show in Fig. 14 an example of this situation. In the diagram A the point 3 is reached by a statistical correlation on the left hand side, and by a dynamical correlation on the right hand side. In the diagram B, the point 4 is reached on both sides only by statistical correlations. In infinite systems, i. e. in the absence of vertex corrections, because of the property (30) of the uncorrelated OBDM, the two diagrams give the

same contribution, except for a minus sign. For this reason, in order to avoid overcounting, we did not consider diagrams of the B type in the evaluation of the  $N_{cc}^{t_1}$  contribution to the TBDF. In finite systems each point is vertex corrected, therefore Eq. (30) cannot be applied to describe the integration over the point 4 in the B diagram, and, consequently, the contribution of the diagram B is different from that of the diagram A.



Figure 14: Two  $N_{cc}(\mathbf{r}_1, \mathbf{r}_2)$  diagrams. In infinite systems they give opposite contributions since the integration over the point 4 in the diagram B recovers the diagram A, except for a minus sign. In finite systems, because of the presence of vertex corrections in the 3 and 4 points, the two diagrams give different contributions.

We take care of this fact by separating the contribution of  $N_{cc}^{t_1}$  in four different terms:

$$\begin{aligned}
 N_{cc}^{t_1}(\mathbf{r}_1, \mathbf{r}_2) &= N_{cc}^{xx t_1}(\mathbf{r}_1, \mathbf{r}_2) + N_{cc}^{x \rho t_1}(\mathbf{r}_1, \mathbf{r}_2) \\
 &+ N_{cc}^{\rho x t_1}(\mathbf{r}_1, \mathbf{r}_2) + N_{cc}^{\rho \rho t_1}(\mathbf{r}_1, \mathbf{r}_2) .
 \end{aligned} \tag{104}$$

The superscripts  $x$  and  $\rho$  refer to the type of correlation reaching the external points. With the label  $\rho$  we indicate that the point is reached by a statistical correlation only, like the point 1 in Fig. 14, while with the label  $x$  we indicate that also dynamical correlations are present, as in the point 2 of the figure.

The full set of FHNC equations containing the vertex corrections, called Renormalized FHNC (RFHNC) equations, is given in Appendix B.

### 3.3 Treatment of the operator dependent correlations

In the discussion done so far for finite nuclei, we have considered scalar correlations only. As in the infinite system case, the use of the operator dependent correlations is treated in the SOC approximation. However, the treatment of these correlations presented in Sect. 2.3 cannot be straightforwardly extended to finite nuclear systems. First, the systems we want to describe are not saturated in isospin, and this changes the treatment of the isospin dependent terms. Second, the  $jj$  coupling of the single-particle wave functions modifies the calculation of the spin traces. In any case, we tackle the problem by using the strategy outlined in Sect. 2.3. We first reduce the product of operators to a sum of single operators, and then we calculate the appropriated traces. We find it convenient to treat separately the spin and isospin operators. For this reason, we use Eq. (51), to express the operator dependent correlation (48) as:

$$F_{ij} = \sum_{p=1}^6 f_p(r_{ij}) O_{ij}^p = \sum_{l=0}^1 (\boldsymbol{\tau}_i \cdot \boldsymbol{\tau}_j)^l \sum_{k=1}^3 f_{2k-1+l}(r_{ij}) P_{ij}^k . \tag{105}$$

As we have already pointed out in the case of infinite systems, we remember that, in addition to the product of operators coming from the dynamical correlations and from the interaction, we have also to deal with the spin and isospin exchange operator Eq. (58), coming from the statistical correlation. Each exchange loop formed by  $n$  statistical correlations  $\rho_0(x_1, x_2)$  carries  $n - 1$  spin-isospin exchange operators. By using the symbols defined in the above equations, we express the operators generated by a single exchange loop as:

$$\frac{1}{4} \sum_{p=1}^6 \Gamma^p O_{12}^p = \frac{1}{4} \sum_{l=0}^1 (\boldsymbol{\tau}_1 \cdot \boldsymbol{\tau}_2)^l \sum_{k=1}^3 \Delta^k P_{ij}^k, \quad (106)$$

where the values of  $\Gamma^p$  are those given in Tab. 9 of Appendix A, from which we see that  $\Delta^k = 1 - \delta_{k,3}$ .

### 3.3.1 Spin traces

We consider a closed loop of statistical correlations (89), involving only two-particles:

$$\begin{aligned} & \rho_0(x_i, x_j) \rho_0(x_j, x_i) = \\ & \sum_{s_1, s'_1, t_1} \rho_0^{s_1 s'_1 t_1}(\mathbf{r}_i, \mathbf{r}_j) \chi_{s_1}^+(i) \chi_{s'_1}(j) \chi_{t_1}^+(i) \chi_{t_1}(j) \times \\ & \sum_{s_2, s'_2, t_2} \rho_0^{s_2 s'_2 t_2}(\mathbf{r}_j, \mathbf{r}_i) \chi_{s_2}^+(j) \chi_{s'_2}(i) \chi_{t_2}^+(j) \chi_{t_2}(i) \\ & = \sum_{s_1, s'_1, t_1} \sum_{s_2, s'_2, t_2} \rho_0^{s_1 s'_1 t_1}(\mathbf{r}_i, \mathbf{r}_j) \rho_0^{s_2 s'_2 t_2}(\mathbf{r}_j, \mathbf{r}_i) \times \\ & \chi_{s_1}^+(j) \chi_{s_2}^+(i) \chi_{t_1}^+(j) \chi_{t_2}^+(i) \Pi^{\sigma, \tau}(i, j) \chi_{s'_1}(j) \chi_{s'_2}(i) \chi_{t_1}(j) \chi_{t_2}(i), \end{aligned}$$

where we have used the operator (58), to exchange the spins and isospin of the bra. Fixing the isospins, which will be treated appart, the kernel of the above equation is:

$$\begin{aligned} & \sum_{s, s'} \rho_0^{s, s', t}(\mathbf{r}_i, \mathbf{r}_j) \chi_s^+(j) \chi_{s'}(j) \\ & = \rho_0^t(\mathbf{r}_i, \mathbf{r}_j) \sum_s \chi_s^+(j) \chi_s(j) \\ & + \rho_{0j}^t(\mathbf{r}_i, \mathbf{r}_j) \sum_s (-1)^{s-1/2} \chi_s^+(j) \chi_{-s}(j), \end{aligned} \quad (107)$$

where we used the uncorrelated OBDMs for parallel and antiparallel spins defined in Eqs. (91,92). The treatment of the parallel spin term is similar to that of the infinite system case. The antiparallel term, which appears only in the  $jj$  coupling scheme, should be treated differently.

Following the scheme presented in Sect. 2.3 we evaluate the spin traces by considering three cases: the product of operators acting on the same nucleonic pair, the product of operator forming a ring (SOR) and the product of more than one operator acting on an internal point. Consistently with the definitions (51) of the operators, in the following expressions the upper indexes  $i, j, k$  can assume the values 1,2 and 3, only.

### 3.3.1.a Parallel spin traces

In analogy to the infinite system we find that the trace of the product of two operators  $P^i$ , acting on the same pair of nucleons is:

$$C(P_{12}^{k_1} P_{12}^{k_2}) = B^{2k_1-1} \delta_{k_1 k_2} = A^{k_1} \delta_{k_1 k_2} , \quad (108)$$

where the values of  $B^p$  are given in Tab. 10. From this table we see that  $A^k = k(k+1)/2$ .

We find that the product of two operators can be reduced to the following sum of single operators:

$$P_{12}^i P_{12}^j = \sum_{k=1}^3 I^{ijk} P_{12}^k , \quad (109)$$

where the matrix  $I^{ijk}$  is constructed by selecting only the values of the odd indexes of the matrix  $K^{pqr}$  given in Tab. 11 of Appendix A:

$$I^{ij1} = \begin{pmatrix} 1 & 0 & 0 \\ 0 & 3 & 0 \\ 0 & 0 & 6 \end{pmatrix} , \quad I^{ij2} = \begin{pmatrix} 0 & 1 & 0 \\ 1 & -2 & 0 \\ 0 & 0 & 2 \end{pmatrix} , \quad I^{ij3} = \begin{pmatrix} 0 & 0 & 1 \\ 0 & 0 & 1 \\ 1 & 1 & -2 \end{pmatrix} . \quad (110)$$

In analogy to Sec. 2.3.1 we can use recursively Eqs. (108) and (109). For example, we find for the trace of the product of three operators the expression:

$$C(P_{12}^i P_{12}^j P_{12}^k) = \sum_{k_1=1}^3 I^{ijk_1} C(P_{12}^{k_1} P_{12}^k) = I^{ijk} A^k . \quad (111)$$

The evaluation of the product of operators forming a closed loop (SOR) follows the steps outlined for the infinite system case. In analogy to Eq. (64), we find that also in the present case this product of operators can be written as a sum of single operators as:

$$\sum_{\sigma_2} \int d\phi_2 P_{12}^i P_{23}^j = \sum_{k=1}^3 \int d\phi_2 \zeta_{123}^{ijk} P_{13}^k , \quad (112)$$

where the values  $\zeta_{123}^{ijk}$  factors are given in Eqs. (65). By using the above equation we find that the trace of multipole operator diagrams, such as those of Fig. 11, can be calculated as:

$$\int d\phi_1 C(P_{mn}^i P_{m1}^j P_{mn}^k P_{n1}^{k'}) = \sum_{k_1=1}^3 J^{ikk_1} \int d\phi_1 \zeta_{m1n}^{jk'k_1} . \quad (113)$$

The matrix  $J^{ijl}$  is built by using the odd index values of the matrix  $L$  given in Tab. 12 of Appendix A:

$$J^{ij1} = \begin{pmatrix} 1 & 0 & 0 \\ 0 & 3 & 0 \\ 0 & 0 & 6 \end{pmatrix} , \quad J^{ij2} = \begin{pmatrix} 0 & 3 & 0 \\ 3 & 6 & 0 \\ 0 & 0 & -6 \end{pmatrix} , \quad J^{ij3} = \begin{pmatrix} 0 & 0 & 6 \\ 0 & 0 & -6 \\ 6 & -6 & 12 \end{pmatrix} . \quad (114)$$

### 3.3.1.b Antiparallel statistical function.

Since the Eqs. (109) and (112) involve only operators, they do not depend upon the spin

structure of the wave function, therefore they are valid also in the antiparallel spin case. The change with respect to the parallel case, is in the basic trace value (108) which is no longer valid. For the antiparallel statistical function of Eq. (107) we write the trace of a single operator as:

$$C_j(P_{12}^k) = \frac{1}{4} \sum_{s_1, s_2} (-1)^{s_1+s_2} \chi_{s_1}^+(1) \chi_{s_2}^+(2) P_{12}^k \chi_{-s_1}(1) \chi_{-s_2}(2) , \quad (115)$$

and we find the values

$$C_j(P_{12}^k) = \delta_{k,2} . \quad (116)$$

We see that the contribution of the scalar operator is zero and that of the spin operator is one, just the opposite results of those of the parallel case. The result (116) for the tensor operator has been obtained under the hypothesis of a spherical symmetry of the system.

### 3.3.2 Isospin expectation values

In a system not saturated in isospin, we should not sum on the isospin third components, since the various diagrams, nodal, elementary, vertex corrections, etc., depend on these quantum numbers. This means that the values of these diagrams are different when they are calculated for protons, neutrons, or mixed, clusters. We do not calculate isospin traces, but the expectation values of products of isospin operators. In order to obtain these expectation values we use the properties of the Pauli matrices which allows us to express the product of  $n$  isospin operator pairs acting on the same pair of nucleons as:

$$(\boldsymbol{\tau}_i \cdot \boldsymbol{\tau}_j)^n = a_n + (1 - a_n) \boldsymbol{\tau}_i \cdot \boldsymbol{\tau}_j , \quad (117)$$

with:

$$a_{n+1} = 3(1 - a_n) , \quad \text{and} \quad a_0 = 1 . \quad (118)$$

The recursive relation (117) expresses the product of isospin operator pairs as a sum of a scalar term plus a term depending from a single isospin operator pair. The expectation value of the operator sequence (117) is:

$$\chi_n^{t_1 t_2} = \chi_{t_1}^+(1) \chi_{t_2}^+(2) (\boldsymbol{\tau}_1 \cdot \boldsymbol{\tau}_2)^n \chi_{t_1}(1) \chi_{t_2}(2) . \quad (119)$$

By using Eqs. (117) and (118) we obtain:

$$\chi_0^{t_1 t_2} = 1 , \quad \text{and} \quad \chi_1^{t_1 t_2} = 2\delta_{t_1 t_2} - 1 , \quad (120)$$

and by applying the recursive relations, we have the more general result:

$$\chi_n^{t_1 t_2} = 2a_n - 1 + 2(1 - a_n) \delta_{t_1 t_2} . \quad (121)$$

This result is the contribution to the cluster expansion of terms like that represented by diagram A of Fig. 15. In this figure we show the various types of diagrams which appear in the calculation of the energy expectation value, and more precisely in the calculation of the expectation value of the two-body interaction:

$$\frac{\langle \Psi | V_2 | \Psi \rangle}{\langle \Psi | \Psi \rangle} = \frac{\langle \Phi | \mathcal{F}^\dagger V_2 \mathcal{F} | \Phi \rangle}{\langle \Psi | \Psi \rangle} \quad (122)$$

In the figure we indicate with the black area joining the external points 1 and 2, the product of the three operators  $O_{12}^p O_{12}^q O_{12}^r$ , where  $O^p$  and  $O^r$  come from the dynamical correlations  $\mathcal{F}$ , while  $O^q$ , always in the middle, comes from the two-body interaction  $V_2$ . All the isospin expectation values necessary for the calculation of the energy expectation value are taken into account by Eq. (121).

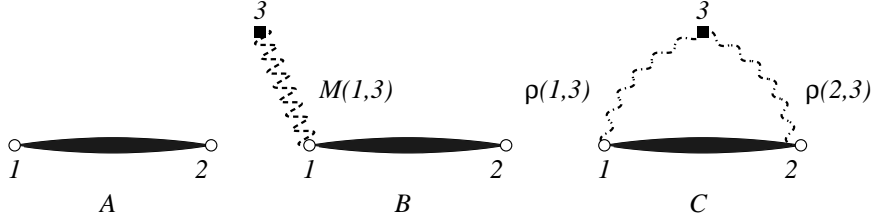


Figure 15: Example of diagrams contributing to the energy expectation value. The black areas indicate the product of three operators  $O_{12}^p O_{12}^q O_{12}^r$ . The two operators  $O^p$ ,  $O^r$  come from the dynamical correlations, while  $O^q$  comes from the interaction. The dashed wiggly line of the diagram B indicates an operator dependent vertex correction  $M$ . This implies the presence of a single operator coming from the correlation, because of the SOC approximation, eventually associated with another operator coming from the spin-isospin exchange term. The wiggly dashed and dotted lines of diagram C indicate the correlated TBDF containing operators of the correlations and those related to the spin-isospin exchange terms.

The case of the A diagram of Fig. 15 is an example of our procedure. We find general recursive relationships connecting the expectation values of isospin operators, and use them to obtain expectation values. The case of the A diagram is the easiest one, but we apply an analogous procedure to calculate the cases of the vertex correction, represented by the B diagram, and the case of the nodal diagram, represented by the C diagram of the figure. The calculation of the isospin expectation values for these two, more involved cases, is presented in detail in Appendix C.

The rules that we have presented in this section to calculate the spin traces and the isospin matrix elements have been used to evaluate the OBDF and the TBDF in the SOC approximation. The expressions of the RFHNC equations which allow us to calculate the cluster expansion of the TBDF in the SOC approximation are given in Appendix B by equations (214-245). The cluster expansion of the TBDF allows us to calculate the energy expectation value. The details of this calculation are given in next section.

## 4 The evaluation of the ground state energy

The discussion of the previous sections was devoted to the calculation of the scalar TBDF defined by Eq. (101) when  $q = 1$ . The TBDF contains all the many-body effects independent from the two-body interaction, whose expectation value can be obtained as indicated by Eq. (11) for the infinite system. For the calculation of the TBDF we developed the cluster expansion techniques and we built a set of hypernetted chain equations which allows us to evaluate in a closed form the contribution of all those diagrams we have called nodal and composite. In this section, we apply these techniques to the calculation of the energy expectation value (9) with a hamiltonian of the form:

$$H = - \sum_{i=1}^A \frac{\hbar^2}{2m} \nabla_i^2 + \sum_{j>i=1}^A V_{ij} + \sum_{k>j>i=1}^A V_{ijk} . \quad (123)$$

The two-body interaction is expressed as:

$$V_{ij} = \sum_{p=1}^8 v^p(r_{ij}) O_{ij}^p , \quad (124)$$

where  $v^p(r_{ij})$  are scalar functions of the distance  $r_{ij}$  of the two interacting nucleons, and the  $p = 1, \dots, 6$  operators are those defined in (49). We consider in addition the spin-orbit operators

$$O_{ij}^{p=7,8} = (\mathbf{L} \cdot \mathbf{S})_{ij}, (\mathbf{L} \cdot \mathbf{S})_{ij} (\boldsymbol{\tau}_i \cdot \boldsymbol{\tau}_j) , \quad (125)$$

where  $\mathbf{L}$  is the relative angular momentum of the two interacting nucleons, and  $\mathbf{S}$  is the sum of their spins. We give in Sect. 4.3 the explicit expression of the three-body interaction  $V_{ijk}$ .

The calculation of the energy expectation values is done by using the trial wave function:

$$\Psi(1, \dots, A) = \mathcal{F}(1, \dots, A) \Phi(1, \dots, A) = \mathcal{S} \left( \prod_{i<j} F_{ij} \right) \Phi(1, \dots, A) , \quad (126)$$

where the two-body correlation function consider only the first six operators as indicated by Eqs. (48) and (105). The uncorrelated state,  $\Phi$ , is a Slater determinant composed by all the single particle wave functions (88) lying below Fermi surface.

In the following, we treat together the kinetic energy and the two-body interaction up to the tensor channels. All the other parts of the hamiltonian, two-body spin orbit interactions, three-body and Coulomb interactions, are treated separately. In the following expressions the  $t$  indexes run on protons and neutrons, the  $p, q, r, s$  labels may assume values from 1 up to 6, and are used to generically identify the different operator channels as in Eq. (49). When we separate the spin and isospin dependence as in Eq. (51) we shall use the indexes  $l=0,1$ , and  $k = 1, 2, 3$ .

### 4.1 Kinetic energy and $V_{12}^6$ part

We evaluate the expectation value of the kinetic energy, by using the Jackson-Feenberg separation scheme [44, 45] as suggested in Ref. [39]. We obtain:

$$\langle T \rangle \equiv T_\phi + T_F - T_{c.m.} , \quad (127)$$



where we have defined

$$T_\phi \equiv -\frac{\hbar^2}{4m} \left( \langle \Phi^* \mathcal{F}^2 \sum_{i=1}^A \nabla_i^2 \Phi \rangle - \langle \sum_{i=1}^A (\nabla_i \Phi^*) \cdot (\mathcal{F}^2 \nabla_i \Phi) \rangle \right), \quad (128)$$

$$T_F \equiv -\frac{\hbar^2}{4m} \langle \Phi^* \left[ \mathcal{F} \left( \sum_{i=1}^A \nabla_i^2 \mathcal{F} \right) - \sum_{i=1}^A (\nabla_i \mathcal{F})^2 \right] \Phi \rangle, \quad (129)$$

and for the contribution of the center of mass term we have:

$$T_{c.m.} = -\frac{\hbar^2}{2mA} \langle \Psi^* \left( \sum_{i=1}^A \nabla_i \right)^2 \Psi \rangle. \quad (130)$$

In the above equations we have used the symbol  $\langle \rangle$ , which has been defined as [27]:

$$\langle X \rangle = \frac{\int dx_1 \dots dx_A X(x_1, \dots, x_A)}{\langle \Psi | \Psi \rangle}. \quad (131)$$

Before attacking the problem of calculating  $\langle T \rangle$  we define some useful quantities:

$$\rho_{T1}^{t1}(\mathbf{r}_1) = \sum_{nljm} \left[ \phi_{nljm}^{t1*}(\mathbf{r}_1) \nabla_1^2 \phi_{nljm}^{t1}(\mathbf{r}_1) - \nabla_1 \phi_{nljm}^{t1*}(\mathbf{r}_1) \cdot \nabla_1 \phi_{nljm}^{t1}(\mathbf{r}_1) \right], \quad (132)$$

$$\rho_{T2}^{t1t2}(\mathbf{r}_1, \mathbf{r}_2) = \rho_0^{t1}(\mathbf{r}_1, \mathbf{r}_2) \nabla_1^2 \rho_0^{t2}(\mathbf{r}_1, \mathbf{r}_2) - \nabla_1 \rho_0^{t1}(\mathbf{r}_1, \mathbf{r}_2) \cdot \nabla_1 \rho_0^{t2}(\mathbf{r}_1, \mathbf{r}_2), \quad (133)$$

$$\rho_{T3}^{t1}(\mathbf{r}_1, \mathbf{r}_2) = 2 \nabla_1^2 \rho_0^{t1}(\mathbf{r}_1, \mathbf{r}_2), \quad (134)$$

$$\begin{aligned} \rho_{T4}^{t1}(\mathbf{r}_1, \mathbf{r}_2) &= \nabla_1 \rho_0^{t1}(\mathbf{r}_1, \mathbf{r}_2) \cdot \nabla_2 \rho_0^{t1}(\mathbf{r}_1, \mathbf{r}_2) \\ &- \rho_0^{t1}(\mathbf{r}_1, \mathbf{r}_2) \nabla_1 \cdot \nabla_2 \rho_0^{t1}(\mathbf{r}_1, \mathbf{r}_2) \\ &+ \nabla_1 \rho_{0j}^{t1}(\mathbf{r}_1, \mathbf{r}_2) \cdot \nabla_2 \rho_{0j}^{t1}(\mathbf{r}_1, \mathbf{r}_2) \\ &- \rho_{0j}^{t1}(\mathbf{r}_1, \mathbf{r}_2) \nabla_1 \cdot \nabla_2 \rho_{0j}^{t1}(\mathbf{r}_1, \mathbf{r}_2). \end{aligned} \quad (135)$$

The above expressions involve neither the interaction nor the correlations, therefore they depend only on the uncorrelated many-body state,  $\Phi$ . The expressions of these quantities in terms of single particle wave functions (88) are given in Appendix D. In terms of these quantities the center of mass contribution can be expressed as:

$$T_{cm} = -\frac{\hbar^2}{4mA} \sum_{t1} \left( \int d\mathbf{r}_1 \rho_{T1}^{t1}(\mathbf{r}_1) - \int d\mathbf{r}_1 d\mathbf{r}_2 \rho_{T4}^{t1}(\mathbf{r}_1, \mathbf{r}_2) \right). \quad (136)$$

The operator structure of  $T_F$  can be easily associated to that required by the calculation of the interaction expectation value. For this reason, we calculate together  $T_F$  and  $V_2 \equiv \sum_{p=1,6} \langle v^p O^p \rangle$ . The contribution of  $T_F + V_2 \equiv W$  is also called *interaction energy* [30].

The structure of the SOC approximation generate various cases that we separate in four parts, i.e. :

$$W = W_0 + W_s + W_c + W_{cs}. \quad (137)$$

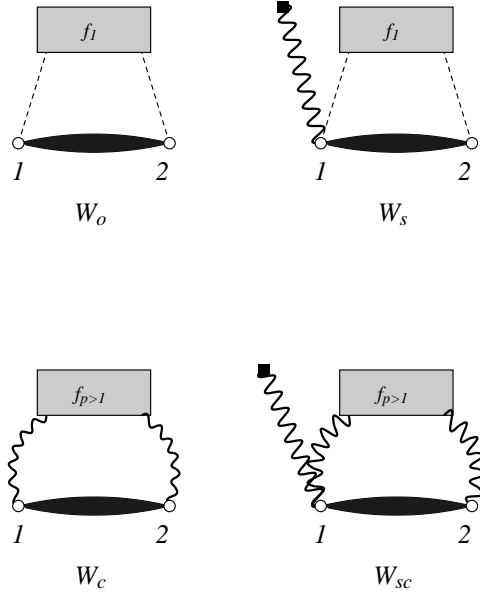


Figure 16: Graphical representation of the  $W$  terms of Eq. (137).

We sketch in Fig. 16 the characteristics of the four terms. The black bands between the interacting points 1 and 2, indicate  $O^p O^q O^r$ , operators  $O^p$  and  $O^r$  coming from the correlation and  $O^q$  from the interaction.

In the term  $W_0$  we calculate the sum of all the diagrams connected to the interaction points by scalar correlation functions only. The interaction points are vertex corrected. If the product  $O^p O^q O^r$  produces a scalar term, the vertex correction contains all the operators types. If, instead, the product  $O^p O^q O^r$  generates operator terms, the vertex correction contains scalar terms only. The explicit expression of  $W_0$  is given in Appendix E.

With  $W_s$  we consider the sum of operator rings touching a single interaction point. These diagrams may include also the presence of scalar operator chains such as those considered in  $W_0$ . The  $W_c$  term is the sum of all the diagrams forming a SOC between the two interacting points. We present in Appendix E the derivation of the explicit expressions of the  $W_s$  and  $W_c$  diagrams.

The contribution of the  $W_{cs}$  term is given by the sum of all the diagrams with operator rings reaching a single interaction point, and, in addition, the SOC between the two interacting points. The  $W_{cs}$  term is obtained by the combination of the topologies of the  $W_s$  and  $W_c$  terms. Because of the large number of operators present in  $W_{cs}$ , we do not calculate explicitly its contribution, but we rather estimate it by using the prescription proposed in [30]:

$$W_{cs} \sim \frac{W_s W_c}{W_0} . \quad (138)$$

Nuclear matter calculations [21] where, more refined computational schemes are used, indicate that the largest contribution of  $W_{cs}$  is two orders of magnitude smaller than those of the other  $W$  terms. We have compared nuclear matter estimations of the values of  $W_{cs}$  obtained with our

prescription with those calculated more accurately in [21], and we have found agreement up to the second significant figure.

In the evaluation of the *interaction energy*  $W$ , the  $T_F$  part of the kinetic energy is included. We describe now how we calculate the contribution of the first term of the kinetic energy (127), the  $T_\phi$  term, where the  $\nabla_1$  operator acts on the mean-field wave functions. In Ref. [27] we found it convenient to separate the contribution of  $T_\phi$  in three parts:

$$T_\phi = T_\phi^{(1)} + T_\phi^{(2)} + T_\phi^{(3)} . \quad (139)$$

where each part is characterized by the type of statistical correlations reaching the interacting point 1. In Fig. 17 we show some diagrams which identify each term. We have denoted the interacting point 1, by an open circle. The nomenclature *interacting point* is due to the fact that this is the point on which the differential operator is acting. In the  $T_\phi^{(1)}$  type of diagrams, the interacting point is connected to the other points by means of dynamical correlations only. In  $T_\phi^{(2)}$ , the statistical correlations reaching the point 1, form a closed loop involving only another single point. In the diagrams of Fig. 17 we call 2 this other point. Finally, in the  $T_\phi^{(3)}$  type of diagrams the statistical correlations reaching the point 1, form close loops which involve at least two other internal points.

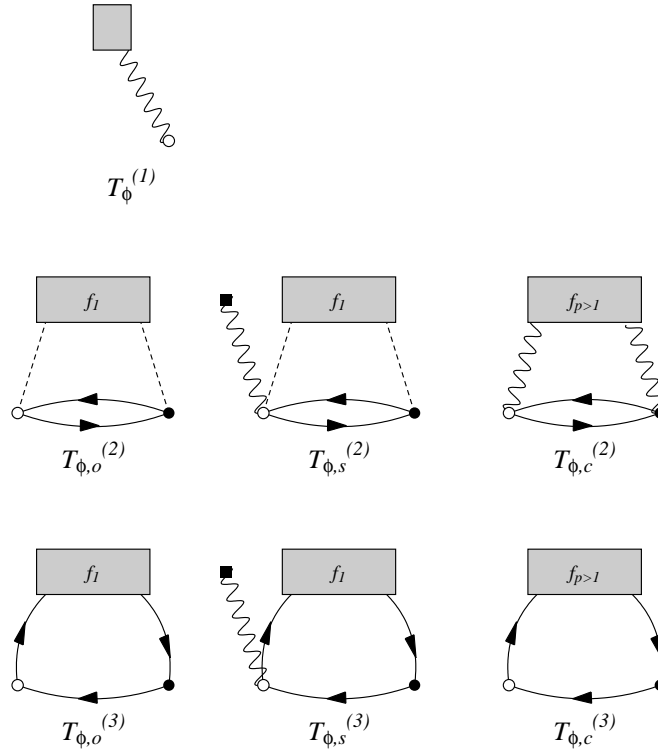


Figure 17: Graphical representation of the  $T_\phi$  terms of Eq. (128).

The expression of the  $T_\phi^{(1)}$  is the expectation value of a one-body operator dressed by the vertex correction, and is given in Appendix E.

The calculation of the other two terms is more involved, since we have to calculate the expectation value of a two-body operator. Nevertheless, the structure of these operators is the same as the ones in the exchange terms of  $W$ . So we further classify the  $T_\phi^{(2)}$  and  $T_\phi^{(3)}$  terms in the same way that we did for the  $W$  terms.

We consider  $T_{\phi,0}^{(2,3)}$  terms where the points 1 and 2 are connected to the other nucleons by a scalar operator chain. As indicated in Fig. 17 this means that these points are reached by scalar correlations only, whose contribution can be calculated in terms of RFHNC diagrams. This is indicated by the  $f_1$  label in the gray box. A second class of diagrams is that we labeled as  $T_{\phi,s}^{(2,3)}$ . In this case, we consider that, in addition to the scalar chains of  $T_{\phi,0}^{(2,3)}$ , the interaction point is reached by a ring of  $p > 1$  operator dependent dynamical correlations. Finally, with  $T_{\phi,c}^{(2,3)}$  we indicate the sum of the diagrams where the points 1 and 2 form a SOC. In the figure, this is indicated by the wiggly lines and by the  $f_{p>1}$  label in the gray box. As in the case of  $W$  terms, we may have also diagrams which are the topological combination of  $T_{\phi,s}^{(2,3)}$  and  $T_{\phi,c}^{(2,3)}$ . We have estimated that their contribution is negligible.

The separation of the  $T_\phi$  contribution in three parts, was proposed, and used, in [27], where the finite nucleon systems treated were saturated in both spin and isospin, and only scalar correlations were considered. The presence of operator dependent correlations, requires a further classification of the various terms. Clearly,  $T_\phi$  depends on the isospin third components of the particles 1 and 2. Furthermore, since we work in a  $jj$  coupling scheme, we have to distinguish in the calculation of the  $T_\phi^{(2,3)}$  terms, the cases when the statistical correlations have parallel and antiparallel spin components. The complete list of expressions of the various terms composing  $T_\phi$  is given in Appendix E.

## 4.2 Spin-orbit and Coulomb terms

The contribution of the Coulomb interaction is:

$$\langle v_{Coul} \rangle = \langle \Psi^* \sum_{j>i=1}^A P_i^{1/2} P_j^{1/2} \frac{e^2}{r_{ij}} \Psi \rangle, \quad (140)$$

where the  $P_i^{1/2}$  projection operator selects the protons. The Coulomb interaction is added to the scalar part of the  $V_{ij}$  interaction when two protons interact. This means that its contribution is consistently calculated following the methodology described in Sect. 4.1 for all the proton-proton  $W$  terms.

We calculate the contribution of the spin-orbit terms of the potential, i.e. the  $p = 7, 8$  channels in Eq. (124), by considering only diagrams containing scalar chains between the interacting points. In other words, for the spin-orbit interaction, we calculate only the  $W_0$  term of Eq. (137). The explicit expression of the spin-orbit contribution is given by Eq. (310) in Appendix E.

## 4.3 The three-body potential

In our calculation we use three-nucleon potentials of Urbana type [46]. The explicit expression of this potential is:

$$V_{ijk} = v_{ijk}^{2\pi} + v_{ijk}^R. \quad (141)$$

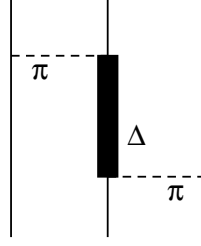


Figure 18: Fujita-Miyazawa term of the three-body force.

The  $v_{ijk}^{2\pi}$  term, describes a three-nucleon force produced when one of the interacting nucleons is transformed into a  $\Delta$  by a first interaction with another nucleon, and it turns back to a nucleonic state after interacting with a third nucleon (see fig. 18). This term called Fujita-Miyazawa [47] describes the long range part of the three-body interaction and produces an attractive contribution. The second term of Eq. (141),  $v_{ijk}^R$ , has a shorter range and a phenomenological origin. The explicit expressions of the two terms of Eq. (141) are:

$$v_{123}^{2\pi} = A_{2\pi} \sum_{cycl} \left( \{X_{31}, X_{32}\} \{ \boldsymbol{\tau}_3 \cdot \boldsymbol{\tau}_1, \boldsymbol{\tau}_3 \cdot \boldsymbol{\tau}_2 \} + \frac{1}{4} [X_{31}, X_{32}] [ \boldsymbol{\tau}_3 \cdot \boldsymbol{\tau}_1, \boldsymbol{\tau}_3 \cdot \boldsymbol{\tau}_2 ] \right), \quad (142)$$

$$v_{123}^R = U_0 \sum_{cycl} T_\pi^2(r_{31}) T_\pi^2(r_{32}). \quad (143)$$

where the sums run on all the possible cyclic combinations of the 1,2 and 3 indexes. In the above equations we have used the terms  $T$  and  $X$  defined by:

$$T_\pi(r) = \frac{e^{-\mu r}}{\mu r} \left[ 1 + \frac{3}{\mu r} + \frac{3}{(\mu r)^2} \right] (1 - e^{-cr^2})^2, \quad (144)$$

$$X_{ij} = Y_\pi(r_{ij}) \boldsymbol{\sigma}_i \cdot \boldsymbol{\sigma}_j + T_\pi(r_{ij}) S_{ij} = \sum_{k=2}^3 X^k(r_{ij}) P_{ij}^k, \quad (145)$$

where:

$$Y_\pi(r) = \frac{e^{-\mu r}}{\mu r} (1 - e^{-cr^2}), \quad (146)$$

where, as usual,  $S_{ij}$  indicates the tensor operator (50), and the symbols  $\{, \}$  and  $[, ]$  indicate the anticommutator and commutator operators, respectively. The values of the constants of the  $v_{123}^{2\pi}$  term are:  $\mu = 0.7 fm^{-1}$ , and  $c = 2 fm^{-2}$ . The parameters  $A_{2\pi}$ , and  $U_0$  of the  $v_{123}^R$  term are fixed to reproduce the  $^3H$  binding energy [46].

In analogy to the calculations in nuclear and neutron matter [21, 46, 24, 40, 25], we evaluate the contribution of the three-body interaction by considering only the sum of the five diagrams presented in Fig. 19. In Ref. [46] it was shown that the diagrams (2.1), (2.2) and (2.3), provide the relevant contribution to  $\langle v_{123}^{2\pi} \rangle$ . The other two diagrams are those important for  $\langle v_{123}^R \rangle$ .

In the diagram (2.1) the pairs of nucleon connected by operators  $X_{ij}$  (pairs 31 and 32) are dressed by scalar correlations, whereas the remaining pair (12) is also dressed by all the other

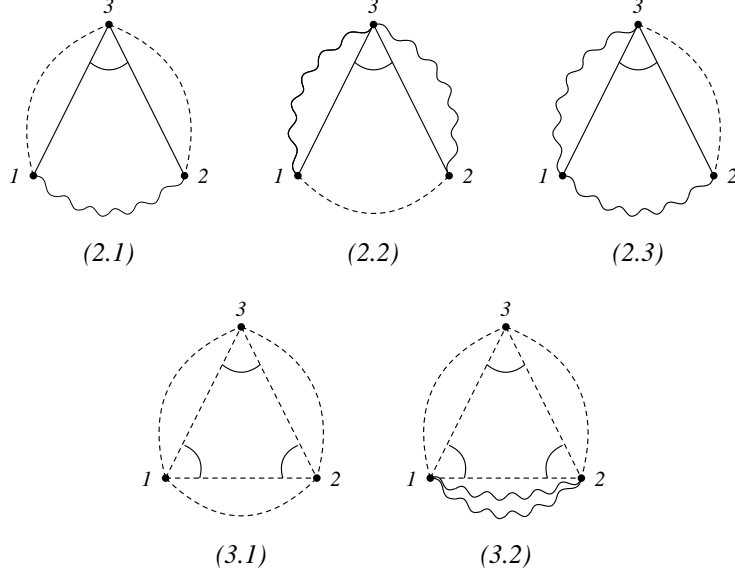


Figure 19: Cluster diagrams considered for the three-body force expectation value. The 2.1, 2.2, 2.3 diagrams are related to the  $\langle v_{ijk}^{2\pi} \rangle$  part of the force, and the 3.1 and 3.2 diagrams are related to  $\langle v_{ijk}^R \rangle$ . The points denote the particle coordinates. The dashed, wavy, and double-wavy lines represent generalized scalar, operator and single-operator ring correlation bonds, respectively.

operator dependent correlations  $p > 1$ , in the SOC approximation. In the (2.2) diagram, the pairs 31 and 32 are linked by operator dependent correlations in the SOC approximation, while the pair 12 is dressed by the scalar correlation. In the (2.3) diagram there is a cyclic permutation of the operator dependent correlations.

The  $\langle v_{123}^R \rangle$  term is calculated by evaluating the (3.1) and (3.2) diagrams. We calculate the case where all the pairs are dressed by scalar correlations at all orders, diagram (3.1) and the case when there is in addition a SOC correction for a single pair of nucleons, diagram (3.2).

The detailed derivation of the expressions of the three-body potential is given in Appendix E.

## 5 Specific applications

We have applied the formalism presented in the previous sections to the description of the  $^{12}\text{C}$ ,  $^{16}\text{O}$ ,  $^{40}\text{Ca}$ ,  $^{48}\text{Ca}$  and  $^{208}\text{Pb}$  nuclei. The only inputs required by our calculations are the two- and three-body nuclear interactions. In Sect. 5.1, we present those chosen for our studies. The single particle wave functions, and the correlation functions, fixed by the minimization procedure (1), are presented in Sects. 5.2 and 5.3, respectively. The theoretical and computational reliability of our calculations has been tested by verifying the exhaustion of some sum rules. This discussion is developed in Sect. 5.4. After that, we discuss in Sect. 5.5 the results regarding the most important observable of our calculations: the binding energy. We compare results obtained by using two different interactions. We continue our discussion by presenting a set of quantities which we have chosen to investigate the effects, and the relevance, of the short-range correlations. These quantities are: matter and charge density distributions, Sect. 5.6, momentum distributions, Sect. 5.7, natural orbits, Sect. 5.8, two-body density distributions, Sect. 5.9, and, finally, quasi-hole wave functions and spectroscopic factors, Sect. 5.10.

### 5.1 The nuclear interaction

The definition of the hamiltonian (123) requires the definition of both two- and three-body forces. We use two-body forces constructed to reproduce the data of the phase-shifts analysis of the large body of nucleon-nucleon scattering [3, 48].

We have used nucleon-nucleon interactions of the Argonne-Urbana family. These interactions are local and non-relativistic, and are expressed as a sum of operator dependent terms as indicated in Eq. (124). The most recent interaction of this type, fitting the phase-shifts of Refs. [3, 48], is the Argonne  $v_{18}$  interaction (AV18) [5], containing 18 operator terms, some of them breaking the charge symmetry.

In our calculations we have considered interactions containing up to eight operators channels, see Eqs. (49) and (125). For this reason, we used a truncated version of the AV18 potential, called Argonne  $v'_8$  (AV8'), and introduced in Ref. [7] because its simpler parameterization allowed a simplification of the numerically involved quantum Monte Carlo calculations. This interaction is not a simple truncation of the full AV18 interaction, but its parameters have been slightly modified to simulate the effects of the missing channels. The AV8' interaction reproduces the results of the full interaction for the  $S$  and  $P$  scattering waves and also the  $^3D_1$  wave. The details of the construction of the AV8' interaction are given in Ref. [7].

The major part of our calculations have been done with the AV8' interaction. However, in order to test the sensitivity of our results to the nuclear interaction, we have also used the Urbana  $v_{14}$  interaction, fixed in Ref. [49], to reproduce the set of phase shifts data available at the beginning of the '80s. In reality we have used only the first eight channels of the interaction, without any readjustment of the parameters values. For this reason, we shall refer to this interaction as UV14, understanding that we used the operator channels only up to the spin-orbit ones.

The two-nucleon interactions are implemented with the three-nucleon interactions fixed to reproduce the  $^3\text{H}$  binding energy. This means that associated to each two-nucleon potential there is a three-body force. Even though more elaborated versions of the three-nucleon forces have been recently proposed [50], in our calculations, we use the original expression [46], as

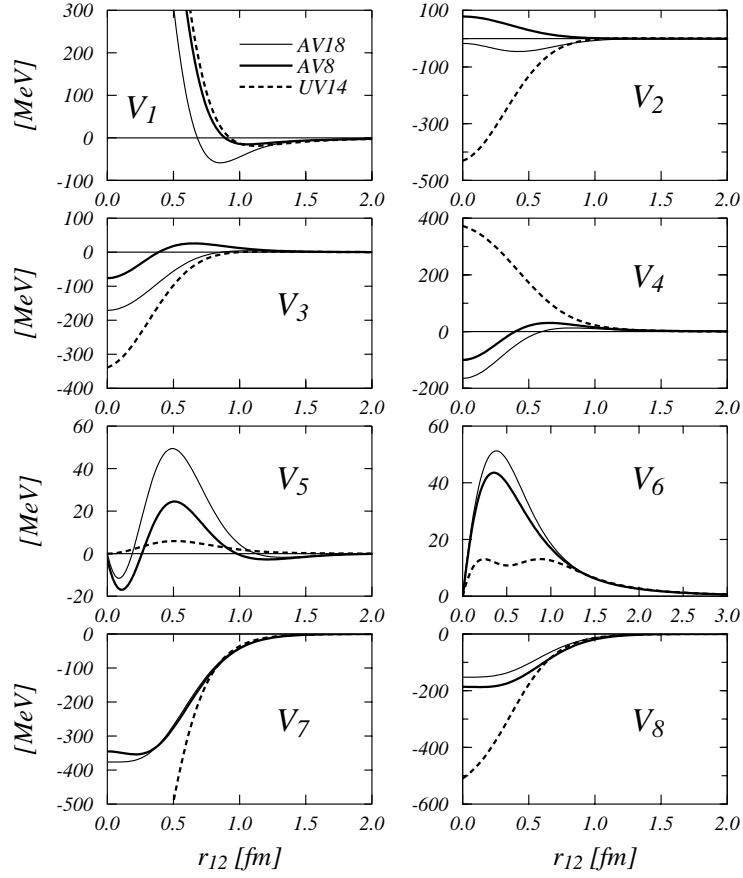


Figure 20: The AV8' and UV14 nucleon-nucleon interactions as a function of the relative distance, in the channels used in our calculations. The continuous thin line, show the behavior of the Argonne  $v_{18}$  potential.



presented in Sect. 4.3.

We use the Urbana UIX three-nucleon interaction [7] together with the AV8' potential, and the Urbana UVII interaction [51] together with the UV14 potential. The values of the parameters of Eqs. (142,...,145), fixing these two forces are given in Tab. 1.

	UVII	UIX
$A_{2\pi}$	-0.03330	-0.02930
$U_0$	0.003700	0.004800

Table 1: Parameters used in Eqs. (142,..., 145) to fix the three-body UVII and UIX interactions. In both cases  $\mu = 0.7 fm^{-1}$  and  $c = 2 fm^{-2}$ .

## 5.2 The single particle wave functions

	$^{12}C$	$^{16}O$	$^{40}Ca$	$^{48}Ca$	$^{208}Pb$
$V_0^p$	-62.00	-52.50	-57.5	-59.50	-60.40
$V_{ls}^p$	-3.20	-7.00	-11.11	-8.55	-6.75
$a_0^p$	0.57	0.53	0.53	0.53	0.79
$a_{ls}^p$	0.57	0.53	0.53	0.53	0.79
$R_0^p$	2.86	3.20	4.10	4.36	7.46
$R_{ls}^p$	2.86	3.20	4.10	4.36	7.46
$R_{Coul}$	2.86	3.20	4.10	4.36	7.46
$V_0^n$	-62.00	-52.50	-55.00	-50.00	-44.32
$V_{ls}^n$	-3.15	-6.54	-8.50	-7.74	-6.08
$a_0^n$	0.57	0.53	0.53	0.53	0.66
$a_{ls}^n$	0.57	0.53	0.53	0.53	0.66
$R_0^n$	2.86	3.20	4.10	4.36	7.46
$R_{ls}^n$	2.86	3.20	4.10	4.36	7.46

Table 2: The values of the parameters of the Woods-Saxon potential well, Eqs. (86) and (87). The superscripts  $p$  and  $n$  indicate protons and neutrons respectively. The values of  $V_0$  and  $V_{ls}$  are expressed in MeV, those of all the other parameters in fm.

In our calculations, the search of the minimum is done by making variations on the correlation function and on the mean-field potential generating the set of single particle states. We have already said in Sect. 3.1 that we used a mean-field basis generated by two Woods-Saxon wells, one for protons and another one for neutrons, both containing spin-orbit terms. The analytical expressions of the Woods-Saxon wells, Eqs. (86) and (87), involve thirteen parameters. Variational calculations done by changing all these parameters would be extremely heavy, from the computational point of view. In reality, we found [31], that the energy minimum is more sensitive to the correlation function, than to the single particle basis. To be more precise, we

found that when the correlation functions provides an energy minimum, changes of the potential do not produce large differences of this value. In Ref. [31] it has been shown that, in  $^{16}\text{O}$ , variations of 47% of the central well changed by only 1.2 % the energy value. In calculations of the  $^{48}\text{Ca}$  nucleus we found a change of 9% in the energy value by doubling the depths of the neutrons and protons wells.

These findings induced us to make calculations by using, for each nucleus, a fixed set of Woods-Saxon parameters. The values of these parameters, given in Tab. 2, are taken from the literature [29]. They have been fixed to reproduce the charge root mean square radii and the single particle energies around the Fermi surface. One could consider the requirement of reproducing these data, a further variational constraint. In any case, we have further verified that our energy minima are only slightly modified by large changes of the potential.

### 5.3 The correlation functions

The correlation function is fixed by the minimization procedure (1), and the result is independent of the starting expression of the correlation function. In practice, however, in order to minimize the computational effort, it is convenient to choose expressions of the correlation functions containing a limited number of parameters, and behaving at large interparticle distances as intuitively expected. This means that asymptotically  $f_1$  should reach the value 1, while the other correlation functions, should be zero. A commonly used expression for the scalar term of the correlation is the gaussian form:

$$f_p(r) = \delta_{p,1} + a_p e^{-b_p r^2}$$

where  $a_p$  and  $b_p$  are the free parameters to be changed in the variation procedure. For example in Refs. [27, 28, 29] correlations of this type have been used.

In our calculations, we found more convenient, from the physical point of view, and also in terms of number of variational parameters, to fix the correlation functions by using what we called the *Euler procedure*. The basic idea is to use as variational parameters the distances where the correlation functions  $f_p(r)$  reach their asymptotic values. For fixed values  $d_p$  of these distances, that we call *healing distances*, the functions  $f_p(r)$  are obtained by doing a minimization of the energy calculated up to the second order cluster expansion. This means that we solve the FHNC/SOC equations when all the nodal diagrams are zero. We give a detailed description of the Euler procedure in Appendix F.

The application of the Euler procedure involves a single variational parameter, the healing distance  $d_p$ , for each operator channel of the correlation, therefore in our calculations we have to deal with six variational parameters. On the other hand, it is known from nuclear and neutron matter calculations [21, 24, 25] that the healing distances of the four central channels  $p \leq 4$  are rather similar, as are those of the two tensor channels  $p = 5, 6$ . For this reason, we performed our calculations by using only two variational parameters, a healing distance  $d_c$  for the four central channels  $p \leq 4$ , and another one  $d_t$ , for the two tensor channels.

The values of the healing distances providing the energy minima for the five nuclei considered, are given in Tab. 3. In this table, we compare the values obtained by using both interactions. In Fig. 21 we show the two-body correlation functions obtained for the AV8'+UIX interaction as a function of the two-nucleon distance.

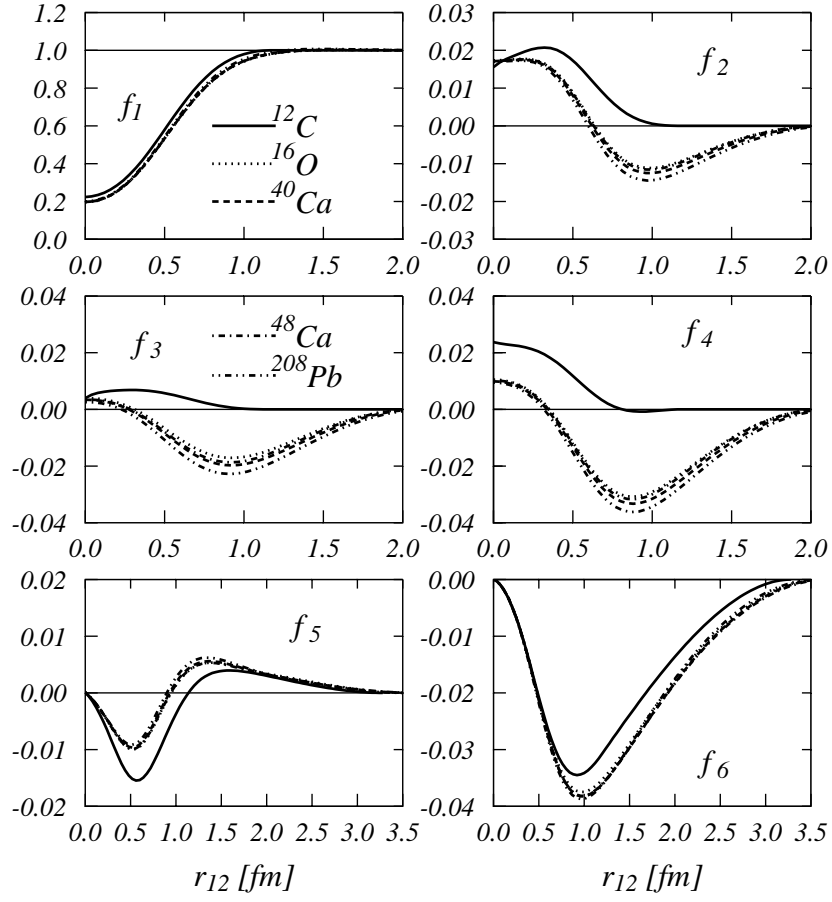


Figure 21: Two-body correlation functions  $f_p$ , obtained with the Euler procedure, as a function of the two-nucleon distance. In this calculations the AV8'+UIX interaction has been used.

		$^{12}\text{C}$	$^{16}\text{O}$	$^{40}\text{Ca}$	$^{48}\text{Ca}$	$^{208}\text{Pb}$
AV8' +	$d_c$	1.20	2.10	2.15	2.10	2.20
UIX	$d_t$	3.30	3.70	3.66	3.70	3.60
UV14 +	$d_c$	1.40	2.10	2.15	2.10	2.20
UVII	$d_t$	3.30	3.80	3.86	3.90	3.80

Table 3: Values, in fm, of the *healing distances*, which minimize the energy functional with the two different interactions we have adopted.

Various remarks are in order after observing these results. The most evident one is the scarce dependence on the type of nucleus, with the only exception of  $^{12}\text{C}$ . We shall see that, also in the calculations of other quantities, this nucleus always produces anomalies in the general trend of our results. We think that this is due to the fact that  $^{12}\text{C}$  is not really a good doubly closed shell nucleus, therefore, open shell effects, not included in our calculations, are relevant. The following observations are done by excluding the  $^{12}\text{C}$  results.

The results of Tab. 3 show the scarce dependence of the healing distances on the interaction model. The values of  $d_c$  are identical for both the interaction models we have used. There are small differences in the  $d_t$  values, those of the UV14+AVII, are slightly larger than those obtained with AV8'+UIX.

Also the dependence on the nucleus is rather weak. The variations of the healing distances are very small, and, the curves of Fig. 21 relative to each nucleus are rather similar for each considered channel.

The values of the scalar correlation functions  $f_1$ , are one order of magnitude larger than those of the other correlations. The behavior of the  $f_1$  functions reflects the presence of the repulsive core in the scalar channel of the nucleon-nucleon force. The correlation function hinders two nucleons from approaching each other too much.

The healing distances of the tensor correlations are larger than those of the central correlations. Also this effect reflects a characteristic of the interaction where the tensor channels have slightly larger interaction range than the central ones (see Fig. 20).

#### 5.4 The sum rules

The numerical solution of the FHNC/SOC equations is not trivial at all. We have to deal with a set of interrelated, hypernetted, integral equations. The numerical technique used to solve this set of equation is based on an iterative procedure. In analogy to what we have discussed in Sect. 2.1 for the HNC equations (22,23,25), we started the calculation of the FHNC/SOC equations by setting the nodal diagrams to zero. The various integrals equations are calculated and they provide new values of the nodal diagrams that are used again to solve the FHNC/SOC equations. The convergence test is done on the energy, and we stop the iterative procedure when the energy calculated in two different iteration loops differ by less than 1 keV. Every calculation is done by using a fixed correlation function. The numerical convergence of the solution does not ensure that this solution is acceptable from the physical point of view. For example we found numerically convergent solutions which provided a wrong number of nucleons.

In addition to these computational problems, we should remember that our calculations do not solve exactly the many-body Schrödinger equation. The solution of the FHNC/SOC set

of equations does not include the elementary diagrams. Furthermore, we do not consider the contribution of those operator dependent terms which are beyond the SOC approximation.

An important tool used to verify the numerical, and theoretical, accuracy of the calculations is, the test of the sum rules exhaustion. For this purpose, we have evaluated the following sum rules:

$$S_1^{t_1} \equiv \frac{1}{\mathcal{N}_{t_1}} \int d\mathbf{r}_1 \rho^{t_1}(\mathbf{r}_1) = 1 , \quad (147)$$

$$\begin{aligned} S_2^{t_1 t_2} &\equiv \frac{1}{\mathcal{N}_{t_1}(\mathcal{N}_{t_2} - \delta_{t_1 t_2})} \int d\mathbf{r}_1 d\mathbf{r}_2 \rho_2^{1, t_1 t_2}(\mathbf{r}_1, \mathbf{r}_2) \\ &= \frac{1}{\mathcal{N}_{t_1}(\mathcal{N}_{t_2} - \delta_{t_1 t_2})} \int d\mathbf{r}_1 d\mathbf{r}_2 \frac{f_{2k_1-1+l_1}(r_{12}) f_{2k_2-1+l_2}(r_{12})}{f_1^2(r_{12})} \\ &\quad \left\{ \rho_{2,dir}^{t_1 t_2}(\mathbf{r}_1, \mathbf{r}_2) A^{k_1} \delta_{k_1 k_2} \chi_{l_1+l_2}^{t_1 t_2} \right. \\ &\quad \left. + \left[ \rho_{2,exc}^{t_1 t_2}(\mathbf{r}_1, \mathbf{r}_2) A^{k_3} I^{k_1 k_2 k_3} + \rho_{2,excj}^{t_1 t_2}(\mathbf{r}_1, \mathbf{r}_2) I^{k_1 k_2 k_4} I^{k_4 k_3 2} \right] \right. \\ &\quad \left. \Delta^{k_3} \sum_{l_3=0}^1 \chi_{l_1+l_2+l_3}^{t_1 t_2} \right\} = 1 , \end{aligned} \quad (148)$$

$$\begin{aligned} S_{2,\sigma} &\equiv \frac{1}{3A} \sum_{t_1 t_2=p,n} \int d\mathbf{r}_1 d\mathbf{r}_2 \rho_2^{3, t_1 t_2}(\mathbf{r}_1, \mathbf{r}_2) \\ &= \frac{1}{3A} \sum_{t_1 t_2=p,n} \int d\mathbf{r}_1 d\mathbf{r}_2 \frac{f_{2k_1-1+l_1}(r_{12}) f_{2k_2-1+l_2}(r_{12})}{f_1^2(r_{12})} \\ &\quad \left\{ \rho_{2,dir}^{t_1 t_2}(\mathbf{r}_1, \mathbf{r}_2) I^{k_1 2 k_2} \chi_{l_1+l_2}^{t_1 t_2} \right. \\ &\quad \left. + \left[ \rho_{2,exc}^{t_1 t_2}(\mathbf{r}_1, \mathbf{r}_2) A^{k_3} I^{k_1 2 k_4} I^{k_4 k_2 k_3} + \rho_{2,excj}^{t_1 t_2}(\mathbf{r}_1, \mathbf{r}_2) I^{k_1 2 k_4} I^{k_4 k_2 k_5} I^{k_5 k_3 2} \right] \right. \\ &\quad \left. \Delta^{k_3} \sum_{l_3=0}^1 \chi_{l_1+l_2+l_3}^{t_1 t_2} \right\} = -1 . \end{aligned} \quad (149)$$

In the above equations, a sum on the repeated indexes is understood. The operator dependent TBDFs  $\rho_2^q$  are defined in Eq. (101). The sum rule  $S_{2,\sigma}$  is related to the two-body density spin function. This sum rule is valid only for spin saturated systems and for correlations not containing tensor operator terms. For this reason, we expect  $S_{2,\sigma}$  to be exhausted in  $^{16}\text{O}$  and  $^{40}\text{Ca}$  nuclei only, and in the absence of the  $O^{p=5,6}$  operator terms in the correlation.

To obtain the expressions (147,...,149) of the sum rules, we have considered all the possible types of correlation operator between the 1 and 2 coordinates, which have been vertex corrected by the scalar correlations. This is the same approach used to calculate the  $W_0$  term of the interaction energy Eq. (137).

In Tab. 4, we show the sum rule values calculated with the AV8'+UIX interaction, by using different types of correlations: purely scalar correlations,  $f_1$ , central correlation,  $f_4$ , and correlations containing also tensor terms,  $f_6$ . To simplify the presentation of the results, we indicate with  $S_2$  the quantity:

$$S_2 = \frac{1}{A(A-1)} \sum_{t_1 t_2} \mathcal{N}_{t_1}(\mathcal{N}_{t_2} - \delta_{t_1 t_2}) S_2^{t_1 t_2} , \quad (150)$$

	$^{12}\text{C}$	$^{16}\text{O}$	$^{40}\text{Ca}$	$^{48}\text{Ca}$	$^{208}\text{Pb}$
$S_1^p(f_1)$	1.000	1.000	1.000	1.000	0.999
$S_1^n(f_1)$	1.000	1.000	1.000	0.999	0.999
$S_1^p(f_4)$	0.998	0.996	0.993	1.005	1.008
$S_1^n(f_4)$	0.998	0.996	0.993	1.004	1.004
$S_1^p(f_6)$	0.997	1.006	1.008	0.994	1.002
$S_1^n(f_6)$	0.997	1.006	1.008	0.996	1.000
$S_2(f_1)$	1.004	1.003	1.001	1.000	0.998
$S_2(f_4)$	0.995	0.999	0.989	1.012	1.014
$S_2(f_6)$	0.996	0.998	0.978	0.994	1.003
$S_{2\sigma}(f_1)$		-0.95	-0.929		
$S_{2\sigma}(f_4)$		-1.080	-1.101		

Table 4: Sum rules exhaustion calculated for the AV8'+UIX interaction. The indexes  $f_p$  indicate the number of operator terms of the correlation.

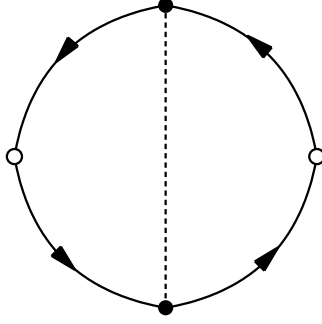


Figure 22: Elementary diagram included in the RFHNC-1 calculations of Ref. [27].

which must be equal to one. The  $f_1$  results give an indication of the error made by neglecting the elementary diagrams. The differences with the other sum rules, is a measure of the validity of the SOC approximation.

Apart from the  $S_{2\sigma}$  values, which we shall discuss separately, the various sum rules are satisfied at the level of few parts per thousand. The  $f_1$  sum rules, give the best results which are only slightly spoiled by the other correlations.

Different remarks should be made for the spin sum rule  $S_{2\sigma}$ . As already pointed out, in our calculations, these sum rules have to be satisfied only for the  $^{16}\text{O}$  and  $^{40}\text{Ca}$  nuclei, and for the  $f_1$  and  $f_4$  cases. The values of Tab. 4 indicate that the  $S_{2\sigma}$  sum rule is satisfied only at the 5-10% level. In Ref. [27], we have verified that the inclusion of the elementary diagram shown in Fig. 22 improves the exhaustion of the  $S_{2\sigma}$  sum rule up to few parts per thousand. This is the same level of accuracy obtained for the other sum rules.

## 5.5 The ground state energies

The most important results of our work are summarized in Tab. 5 where we give the values of the binding energies per nucleon, for all the five nuclei considered. We show the results obtained with the two interactions AV8'+UIX and U14+UVII, and we compare them with the experimental energies [52]. We present the various terms contributing to the total energy: the kinetic energy  $T$ , the two-body interaction, where the contribution of the first six channels  $V_{2-body}^6$  and that of the spin-orbit interaction  $V_{LS}$  are separately given, the Coulomb interaction  $V_{Coul}$  and the three-body force  $V_{3-body}$ . In the kinetic energy term the spurious contribution of the center of mass motion, Eq. (130), calculated as discussed in [27], has already been subtracted.

The various terms show some saturation properties. For example, the values of the kinetic energies per nucleon,  $T$ , increase up to  $^{40}\text{Ca}$  and then they remain almost stable. An analogous behavior is shown by the  $V_{2-body}^6$  terms whose contribution per nucleon increases with increasing number of nucleons up to  $^{40}\text{Ca}$ , and afterword it remains almost constant.

We have mentioned the fact that the spin-orbit terms are not treated consistently in the FHNC/SOC computational scheme, but they are evaluated by using some approximation. In any case, in all the nuclei considered, their contributions are of the order of a few percent with respect to the  $V_{2-body}^6$  contributions. We have done calculations in  $^{16}\text{O}$  and  $^{40}\text{Ca}$  after switching off the spin-orbit terms in the mean field potential. In this case the spin-orbit partner single particle wave functions are identical. The differences in the total spin-orbit contributions, with respect to the values given in Tab. 5 are within the numerical uncertainty.

As expected, the results of Tab. 5 show that the binding is obtained by a subtle subtraction between the repulsive kinetic energy term and the attractive contribution of the two-body potential. The sum of only these contributions for the AV8' interaction, provide -2.25, -6.20, -8.30, -7.31 and -9.32 MeV for the  $^{12}\text{C}$ ,  $^{16}\text{O}$ ,  $^{40}\text{Ca}$ ,  $^{48}\text{Ca}$  and  $^{208}\text{Pb}$  nuclei respectively. The sum in the U14 model provide -2.40, -6.56, -9.25, -8.19 and -10.17 MeV. It is evident that the U14 interaction is more attractive than the AV8'. This depends on the intrinsic structure of the interaction and its parametrization.

The contribution of the Coulomb term  $V_{Coul}$  is evaluated within the complete FHNC/SOC computational scheme. As expected, the behavior with increasing size of the nucleus does not show saturation because of the long range nature of the interaction. The Coulomb terms behave as expected, their contributions increase with increasing number of protons. The apparent inversion of this trend from  $^{40}\text{Ca}$  to  $^{48}\text{Ca}$  is due to the representation in terms of energy per nucleon, which in this case is misleading, since the proton number is the same for the two nuclei. In this case it is better to compare the total values of the Coulomb energies, 78.80 MeV for  $^{40}\text{Ca}$  and 75.36 for  $^{48}\text{Ca}$ . The 4.4% difference between these two values is due to the different structure of the two nuclei. The inclusion of the Coulomb repulsion reduces the nuclear binding energies.

In addition, there is the contribution of the three-body force. As discussed in sect. 4.3 the two terms composing this interactions provide contributions of different sign; the Fujita-Miyazawa term  $v_{123}^{2\pi}$  is attractive, while the other term  $v_{123}^R$  is repulsive. In our calculations, the total contribution of the UVII and UIX three-body interactions is always globally repulsive. This feature is common to the FHNC/SOC nuclear matter results [24, 25].

The comparison with the experimental energies indicates a general underbinding of about

AV8'+UIX	<sup>12</sup> C	<sup>16</sup> O	<sup>40</sup> Ca	<sup>48</sup> Ca	<sup>208</sup> Pb
$T$	27.13	32.33	41.06	39.64	39.56
$V_{2-body}^6$	-29.13	-38.15	-48.97	-46.60	-48.43
$V_{Coul}$	0.67	0.86	1.97	1.57	3.97
$V_{LS}$	-0.25	-0.38	-0.39	-0.35	-0.45
$T + V_2$	-1.58	-5.34	-6.34	-5.74	-5.35
$V_{3-body}$	0.67	0.86	1.76	1.61	1.91
$E$	-0.91	-4.48	-4.58	-4.14	-3.43
U14+UVII	<sup>12</sup> C	<sup>16</sup> O	<sup>40</sup> Ca	<sup>48</sup> Ca	<sup>208</sup> Pb
$T$	24.63	29.25	37.32	36.12	36.07
$V_{2-body}^6$	-27.08	-35.84	-46.65	-44.40	-46.28
$V_{Coul}$	0.68	0.88	2.01	1.59	4.00
$V_{LS}$	0.05	0.03	0.08	0.09	0.04
$T + V_2$	-1.72	-5.68	-7.24	-6.71	-6.17
$V_{3-body}$	0.54	0.69	1.46	1.32	1.61
$E$	-1.18	-4.99	-5.77	-5.27	-4.55
$E_{exp}$	-7.68	-7.97	-8.55	-8.66	-7.86

Table 5: Energies per nucleon in MeV, obtained by using the  $AV8'+UIX$  and  $U14+UVII$  interactions. We have indicated with  $T$  the kinetic energy, with  $V_{2-body}^6$  the contribution of the first six channels of the two-body interaction, with  $V_{LS}$  the spin-orbit contribution, with  $V_{Coul}$  the contribution of the Coulomb interaction and with  $V_{3-body}$  the total contribution of the three-body force. The rows labeled  $T + V_2$  show the energies obtained by considering the two-body interactions only. The experimental energies are from Ref. [52].

4.0 MeV per nucleon. This is roughly the same underbinding obtained, at the saturation density, by the most recent FHNC/SOC nuclear matter calculations [25].

The behavior of the <sup>12</sup>C nucleus is anomalous in this general trend. This nucleus is barely bound in our calculations. Some crucial physics ingredient, relevant in <sup>12</sup>C, but negligible for the other nuclei, is missing in our approach. Probably, this has to do with soft deformations of the <sup>12</sup>C nucleus, effects which we are unable to treat.

The comparison between the two interactions indicates that the UV14+UVII interaction is more attractive than the AV8'+UIX force. This fact is already present when only the two-body interactions are considered, and it is enhanced by the inclusion of the three-body force. The contributions of the spin-orbit term in the two cases have different sign, they are attractive for AV8' and slightly repulsive for UV14. Globally, the differences in the total energies, calculated with the two interactions, vary from a minimum of 5% (<sup>16</sup>O) to a maximum of 18% (<sup>208</sup>Pb).

We have done a detailed study of the relevance of the various terms contributing to the energy, as they have been presented in Sect. 4. As an example, we show in Tab. 6 the various contributions obtained in the calculation of the <sup>208</sup>Pb energy with the AV8'+UIX interaction. We have obtained analogous results for all the other nuclei investigated and also for the other interaction.

The larger contributions to the energy come from the terms calculated with what we have called the (0) approximation in Eq. (137). This is the contribution of those diagrams containing



	(0)	(s)	(c)	(0) + (s) + (c)
$T_{\Phi}^{(1)}$	16.05			16.05
$T_{\Phi}^{(2)}$	4.16	-0.35	-0.13	3.68
$T_{\Phi}^{(3)}$	0.42	-0.08		0.34
$T_F$	17.34	1.62	0.55	19.51
$T_{\Phi j}^{(2)}$	0.17			0.17
$T_{\Phi j}^{(3)}$	-0.012			-0.012
$T_{Fj}$	0.0			0.0
$T_{c.m.}$	0.02			0.02
$v^1$	-0.03	-0.10	-0.47	-0.6
$v^2$	-1.29	0.04	-0.19	-1.44
$v^3$	-3.87	0.18	-0.67	-4.36
$v^4$	-17.57	-0.41	-1.49	-19.47
$v^5$	0.11	-0.02	0.04	0.13
$v^6$	-21.42	-1.37	0.10	-22.69
$v_j^1$	0.006			0.006
$v_j^2$	0.0			0.0
$v_j^3$	0.004			0.004
$v_j^4$	0.012			0.012
$v_j^5$	0.0			0.0
$v_j^6$	-0.005			-0.005
$v_{123}^R$				3.282
$v_{123}^{2\pi}$				-1.368

Table 6: Contributions, in MeV, of the various terms forming the  $^{208}\text{Pb}$  energy, calculated with the AV8'+UIX interaction. The various terms are defined in Sect. 4. The terms T of the kinetic energy are defined by Eqs. (127, 128, 129, 139). The  $v^p$  terms indicate the six-channels of the two-body interaction. The three-body terms are defined in Eqs. (142,143). The subscript  $j$  indicate the contribution produced by antiparallel spin densities. The labels (0), (s) and (c) indicate the various approximation of the energy related to the pieces  $W_0$ ,  $W_s$ , and  $W_c$  as defined in Eq. (137).

all the scalar dressings of the (1,2) pair. The (s) and (c) terms, more difficult to calculate, give much smaller contributions.

It is interesting to observe that, the contributions given by the terms depending on one-body densities with antiparallel spins, i. e. the terms labeled with the  $j$  subscript in the table, are very small. In Tab. 6 we show their largest values, since we found their contributions to be even smaller for nuclei with saturated  $l$  shells such as  $^{16}\text{O}$  and  $^{40}\text{Ca}$ .

The study of the contributions of the various channels of the two-body interaction, indicates that the spin-isospin ( $p = 4$ ) and tensor-isospin ( $p = 6$ ) terms are the main source for the binding. This is a common feature for all the nuclei we have considered [53].

The results for the UV14+UVII interaction are analogous to those shown in Tab. 6 for the AV8'+UIX interaction. In the remaining part of Sect. 5, we shall present some quantities with the aim of studying the effects of the Short-Range Correlations (SRC). We have found that the

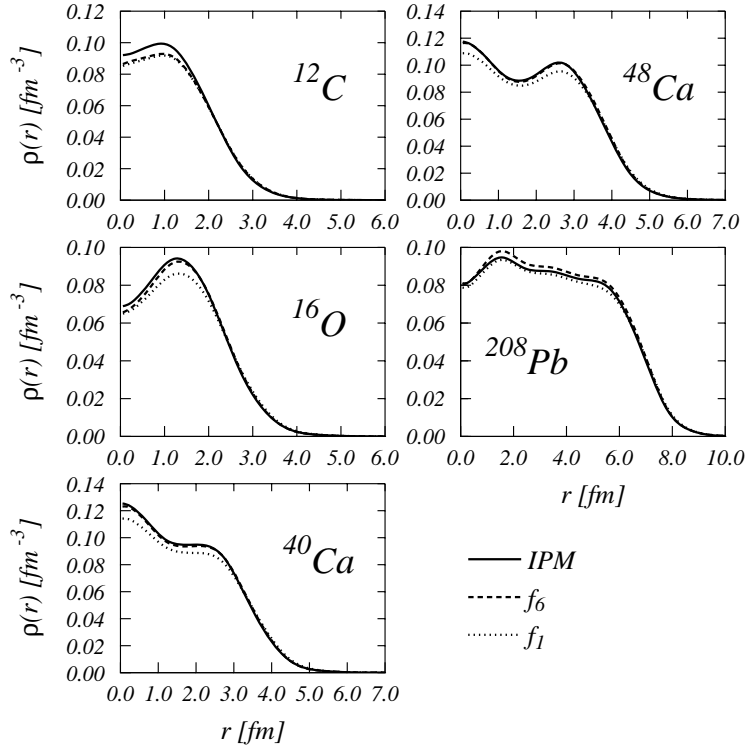


Figure 23: Neutron density distributions. The full lines are the IPM distributions, the dotted ones have been obtained by using scalar correlations only, and the dashed lines show the results of the complete calculation.

differences between the results obtained with the two interaction models are smaller than the effects we are looking for. For this reason, henceforth, we shall present only the results obtained by using the AV8'+UIX interaction.

## 5.6 The one-body distribution functions

The OBDF,  $\rho^t(\mathbf{r})$ , has been defined by Eq. (100). The physical meaning of this quantity is the probability density of finding a nucleon of type  $t$ , in the position  $\mathbf{r}$  with respect to the nuclear center. Since we have assumed that our systems are spherical, this probability depends only on the distance from the center of the nucleus. The expression of the density distribution in terms of the FHNC/SOC quantities is given by Eqs. (103) and (239).

We show in Fig. 23 the neutron density distributions for the five nuclei we have considered. The full lines show the IPM results, the dotted lines those obtained by using scalar,  $f_1$ , correlations only, and the dashed lines show the results of the full FHNC/SOC calculations. In an analogous way we show in Fig. 24 the charge distributions, obtained by folding the proton distributions with the proton electromagnetic form factor. We have used a dipole form for this form factor. In this figure the continuous thick lines indicate the empirical charge distributions extracted from elastic electron scattering experiments [54].

The results obtained with scalar interactions produce distributions which are smaller at the

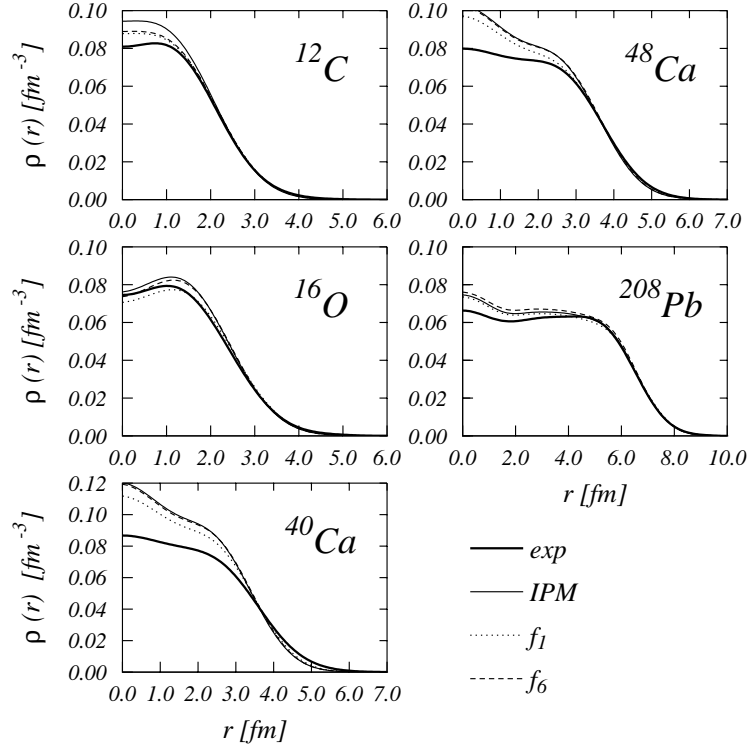


Figure 24: Charge density distributions, obtained by folding the proton distributions with the electromagnetic form factor. The full thick lines show the empirical distributions [54]. The other curves have the same meaning as in Fig. 23.

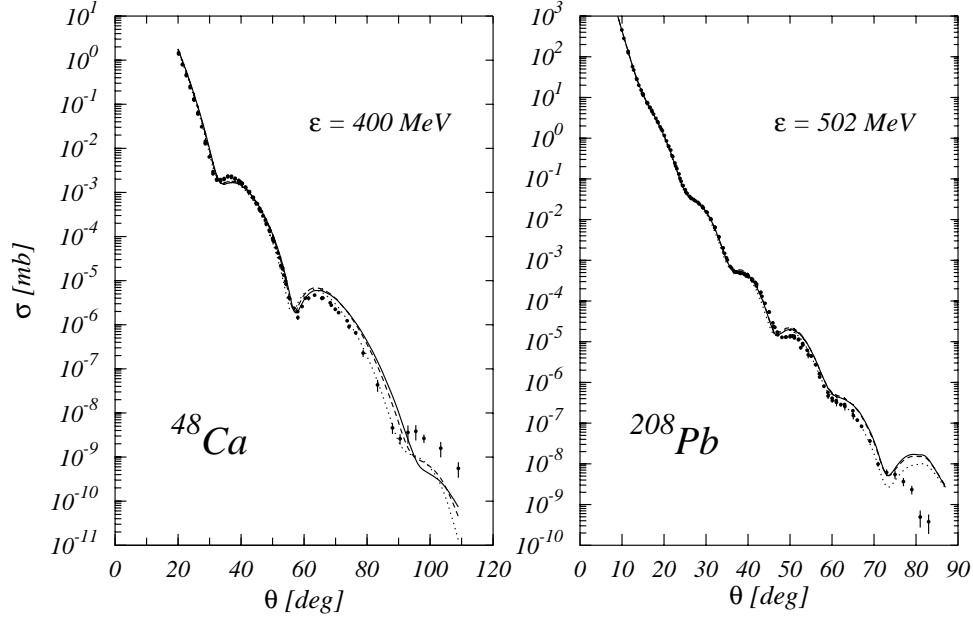


Figure 25: Elastic electron scattering cross sections on  $^{48}\text{Ca}$  and  $^{208}\text{Pb}$  target nuclei, as a function of the scattering angle. The theoretical cross sections have been calculated in distorted wave Born approximation [56, 57]. The full lines show the IPM results, the dotted lines the results obtained with the  $f_1$  correlations, the dashed lines with the  $f_6$  correlations. We have indicated with  $\epsilon$  the electron energy.

center of the nucleus with respect to the mean-field distributions. This effect is reduced when all the correlations are included in the calculation. These findings are in agreement with the results of Ref. [55] where a first-order cluster expansion was used.

We used the charge density distributions to calculate the elastic electron scattering cross sections within a distorted wave Born approximation [56, 57]. We compare in Fig. 25 our results with the experimental data of the  $^{48}\text{Ca}$  and  $^{208}\text{Pb}$  nuclei [58, 59]. In Ref. [31] a similar figure for the  $^{16}\text{O}$  and  $^{40}\text{Ca}$  nuclei is shown. It is evident that the main discrepancies with the data appear at large scattering angles. The use of the correlations slightly improves the agreement with the experiment. The effects of the  $f_6$  correlations go in the opposite direction of those of the  $f_1$  correlation (as has already been remarked) in the neutron density, and in the charge distributions cases.

We would like to point out here that the density distributions are the only quantities amongst those we have investigated where the use of operator dependent correlations reduces the effects of purely scalar correlations. In all the other cases, as we are going to show, the effects of the  $f_6$  correlations are larger than those of the  $f_1$  correlation.

## 5.7 Momentum distributions

The momentum distribution is related to the probability of finding a nucleon with a certain value of the momentum. This quantity is related to the Fourier transform of the OBDM, which is defined in analogy to the OBDF (100) but for different values of the non integrated variable:

$$\begin{aligned}\rho(x_1, x'_1) &= \sum_{s,s',t} \rho^{s,s',t}(\mathbf{r}_1, \mathbf{r}'_1) \chi_s^+(1) \chi_t^+(1) \chi_{s'}(1') \chi_t(1') \\ &= \frac{A}{\langle \Psi | \Psi \rangle} \int dx_2 \dots dx_A \Psi^\dagger(x_1, x_2, \dots, x_A) \Psi(x'_1, x_2, \dots, x_A) .\end{aligned}\quad (151)$$

The evaluation of this quantity merits some comments. For simplicity, we consider in this discussion only scalar correlations. In order to perform the cluster expansion of the OBDM, it is necessary to define a new dynamical correlation function:

$$h_w(r_{ij}) = f_1(r_{ij}) - 1 , \quad (152)$$

where  $i$  can be either 1 or  $1'$ , and  $j = 2, \dots, A$ . This takes into account the fact that the coordinate  $x_1$  is present only in the bra, while the coordinate  $x'_1$  is present only in the ket. The coordinates describing the other particles can appear in both bra and ket states, and generate the usual  $h = f_1^2 - 1$  dynamical correlation function. For the calculation of Eq. (151), we found it convenient to define a new type of sub-determinant, in analogy to what has been done in Eq. (31):

$$\Delta'_p(1, 1', 2, \dots, p) = \begin{vmatrix} \rho_0(x_1, x_{1'}) & \rho_0(x_1, x_2) & \dots & \rho_0(x_1, x_p) \\ \rho_0(x_2, x_{1'}) & \rho_0(x_2, x_2) & \dots & \rho_0(x_2, x_p) \\ \vdots & \vdots & \ddots & \vdots \\ \rho_0(x_p, x_{1'}) & \rho_0(x_p, x_2) & \dots & \rho_0(x_p, x_p) \end{vmatrix} . \quad (153)$$

Also for this new sub-determinant the properties (32... 34) remain valid, therefore we can apply the usual cluster expansion techniques, developed for the calculation of the TBDF. However, we have to consider that the separation of the  $x_1$  and  $x_{1'}$  coordinates which refer to the same particle, implies the absence of dynamical correlations between these two coordinates, as is shown in the diagrams of Fig. 26. In addition, we should take care of the fact that the statistical loops containing the coordinate  $x_1$  must contain also  $x_{1'}$  and must be open in these two points, see again the diagrams of Fig. 26.

The calculation of the OBDM proceeds in analogy to that of the TBDF. The denominator of Eq. (151) simplifies the contribution of the unlinked diagrams of the numerator. At this point, we encounter a difficulty, since it is not possible to cancel those reducible diagrams where the articulation point is one of the points in the open statistical loop containing to 1 and  $1'$ . This is not a specific problem of the finite systems. Its solution is based on the use of the vertex corrections which have been introduced for the first time to calculate the momentum distribution of an infinite system of particles [43].

Coming back to our specific case, we found that the calculation of the OBDM requires the use of a new vertex correction, which we call  $C_w(\mathbf{r}_i)$ , understanding that  $i$  can be 1 or  $1'$ . New types of diagrams appear. We call them  $wd$ ,  $we$ ,  $ww$ ,  $w_c c$ , and  $w_c w_c$ . The label  $w$  is associated to the new dynamical correlation  $h_w$  and, as  $d$ , denotes that no statistical line arrive at the corresponding point. With the label  $w_c$  we indicate diagrams analogous to those we have called

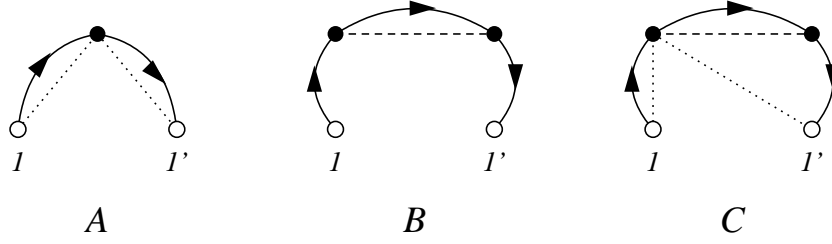


Figure 26: Example of diagrams used to calculate the OBDM (151). The dotted lines indicate the new dynamical correlation function  $h_w = f_1 - 1$ , while the dashed line indicate the usual dynamical correlation function  $h = f_1^2 - 1$ .

$c$  in the calculation of the TBDF. These diagrams have an open statistical loop with the  $h_w$  dynamical correlations, as the diagrams of Fig. 26. The diagrams contributing to the OBDM are of  $w_c w_c$  type and the rest of classes diagrams are auxiliary quantities needed to calculate them. The RFHNC/SOC expressions of the different quantities involved in the calculation of the OBDM, are presented in Appendix B where the parallels with the TBDF expressions are also pointed out.

Because of the spherical symmetry of the systems we are describing, the quantity of interest in our calculations is:

$$\rho^t(\mathbf{r}_1, \mathbf{r}'_1) = \sum_{s=\pm 1/2} [\rho^{s,s;t}(\mathbf{r}_1, \mathbf{r}'_1) + \rho^{s,-s;t}(\mathbf{r}_1, \mathbf{r}'_1)] , \quad (154)$$

whose diagonal part,  $\mathbf{r}'_1 = \mathbf{r}_1$ , is the OBDF. We obtain the momentum distributions of protons or neutrons as:

$$n^t(k) = \frac{1}{(2\pi)^3} \frac{1}{\mathcal{N}_t} \int d\mathbf{r}_1 d\mathbf{r}'_1 e^{i\mathbf{k} \cdot (\mathbf{r}_1 - \mathbf{r}'_1)} \rho^t(\mathbf{r}_1, \mathbf{r}'_1) , \quad (155)$$

which is normalized:

$$\int d\mathbf{k} n^t(k) = 1 . \quad (156)$$

The uncorrelated OBDMs are obtained by inserting in Eq. (89) the Slater determinant,  $\Phi$ , formed by the single particle wave functions (88). We obtain the expressions (91) for  $s' = s$  and (92) for  $s' \neq s$ .

For the correlated OBDM we obtain the expression:

$$\begin{aligned} \rho^t(\mathbf{r}_1, \mathbf{r}'_1) = & -2C_{w,11}^t(\mathbf{r}_1)C_{w,11}^t(\mathbf{r}'_1)g_{w_c w_c}^t(\mathbf{r}_1, \mathbf{r}'_1) \\ & -2C_{w,22}^t(\mathbf{r}_1)C_{w,22}^t(\mathbf{r}'_1) \sum_{p>1} A^k \Delta^k g_{w_c w_c, p}^t(\mathbf{r}_1, \mathbf{r}'_1) . \end{aligned} \quad (157)$$

with  $p = 2k - 1 + l$ . All the FHNC/SOC quantities have been defined in Appendix B.

In Fig. 27 we compare the  $^{12}\text{C}$ ,  $^{16}\text{O}$ ,  $^{40}\text{Ca}$ ,  $^{48}\text{Ca}$  and  $^{208}\text{Pb}$  momentum distributions calculated in the IPM model, with those obtained by using  $f_1$  and  $f_6$  correlations.

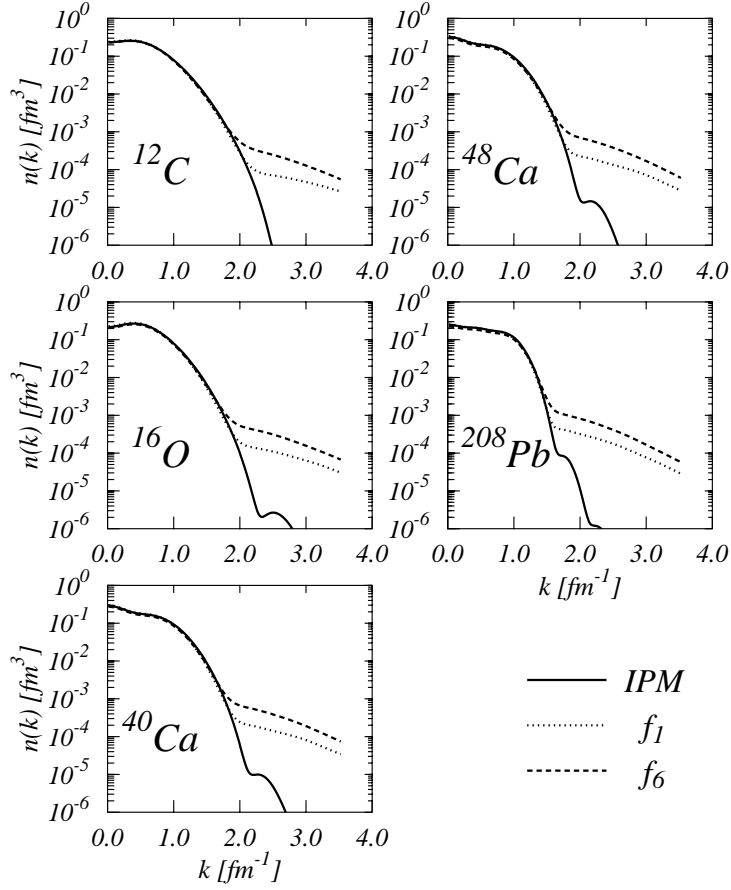


Figure 27: The proton momentum distributions of the  $^{12}\text{C}$ ,  $^{16}\text{O}$ ,  $^{40}\text{Ca}$ ,  $^{48}\text{Ca}$  and  $^{208}\text{Pb}$  nuclei calculated in the IPM model (full lines), by using the scalar correlation only (dotted lines) and the full operator dependent correlations (dashed lines).

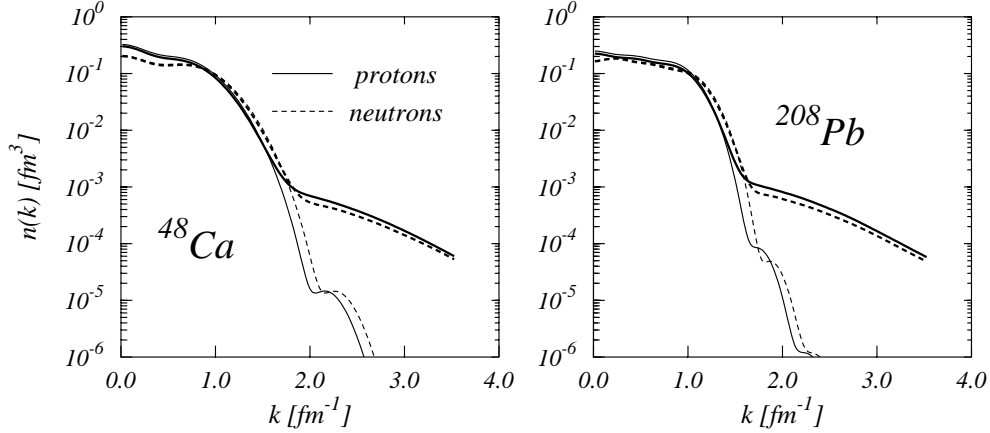


Figure 28: Protons (full lines) and neutrons (dashed lines) momentum distributions of the  $^{48}\text{Ca}$  and  $^{208}\text{Pb}$ . The thick lines show the results of our calculations, the thin lines the IPM results.

The general behavior of the momentum distributions, is very similar for all the nuclei we have considered. Correlated and IPM distributions almost coincide in the low momentum region up to a precise value, when they start to deviate. The correlated distributions show high momentum tails, which are orders of magnitudes larger than the IPM results. The value of  $k$  of which uncorrelated and correlated momentum distributions start to deviate is smaller the heavier is the nucleus. It is about  $1.9 \text{ fm}^{-1}$  for  $^{12}\text{C}$ , and  $1.5 \text{ fm}^{-1}$  for  $^{208}\text{Pb}$ . We recall that the value of the Fermi momentum of symmetric nuclear matter at the saturation point is  $1.36 \text{ fm}^{-1}$ . The results presented in Fig. 27 clearly show that the effects of the scalar correlations are smaller than those obtained by including the operator dependent terms.

In our calculations, we have found that the proton and neutron momentum distributions for nuclei with  $N = Z$  are very similar. For this reason, we show in Fig. 28 the proton and neutron momentum distributions of the two nuclei we have investigated with  $N \neq Z$ : the  $^{48}\text{Ca}$  and  $^{208}\text{Pb}$  nuclei. The thicker lines show the results of our RFHNC/SOC calculations, while the thinner ones the IPM distributions. The main differences between the two distributions are in the zone where the  $n(k)$  values drop by orders of magnitudes. This zone, corresponds, in the infinite systems, to the discontinuity region of the momentum distribution, related to the Fermi momentum. In a finite system, the larger number of neutrons implies that the neutron Fermi energy and, consequently, the effective Fermi momentum, is larger than that of the protons. For this reason, the discontinuity regions of the neutron momentum distributions are located at larger values of  $k$  with respect to the protons momentum distributions.

After the discontinuity region, the behaviors of the distributions are dominated by the SRC effects, and the protons and neutrons results are very close. In terms of relative difference, the SRC effects are essentially the same for protons and neutrons [60]. A discussion about the role of SRC effects on the proton and neutron momentum distributions in asymmetric nuclear matter is open, and our results are in agreement with the findings of Ref. [61], but disagree with those of Ref. [62].

The increase of the momentum distribution at large  $k$  values, induced by the SRC, is a well



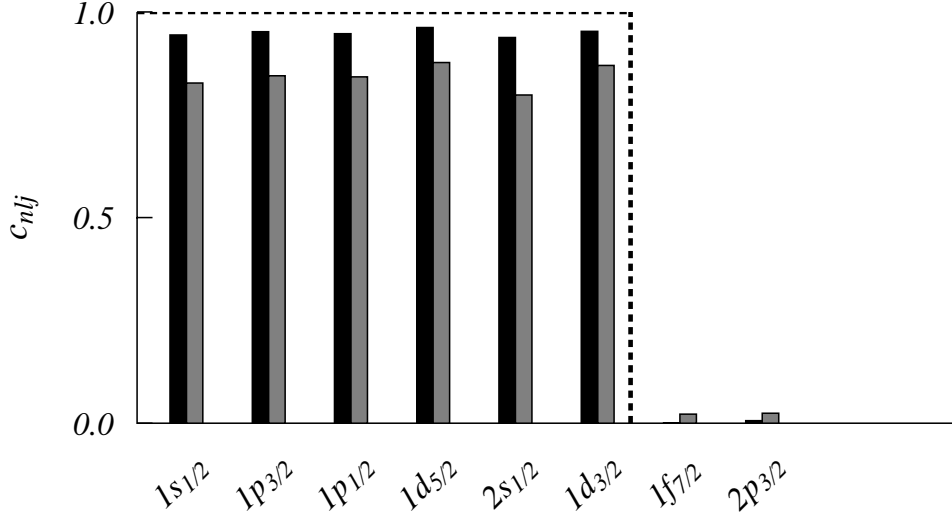


Figure 29: Occupation numbers of the proton natural orbits of the  $^{48}\text{Ca}$  nucleus. The dashed line indicates the IPM values. The black bars show the values obtained with the scalar correlation and the gray bars those values obtained with the full correlation.

known result in the literature, see for example the review of Ref. [63]. The momentum distributions of medium-heavy nuclei, have been usually obtained by using approximated descriptions of the cluster expansion, which is instead considered at all orders in our treatment. We found in [60] that the results of the approximate treatment provide only a qualitative description of the correlation effects. They produce a high-momentum enhancement, but they underestimate the correct results by orders of magnitude.

## 5.8 Natural orbits

We have studied the effects of the SRC on the natural orbits which are defined as those single particle wave functions forming the basis where the OBDM is diagonal:

$$\rho^t(\mathbf{r}_1, \mathbf{r}'_1) = \sum_{nlj} c_{nlj}^t \phi_{nlj}^{*t, NO}(\mathbf{r}_1) \phi_{nlj}^{t, NO}(\mathbf{r}'_1). \quad (158)$$

In the above equation the  $c_{nlj}^t$  coefficients, called occupation numbers, are real numbers. In the IPM the natural orbits correspond to the mean-field wave functions of Eq. (88), and the  $c_{nlj}^t$  numbers are 1, for the states below the Fermi surface and 0 for those above it.

In order to obtain the natural orbits we found it convenient to express the OBDM of Eq. (158) as:

$$\rho^t(\mathbf{r}_1, \mathbf{r}'_1) = A^t(\mathbf{r}_1, \mathbf{r}'_1) \rho_0^t(\mathbf{r}_1, \mathbf{r}'_1) + B^t(\mathbf{r}_1, \mathbf{r}'_1), \quad (159)$$

where  $\rho_0^t(\mathbf{r}_1, \mathbf{r}'_1)$  is the uncorrelated OBDM of Eq. (91), and the other two quantities are defined as:

$$A^t(\mathbf{r}_1, \mathbf{r}'_1) = 2C_{w,11}^t(\mathbf{r}_1)C_{w,11}^t(\mathbf{r}'_1)g_{ww}^{tt}(\mathbf{r}_1, \mathbf{r}'_1) +$$

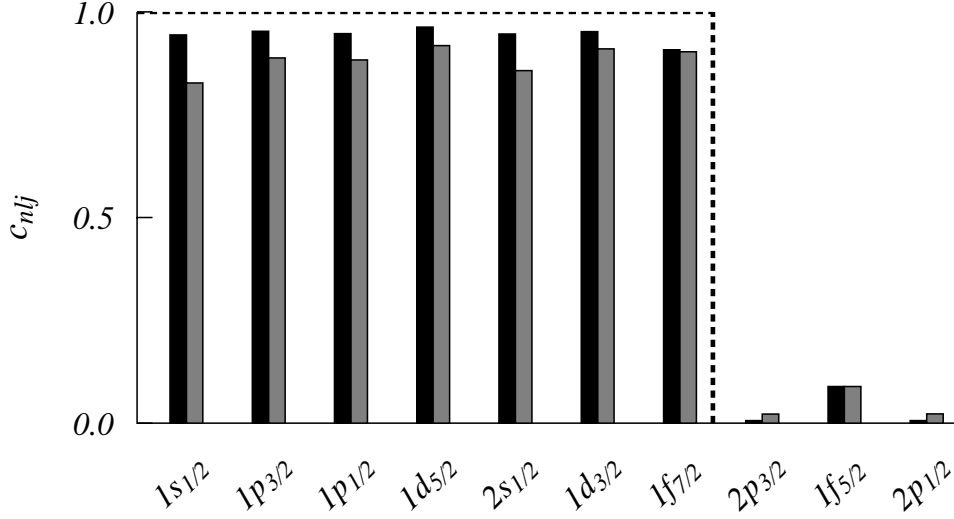


Figure 30: The same as Fig. 29 for the neutron natural orbits of the  $^{48}\text{Ca}$  nucleus.

$$\begin{aligned}
& 2C_{w,22}^t(\mathbf{r}_1)C_{w,22}^t(\mathbf{r}'_1) \sum_{p>1} A^k \Delta^k g_{ww,p}^{tt}(\mathbf{r}_1, \mathbf{r}'_1) , \\
B^t(\mathbf{r}_1, \mathbf{r}'_1) = & -2C_{w,11}^t(\mathbf{r}_1)C_{w,11}^t(\mathbf{r}'_1)g_{ww}^{tt}(\mathbf{r}_1, \mathbf{r}'_1)N_{w_c w_c}^t(\mathbf{r}_1, \mathbf{r}'_1) - \\
& 2C_{w,22}^t(\mathbf{r}_1)C_{w,22}^t(\mathbf{r}'_1) \sum_{p>1} A^k \Delta^k \left[ g_{ww,p}^{tt}(\mathbf{r}_1, \mathbf{r}'_1)N_{w_c w_c}^t(\mathbf{r}_1, \mathbf{r}'_1) + \right. \\
& \left. g_{ww}^{tt}(\mathbf{r}_1, \mathbf{r}'_1)N_{w_c w_c,p}^t(\mathbf{r}_1, \mathbf{r}'_1) \right] .
\end{aligned} \tag{160}$$

The expressions of the various FHNC/SOC quantities used in the above equations are given in Appendix B.

We expand the OBDM on a basis of spin spherical harmonics  $\mathbf{Y}_{lj}^m$  defined in Eq. (88),

$$\rho^t(\mathbf{r}_1, \mathbf{r}'_1) = \sum_{ljm} \frac{1}{2j+1} [\mathcal{A}_{lj}^t(r_1, r'_1) + \mathcal{B}_{lj}^t(r_1, r'_1)] \mathbf{Y}_{lj}^{*m}(\Omega) \mathbf{Y}_{lj}^m(\Omega') \tag{161}$$

where  $\Omega$  and  $\Omega'$  indicate the polar angles identifying  $\mathbf{r}_1$  and  $\mathbf{r}'_1$ . The explicit expressions of the  $\mathcal{A}$  and  $\mathcal{B}$  coefficients are:

$$\begin{aligned}
\mathcal{A}_{lj}^t(r_1, r'_1) = & (2l+1) \sum_{nl_1 l_2 j_2} (2l_2+1)(2j_2+1) \begin{pmatrix} l & l_1 & l_2 \\ 0 & 0 & 0 \end{pmatrix}^2 \left\{ \begin{matrix} j_2 & l_1 & j \\ l & \frac{1}{2} & l_2 \end{matrix} \right\}^2 \\
& R_{nl_2 j_2}^t(r_1) R_{nl_2 j_2}^t(r_2) A_{l_1}^t(r_1, r'_1)
\end{aligned} \tag{162}$$

with

$$A_l^t(r_1, r'_1) = \frac{2}{2l+1} \int d\Omega A^t(\mathbf{r}_1, \mathbf{r}'_1) P_l(\cos \theta_{11'}) \tag{163}$$

and

$$\mathcal{B}_{lj}^t(r_1, r'_1) = \frac{4\pi}{2l+1} \int d(\cos \theta_{11'}) B^t(\mathbf{r}_1, \mathbf{r}'_1) P_l(\cos \theta_{11'}) \tag{164}$$

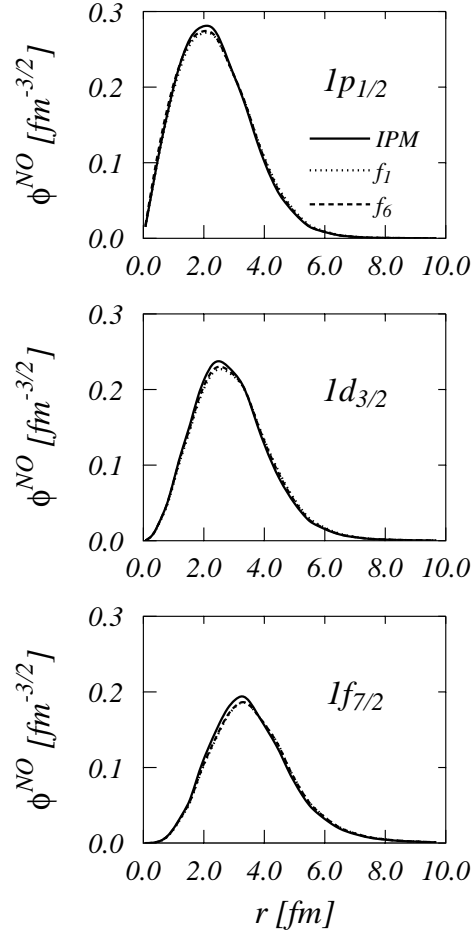


Figure 31: Natural orbits for some neutron states in  $^{48}\text{Ca}$ . The full lines indicate the IPM orbits, the dotted lines those obtained with scalar correlations only and the dashed lines those obtained with the complete operator dependent correlation.

State	$\alpha = 1$			$\alpha = 2$			$\alpha = 3$		
	$f_1$	$f_6$	PMD	$f_1$	$f_6$	PMD	$f_1$	$f_6$	PMD
$1s_{1/2}$ (p)	0.956	0.873	0.921	0.011	0.038	0.013	0.002	0.007	0.002
(n)	0.957	0.873		0.012	0.039		0.003	0.008	
$1p_{3/2}$ (p)	0.973	0.921	0.947	0.004	0.013	0.007	0.001	0.003	0.001
(n)	0.973	0.924		0.004	0.014		0.002	0.004	
$1p_{1/2}$ (p)	0.970	0.923	0.930	0.003	0.012	0.008	0.001	0.003	0.002
(n)	0.970	0.922		0.004	0.013		0.002	0.003	
$1d_{5/2}$ (p)	0.001	0.005	0.016	0.013	0.003	0.003	0.000	0.000	0.000
(n)	0.001	0.005		0.001	0.003		0.000	0.000	
$1d_{3/2}$ (p)	0.002	0.005	0.019	0.001	0.003	0.005	0.000	0.000	0.001
(n)	0.001	0.005		0.001	0.003		0.000	0.000	

Table 7: Protons (p) and neutrons (n) natural orbits occupation numbers for  $^{16}\text{O}$ . The PMD values are those of Ref. [65]. The  $f_1$  values have been obtained with scalar correlations only, and the  $f_6$  values with the complete state dependent correlation function.

In the above equations we have used the 3j and 6j Wigner symbols [42] and we have indicated with  $\theta_{11'}$  the angle between  $\mathbf{r}_1$  and  $\mathbf{r}'_{1'}$ . The term  $\mathcal{A}$  depends on both orbital and total angular momenta of the single particle,  $l$  and  $j$  respectively, and  $\mathcal{B}$  depends only on the orbital angular momentum  $l$ .

As has been done in Refs. [64] and [65] we identify the various natural orbits with a number,  $\alpha$ , ordering them with respect to the decreasing value of the occupation probability. The general behavior of our results, is analogous to that described in Ref. [64] where a system of  $^3\text{He}$  drops, composed by 70 atoms, have been studied. The orbits corresponding to states below the Fermi level in the IPM picture, have occupation numbers very close to unity for  $\alpha = 1$ , and very small in all the other cases.

As example of our results, we show in Figs. 29 and 30 the protons and neutrons occupation numbers for the natural orbits with  $\alpha = 1$  of the  $^{48}\text{Ca}$  nucleus. In the figures, the IPM results are indicated by the dashed lines. The black bars show the values obtained by using scalar correlations only, the gray bars those obtained with the complete operator dependent correlations.

The correlated occupation numbers are smaller than one for orbits below the Fermi surface, and larger than zero for those orbits above the Fermi surface. This effect is enhanced by the operator dependent correlations. We observe that for the states above the Fermi surface the gray bars are larger than the black ones, indicating that also for these states the operator dependent correlations, produce larger effects than the scalar ones.

We show in Fig. 31 some  $\alpha = 1$  natural orbits for three neutron states in  $^{48}\text{Ca}$ . In this figure, we compare the IPM results (full lines) with those obtained with scalar correlation only (dotted lines), and with the full operator dependent correlation (dashed lines). The effect of the correlations is a lowering of the peak and a small widening of the function. Despite the small effect, it is interesting to notice the inclusion of operator dependent terms diminishes the correlation effect. This fact is consistent with the results on the density distributions we have presented in Sect. 5.6.

In Tab. 7 we show the occupation numbers of the  $^{16}\text{O}$  protons and neutrons natural orbits

also for  $\alpha > 1$ , and we make a direct comparison with the results of Ref. [65]. As already said in the discussion of the  $^{48}\text{Ca}$  results, the inclusion of the state dependent correlations increases the differences with respect to the IPM. The occupation numbers of the orbits below the Fermi surface are smaller than those obtained with scalar correlations only. The situation is reversed for the orbits with  $\alpha > 1$  or above the Fermi level. For the states below the Fermi surface, our full calculations produce correlation effects slightly larger than those found in [65], whose results are closer to those we obtain with scalar correlations only. For orbits above the IPM Fermi surface, our occupation numbers are always smaller than those of Ref. [65].

## 5.9 The two-body distribution functions

We have already defined the state dependent TBDF in Eq. (101). In our FHNC/SOC computational scheme, we calculate the TBDF as:

$$\begin{aligned} \rho_2^{2k_3-1+l_3, t_1 t_2}(\mathbf{r}_1, \mathbf{r}_2) &= \frac{f_{2k_1-1+l_1}(r_{12}) f_{2k_2-1+l_2}(r_{12})}{f_1^2(r_{12})} \\ &\quad \left\{ I^{k_1 k_3 k_2} A^{k_2} \chi_{l_1+l_2+l_3}^{t_1 t_2} \rho_{2,dir}^{t_1 t_2}(\mathbf{r}_1, \mathbf{r}_2) \right. \\ &\quad + \left[ I^{k_4 k_1 k_5} I^{k_3 k_2 k_5} A^{k_5} \rho_{2,exc}^{t_1 t_2}(\mathbf{r}_1, \mathbf{r}_2) \right. \\ &\quad \left. + I^{k_4 k_1 k_5} I^{k_3 k_2 k_6} I^{k_5 k_6 2} \rho_{2,excj}^{t_1 t_2}(\mathbf{r}_1, \mathbf{r}_2) \right] \\ &\quad \left. \Delta^{k_4} \sum_{l_4=0}^1 \chi_{l_1+l_2+l_3+l_4}^{t_1 t_2} \right\} \end{aligned} \quad (165)$$

where a sum is understood on every repeated index. The FHNC/SOC quantities are defined in Appendix B.

We first discuss the case  $q = 1$  which, apart from some constant factors, gives the probability of finding a nucleon in  $\mathbf{r}_1$ , and at the same time, another nucleon in  $\mathbf{r}_2$ . The IPM two-body densities are obtained by inserting a Slater determinant in Eq. (167). For  $q = 1$  TBDF we obtain the expression:

$$\rho_{2,0}^{t_1 t_2}(\mathbf{r}_1, \mathbf{r}_2) = \rho_0^{t_1}(\mathbf{r}_1) \rho_0^{t_2}(\mathbf{r}_2) - 2\delta_{t_1 t_2} \left\{ \left[ \rho_0^{t_1}(\mathbf{r}_1, \mathbf{r}_2) \right]^2 + \left[ \rho_{0j}^{t_1}(\mathbf{r}_1, \mathbf{r}_2) \right]^2 \right\}, \quad (166)$$

where the  $\rho_{0(j)}^{t_1}(\mathbf{r}_1, \mathbf{r}_2)$  are the uncorrelated OBDs defined in Eqs. (91) and (92).

The relevant information about the TBDF is contained in the function:

$$\rho_2^{q, t_1 t_2}(r_{12}) = \int d\mathbf{R}_{12} \rho_2^{q, t_1 t_2}(\mathbf{r}_1, \mathbf{r}_2), \quad (167)$$

where  $r_{12} = |\mathbf{r}_1 - \mathbf{r}_2|$  is the relative distance and  $\mathbf{R}_{12} = (\mathbf{r}_1 + \mathbf{r}_2)/2$  the center-of-mass of the nucleonic pair.

We show in Fig. 32 the proton-proton scalar,  $q=1$ , TBDFs, Eq. (167), for all the nuclei considered as a function of the relative distance of the pair. The dotted lines represent the uncorrelated joint probability density of finding the two nucleons at a certain distance, as often given in the literature (see e.g. Ref. [66]). These lines have been obtained as a product of the uncorrelated one-body densities. This definition of the uncorrelated two-body densities

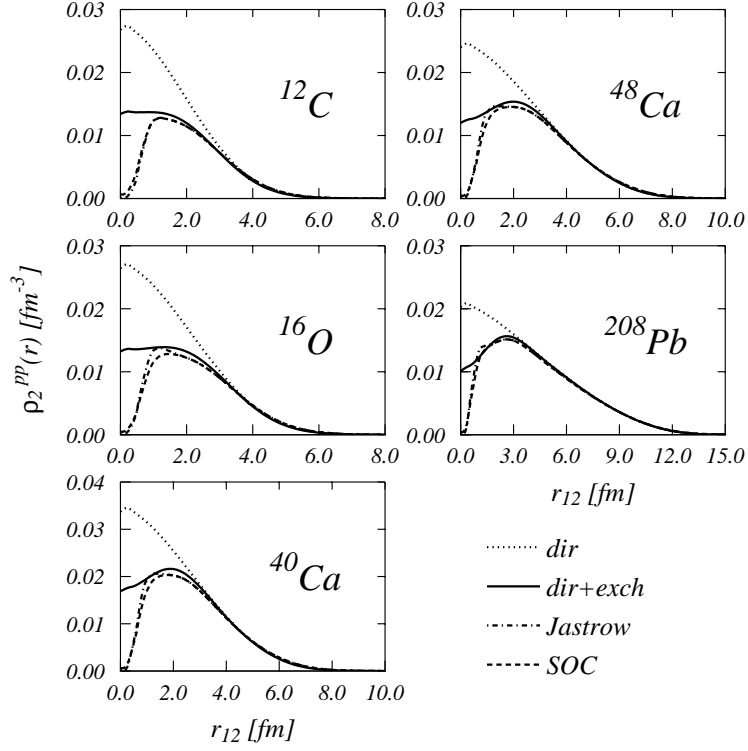


Figure 32: Proton-proton scalar (q=1) TBDFs (101) as a function of the distance between two nucleons. The dotted lines show the uncorrelated TBDF obtained as a product of two uncorrelated OBDMs. The full lines show the uncorrelated TBDF obtained by using in Eq. (101) Slater determinants. The other lines have been obtained with the scalar ( $f_1$ ) and full ( $f_6$ ) correlations.

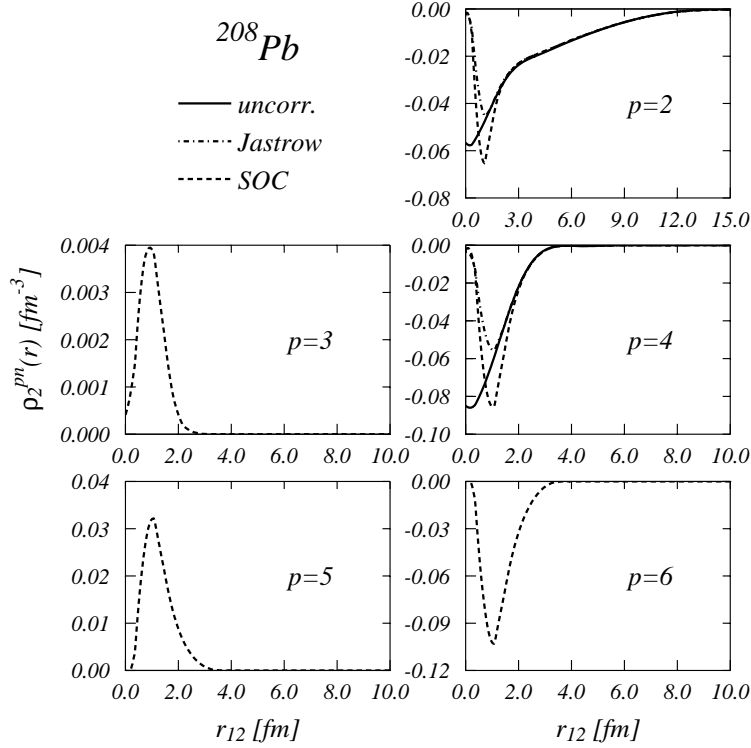


Figure 33: Proton-neutron operator dependent ( $q>1$ ) TBDFs (101) as a function of the distance between two nucleons for the  $^{208}\text{Pb}$  nucleus.

can be meaningful from the probabilistic point of view, but it is misleading in our framework, since it corresponds to using only the first, direct, term of Eq. (166). In fermionic systems the uncorrelated two-body density is given by the full expression (166) which contains also the exchange term. These complete uncorrelated TBDF are shown by the full lines. The effects of the SRC can be deduced by comparing these lines with the dashed-dotted lines obtained with the  $f_1$  scalar correlations only, and with the dashed lines showing the full FHNC/SOC results.

In all our results the correlations reduce the values of the TBDF at short internucleon distances. The exchange term of the uncorrelated density already contributes to this reduction, but the major effect is produced by the SRC, and mainly by the scalar correlations. We found similar results for the neutron-neutron TBDF. When the TBDF are composed of different particles, the results change only slightly. Beside a strong reduction at small distances, the correlations produce enhancements, with respect to the IPM results, around 2 fm, in all the nuclei considered [33].

To discuss the effects of the correlations on the other operator dependent TBDFs (101) we show in Fig. 33 the TBDFs for the  $^{208}\text{Pb}$  nucleus, for the various operators. We first notice that the tensor TBDFs,  $p = 5, 6$ , are different from zero only when the  $f_6$  correlation is used. This occurs because, in order to get a spin trace different from zero in Eq. (101), at least two-tensor operators are needed. Also the spin term  $p = 3$  differs from zero in the  $f_6$  case only. Here there are different reasons why both terms of Eq. (166) are zero. The first term is zero because of the

spin trace, while the second term vanishes because the two nucleons have different isospin.

The most remarkable feature is the range of the various TBDFs. The scalar TBDFs of Fig. 32 and the isospin TBDF of Fig. 33 extend up to relative distances comparable to the dimensions of the nucleus, 15 fm. In contrast, all the other density functions have much smaller ranges, of the order of 3-4 fm. We found similar results for all the nuclei considered [33, 53].

## 5.10 Quasi-hole wave functions and spectroscopic factors

The quasi-hole wave function is defined as:

$$\psi_{nljm}^t(x) = \frac{\sqrt{A} \langle \Psi_{nljm}^t(1, \dots, A-1) | \delta(x - x_A) P_A^t | \Psi(1, \dots, A) \rangle}{\langle \Psi_{nljm}^t | \Psi_{nljm}^t \rangle^{1/2} \langle \Psi | \Psi \rangle^{1/2}}, \quad (168)$$

where  $\Psi_{nljm}^t(1, \dots, A-1)$  and  $\Psi(1, \dots, A)$  are the states of the nuclei formed by  $A-1$  and  $A$  nucleons respectively, and  $P_A^t$  is the isospin projector. In analogy to the ansatz (2), we assume that the state of the nucleus with  $A-1$  nucleons can be described as:

$$\Psi_{nljm}^t(1, \dots, A-1) = \mathcal{F}(1, \dots, A-1) \Phi_{nljm}^t(1, \dots, A-1), \quad (169)$$

where  $\Phi_{nljm}^t(1, \dots, A-1)$  is the Slater determinant obtained by removing from  $\Phi(1, \dots, A)$  a single state characterized by the quantum numbers  $nljmt$ . For the system of  $A-1$  nucleons we use the same correlation function fixed for the system of  $A$  nucleons. In an uncorrelated system the quasi-hole wave functions coincide with the hole mean-field wave functions (88).

We are interested in the radial part of the quasi-hole wave function, which we obtain by multiplying equation (168) by the vector spherical harmonics  $\mathbf{Y}_{lj}^{*m}(\Omega)$  and, then, by integrating over the angular coordinates  $\Omega$ , and summing over  $m$ . It is useful to rewrite the radial part of the quasi-hole wave function as [32]:

$$\begin{aligned} \psi_{nlj}^t(r) &= \frac{1}{2j+1} \sum_m \int d\Omega \mathbf{Y}_{lj}^{*m}(\Omega) \psi_{nljm}^t(x) \\ &= \frac{1}{2j+1} \sum_m \mathcal{X}_{nljmt}^t(r) [\mathcal{N}_{nlj}^t]^{1/2}, \end{aligned} \quad (170)$$

where we have defined:

$$\mathcal{X}_{nljmt}^t(r) = \frac{\sqrt{A} \langle \Psi_{nljm}^t(A-1) | \mathbf{Y}_{lj}^{*m}(\Omega) \delta(\mathbf{r} - \mathbf{r}_A) P_A^t | \Psi(A) \rangle}{\langle \Psi_{nljm}^t | \Psi_{nljm}^t \rangle}, \quad (171)$$

and

$$\mathcal{N}_{nljmt}^t = \frac{\langle \Psi_{nljm}^t(1, \dots, A-1) | \Psi_{nljm}^t(1, \dots, A-1) \rangle}{\langle \Psi(1, \dots, A) | \Psi(1, \dots, A) \rangle}. \quad (172)$$

Following the procedure outlined in Ref. [32], we consider separately the cluster expansions of the two terms  $\mathcal{N}^t$  and  $\mathcal{X}^t$ . For  $\mathcal{X}^t$  we have:

$$\begin{aligned} \mathcal{X}_\alpha^t(r) &= C_{w,11}^{t,\alpha}(\mathbf{r}) \left\{ R_{nlj}^t(r) + \int d\mathbf{r}_1 R_{nlj}^t(r_1) P_l(\cos \theta) \left[ g_{wc}^{t,\alpha}(\mathbf{r}, \mathbf{r}_1) C_{d,11}^{t,\alpha}(\mathbf{r}_1) \right. \right. \\ &\quad \left. \left. + \rho_0^{t,\alpha}(\mathbf{r}, \mathbf{r}_1) - N_{cw}^{(\rho)t,\alpha}(\mathbf{r}_1, \mathbf{r}) \right] \right\} \\ &\quad + C_{w,22}^{t,\alpha}(\mathbf{r}) \int d\mathbf{r}_1 R_{nlj}^t(r_1) P_l(\cos \theta) \mathcal{X}_{SOC}^t(\mathbf{r}, \mathbf{r}_1), \end{aligned} \quad (173)$$



and for  $\mathcal{N}^t$  we obtain:

$$\begin{aligned} [\mathcal{N}_\alpha^t]^{-1} &= \int d\mathbf{r} C_{d,11}^{t,\alpha}(\mathbf{r}) \left\{ |\phi_\alpha^t(\mathbf{r})|^2 + \int d\mathbf{r}_1 \phi_\alpha^{t*}(\mathbf{r}) \phi_\alpha^t(\mathbf{r}_1) 2 \left[ g_{cc}^{t,\alpha}(\mathbf{r}, \mathbf{r}_1) C_{d,11}^{t,\alpha}(\mathbf{r}_1) \right. \right. \\ &\quad \left. \left. + \rho_0^{t,\alpha}(\mathbf{r}, \mathbf{r}_1) - N_{cc}^{(\rho)t,\alpha}(\mathbf{r}_1, \mathbf{r}) \right] \right\} \\ &\quad + \int d\mathbf{r} \phi_\alpha^{t*}(\mathbf{r}) C_{d,22}^{t,\alpha}(\mathbf{r}) \int d\mathbf{r}_1 \phi_\alpha^t(\mathbf{r}_1) \mathcal{N}_{SOC}^t(\mathbf{r}, \mathbf{r}_1) , \end{aligned} \quad (174)$$

where we have indicated with  $\alpha$  the set of the  $nljm$  quantum numbers. All the FHNC quantities have a superscript  $\alpha$  since these equations must be built by using:

$$\rho_0^{t,\alpha}(\mathbf{r}, \mathbf{r}_1) = \rho_0^t(\mathbf{r}, \mathbf{r}_1) - \phi_\alpha^{t*}(\mathbf{r}) \phi_\alpha^t(\mathbf{r}_1) , \quad (175)$$

instead of  $\rho_0^t(\mathbf{r}, \mathbf{r}_1)$ . The expressions of  $\mathcal{N}_{SOC}^t(\mathbf{r}, \mathbf{r}_1)$  and  $\mathcal{X}_{SOC}^t(\mathbf{r}, \mathbf{r}_1)$ , are:

$$\begin{aligned} \mathcal{X}_{SOC}^{t_1}(\mathbf{r}, \mathbf{r}_1) &= \sum_{k=1}^3 A^k \sum_{t_2=p,n} \left\{ (1 - \delta_{k,1}) \mathcal{X}_{2k-1,2k-1}^{t_1 t_2}(\mathbf{r}, \mathbf{r}_1) \right. \\ &\quad \left. + \chi_1^{t_1 t_2} \left[ \mathcal{X}_{2k-1,2k}^{t_1 t_2}(\mathbf{r}, \mathbf{r}_1) + \mathcal{X}_{2k,2k-1}^{t_1 t_2}(\mathbf{r}, \mathbf{r}_1) \right] \right. \\ &\quad \left. + \chi_2^{t_1 t_2} \mathcal{X}_{2k,2k}^{t_1 t_2}(\mathbf{r}, \mathbf{r}_1) \right\} , \end{aligned} \quad (176)$$

$$\begin{aligned} \mathcal{N}_{SOC}^{t_1}(\mathbf{r}, \mathbf{r}_1) &= \sum_{k=1}^3 A^k \sum_{t_2=p,n} \left\{ (1 - \delta_{k,1}) \mathcal{N}_{2k-1,2k-1}^{t_1 t_2}(\mathbf{r}, \mathbf{r}_1) \right. \\ &\quad \left. + \chi_1^{t_1 t_2} \left[ \mathcal{N}_{2k-1,2k}^{t_1 t_2}(\mathbf{r}, \mathbf{r}_1) \right. \right. \\ &\quad \left. \left. + \mathcal{X}_{2k,2k-1}^{t_1 t_2}(\mathbf{r}, \mathbf{r}_1) \right] + \chi_2^{t_1 t_2} \mathcal{N}_{2k,2k}^{t_1 t_2}(\mathbf{r}, \mathbf{r}_1) \right\} . \end{aligned} \quad (177)$$

where the indexes  $t$  refer to the isospin and the functions and we have defined:

$$\begin{aligned} \mathcal{X}_{pq}^{t_1 t_2}(\mathbf{r}, \mathbf{r}_1) &= \frac{1}{2} \left\{ h_{w,p}^{t_1 t_2, \alpha}(\mathbf{r}, \mathbf{r}_1) g_{wd}^{t_1 t_2, \alpha}(\mathbf{r}, \mathbf{r}_1) C_{d,pq}^{t_2, \alpha}(\mathbf{r}_1) \right. \\ &\quad \left[ -\rho_0^{t_2, \alpha}(\mathbf{r}, \mathbf{r}_1) + N_{wc}^{t_2, \alpha}(\mathbf{r}, \mathbf{r}_1) \right] \\ &\quad + g_{wd}^{t_1 t_2, \alpha}(\mathbf{r}, \mathbf{r}_1) C_{d,pq}^{t_2, \alpha}(\mathbf{r}_1) N_{wc,p}^{t_2, \alpha}(\mathbf{r}, \mathbf{r}_1) - \\ &\quad \left. N_{cw,p}^{(\rho)t_2, \alpha}(\mathbf{r}_1, \mathbf{r}) \right\} \Delta^{k_2} , \end{aligned} \quad (178)$$

$$\begin{aligned} \mathcal{N}_{pq}^{t_1 t_2}(\mathbf{r}, \mathbf{r}_1) &= \left\{ h_p^{t_1 t_2, \alpha}(\mathbf{r}, \mathbf{r}_1) g_{dd}^{t_1 t_2, \alpha}(\mathbf{r}, \mathbf{r}_1) C_{d,pq}^{t_2, \alpha}(\mathbf{r}_1) \right. \\ &\quad \left[ -\rho_0^{t_2, \alpha}(\mathbf{r}, \mathbf{r}_1) + N_{cc}^{t_2, \alpha}(\mathbf{r}, \mathbf{r}_1) \right] \\ &\quad \left. + g_{dd}^{t_1 t_2}(\mathbf{r}, \mathbf{r}_1) C_{d,pq}^{t_2, \alpha}(\mathbf{r}_1) N_{cc,p}^{t_2, \alpha}(\mathbf{r}, \mathbf{r}_1) - N_{cc,p}^{(\rho)t_2, \alpha}(\mathbf{r}_1, \mathbf{r}) \right\} \Delta^{k_2} , \end{aligned} \quad (179)$$

with  $q = 2k_2 - 1 + l$ . The other terms are defined in Appendix B.

The knowledge of the quasi-hole functions allows us to calculate the spectroscopic factors:

$$S_{nlj}^t = \int dr r^2 |\psi_{nlj}^t(r)|^2 . \quad (180)$$

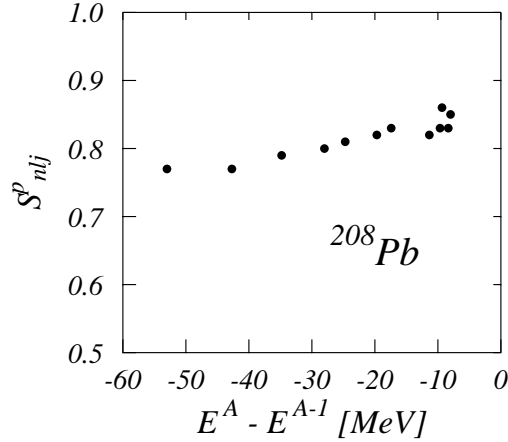


Figure 34: Protons spectroscopic factors of the  $^{208}\text{Pb}$  nucleus as a function of the separation energies.

The inclusion of the correlations produce spectroscopic factors smaller than one, the mean-field value. In general, this effect increases together with the complexity of the correlation. The  $f_6$  results are smaller than those of  $f_4$ , which are smaller than those obtained with  $f_1$ .

We found that in our calculations the effects of the correlations are larger on the internal shells [60]. This fact emerges by observing that for a fixed set of  $lj$  quantum numbers, the spectroscopic factors increases with  $n$  and at the same time, that values of the spectroscopic factors become larger when  $n$  and  $lj$  values increase. This effect is well represented in Fig. 34 where we show with the black points the proton spectroscopic factors of the  $^{208}\text{Pb}$  nucleus as a function of the separation energies, defined as the difference between the energy of the  $A$ -nucleons system and that of the correspondent  $A-1$ -nucleons system. We have associated the spectroscopic factor of each level to its empirical separation energy. The behavior of the black points of the figure indicates that, in our calculations, correlation effects are larger on the more bound levels.

In Fig. 35, as example of the correlations effects on the quasi-hole wave functions, we show the squares of the proton  $3s_{1/2}$  and neutron  $3p_{1/2}$  quasi-hole wave functions. The global effect is a lowering of the wave function in the nuclear interior, and this effect increases with increasing complexity of the correlation.

In Fig. 36 we show with a gray band the difference between the empirical charge distributions of  $^{206}\text{Pb}$  and  $^{205}\text{Tl}$  [67]. The dashed dotted line, labeled as IPM, has been obtained by using the fact that the difference between the two charge distributions can be described as a single  $3s_{1/2}$  proton hole in the core of the lead nucleus. This curve has been obtained by folding the IPM line of Fig. 35 with the electric proton form factor in its dipole form. In a slightly more elaborated picture, the ground state of the  $^{205}\text{Tl}$  is composed of the  $3s_{1/2}$  proton hole in the  $^{206}\text{Pb}$  ground state, plus the coupling of the  $2d_{5/2}$  and  $2d_{3/2}$  protons levels with the first  $2^+$  excited state of  $^{206}\text{Pb}$  [68, 69]. This description of the  $^{205}\text{Tl}$ , charge distribution, labeled IPM\*, and shown by the dotted line, is still in a IPM framework. The dashed line has been obtained by adding to the dotted line the core polarization effects produced by long-range correlations.

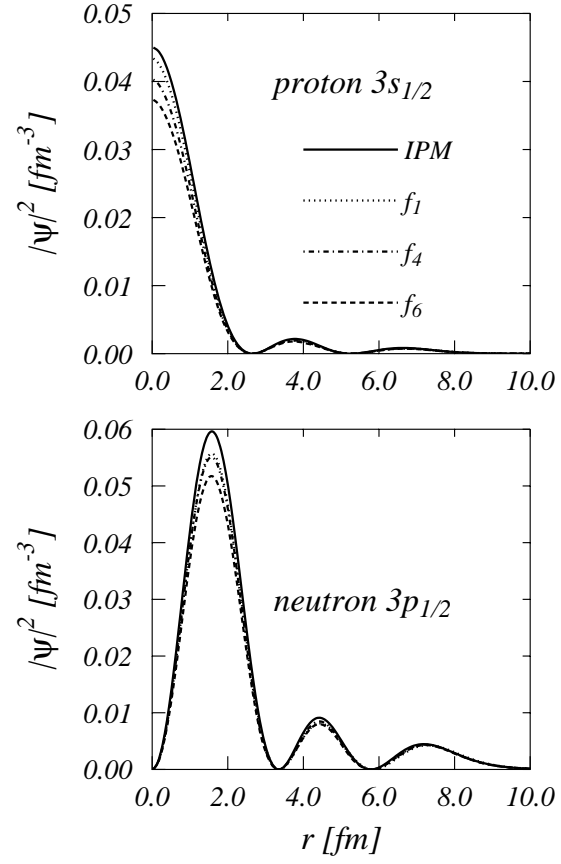


Figure 35: Square of the  $^{208}\text{Pb}$  proton  $3s_{1/2}$  and neutron  $3p_{1/2}$  quasi-hole functions. The various lines show the results obtained by using different type of correlations.

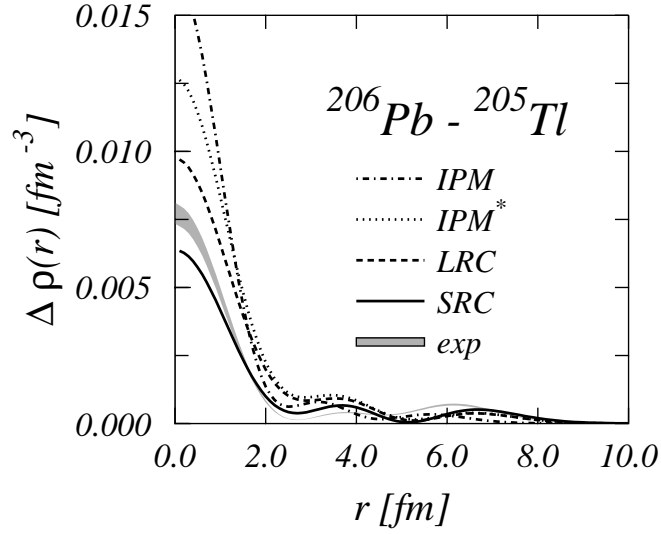


Figure 36: Differences between charge density distributions of  $^{206}\text{Pb}$  and  $^{205}\text{Tl}$ . See the text for the explanation of the various lines.

These effects have been calculated by following the Random Phase Approximation approach of Refs. [70, 71]. The full line has been obtained when our SRC effects are also included.

The various effects presented in Fig. 36 have been obtained in different theoretical frameworks, and the final result does not have any pretense of being a well grounded and coherent description of the empirical charge differences. The point we want to make by showing this figure is that the effects of the SRC are of the same order of magnitude as those commonly considered in nuclear structure calculations.

## 6 Perspectives

In this section we give a short review of the possible developments of the theory. We present only those topics which have been already formulated. Some of these subjects have been already well studied in nuclear matter, and the work to be done consists in adapting the formulation to the case of finite nuclei. Other topics are still at the level of a very abstract general formulation, valid for any kind of many-body systems. We first present some possible applications of the theory, which do not require changes in its basic hypotheses. Then, we discuss some extensions of the theory.

The main goal of the RFHNC/SOC equations is the evaluation of the hamiltonian expectation value, in order to apply the variational principle. Once the parameters of the correlation function and of the mean-field potential which minimize the energy functional, Eq. (1), have been found, it is relatively straightforward to apply the RFHNC/SOC equations to evaluate expectation values of other operators. This is the strategy used in Sect. 5, to calculate all the quantities other than the energy.

So far our approach is aimed at the description of the nuclear ground state, therefore we can only obtain expectation values of ground state observables. On the other hand, a clever use of completeness relations allows us to get information on excited states by calculating expectation values of operators between ground states. This is, for example, the case of the sum rules. The enhancement factor of the electric-dipole sum rule has been calculated in nuclear matter [72], and the same approach can be applied to finite nuclei.

Dynamical response functions and hole spectral functions have been calculated in nuclear matter by using the FHNC/SOC formalism [23, 73, 74, 75]. The responses of the system for a momentum transfer  $\mathbf{q}$  and an excitation energy  $\omega$  have been evaluated by using the expression [76]:

$$S(\mathbf{q}, \omega) = \frac{1}{\pi} \text{Im} \left( \langle \Psi_0 | \frac{\rho^\dagger(\mathbf{q})\rho(\mathbf{q})}{H - E_0 - \omega - i\eta} | \Psi_0 \rangle \langle \Psi_0 | \Psi_0 \rangle^{-1} \right), \quad (181)$$

where  $\Psi_0$  and  $E_0$  are the ground state wave function and energy respectively,  $H$  the nuclear hamiltonian and  $\rho$  the external operator exciting the system. Analogous expressions have been used to calculate the spectral functions. Also in this case the completeness of the excited states has been used, and the response is expressed as the ground state expectation value of an operator. Formally, the cluster expansion and the RFHNC/SOC resummation techniques can be applied without any major problems to evaluate these expectation values. However, from the pragmatical point of view, we have to consider that the expression of the global operator is extremely involved, as is shown by Eq. (181). This global operator combines the operator describing the effect of the external probe, usually a relatively simple one-body operator, with the hamiltonian (123) composed by one- two- and three-body terms. The effort will be rewarded by the results, since the evaluation of the response functions gives direct access to the calculation of the cross sections, and of other observables.

The RFHNC/SOC theory can be applied to describe hypernuclei by considering the hyperon as an impurity in the nucleonic fluid. The FHNC equations for an impurity in homogeneous matter have been derived in Refs. [77, 78] to describe the presence of atomic  $^4\text{He}$  in liquid  $^3\text{He}$ . A first application of this theory to the case of single  $\Lambda$  hypernuclei has been done in Ref. [79]. In these calculations we used simple interactions and correlations. The nucleon-nucleon interaction contained only the first four central channels, and the  $\Lambda$ -nucleon interaction the scalar and spin

channels only. All the correlations were purely scalar functions.

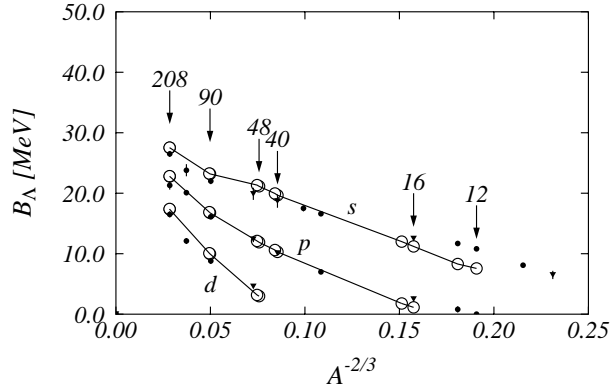


Figure 37: Binding energy of the  $\Lambda$  hyperon for the  $1s$ ,  $1p$  and  $1d$  states as a function of  $A^{-2/3}$ . The white circles are the energies calculated as indicated in Ref. [79] by using a Woods-Saxon mean-field well for the hyperon. The experimental energies are from Ref. [80] (triangles) and [81] (squares). The full lines connecting the theoretical values have been drawn to guide the eye.

Despite the simple ingredients used in the calculations, the agreement with the experimental  $\Lambda$  binding energies of Refs. [80, 81] is rather good, as is seen in Fig. 37. The extension of the formalism of Ref. [79] to the case of operator dependent correlations, which allows us to deal with realistic hamiltonians, is technically rather involved. On the other hand, the results of Fig. 37 are very encouraging and the potentialities of our technology to make predictions are wide, and rather unique.

In the introduction, we have mentioned that our approach is the lowest order approximation of the CBF theory formulated at the beginning of the '60s [82, 83, 84]. The starting point of the CBF theory is the construction of a basis of normalized, but in general non-orthogonal, state vectors of the type:

$$|\Psi_m(1, \dots, A)\rangle = \frac{F(1, \dots, A)|\Phi_m(1, \dots, A)\rangle}{\langle \Phi_m | F^\dagger F | \Phi_m \rangle^{1/2}}, \quad (182)$$

where  $F$  is the many-body correlation function acting on a complete orthonormal set of model states  $|\Phi_m\rangle$ . The CBF theory constructs a coherent perturbation theory on the correlated basis formed by the states given by Eq. (182), [13]. In the limit  $F \rightarrow 1$  the application of the variational principle would provide the Hartree-Fock equations, and the excited states (182) would be constructed as particle-hole excitations of the single particle basis. The so-called residual interaction would mix these single particle excitations in a perturbative expansion. It appears evident how our calculations, based on the application of the variational principle (1), can be considered, in the CBF framework, as the first step of a perturbation expansion. This first step is necessary to fix the correlation function  $F$  and the wave functions basis.

An improvement of our work consists in the inclusion of higher-order perturbative terms in the CBF expansion. This has already been done for nuclear matter, where perturbative corrections to the binding energy [85], momentum distributions [22], responses [23, 74, 75], and

spectral functions [73, 86], have been evaluated. With the help of the perturbative expansion, the nucleon-self energy in nuclear matter has also been calculated and the optical potential has been evaluated [87, 85].

The use of the CBF theory allows the description of nuclear excited states. In this respect, they can be treated within the correlated Random Phase Approximation theory, whose basic equations have been obtained by using a time-dependent Hartee-Fock approach [88, 89, 90, 13].

Another line of development of our theory consists in modifying the Jastrow ansatz (3). For example, correlation functions composed of scalar Jastrow function and linear state-dependent correlations have been proposed in Ref. [41]. These correlations have been applied to the description of light nuclei using Variational Monte Carlo techniques with promising results [91, 92]. With linear state-dependent correlations, the structure of our RFHNC equations becomes simpler. However, this approach has serious drawbacks, since it requires the use of up to six-body distribution functions.

The developments described so far are thought to be applied to doubly closed shell nuclei. The description of other nuclei is related to a change of the single particle basis, which should consider open shell and deformations. Also in this case, there are no problems in principal in applying our theory, but the technicalities are rather involved.

## 7 Closing remarks

The theory we have presented aims to describe the properties of medium-heavy nuclei by solving the many-body Schrödinger equation with microscopic nucleon-nucleon interactions. This is an *ab initio* calculation, since there are no free parameters to be adjusted. However, the technique of solving the many-body Schrödinger equation requires some approximations.

The most basic approximation is related to the use of the variational principle. The search for the minimum of the energy functional, Eq. (1), is done by spanning the space of many-body wave functions which can be expressed as a product of a correlation function times an independent particle model wave function, see Eq. (2). The many-body correlation function is expressed as a product of two-body correlation functions which hinder two nucleons from approaching each other for distances smaller than the range of the strongly repulsive core of the nucleon-nucleon interaction. The use of the ansatz (2) allows an explicit treatment of a great number of correlations. However, these are not all the possible correlations, and they are specifically related to the strongly repulsive core of the interaction. Other types of correlations, such as those produced by collective motions of the nucleons, are not so well described. Since this is the starting hypothesis of the theory, we cannot test its validity within the theory itself. The only possibility of making this test, is a comparison of our results with those obtained by other microscopic theories which are approximation free, such as Quantum Monte Carlo calculations. The validity of the variational ansatz has been tested in the literature by comparing Variational Monte Carlo and Quantum Monte Carlo results for light nuclei. This comparison, done for nuclei with  $A < 8$ , indicates a minimum difference of 0.1 MeV per nucleon in  $^4\text{He}$  and a maximum one of about 1.0 MeV per nucleon in  $^8\text{Li}$  [93]. Hence, this difference seems to increase with the number of nucleons.

The evaluation of the variational energy functional (1) in Ref. [93] is done with a Monte Carlo integration technique, i. e. without approximation. In our approach we calculate the energy functional by doing a cluster expansion. After a topological analysis of the various diagrams, we sum two categories of diagrams, the nodal and the composite ones, in closed form, by solving the RFHNC integral equations. The procedure we have used does not consider a certain type of diagrams, the elementary ones. This is another approximation of our computational scheme. The role of the elementary diagrams has been studied in quantum liquids and in nuclear matter, and they have been found to be more important in the former systems than in the latter ones. This is because, in many-body jargon, liquid helium is denser than nuclear matter. This means that the number of particles in a volume characterized by the range of the repulsive core of the interaction, is larger in liquid helium than in nuclear matter.

We have calculated in Ref. [27] the contribution of the elementary diagram of Fig. 8, the simplest one. The calculation has been done for a simple interaction, the B1 force of Brink and Boeker [94], with scalar correlations and in model nuclei with isospin degeneracy and single particle wave functions treated in the *ls* coupling scheme. We obtained for  $^{16}\text{O}$  and  $^{40}\text{Ca}$  a repulsive contribution of about 1.1 MeV per nucleon. This is about 2% of the contribution of the potential energy produced by the interaction. However, the total energy is obtained as a difference between kinetic and potential energies, and, in this case, 1 MeV is not negligible. The contribution of the elementary diagrams should be further investigated.

The third approximation of our computational scheme is the SOC. It is clear that the *ad hoc* SOC approximation breaks the formal completeness of the FHNC theory which holds when only scalar correlations are used. We have difficulties in making estimates of the contribution to



the energy of the diagrams excluded by the SOC approximation. We can only say that the sum rules exhaustions are slightly worsened when the SOC approximation is used. We are talking in any case of few parts on a thousand. On the other hand, we cannot exclude that the diagrams not considered are irrelevant for the sum rules, but not totally negligible for the calculation of the energy.

The three approximations just discussed are somehow intrinsic to the computational scheme. We now talk about the simplifications we have done in the specific applications of the RFHNC/SOC formalism. In our calculation we have used a nucleon-nucleon interaction limited to the first eight channels. Modern interactions, with isospin symmetry breaking terms, have up to eighteen channels. Our correlation functions are also limited to the first six channels. We have estimated the contribution of these missing terms of the interaction and of the correlation by doing a bold extrapolation of nuclear matter results. The results of this estimate are shown in Tab. 8. The contribution of the neglected channels is small when compared with the contribution of the interaction term,  $v_{2-body}^6$  in Tab. 5. However, since the energy is obtained by a subtracting potential energy to the kinetic one, their contribution is not negligible on the final result.

	$^{12}\text{C}$	$^{16}\text{O}$	$^{40}\text{Ca}$	$^{48}\text{Ca}$	$^{208}\text{Pb}$
$\langle k_F \rangle$	1.09	1.09	1.19	1.19	1.21
$E$	-0.91	-4.48	-4.58	-4.14	-3.43
$\Delta E$	-0.93	-0.93	-1.37	-1.37	-1.48
$E+\Delta E$	-1.84	-5.41	-5.95	-5.51	-4.91

Table 8: Average Fermi momenta  $\langle k_F \rangle$ , in  $\text{fm}^{-1}$ , used to estimate the corrections to the binding energies produced by the interaction channels beyond the spin-orbit ones, from nuclear matter calculations. All the energy values are expressed in MeV. The  $E$  rows gives the results of Tab. 5 for the AV8'+UIX interaction. The  $\Delta E$  rows values have been obtained by doing a local density approximation interpolation of the nuclear matter results given in Tab. III of Ref. [31].

Our minimization procedure has been done on two parameters only, the healing distance for all the central correlation channels, and that of the two tensor correlations. In principle, our model could handle six variational parameters for the correlation, plus other thirteen describing the mean field Woods-Saxon potential generating protons and neutrons single particle states. The choice of using only two variational parameters, dictated mainly by computational reasons, could seem rather limiting. In reality, we are confident that our minima are rather close to the minima that a full minimization with all the variational parameters could obtain. Concerning the correlations, there is a nuclear matter experience [21] indicating that the four central correlations heal at the same distance, noticeably different from the tensor healing distance. We have done some calculations in  $^{40}\text{Ca}$  by changing the healing distances of all the correlations, and we did not find significant improvements of the energy value. The case of the single particle basis has been discussed with some detail in Sect. 5.2. Also in this case, we have tested that, when the minimization on the correlation function has been done, even large changes of the mean-field potential do not produce sensitive changes in the energy minimum.

At present, the most evident problem of our calculations is related to the behavior of the three-body force. In few body and light nuclei the contribution of this part of the hamiltonian is attractive, while in our calculations it is repulsive. This happens also in variational nuclear

matter calculations [24, 25]. There are two possible solution of the puzzle. The one which should be explored first, is that our present treatment of the three-body force is not accurate enough. For example, we could find that the set of diagrams we are now considering, see Sect. 4.3, is not sufficient, or that the inclusion of a three-nucleon correlation function is necessary. If after improving the description of the three-body force, its contribution remains repulsive, we have to deduce that the three-body interactions we use, are tailored to provide good descriptions of few body systems and light nuclei, but they are not adequate for medium, heavy and infinite nuclear systems.

The three-body force puzzle, is an example of the potentiality of our approach, and, in general, of all the microscopic calculations, in nuclear structure. These calculations allows us to investigate phenomena that mean-field based effective theories cannot study. We have pointed out a few examples, by showing the effects of the SRC on momentum distributions, natural orbits, quasi-hole wave functions and spectroscopic factors. But the relevance of microscopic calculations goes beyond that, since these calculations have reached such an accuracy to put constraints on the nuclear hamiltonian itself. Microscopic nuclear structure calculations will become more and more important in the near future, and, among them, the RFHNC/SOC computational scheme will play a relevant role.

## Final note

We had just started to write this article, when Adelchi Fabrocini passed away. The reader who had the privilege of knowing him is certainly aware of the absence of his touch in the writing of this article. Adelchi's contribution to the realization of the work presented here, has been enormous and fundamental. We miss his talent, his leadership, his experience and, not least, his subtle sense of humor.

## Acknowledgments

We thank S. Fantoni who triggered the idea of the project and, with us, started the work. We thank P. Folgarait and I. E. Lagaris for their contributions in the early stages of the work. A special thank to P. Rotelli whose careful, and critical, reading of the manuscript helped us a lot in improving the presentation. This work has been partially supported by the agreement INFN-CICYT, by the Spanish Ministerio de Educación y Ciencia (FIS2005-02145) and by the MURST through the PRIN *Teoria della struttura nucleare e della materia nucleare*.

## A Matrices of the spin and isospin traces

In this appendix we give the numerical values of the various matrices used to calculate the spin and isospin traces, when state dependent correlations are used.

$p$	1	2	3	4	5	6
$\Gamma^p$	1	1	1	1	0	0

Table 9: The values of  $\Gamma^p$  defined in Eq. (58). The values of  $p$  indicate the operator channel.

$p$	1	2	3	4	5	6
$B^p$	1	3	3	9	6	18

Table 10: The values of  $B^p$  defined in Eq. (62).

$K^{pqr}$		q												
	p	1	2	3	4	5	6		1	2	3	4	5	6
r=1	1	1	0	0	0	0	0	r=2	0	1	0	0	0	0
	2	0	3	0	0	0	0		1	-2	0	0	0	0
	3	0	0	3	0	0	0		0	0	0	3	0	0
	4	0	0	0	9	0	0		0	0	3	-6	0	0
	5	0	0	0	0	6	0		0	0	0	0	0	6
	6	0	0	0	0	0	18		0	0	0	0	6	-12
r=3	1	0	0	1	0	0	0	r=4	0	0	0	1	0	0
	2	0	0	0	3	0	0		0	0	1	-2	0	0
	3	1	0	-2	0	0	0		0	1	0	-2	0	0
	4	0	3	0	-6	0	0		1	-2	-2	4	0	0
	5	0	0	0	0	2	0		0	0	0	0	0	2
	6	0	0	0	0	0	6		0	0	0	0	2	-4
r=5	1	0	0	0	0	1	0	r=6	0	0	0	0	0	1
	2	0	0	0	0	0	3		0	0	0	0	1	-2
	3	0	0	0	0	1	0		0	0	0	0	0	1
	4	0	0	0	0	0	3		0	0	0	0	1	-2
	5	1	0	1	0	-2	0		0	1	0	1	0	-2
	6	0	3	0	3	0	-6		1	-2	1	-2	-2	4

Table 11: The values of the matrix  $K^{pqr}$  defined in Eq. (63). The values of  $p, q$  and  $r$  indicate the operator channel.

$L^{pqr}$		q												
	p	1	2	3	4	5	6		1	2	3	4	5	6
r=1	1	1	0	0	0	0	0	r=2	0	3	0	0	0	0
	2	0	3	0	0	0	0		3	6	0	0	0	0
	3	0	0	3	0	0	0		0	0	0	9	0	0
	4	0	0	0	9	0	0		0	0	9	18	0	0
	5	0	0	0	0	6	0		0	0	0	0	0	18
	6	0	0	0	0	0	18		0	0	0	0	18	36
r=3	1	0	0	3	0	0	0	r=4	0	0	0	9	0	0
	2	0	0	0	9	0	0		0	0	9	18	0	0
	3	3	0	6	0	0	0		0	9	0	18	0	0
	4	0	9	0	18	0	0		9	18	18	36	0	0
	5	0	0	0	0	-6	0		0	0	0	0	0	-18
	6	0	0	0	0	0	-18		0	0	0	0	-18	-36
r=5	1	0	0	0	0	6	0	r=6	0	0	0	0	0	18
	2	0	0	0	0	0	18		0	0	0	0	18	36
	3	0	0	0	0	-6	0		0	0	0	0	0	-18
	4	0	0	0	0	0	-18		0	0	0	0	-18	-36
	5	6	0	-6	0	12	0		0	18	0	-18	0	36
	6	0	18	0	-18	0	36		18	36	-18	-36	36	72

Table 12: The values of the matrix  $L^{pqr}$  defined in Eq. (67). The values of  $p, q$  and  $r$  indicate the operator channel.

p		q					
q		1	2	3	4	5	6
1		0	0	0	0	0	0
2		0	$-\frac{4}{3}$	0	$-\frac{4}{3}$	0	$-\frac{4}{3}$
3		0	0	$-\frac{4}{3}$	$-\frac{4}{3}$	$-\frac{4}{3}$	$-\frac{4}{3}$
4		0	$-\frac{4}{3}$	$-\frac{4}{3}$	$-\frac{8}{3}$	$-\frac{4}{3}$	$-\frac{8}{3}$
5		0	0	$-\frac{4}{3}$	$-\frac{4}{3}$	$-\frac{4}{3}$	$-\frac{4}{3}$
6		0	$-\frac{4}{3}$	$-\frac{4}{3}$	$-\frac{8}{3}$	$-\frac{4}{3}$	$-\frac{8}{3}$

Table 13: The values of the matrix  $E_{pq}$  defined in Eq. (69).

## B The RFHNC/SOC equations for nuclear finite systems

We present here the set of RFHNC equations for finite nuclear systems with different number of protons and neutrons, and in a  $jj$  coupling scheme. The upper index  $t$  distinguishes the contributions of protons and neutrons. In this appendix, in addition to the terms necessary to calculate the one- and two-body density functions, which are used for the evaluation of the energy of the system, we present also those terms which are required in the evaluation of the OBDM, necessary ingredients for the calculation of the momentum distribution.

We show the expressions of the various parts necessary to build the one- and two-body density functions used in the calculation of the energy of the nucleus, and also those parts required to obtain the OBDM necessary for the momentum distribution evaluation.

The various terms can be written in general as  $Y_{mn}^{t_i t_j}(\mathbf{r}_i, \mathbf{r}_j)$ . An important simplification in the writing of the equations is the property:

$$Y_{mn}^{t_i t_j}(\mathbf{r}_i, \mathbf{r}_j) = Y_{nm}^{t_j t_i}(\mathbf{r}_j, \mathbf{r}_i) . \quad (183)$$

We present first the set of RFHNC equations for the scalar part of the correlation  $f_1$ , and, in a second step, the equations involving operator dependent correlations, i.e. the RFHNC/SOC equations.

We start our presentation by considering the dynamical diagrams, i.e. those where the external points are reached only by dynamical correlations. We used two types of dynamical correlations,  $h_d = f_1^2 - 1$ , and  $h_w = f_1 - 1$ . This last correlation appears in the calculation of the OBDM, where it connects only the external points. The dynamical TBDFs can be written as:

$$g_{dd}^{t_1 t_2}(\mathbf{r}_1, \mathbf{r}_2) = f_1^2(r_{12}) \exp \left[ N_{dd}^{t_1 t_2}(\mathbf{r}_1, \mathbf{r}_2) + E_{dd}^{t_1 t_2}(\mathbf{r}_1, \mathbf{r}_2) \right] , \quad (184)$$

$$g_{wd}^{t_1 t_2}(\mathbf{r}_1, \mathbf{r}_2) = f_1(r_{12}) \exp \left[ N_{wd}^{t_1 t_2}(\mathbf{r}_1, \mathbf{r}_2) + E_{wd}^{t_1 t_2}(\mathbf{r}_1, \mathbf{r}_2) \right] , \quad (185)$$

$$g_{ww}^{t_1 t_2}(\mathbf{r}_1, \mathbf{r}_2) = \exp \left[ N_{ww}^{t_1 t_2}(\mathbf{r}_1, \mathbf{r}_2) + E_{ww}^{t_1 t_2}(\mathbf{r}_1, \mathbf{r}_2) \right] . \quad (186)$$

These distribution functions are related to the non-nodal diagrams  $X^{t_1 t_2}$  by the equation:

$$g_{mn}^{t_1 t_2}(\mathbf{r}_1, \mathbf{r}_2) = 1 + N_{mn}^{t_1 t_2}(\mathbf{r}_1, \mathbf{r}_2) + X_{mn}^{t_1 t_2}(\mathbf{r}_1, \mathbf{r}_2) , \quad (187)$$

with  $m, n = d, w$ . In the presence of purely scalar correlation functions, the dynamical functions do not depend on the isospin of the external particles. However, in the above equations, we wrote the explicit isospin dependence in view of the treatment with the state dependent correlations.

The next step is to consider the case when the dynamical correlations link only one external point, let's say point 1, while the other point is reached by the statistical correlations, forming an exchange loop. In this case, the functions to be considered are:

$$\begin{aligned} g_{me}^{t_1 t_2}(\mathbf{r}_1, \mathbf{r}_2) &= g_{md}^{t_1 t_2}(\mathbf{r}_1, \mathbf{r}_2) \left[ N_{me}^{t_1 t_2}(\mathbf{r}_1, \mathbf{r}_2) + E_{me}^{t_1 t_2}(\mathbf{r}_1, \mathbf{r}_2) \right] \\ &= N_{me}^{t_1 t_2}(\mathbf{r}_1, \mathbf{r}_2) + X_{me}^{t_1 t_2}(\mathbf{r}_1, \mathbf{r}_2) , \end{aligned} \quad (188)$$

with  $m = d, w$ .

In the case when both the two external points are reached by exchange loops, the equations are:

$$\begin{aligned} g_{ee}^{t_1 t_2}(\mathbf{r}_1, \mathbf{r}_2) &= g_{ee,dir}^{t_1 t_2}(\mathbf{r}_1, \mathbf{r}_2) + 2\delta_{t_1 t_2} g_{ee,exc}^{t_1 t_2}(\mathbf{r}_1, \mathbf{r}_2) + 2\delta_{t_1 t_2} g_{ee,excj}^{t_1 t_2}(\mathbf{r}_1, \mathbf{r}_2) \\ &= N_{ee}^{t_1 t_2}(\mathbf{r}_1, \mathbf{r}_2) + X_{ee}^{t_1 t_2}(\mathbf{r}_1, \mathbf{r}_2), \end{aligned} \quad (189)$$

$$\begin{aligned} g_{ee,dir}^{t_1 t_2}(\mathbf{r}_1, \mathbf{r}_2) &= g_{dd}^{t_1 t_2}(\mathbf{r}_1, \mathbf{r}_2) \left[ N_{ee}^{t_1 t_2}(\mathbf{r}_1, \mathbf{r}_2) + E_{ee,dir}^{t_1 t_2}(\mathbf{r}_1, \mathbf{r}_2) \right. \\ &\quad + \left( N_{ed}^{t_1 t_2}(\mathbf{r}_1, \mathbf{r}_2) + E_{ed}^{t_1 t_2}(\mathbf{r}_1, \mathbf{r}_2) \right) \\ &\quad \left. \left( N_{de}^{t_1 t_2}(\mathbf{r}_1, \mathbf{r}_2) + E_{de}^{t_1 t_2}(\mathbf{r}_1, \mathbf{r}_2) \right) \right], \end{aligned} \quad (190)$$

$$\begin{aligned} g_{ee,exc}^{t_1 t_2}(\mathbf{r}_1, \mathbf{r}_2) &= g_{dd}^{t_1 t_2}(\mathbf{r}_1, \mathbf{r}_2) \left[ E_{ee,exc}^{t_1 t_2}(\mathbf{r}_1, \mathbf{r}_2) \right. \\ &\quad - \left( N_{cc}^{t_1}(\mathbf{r}_1, \mathbf{r}_2) + E_{cc}^{t_1}(\mathbf{r}_1, \mathbf{r}_2) - \rho_0^{t_1}(\mathbf{r}_1, \mathbf{r}_2) \right) \\ &\quad \left. \left( N_{cc}^{t_2}(\mathbf{r}_1, \mathbf{r}_2) + E_{cc}^{t_2}(\mathbf{r}_1, \mathbf{r}_2) - \rho_0^{t_2}(\mathbf{r}_1, \mathbf{r}_2) \right) \right], \end{aligned} \quad (191)$$

$$\begin{aligned} g_{ee,excj}^{t_1 t_2}(\mathbf{r}_1, \mathbf{r}_2) &= g_{dd}^{t_1 t_2}(\mathbf{r}_1, \mathbf{r}_2) \left[ E_{ee,excj}^{t_1 t_2}(\mathbf{r}_1, \mathbf{r}_2) \right. \\ &\quad - \left( N_{ccj}^{t_1}(\mathbf{r}_1, \mathbf{r}_2) + E_{ccj}^{t_1}(\mathbf{r}_1, \mathbf{r}_2) - \rho_{0j}^{t_1}(\mathbf{r}_1, \mathbf{r}_2) \right) \\ &\quad \left. \left( N_{ccj}^{t_2}(\mathbf{r}_1, \mathbf{r}_2) + E_{ccj}^{t_2}(\mathbf{r}_1, \mathbf{r}_2) - \rho_{0j}^{t_2}(\mathbf{r}_1, \mathbf{r}_2) \right) \right], \end{aligned} \quad (192)$$

In the above expression the subindex *dir* denotes the case when the two external particles are linked to different statistical loops, and *exc(j)* when they are connected to the same loop. In this last case, a spin-isospin exchange operator is present, whose trace in the isospin space is  $2\delta_{t_1 t_2}$ . In the *exc(j)* case, we further distinguish the parallel spin case, *exc*, from the antiparallel one, *excj*.

Finally, in the construction of the exchange parts, we have to introduce the contribution of diagrams with open statistical loops. These open loops appear in both the calculation of the energy and of the OBDM. We have to distinguish, also in this situation, the case where the external particles have parallel or antiparallel spins. In either case, the exchange loops may be combined with the two kinds of dynamical correlations, therefore we define:

$$\begin{aligned} g_{cc(j)}^{t_1}(\mathbf{r}_1, \mathbf{r}_2) &= g_{dd}^{t_1 t_1}(\mathbf{r}_1, \mathbf{r}_2) \\ &\quad \left[ N_{cc(j)}^{t_1}(\mathbf{r}_1, \mathbf{r}_2) + E_{cc(j)}^{t_1}(\mathbf{r}_1, \mathbf{r}_2) - \rho_{0(j)}^{t_1}(\mathbf{r}_1, \mathbf{r}_2) \right], \end{aligned} \quad (193)$$

$$\begin{aligned} g_{w_c c(j)}^{t_1}(\mathbf{r}_1, \mathbf{r}_2) &= g_{wd}^{t_1 t_1}(\mathbf{r}_1, \mathbf{r}_2) \\ &\quad \left[ N_{w_c c(j)}^{t_1}(\mathbf{r}_1, \mathbf{r}_2) + E_{w_c c(j)}^{t_1}(\mathbf{r}_1, \mathbf{r}_2) - \rho_{0(j)}^{t_1}(\mathbf{r}_1, \mathbf{r}_2) \right], \end{aligned} \quad (194)$$

$$\begin{aligned} g_{w_c w_c(j)}^{t_1}(\mathbf{r}_1, \mathbf{r}_2) &= g_{ww}^{t_1 t_1}(\mathbf{r}_1, \mathbf{r}_2) \\ &\quad \left[ N_{w_c w_c(j)}^{t_1}(\mathbf{r}_1, \mathbf{r}_2) + E_{w_c w_c(j)}^{t_1}(\mathbf{r}_1, \mathbf{r}_2) - \rho_{0(j)}^{t_1}(\mathbf{r}_1, \mathbf{r}_2) \right], \end{aligned} \quad (195)$$

where with  $(j)$  we have indicated the possible presence of the label  $j$ . For all these six partial distribution functions we can write:

$$g_{mn(j)}^{t_1}(\mathbf{r}_1, \mathbf{r}_2) = N_{mn(j)}^{t_1}(\mathbf{r}_1, \mathbf{r}_2) + X_{mn(j)}^{t_1}(\mathbf{r}_1, \mathbf{r}_2) - \rho_{0(j)}^{t_1}(\mathbf{r}_1, \mathbf{r}_2). \quad (196)$$

The RFHNC expressions of all the nodal diagrams which do not have open statistical loops, can be written in a compact form as:

$$N_{mn}^{t_1 t_2}(\mathbf{r}_1, \mathbf{r}_2) = \sum_{t_3=p,n} \sum_{m'n'} \left( X_{mm'}^{t_1 t_3}(\mathbf{r}_1, \mathbf{r}_3) V_{m'n'}^{t_3}(\mathbf{r}_3) \left| N_{n'n}^{t_3 t_2}(\mathbf{r}_3, \mathbf{r}_2) + X_{n'n}^{t_3 t_2}(\mathbf{r}_3, \mathbf{r}_2) \right. \right), \quad (197)$$

where  $m, n = d, w, e$ . In the previous equation, due to the diagrammatic rules, the sums are limited to the values  $(m'n') = dd, de, ed$ . Furthermore we have defined:

$$V_{mn}^{t_3}(i) = \begin{cases} C^{t_3}(i) & \text{for } (mn) = dd \\ C_d^{t_3}(i) & \text{otherwise} \end{cases}. \quad (198)$$

The expressions of the nodal diagrams with open statistical loops in the external particles, such as the diagrams of Fig. 14, follow the classification presented in Eq. (104):

$$\begin{aligned} N_{mn}^{(x)t_1}(\mathbf{r}_1, \mathbf{r}_2) &= \left( X_{mc}^{t_1}(\mathbf{r}_1, \mathbf{r}_3) C_d^{t_1}(\mathbf{r}_3) \left| g_{cn}^{t_1}(\mathbf{r}_3, \mathbf{r}_2) \right. \right) \\ &- \left( X_{mcj}^{t_1}(\mathbf{r}_1, \mathbf{r}_3) C_d^{t_1}(\mathbf{r}_3) \left| g_{cnj}^{t_1}(\mathbf{r}_3, \mathbf{r}_2) \right. \right), \end{aligned} \quad (199)$$

$$\begin{aligned} N_{mn}^{(\rho)t_1}(\mathbf{r}_1, \mathbf{r}_2) &= - \left( \rho_0^{t_1}(\mathbf{r}_1, \mathbf{r}_3) C_d^{t_1}(\mathbf{r}_3) \left| N_{cn}^{(x)t_1}(\mathbf{r}_3, \mathbf{r}_2) + X_{cn}^{t_1}(\mathbf{r}_3, \mathbf{r}_2) \right. \right) \\ &- \left( \rho_0^{t_1}(\mathbf{r}_1, \mathbf{r}_3) (C_d^{t_1}(\mathbf{r}_3) - 1) \left| N_{cn}^{(\rho)t_1}(\mathbf{r}_3, \mathbf{r}_2) - \rho_0^{t_1}(\mathbf{r}_3, \mathbf{r}_2) \right. \right) \\ &+ \left( \rho_{0j}^{t_1}(\mathbf{r}_1, \mathbf{r}_3) C_d^{t_1}(\mathbf{r}_3) \left| N_{cnj}^{(x)t_1}(\mathbf{r}_3, \mathbf{r}_2) + X_{cnj}^{t_1}(\mathbf{r}_3, \mathbf{r}_2) \right. \right) \\ &+ \left( \rho_{0j}^{t_1}(\mathbf{r}_1, \mathbf{r}_3) (C_d^{t_1}(\mathbf{r}_3) - 1) \left| N_{cnj}^{(\rho)t_1}(\mathbf{r}_3, \mathbf{r}_2) - \rho_{0j}^{t_1}(\mathbf{r}_3, \mathbf{r}_2) \right. \right), \end{aligned} \quad (200)$$

$$\begin{aligned} N_{mnj}^{(x)t_1}(\mathbf{r}_1, \mathbf{r}_2) &= \left( X_{mcj}^{t_1}(\mathbf{r}_1, \mathbf{r}_3) C_d^{t_1}(\mathbf{r}_3) \left| g_{cn}^{t_1}(\mathbf{r}_3, \mathbf{r}_2) \right. \right) \\ &+ \left( X_{mc}^{t_1}(\mathbf{r}_1, \mathbf{r}_3) C_d^{t_1}(\mathbf{r}_3) \left| g_{cnj}^{t_1}(\mathbf{r}_3, \mathbf{r}_2) \right. \right), \end{aligned} \quad (201)$$

$$\begin{aligned} N_{mnj}^{(\rho)t_1}(\mathbf{r}_1, \mathbf{r}_2) &= - \left( \rho_{0j}^{t_1}(\mathbf{r}_1, \mathbf{r}_3) C_d^{t_1}(\mathbf{r}_3) \left| N_{cn}^{(x)t_1}(\mathbf{r}_3, \mathbf{r}_2) + X_{cn}^{t_1}(\mathbf{r}_3, \mathbf{r}_2) \right. \right) \\ &- \left( \rho_{0j}^{t_1}(\mathbf{r}_1, \mathbf{r}_3) (C_d^{t_1}(\mathbf{r}_3) - 1) \left| N_{cn}^{(\rho)t_1}(\mathbf{r}_3, \mathbf{r}_2) - \rho_0^{t_1}(\mathbf{r}_3, \mathbf{r}_2) \right. \right) \\ &- \left( \rho_0^{t_1}(\mathbf{r}_1, \mathbf{r}_3) C_d^{t_1}(\mathbf{r}_3) \left| N_{cnj}^{(x)t_1}(\mathbf{r}_3, \mathbf{r}_2) + X_{cnj}^{t_1}(\mathbf{r}_3, \mathbf{r}_2) \right. \right) \\ &- \left( \rho_0^{t_1}(\mathbf{r}_1, \mathbf{r}_3) (C_d^{t_1}(\mathbf{r}_3) - 1) \left| N_{cnj}^{(\rho)t_1}(\mathbf{r}_3, \mathbf{r}_2) - \rho_{0j}^{t_1}(\mathbf{r}_3, \mathbf{r}_2) \right. \right), \end{aligned} \quad (202)$$

where  $m, n = c, w_c$ . In the above equation, we have used the definitions:

$$N_{mn(j)}^{(x)t_1}(\mathbf{r}_1, \mathbf{r}_2) = N_{mn(j)}^{xx t_1}(\mathbf{r}_1, \mathbf{r}_2) + N_{mn(j)}^{x \rho t_1}(\mathbf{r}_1, \mathbf{r}_2),$$

and

$$N_{mn(j)}^{(\rho)t_1}(\mathbf{r}_1, \mathbf{r}_2) = N_{mn(j)}^{\rho x t_1}(\mathbf{r}_1, \mathbf{r}_2) + N_{mn(j)}^{\rho \rho t_1}(\mathbf{r}_1, \mathbf{r}_2).$$

It is worth to point out that Eq. (200) indicates that  $N_{mn(j)}^{(\rho)t_1}(\mathbf{r}_1, \mathbf{r}_2)$  does not depend on  $m$ .

The results of Sect. 3.2 indicate that the vertex corrections are given by:

$$C_m^{t_1}(\mathbf{r}_1) = \exp[U_m^{t_1}(\mathbf{r}_1)], \quad (203)$$

$$C_d^{t_1}(\mathbf{r}_1) = C_d^{t_1}(\mathbf{r}_1)[U_e^{t_1}(\mathbf{r}_1) + \rho_0^{t_1}(\mathbf{r}_1)] = \rho(\mathbf{r}_1), \quad (204)$$



with  $m = d, w$ . In order to simplify the writing of the RFHNC expressions for  $U_{d,w,e}$ , we have defined the quantity:

$$S_{mn}^{t_1 t_2}(\mathbf{r}_1, \mathbf{r}_2) \equiv \frac{1}{2} N_{mn}^{t_1 t_2}(\mathbf{r}_1, \mathbf{r}_2) + E_{mn}^{t_1 t_2}(\mathbf{r}_1, \mathbf{r}_2) . \quad (205)$$

and we obtain:

$$\begin{aligned} U_m^{t_1}(\mathbf{r}_1) = & \int d\mathbf{r}_2 \sum_{t_2=p,n} \left\{ C^{t_2}(\mathbf{r}_2) \left[ X_{md}^{t_1 t_2}(\mathbf{r}_1, \mathbf{r}_2) - E_{md}^{t_1 t_2}(\mathbf{r}_1, \mathbf{r}_2) \right. \right. \\ & - S_{md}^{t_1 t_2}(\mathbf{r}_1, \mathbf{r}_2) (g_{md}^{t_1 t_2}(\mathbf{r}_1, \mathbf{r}_2) - 1) \Big] \\ & + C_d^{t_2}(\mathbf{r}_2) \left[ X_{me}^{t_1 t_2}(\mathbf{r}_1, \mathbf{r}_2) - E_{me}^{t_1 t_2}(\mathbf{r}_1, \mathbf{r}_2) \right. \\ & - S_{me}^{t_1 t_2}(\mathbf{r}_1, \mathbf{r}_2) (g_{md}^{t_1 t_2}(\mathbf{r}_1, \mathbf{r}_2) - 1) \\ & \left. \left. - S_{md}^{t_1 t_2}(\mathbf{r}_1, \mathbf{r}_2) g_{me}^{t_1 t_2}(\mathbf{r}_1, \mathbf{r}_2) \right] \right\} + E_m^{t_1}(\mathbf{r}_1) , \end{aligned} \quad (206)$$

$$\begin{aligned} U_e^{t_1}(\mathbf{r}_1) = & \int d\mathbf{r}_2 \sum_{t_2=p,n} \left\{ C^{t_2}(\mathbf{r}_2) \left[ X_{ed}^{t_1 t_2}(\mathbf{r}_1, \mathbf{r}_2) - E_{ed}^{t_1 t_2}(\mathbf{r}_1, \mathbf{r}_2) \right. \right. \\ & - S_{ed}^{t_1 t_2}(\mathbf{r}_1, \mathbf{r}_2) (g_{dd}^{t_1 t_2}(\mathbf{r}_1, \mathbf{r}_2) - 1) - S_{dd}^{t_1 t_2}(\mathbf{r}_1, \mathbf{r}_2) g_{ed}^{t_1 t_2}(\mathbf{r}_1, \mathbf{r}_2) \Big] \\ & + C_d^{t_2}(\mathbf{r}_2) \left[ X_{ee}^{t_1 t_2}(\mathbf{r}_1, \mathbf{r}_2) - E_{ee}^{t_1 t_2}(\mathbf{r}_1, \mathbf{r}_2) \right. \\ & - S_{ee}^{t_1 t_2}(\mathbf{r}_1, \mathbf{r}_2) (g_{dd}^{t_1 t_2}(\mathbf{r}_1, \mathbf{r}_2) - 1) - S_{ed}^{t_1 t_2}(\mathbf{r}_1, \mathbf{r}_2) g_{de}^{t_1 t_2}(\mathbf{r}_1, \mathbf{r}_2) \\ & \left. - S_{de}^{t_1 t_2}(\mathbf{r}_1, \mathbf{r}_2) g_{ed}^{t_1 t_2}(\mathbf{r}_1, \mathbf{r}_2) - S_{dd}^{t_1 t_2}(\mathbf{r}_1, \mathbf{r}_2) g_{ee}^{t_1 t_2}(\mathbf{r}_1, \mathbf{r}_2) \right] \\ & + 2\delta_{t_1 t_2} \left[ C_d^{t_2}(\mathbf{r}_2) [S_{cc}^{t_1}(\mathbf{r}_1, \mathbf{r}_2) g_{cc}^{t_2}(\mathbf{r}_1, \mathbf{r}_2) + S_{ccj}^{t_1}(\mathbf{r}_1, \mathbf{r}_2) g_{ccj}^{t_2}(\mathbf{r}_1, \mathbf{r}_2)] \right. \\ & - \rho_0^{t_1}(\mathbf{r}_1, \mathbf{r}_2) (N_{cc}^{(\rho)t_2}(\mathbf{r}_1, \mathbf{r}_2) - \rho_0^{t_2}(\mathbf{r}_1, \mathbf{r}_2)) \\ & \left. \left. - \rho_{0j}^{t_1}(\mathbf{r}_1, \mathbf{r}_2) (N_{ccj}^{(\rho)t_2}(\mathbf{r}_1, \mathbf{r}_2) - \rho_{0j}^{t_2}(\mathbf{r}_1, \mathbf{r}_2)) \right] \right\} + E_e^{t_1}(\mathbf{r}_1) , \end{aligned} \quad (207)$$

with  $m = w, d$ . The expressions (184-207) form the close set of RFHNC equations, valid for the scalar part of the correlation. In terms of these quantities and defining other useful ones, we can express the TBDF and the OBDM as:

$$\rho_2^{1, t_1 t_2}(\mathbf{r}_1, \mathbf{r}_2) = \rho_{2, dir}^{t_1 t_2}(\mathbf{r}_1, \mathbf{r}_2) + 2\delta_{t_1 t_2} \left( \rho_{2, exc}^{t_1 t_2}(\mathbf{r}_1, \mathbf{r}_2) + \rho_{2, excj}^{t_1 t_2}(\mathbf{r}_1, \mathbf{r}_2) \right) \quad (208)$$

$$\begin{aligned} \rho_{2, dir}^{t_1 t_2}(\mathbf{r}_1, \mathbf{r}_2) = & C^{t_1}(\mathbf{r}_1) (C^{t_2}(\mathbf{r}_2) g_{dd}^{t_1 t_2}(\mathbf{r}_1, \mathbf{r}_2) + C_d^{t_2}(\mathbf{r}_2) g_{de}^{t_1 t_2}(\mathbf{r}_1, \mathbf{r}_2)) \\ & + C_d^{t_1}(\mathbf{r}_1) (C^{t_2}(\mathbf{r}_2) g_{ed}^{t_1 t_2}(\mathbf{r}_1, \mathbf{r}_2) + C_d^{t_2}(\mathbf{r}_2) g_{ee, dir}^{t_1 t_2}(\mathbf{r}_1, \mathbf{r}_2)) , \end{aligned} \quad (209)$$

$$\rho_{2, exc}^{t_1 t_2}(\mathbf{r}_1, \mathbf{r}_2) = C_d^{t_1}(\mathbf{r}_1) C_d^{t_2}(\mathbf{r}_2) g_{ee, exc}^{t_1 t_2}(\mathbf{r}_1, \mathbf{r}_2) , \quad (210)$$

$$\rho_{2, excj}^{t_1 t_2}(\mathbf{r}_1, \mathbf{r}_2) = C_d^{t_1}(\mathbf{r}_1) C_d^{t_2}(\mathbf{r}_2) g_{ee, excj}^{t_1 t_2}(\mathbf{r}_1, \mathbf{r}_2) , \quad (211)$$

$$\rho^{t_1}(\mathbf{r}_1, \mathbf{r}_2) = -2C_w^{t_1}(\mathbf{r}_1) C_w^{t_1}(\mathbf{r}_2) g_{w_c w_c}^{t_1 t_1}(\mathbf{r}_1, \mathbf{r}_2) \quad (212)$$

We discuss now the case of state-dependent correlations, in the SOC approximation. We have mentioned in Sect. 3.3, the need of separating the spin and isospin dependence of the TBDF in order to describe nuclei not saturated in isospin. In these systems, the contribution of the linear isospin operators is not zero, therefore we distinguish the proton and neutron dependence of the

various RFHNC/SOC terms. This affects the chain equations in the calculation of the nodal  $N_{xy,p}^{t_1 t_2}(\mathbf{r}_1, \mathbf{r}_2)$  functions. In order to generate these chains, we have to consider the following folding products: those of a function  $X_{xy,p}(\mathbf{r}_1, \mathbf{r}_3)$  with another function  $X_{xy,q}(\mathbf{r}_3, \mathbf{r}_2)$ , those of  $X_{xy,p}(\mathbf{r}_1, \mathbf{r}_3)$  with  $N_{xy,q}(\mathbf{r}_1, \mathbf{r}_3)$ , and those of  $X_{xy,p}(\mathbf{r}_1, \mathbf{r}_3)$ , or  $N_{xy,q}(\mathbf{r}_1, \mathbf{r}_3)$ , with  $\rho_0(\mathbf{r}_3, \mathbf{r}_2)$ . These combinations are present also in isospin saturated systems. In addition, we should also consider that the action of a single isospin operator on a single external point of the nodal function, produces a non zero contribution.

We give in the following the expressions of the vertex corrections of the nodal terms in SOC approximation, and also those of the various terms of the TBDF. In these expressions we use the index  $k$  which can assume the values 1,2 and 3 and the index  $l$  which can be 0 or 1. The  $p$ ,  $q$  and  $r$  indexes indicate the operator channels and can assume values from 1 up to 6.

The expressions of the nodal functions without open statistical loops can be written as:

$$\begin{aligned} N_{mn,2k_1-1}^{t_1 t_2}(\mathbf{r}_1, \mathbf{r}_2) &= \sum_{k_2 k_3=1}^3 \sum_{t_3=p,n} \left[ N_{mn,2k_1-1,2k_2-1,2k_3-1}^{t_1 t_2 t_3}(\mathbf{r}_1, \mathbf{r}_2) \right. \\ &+ (2\delta_{t_1 t_3} - 1) N_{mn,2k_1-1,2k_2,2k_3-1}^{t_1 t_2 t_3}(\mathbf{r}_1, \mathbf{r}_2) \\ &+ \left. (2\delta_{t_2 t_3} - 1) N_{mn,2k_1-1,2k_2-1,2k_3}^{t_1 t_2 t_3}(\mathbf{r}_1, \mathbf{r}_2) \right], \end{aligned} \quad (213)$$

$$N_{mn,2k_1}^{t_1 t_2}(\mathbf{r}_1, \mathbf{r}_2) = \sum_{k_2, k_3=1}^3 \sum_{t_3=p,n} N_{mn,2k_1,2k_2,2k_3}^{t_1 t_2 t_3}(\mathbf{r}_1, \mathbf{r}_2), \quad (214)$$

where we have defined:

$$\begin{aligned} N_{mn,pqr}^{t_1 t_2 t_3}(\mathbf{r}_1, \mathbf{r}_2) &= \left( X_{md,q}^{t_1 t_3}(\mathbf{r}_1, \mathbf{r}_3) \zeta_{132}^{k_2 k_3 k_1} C_{qr}^{t_3}(\mathbf{r}_3) \right) \left| X_{dn,r}^{t_3 t_2}(\mathbf{r}_3, \mathbf{r}_2) + N_{dn,r}^{t_3 t_2}(\mathbf{r}_3, \mathbf{r}_2) \right| \\ &+ \left( X_{me,q}^{t_1 t_3}(\mathbf{r}_1, \mathbf{r}_3) \zeta_{132}^{k_2 k_3 k_1} C_{d,qr}^{t_3}(\mathbf{r}_3) \right) \left| X_{dn,r}^{t_3 t_2}(\mathbf{r}_3, \mathbf{r}_2) + N_{dn,r}^{t_3 t_2}(\mathbf{r}_3, \mathbf{r}_2) \right| \\ &+ \left( X_{md,q}^{t_1 t_3}(\mathbf{r}_1, \mathbf{r}_3) \zeta_{132}^{k_2 k_3 k_1} C_{d,qr}^{t_3}(\mathbf{r}_3) \right) \left| X_{en,r}^{t_3 t_2}(\mathbf{r}_3, \mathbf{r}_2) + N_{en,r}^{t_3 t_2}(\mathbf{r}_3, \mathbf{r}_2) \right|. \end{aligned} \quad (215)$$

In the above equations we have defined  $p = 2k_1 - 1 + l_1$ ,  $q = 2k_2 - 1 + l_2$ , and  $r = 2k_3 - 1 + l_3$ . The sub-indexes  $m$  and  $n$  indicate the type of link with the two external points, specifically  $m, n = d, w, e$ .

Since in the calculations of  $ww$  diagrams, we must include the isospin trace, for this case, we substitute Eq.(214) with:

$$N_{ww,2k_1}^{t_1 t_1}(\mathbf{r}_1, \mathbf{r}_2) = \sum_{k_2, k_3=1}^3 \sum_{t_3=p,n} \chi_2^{t_1 t_3} N_{ww,2k_1,2k_2,2k_3}^{t_1 t_1 t_3}(\mathbf{r}_1, \mathbf{r}_2). \quad (216)$$

The expressions of the nodal diagrams with open statistical loops are:

$$N_{mn,p}^{t_1}(\mathbf{r}_1, \mathbf{r}_2) = N_{mn,p}^{(x)t_1}(\mathbf{r}_1, \mathbf{r}_2) + N_{mn,p}^{(\rho)t_1}(\mathbf{r}_1, \mathbf{r}_2) \quad p = 1, \dots, 6, \quad (217)$$

$$N_{mnj,p}^{t_1}(\mathbf{r}_1, \mathbf{r}_2) = N_{mnj,p}^{(x)t_1}(\mathbf{r}_1, \mathbf{r}_2) + N_{mnj,p}^{(\rho)t_1}(\mathbf{r}_1, \mathbf{r}_2) \quad p = 1, 2, \quad (218)$$

with  $m, n = c, w, e$ . We have used a symbology analogous to that of Eqs. (200 - 202), to indicate the parallel spin case, Eq. (217), and the antiparallel one, Eq. (218). In this last case, we have

considered only the contribution of the first two channels of the interaction,  $p = 1, 2$ , in order to simplify our calculations. This is a good approximation since the relevance of the antiparallel loops is small. The explicit expressions of the nodal functions present in the Eqs. (217) and (218) are:

$$N_{mn(j),2k_1-1}^{(y)t_1}(\mathbf{r}_1, \mathbf{r}_2) = \sum_{k_2, k_3=1}^3 \sum_{t_3=p, n} \left[ N_{mn(j),2k_1-1,2k_2-1,2k_3-1}^{(y)t_1 t_3}(\mathbf{r}_1, \mathbf{r}_2) + (2\delta_{t_1 t_3} - 1) \left( N_{mn(j),2k_1-1,2k_2,2k_3-1}^{(y)t_1 t_3}(\mathbf{r}_1, \mathbf{r}_2) + N_{mn(j),2k_1-1,2k_2-1,2k_3}^{(y)t_1 t_3}(\mathbf{r}_1, \mathbf{r}_2) \right) \right], \quad (219)$$

$$N_{mn(j),2k_1}^{(y)t_1}(\mathbf{r}_1, \mathbf{r}_2) = \sum_{k_2, k_3=1}^3 \sum_{t_3=p, n} N_{mn(j),2k_1,2k_2,2k_3}^{(y)t_1 t_3}(\mathbf{r}_1, \mathbf{r}_2), \quad (220)$$

where  $y = x, \rho$ . The other terms are:

$$\begin{aligned} N_{mn,pqr}^{(x)t_1 t_3}(\mathbf{r}_1, \mathbf{r}_2) &= \left( X_{mc,q}^{t_1}(\mathbf{r}_1, \mathbf{r}_3) \zeta_{132}^{k_2 k_3 k_1} C_{d,qr}^{t_3}(\mathbf{r}_3) \frac{\Delta^{k_3}}{2} \left| g_{cn}^{t_3}(\mathbf{r}_3, \mathbf{r}_2) \right| \right) \\ &+ (1 - \delta_{r,1}) \left( X_{mc}^{t_1}(\mathbf{r}_1, \mathbf{r}_3) \frac{\Delta^{k_2}}{2} \zeta_{132}^{k_2 k_3 k_1} C_{d,qr}^{t_3}(\mathbf{r}_3) \left| g_{cn,r}^{t_3}(\mathbf{r}_3, \mathbf{r}_2) \right| \right) \\ &- \delta_{k_1 1} \delta_{k_2 1} \delta_{k_3 1} \left[ \left( X_{mcj,q}^{t_1}(\mathbf{r}_1, \mathbf{r}_3) C_{d,qr}^{t_3}(\mathbf{r}_3) \frac{1}{2} \left| g_{cnj}^{t_3}(\mathbf{r}_3, \mathbf{r}_2) \right| \right) \right. \\ &\left. + (1 - \delta_{r,1}) \left( X_{mcj}^{t_1}(\mathbf{r}_1, \mathbf{r}_3) C_{d,qr}^{t_3}(\mathbf{r}_3) \frac{1}{2} \left| g_{cnj,r}^{t_3}(\mathbf{r}_3, \mathbf{r}_2) \right| \right) \right], \quad (221) \end{aligned}$$

$$\begin{aligned} N_{mn,pqr}^{(\rho)t_1 t_3}(\mathbf{r}_1, \mathbf{r}_2) &= - \left( \rho_0^{t_1}(\mathbf{r}_1, \mathbf{r}_3) \frac{\Delta^{k_2}}{2} \zeta_{132}^{k_2 k_3 k_1} C_{d,qr}^{t_3}(\mathbf{r}_3) \left| X_{cn,r}^{t_3}(\mathbf{r}_3, \mathbf{r}_2) \right| \right) \\ &- \left( \rho_0^{t_1}(\mathbf{r}_1, \mathbf{r}_3) \frac{\Delta^{k_2}}{2} \zeta_{132}^{k_2 k_3 k_1} C_{d,qr}^{t_3}(\mathbf{r}_3) \left| N_{cn,r}^{(x)t_3}(\mathbf{r}_3, \mathbf{r}_2) \right| \right) \\ &- \left( \rho_0^{t_1}(\mathbf{r}_1, \mathbf{r}_3) \frac{\Delta^{k_2}}{2} \zeta_{132}^{k_2 k_3 k_1} (C_{d,qr}^{t_3}(\mathbf{r}_3) - 1) \left| N_{cn,r}^{(\rho)t_3}(\mathbf{r}_3, \mathbf{r}_2) \right| \right) \\ &+ \delta_{r,1} \left( \rho_0^{t_1}(\mathbf{r}_1, \mathbf{r}_3) \frac{\Delta^{k_2}}{2} \zeta_{132}^{k_2 k_3 k_1} (C_{d,qr}^{t_3}(\mathbf{r}_3) - 1) \left| \rho_0^{t_3}(\mathbf{r}_3, \mathbf{r}_2) \right| \right) \\ &+ \frac{\delta_{k_1 1} \delta_{k_2 1} \delta_{k_3 1}}{2} \left[ \left( \rho_{0j}^{t_1}(\mathbf{r}_1, \mathbf{r}_3) C_{d,qr}^{t_3}(\mathbf{r}_3) \left| X_{cnj,r}^{t_3}(\mathbf{r}_3, \mathbf{r}_2) \right| \right) \right. \\ &+ \left( \rho_{0j}^{t_1}(\mathbf{r}_1, \mathbf{r}_3) C_{d,qr}^{t_3}(\mathbf{r}_3) \left| N_{cnj,r}^{t_3}(\mathbf{r}_3, \mathbf{r}_2) \right| \right) \\ &+ \left( \rho_{0j}^{t_1}(\mathbf{r}_1, \mathbf{r}_3) (C_{d,qr}^{t_3}(\mathbf{r}_3) - 1) \left| N_{cnj,r}^{t_3}(\mathbf{r}_3, \mathbf{r}_2) \right| \right) \\ &\left. - \delta_{r,1} \left( \rho_{0j}^{t_1}(\mathbf{r}_1, \mathbf{r}_3) (C_{d,qr}^{t_3}(\mathbf{r}_3) - 1) \left| \rho_{0j}^{t_3}(\mathbf{r}_3, \mathbf{r}_2) \right| \right) \right], \quad (222) \end{aligned}$$

$$\begin{aligned} N_{mnj,pst}^{(x)t_1 t_3}(\mathbf{r}_1, \mathbf{r}_2) &= \left( X_{mc,s}^{t_1}(\mathbf{r}_1, \mathbf{r}_3) C_{d,st}^{t_3}(\mathbf{r}_3) \frac{1}{2} \left| g_{cnj}^{t_3}(\mathbf{r}_3, \mathbf{r}_2) \right| \right) \\ &+ (1 - \delta_{t,1}) \left( X_{mc}^{t_1}(\mathbf{r}_1, \mathbf{r}_3) C_{d,st}^{t_3}(\mathbf{r}_3) \frac{1}{2} \left| g_{cnj,t}^{t_3}(\mathbf{r}_3, \mathbf{r}_2) \right| \right) \\ &+ \left( X_{mcj,s}^{t_1}(\mathbf{r}_1, \mathbf{r}_3) C_{d,st}^{t_3}(\mathbf{r}_3) \frac{1}{2} \left| g_{cn}^{t_3}(\mathbf{r}_3, \mathbf{r}_2) \right| \right) \\ &+ (1 - \delta_{t,1}) \left( X_{mcj}^{t_1}(\mathbf{r}_1, \mathbf{r}_3) C_{d,st}^{t_3}(\mathbf{r}_3) \frac{1}{2} \left| g_{cn,t}^{t_3}(\mathbf{r}_3, \mathbf{r}_2) \right| \right), \quad (223) \end{aligned}$$

$$\begin{aligned}
N_{mnj,pst}^{(\rho)t_1t_3}(\mathbf{r}_1, \mathbf{r}_2) &= -\left(\rho_0^{t_1}(\mathbf{r}_1, \mathbf{r}_3)C_{d,st}^{t_3}(\mathbf{r}_3)\frac{1}{2}\left|X_{cnj,t}^{t_3}(\mathbf{r}_3, \mathbf{r}_2) + N_{cnj,t}^{(x)t_3}(\mathbf{r}_3, \mathbf{r}_2)\right.\right) \\
&- \left(\rho_0^{t_1}(\mathbf{r}_1, \mathbf{r}_3)(C_{d,st}^{t_3}(\mathbf{r}_3) - 1)\frac{1}{2}\left|N_{cnj,t}^{(\rho)t_3}(\mathbf{r}_3, \mathbf{r}_2)\right.\right) \\
&+ \delta_{t,1}\left(\rho_0^{t_1}(\mathbf{r}_1, \mathbf{r}_3)(C_{d,st}^{t_3}(\mathbf{r}_3) - 1)\frac{1}{2}\left|\rho_{0j}^{t_3}(\mathbf{r}_3, \mathbf{r}_2)\right.\right) \\
&- \left(\rho_{0j}^{t_1}(\mathbf{r}_1, \mathbf{r}_3)C_{d,st}^{t_3}(\mathbf{r}_3)\frac{1}{2}\left|X_{cn,t}^{t_3}(\mathbf{r}_3, \mathbf{r}_2) + N_{cn,t}^{(x)t_3}(\mathbf{r}_3, \mathbf{r}_2)\right.\right) \\
&- \left(\rho_{0j}^{t_1}(\mathbf{r}_1, \mathbf{r}_3)(C_{d,st}^{t_3}(\mathbf{r}_3) - 1)\frac{1}{2}\left|N_{cn,t}^{(\rho)t_3}(\mathbf{r}_3, \mathbf{r}_2)\right.\right) \\
&+ \delta_{t,1}\left(\rho_{0j}^{t_1}(\mathbf{r}_1, \mathbf{r}_3)(C_{d,st}^{t_3}(\mathbf{r}_3) - 1)\frac{1}{2}\left|\rho_0^{t_3}(\mathbf{r}_3, \mathbf{r}_2)\right.\right). \tag{224}
\end{aligned}$$

In the above equations the symbols  $s$  and  $t$  can assume the values 1 and 2.

In the calculations of  $w_c w_c$  diagrams, we must include the isospin trace, therefore we use:

$$N_{w_c w_c, 2k_1}^{t_1}(\mathbf{r}_1, \mathbf{r}_2) = \sum_{k_2, k_3=1}^3 \sum_{t_3=p, n} \chi_2^{t_1 t_3} N_{w_c w_c, 2k_1, 2k_2, 2k_3}^{t_1 t_3}(\mathbf{r}_1, \mathbf{r}_2). \tag{225}$$

The expressions of the TBDFs are rather similar to those of the symmetric nuclear matter case. We define the quantities:

$$h_{dd,p}^{t_1 t_2}(\mathbf{r}_1, \mathbf{r}_2) = \frac{2f_p(r_{12})}{f_1(r_{12})} + N_{dd,p}^{t_1 t_2}(\mathbf{r}_1, \mathbf{r}_2), \tag{226}$$

$$h_{wd,p}^{t_1 t_2}(\mathbf{r}_1, \mathbf{r}_2) = \frac{f_p(r_{12})}{f_1(r_{12})} + N_{wd,p}^{t_1 t_2}(\mathbf{r}_1, \mathbf{r}_2), \tag{227}$$

$$h_{ww,p}^{t_1 t_2}(\mathbf{r}_1, \mathbf{r}_2) = N_{ww,p}^{t_1 t_2}(\mathbf{r}_1, \mathbf{r}_2), \tag{228}$$

with  $p = 2k - 1 + l > 1$ . We obtain:

$$\begin{aligned}
g_{mn,p}^{t_1 t_2}(\mathbf{r}_1, \mathbf{r}_2) &= g_{mn}^{t_1 t_2}(\mathbf{r}_1, \mathbf{r}_2)h_{mn,p}^{t_1 t_2}(\mathbf{r}_1, \mathbf{r}_2) \\
&= X_{mn,p}^{t_1 t_2}(\mathbf{r}_1, \mathbf{r}_2) + N_{mn,p}^{t_1 t_2}(\mathbf{r}_1, \mathbf{r}_2), \\
g_{me,p}^{t_1 t_2}(\mathbf{r}_1, \mathbf{r}_2) &= g_{me}^{t_1 t_2}(\mathbf{r}_1, \mathbf{r}_2)h_{md,p}^{t_1 t_2}(\mathbf{r}_1, \mathbf{r}_2) + g_{md}^{t_1 t_2}(\mathbf{r}_1, \mathbf{r}_2)N_{me,p}^{t_1 t_2}(\mathbf{r}_1, \mathbf{r}_2) \\
&= X_{me,p}^{t_1 t_2}(\mathbf{r}_1, \mathbf{r}_2) + N_{me,p}^{t_1 t_2}(\mathbf{r}_1, \mathbf{r}_2), \tag{229}
\end{aligned}$$

$$\begin{aligned}
g_{ee,p}^{t_1 t_2}(\mathbf{r}_1, \mathbf{r}_2) &= g_{ee,dir,p}^{t_1 t_2}(\mathbf{r}_1, \mathbf{r}_2) + g_{ee,exc,p}^{t_1 t_2}(\mathbf{r}_1, \mathbf{r}_2) + g_{ee,excj,p}^{t_1 t_2}(\mathbf{r}_1, \mathbf{r}_2) \\
&= X_{ee,p}^{t_1 t_2}(\mathbf{r}_1, \mathbf{r}_2) + N_{ee,p}^{t_1 t_2}(\mathbf{r}_1, \mathbf{r}_2), \tag{230}
\end{aligned}$$

$$\begin{aligned}
g_{ee,dir,p}^{t_1 t_2}(\mathbf{r}_1, \mathbf{r}_2) &= g_{ee,dir}^{t_1 t_2}(\mathbf{r}_1, \mathbf{r}_2)h_{dd,p}^{t_1 t_2}(\mathbf{r}_1, \mathbf{r}_2) \\
&+ g_{dd}^{t_1 t_2}(\mathbf{r}_1, \mathbf{r}_2)N_{ee,p}^{t_1 t_2}(\mathbf{r}_1, \mathbf{r}_2) \\
&+ g_{de}^{t_1 t_2}(\mathbf{r}_1, \mathbf{r}_2)N_{ed,p}^{t_1 t_2}(\mathbf{r}_1, \mathbf{r}_2) \\
&+ g_{ed}^{t_1 t_2}(\mathbf{r}_1, \mathbf{r}_2)N_{de,p}^{t_1 t_2}(\mathbf{r}_1, \mathbf{r}_2), \tag{231}
\end{aligned}$$

$$g_{ee,exc,p}^{t_1 t_2}(\mathbf{r}_1, \mathbf{r}_2) = \Delta^k g_{ee,exc}^{t_1 t_2}(\mathbf{r}_1, \mathbf{r}_2), \tag{232}$$

$$g_{ee,excj,p}^{t_1 t_2}(\mathbf{r}_1, \mathbf{r}_2) = \Delta^k g_{ee,excj}^{t_1 t_2}(\mathbf{r}_1, \mathbf{r}_2), \tag{233}$$

with  $m, n = d, w$ .

For the other diagrams we can write:

$$\begin{aligned} g_{cc(j),p}^{t_1}(\mathbf{r}_1, \mathbf{r}_2) &= g_{cc(j)}^{t_1}(\mathbf{r}_1, \mathbf{r}_2) h_{dd,p}^{t_1 t_1}(\mathbf{r}_1, \mathbf{r}_2) \\ &+ g_{dd}^{t_1 t_1}(\mathbf{r}_1, \mathbf{r}_2) N_{cc(j),p}^{t_1}(\mathbf{r}_1, \mathbf{r}_2) , \end{aligned} \quad (234)$$

$$\begin{aligned} g_{wc(j),p}^{t_1}(\mathbf{r}_1, \mathbf{r}_2) &= g_{wc(j)}^{t_1}(\mathbf{r}_1, \mathbf{r}_2) h_{wd,p}^{t_1 t_1}(\mathbf{r}_1, \mathbf{r}_2) \\ &+ g_{wd}^{t_1 t_1}(\mathbf{r}_1, \mathbf{r}_2) N_{wc(j),p}^{t_1}(\mathbf{r}_1, \mathbf{r}_2) , \end{aligned} \quad (235)$$

$$\begin{aligned} g_{wcwc(j),p}^{t_1}(\mathbf{r}_1, \mathbf{r}_2) &= g_{wcwc(j)}^{t_1}(\mathbf{r}_1, \mathbf{r}_2) h_{ww,p}^{t_1 t_1}(\mathbf{r}_1, \mathbf{r}_2) \\ &+ g_{ww}^{t_1 t_1}(\mathbf{r}_1, \mathbf{r}_2) N_{wcwc(j),p}^{t_1}(\mathbf{r}_1, \mathbf{r}_2) . \end{aligned} \quad (236)$$

All the TBDFs can be expressed in terms of nodal and non nodal diagrams, and for all of them, we can write:

$$g_{mn(j),p}^{t_1}(\mathbf{r}_1, \mathbf{r}_2) = X_{mn(j),p}^{t_1}(\mathbf{r}_1, \mathbf{r}_2) + N_{mn(j),p}^{t_1}(\mathbf{r}_1, \mathbf{r}_2) . \quad (237)$$

The expressions of the vertex corrections for the operator dependent part of the correlations are:

$$C_{m,pq}^{t_1}(\mathbf{r}_1) = C_m^{t_1}(\mathbf{r}_1) \left[ 1 + \delta_{pq,11} U_{m,SOC}^{t_1}(\mathbf{r}_1) \right] , \quad (238)$$

$$\begin{aligned} C_{pq}^{t_1}(\mathbf{r}_1) &= C_{d,pq}^{t_1}(\mathbf{r}_1) \left[ \rho_0^{t_1}(\mathbf{r}_1) + U_e^{t_1}(\mathbf{r}_1) \right] \\ &+ \delta_{pq,11} C_d^{t_1}(\mathbf{r}_1) \left[ U_{e,SOC}^{t_1}(\mathbf{r}_1) + U_{ej,SOC}^{t_1}(\mathbf{r}_1) \right] , \end{aligned} \quad (239)$$

with  $m = w, d$  and where we have used:

$$\begin{aligned} U_{m,SOC}^{t_1}(\mathbf{r}_1) &= \sum_{k_1=1}^3 A^k \sum_{t_2=p,n} \left\{ (1 - \delta_{k_1 1}) U_{m,2k_1-1,2k_1-1}^{t_1 t_2}(\mathbf{r}_1) \right. \\ &+ \chi_1^{t_1 t_2} \left[ U_{m,2k_1-1,2k_1}^{t_1 t_2}(\mathbf{r}_1) + U_{m,2k_1,2k_1-1}^{t_1 t_2}(\mathbf{r}_1) \right] \\ &+ \left. \chi_2^{t_1 t_2} U_{m,2k_1,2k_1}^{t_1 t_2}(\mathbf{r}_1) \right\} , \end{aligned} \quad (240)$$

$$\begin{aligned} U_{ej,SOC}^{t_1}(\mathbf{r}_1) &= \sum_{k_1 k_2=1}^3 I^{k_1 k_2 2} \sum_{t_2=p,n} \left\{ U_{ej,2k_1-1,2k_2-1}^{t_1 t_2}(\mathbf{r}_1) \right. \\ &+ \chi_1^{t_1 t_2} \left[ U_{ej,2k_1-1,2k_2}^{t_1 t_2}(\mathbf{r}_1) + U_{ej,2k_1,2k_2-1}^{t_1 t_2}(\mathbf{r}_1) \right] \\ &+ \left. \chi_2^{t_1 t_2} U_{ej,2k_1,2k_2}^{t_1 t_2}(\mathbf{r}_1) \right\} , \end{aligned} \quad (241)$$

and we have considered  $m = d, w, e$ , the relation  $p = 2k_1 - 1 + l_1$  and  $q = 2k_2 - 1 + l_2$ . The expressions of the  $U$  coefficients are:

$$U_{d,pq}^{t_1 t_2}(\mathbf{r}_1) = \int d\mathbf{r}_2 h_p^{t_1 t_2}(\mathbf{r}_1, \mathbf{r}_2) \left\{ \left[ g_{dd}^{t_1 t_2}(\mathbf{r}_1, \mathbf{r}_2) C_{pq}^{t_2}(\mathbf{r}_2) \right. \right.$$

$$\begin{aligned}
& + g_{de}^{t_1 t_2}(\mathbf{r}_1, \mathbf{r}_2) C_{d,pq}^{t_2}(\mathbf{r}_2) \Big] h_q^{t_1 t_2}(\mathbf{r}_1, \mathbf{r}_2) \\
& + g_{dd}^{t_1 t_2}(\mathbf{r}_1, \mathbf{r}_2) C_{d,pq}^{t_2}(\mathbf{r}_2) (1 - \delta_{q,1}) N_{de,q}^{t_1 t_2}(\mathbf{r}_1, \mathbf{r}_2) \Big\} , \tag{242}
\end{aligned}$$

$$\begin{aligned}
U_{w,pq}^{t_1 t_2}(\mathbf{r}_1) &= \int d\mathbf{r}_2 h_{w,p}^{t_1 t_2}(\mathbf{r}_1, \mathbf{r}_2) (1 - \delta_{q,1}) \Big\{ \Big[ g_{wd}^{t_1 t_2}(\mathbf{r}_1, \mathbf{r}_2) C_{pq}^{t_2}(\mathbf{r}_2) \\
& + g_{we}^{t_1 t_2}(\mathbf{r}_1, \mathbf{r}_2) C_{d,pq}^{t_2}(\mathbf{r}_2) \Big] N_{wd,q}^{t_1 t_2}(\mathbf{r}_1, \mathbf{r}_2) \\
& + g_{wd}^{t_1 t_2}(\mathbf{r}_1, \mathbf{r}_2) C_{d,pq}^{t_2}(\mathbf{r}_2) N_{we,q}^{t_1 t_2}(\mathbf{r}_1, \mathbf{r}_2) \Big\} , \tag{243}
\end{aligned}$$

$$\begin{aligned}
U_{e,pq}^{t_1 t_2}(\mathbf{r}_1) &= \int d\mathbf{r}_2 h_p^{t_1 t_2}(\mathbf{r}_1, \mathbf{r}_2) \Big\{ \Big[ g_{ed}^{t_1 t_2}(\mathbf{r}_1, \mathbf{r}_2) C_{pq}^{t_2}(\mathbf{r}_2) \\
& + g_{ee,dir}^{t_1 t_2}(\mathbf{r}_1, \mathbf{r}_2) C_{d,pq}^{t_2}(\mathbf{r}_2) \Big] h_q^{t_1 t_2}(\mathbf{r}_1, \mathbf{r}_2) \\
& + g_{dd}^{t_1 t_2}(\mathbf{r}_1, \mathbf{r}_2) C_{pq}^{t_2}(\mathbf{r}_2) (1 - \delta_{q,1}) N_{ed,q}^{t_1 t_2}(\mathbf{r}_1, \mathbf{r}_2) + g_{dd}^{t_1 t_2}(\mathbf{r}_1, \mathbf{r}_2) C_{d,pq}^{t_2}(\mathbf{r}_2) \\
& \times (1 - \delta_{q,1}) \Big[ N_{ee,q}^{t_1 t_2}(\mathbf{r}_1, \mathbf{r}_2) + N_{de,q}^{t_1 t_2}(\mathbf{r}_1, \mathbf{r}_2) N_{ed}^{t_1 t_2}(\mathbf{r}_1, \mathbf{r}_2) \\
& + N_{ed,q}^{t_1 t_2}(\mathbf{r}_1, \mathbf{r}_2) N_{de}^{t_1 t_2}(\mathbf{r}_1, \mathbf{r}_2) \Big] \Big\} \\
& + (1 - \delta_{p,1}) \Delta^{k_2} \int d\mathbf{r}_2 \Big\{ h_p^{t_1 t_2}(\mathbf{r}_1, \mathbf{r}_2) 2 g_{ee,exc}^{t_1 t_2}(\mathbf{r}_1, \mathbf{r}_2) C_{d,pq}^{t_2}(\mathbf{r}_2) \\
& - N_{cc,p}^{t_1}(\mathbf{r}_1, \mathbf{r}_2) g_{cc}^{t_2}(\mathbf{r}_1, \mathbf{r}_2) C_{d,pq}^{t_2}(\mathbf{r}_2) \\
& + N_{cc,p}^{(\rho)t_1}(\mathbf{r}_2, \mathbf{r}_1) \Big[ N_{cc}^{(\rho)t_2}(\mathbf{r}_2, \mathbf{r}_1) - \rho_0^{t_2}(\mathbf{r}_1, \mathbf{r}_2) \Big] \Big\} , \tag{244}
\end{aligned}$$

$$\begin{aligned}
U_{ej,pq}^{t_1 t_2} &= (1 - \delta_{p,1}) \Delta^{k_2} \int d\mathbf{r}_2 \Big\{ h_p^{t_1 t_2}(\mathbf{r}_1, \mathbf{r}_2) 2 g_{ee,excj}^{t_1 t_2}(\mathbf{r}_1, \mathbf{r}_2) C_{d,pq}^{t_2}(\mathbf{r}_2) \\
& - N_{cc,p}^{t_1}(\mathbf{r}_1, \mathbf{r}_2) g_{ccj}^{t_2}(\mathbf{r}_1, \mathbf{r}_2) C_{d,pq}^{t_2}(\mathbf{r}_2) \\
& + N_{cc,p}^{(\rho)t_1}(\mathbf{r}_2, \mathbf{r}_1) \Big[ N_{ccj}^{(\rho)t_2}(\mathbf{r}_2, \mathbf{r}_1) - \rho_{0j}^{t_2}(\mathbf{r}_1, \mathbf{r}_2) \Big] \Big\} \tag{245}
\end{aligned}$$

In the above equations we have used the functions

$$\begin{aligned}
h_q^{t_1 t_2}(\mathbf{r}_1, \mathbf{r}_2) &= \frac{f_q(r_{12})}{f_1(r_{12})} + (1 - \delta_{q,1}) N_{dd,q}^{t_1 t_2}(\mathbf{r}_1, \mathbf{r}_2) , \\
h_{w,q}^{t_1 t_2}(\mathbf{r}_1, \mathbf{r}_2) &= \frac{f_q(r_{12})}{f_1(r_{12})} + (1 - \delta_{q,1}) N_{wd,q}^{t_1 t_2}(\mathbf{r}_1, \mathbf{r}_2) .
\end{aligned}$$

In addition we remark that, since there is no contribution in the case  $p = q = 1$ , we have

$$C_{m,pq}^{t_2}(\mathbf{r}_2) = C_{m,22}^{t_2}(\mathbf{r}_2) .$$

## C The isospin matrix elements

In Sect. 3.3.2 we have shown how to calculate the expectation value of the diagram A of Fig. 15 by using the properties of the Pauli matrices. We found a recursive relation which allowed us to express a set of  $n$  pairs of isospin operators as a scalar term plus a single isospin operator pair, Eq. (117). This recursive relation was used to evaluate the expectation value of a set of  $n$  isospin operator pairs between two external points, Eq. (121).

In this Appendix we calculate the isospin expectation value for the situations represented by the B and C diagrams of Fig. 15. We call these diagrams vertex correction and nodal diagram, respectively.

The starting point is a general expression for the expectation value of a product of isospin operators between the external points 1 and 2, and a generic internal point, we label it as 3. Since this expression is symmetric in the external points, we write it in a general manner and we understand that the  $i$  and  $j$  points can be either 1 or 2. We define the expectation value:

$$\begin{aligned} \mathcal{T}_{l_1 l_2 l_3 l_4 l_5}^{t_1 t_2 t_3}(i, j) &\equiv \chi_{t_1}^+(1) \chi_{t_2}^+(2) \chi_{t_3}^+(3) (\boldsymbol{\tau}_1 \cdot \boldsymbol{\tau}_2)^{l_1} (\boldsymbol{\tau}_i \cdot \boldsymbol{\tau}_3)^{l_2} \\ &\quad (\boldsymbol{\tau}_1 \cdot \boldsymbol{\tau}_2)^{l_3} (\boldsymbol{\tau}_j \cdot \boldsymbol{\tau}_3)^{l_4} (\boldsymbol{\tau}_1 \cdot \boldsymbol{\tau}_2)^{l_5} \chi_{t_1}(1) \chi_{t_2}(2) \chi_{t_3}(3) \\ &= b'_1 + b'_2 \delta_{t_1 t_2} + b'_3 \delta_{t_1 t_3} + b'_4 \delta_{t_2 t_3} + b'_5 \delta_{t_1 t_2} \delta_{t_1 t_3} \delta_{t_2 t_3} , \end{aligned} \quad (246)$$

where the  $b'_{1,5}$  coefficients are real numbers depending on  $l_{1,\dots,5}$  which indicate the number of isospin pairs appearing in the expression. For the properties of the Kronecker's  $\delta$  symbol we have that:

$$\delta_{t_1 t_2} \delta_{t_1 t_3} \delta_{t_2 t_3} = \frac{1}{2} (\delta_{t_1 t_2} + \delta_{t_1 t_3} + \delta_{t_2 t_3} - 1) , \quad (247)$$

therefore we obtain:

$$\mathcal{T}_{l_1 l_2 l_3 l_4 l_5}^{t_1 t_2 t_3}(i, j) = b_1 + b_2 \delta_{t_1 t_2} + b_3 \delta_{t_1 t_3} + b_4 \delta_{t_2 t_3} , \quad (248)$$

where we have defined  $b_1 = b'_1 - b'_5/2$  and  $b_k = b'_k + b'_5/2$  for  $k = 2, 3, 4$ . By exchanging the coordinates 1 and 2 in Eq. (246) we find that:

$$\mathcal{T}_{l_1 l_2 l_3 l_4 l_5}^{t_1 t_2 t_3}(3-i, 3-j) = \mathcal{T}_{l_1 l_2 l_3 l_4 l_5}^{t_2 t_1 t_3}(i, j) . \quad (249)$$

Eq. (246) represents the most general expression for all the cases we want to treat. All the possible combinations of isospin operator pairs of our calculations, can be reconducted to this expression, by appropriately redefining the values of the  $l$  powers, and those of the  $i$  and  $j$  coordinates. The structure of the sequence of operator pairs can be interpreted as follows. The isospin pairs with exponent  $l_1$  and  $l_5$  represent the operators coming from the dynamical correlations, and, eventually those coming from a statistical correlation line applied to the points 1 and 2. The pair with  $l_3$  represents the operator of the interaction. The isospin pairs with power  $l_2$  and  $l_4$  are associated to the operators of the vertex correction in the case  $j = i$ , and to the nodal diagram in the case  $j = 3 - i$ . Since we work in SOC approximation, there is only a single pair of isospin operators acting on these particles, therefore  $l_2, l_4 = 0, 1$ . On the other hand, there are no limitations on the values that the other  $l$  indexes can assume. We discuss below the three possible cases, compatible with the SOC approximation.

When  $l_2 = l_4 = 0$  we have a structure analogous to that treated in Sect. 3.3.2 and therefore:

$$\mathcal{T}_{l_1 0 l_3 0 l_5}^{t_1 t_2 t_3}(i, j) = \chi_{l_1 + l_3 + l_5}^{t_1 t_2} , \quad (250)$$

with  $\chi_{l_1+l_3+l_5}^{t_1 t_2}$  given by Eq. (121).

For the case  $l_2 \neq l_4$ , obviously one of the  $l$  indexes is 1 and the other one is 0. The expression of Eq. (246) can be written, with an appropriated redefinition of the power indexes, to an expression of the kind:

$$T_{l_1 l_2}^{t_1 t_2 t_3}(i) = \chi_{t_1}^+(1) \chi_{t_2}^+(2) \chi_{t_3}^+(3) (\boldsymbol{\tau}_1 \cdot \boldsymbol{\tau}_2)^{l_1} (\boldsymbol{\tau}_i \cdot \boldsymbol{\tau}_3) (\boldsymbol{\tau}_1 \cdot \boldsymbol{\tau}_2)^{l_2} \chi_{t_1}(1) \chi_{t_2}(2) \chi_{t_3}(3) . \quad (251)$$

These coefficients are related to the  $\mathcal{T}$  coefficients by the relations:

$$\mathcal{T}_{l_1 0 l_3 1 l_5}^{t_1 t_2 t_3}(i, j) = \mathcal{T}_{l_1 + l_3 l_5}^{t_1 t_2 t_3}(j) , \quad (252)$$

$$\mathcal{T}_{l_1 1 l_3 0 l_5}^{t_1 t_2 t_3}(i, j) = \mathcal{T}_{l_1 l_3 + l_5}^{t_1 t_2 t_3}(i) . \quad (253)$$

By using the recursive relation (118), we find for  $T_{l_1 l_2}^{t_1 t_2 t_3}(i)$  the following expression:

$$T_{l_1 l_2}^{t_1 t_2 t_3}(i) = a_{l_1} a_{l_2} T_{00}^{t_1 t_2 t_3}(i) + [a_{l_1}(1 - a_{l_2}) + (1 - a_{l_1})a_{l_2}] T_{10}^{t_1 t_2 t_3}(i) + (1 - a_{l_1})(1 - a_{l_2}) T_{11}^{t_1 t_2 t_3}(i) . \quad (254)$$

		$T_{l_1 l_2}^{t_1 t_2 t_3}(1)$			
$l_1$	$l_2$	$b_1$	$b_2$	$b_3$	$b_4$
0	0	-1	0	2	0
1	0	-1	0	0	2
1	1	-1	0	-2	4

Table 14: The values of the  $b$  coefficients of Eq. (248) used to calculate the basic  $T_{l_1 l_2}^{t_1 t_2 t_3}(1)$  terms of Eq. (254).

The values of the  $b$  coefficients for each term of Eq. (254) are given in Tab. 14 and have been calculated by using the expression:

$$\boldsymbol{\tau}_i \cdot \boldsymbol{\tau}_j \chi_{t_i}(i) \chi_{t_j}(j) = 2 \chi_{t_j}(i) \chi_{t_i}(j) - \chi_{t_i}(i) \chi_{t_j}(j) . \quad (255)$$

The values presented in Tab. 14 refer to the  $i = 1$  case. By using Eq. (249) we have:

$$T_{l_1 l_2}^{t_1 t_2 t_3}(2) = T_{l_1 l_2}^{t_2 t_1 t_3}(1) .$$

The last case we have to analyze is:  $l_2 = l_4 = 1$ . In this case, we can write:

$$\begin{aligned} \mathcal{T}_{l_1 1 l_3 1 l_5}^{t_1 t_2 t_3}(i, j) &= a_{l_1} a_{l_3} [a_{l_5} \mathcal{T}_{01010}^{t_1 t_2 t_3}(i, j) + (1 - a_{l_5}) \mathcal{T}_{01011}^{t_1 t_2 t_3}(i, j)] + \\ &\quad (1 - a_{l_1}) a_{l_3} [a_{l_5} \mathcal{T}_{11010}^{t_1 t_2 t_3}(i, j) + (1 - a_{l_5}) \mathcal{T}_{11011}^{t_1 t_2 t_3}(i, j)] + \\ &\quad a_{l_1} (1 - a_{l_3}) [a_{l_5} \mathcal{T}_{01110}^{t_1 t_2 t_3}(i, j) + (1 - a_{l_5}) \mathcal{T}_{01111}^{t_1 t_2 t_3}(i, j)] + \\ &\quad (1 - a_{l_1}) (1 - a_{l_3}) [a_{l_5} \mathcal{T}_{11110}^{t_1 t_2 t_3}(i, j) + (1 - a_{l_5}) \mathcal{T}_{11111}^{t_1 t_2 t_3}(i, j)] . \end{aligned} \quad (256)$$

The values of the matrix elements  $\mathcal{T}$  of the previous equations are given in Tab. 15 for  $i = 1$  and  $j = 1, 2$ . The other cases are calculated using Eq. (249).



$l_1$	$l_3$	$l_5$	$\mathcal{T}_{l_1 l_3 l_5}^{t_1 t_2 t_3}(1, 1)$				$\mathcal{T}_{l_1 l_3 l_5}^{t_1 t_2 t_3}(1, 2)$			
			$b_1$	$b_2$	$b_3$	$b_4$	$b_1$	$b_2$	$b_3$	$b_4$
0	0	0	5	0	-4	0	-1	2	0	0
1	0	0	-1	6	0	-4	5	-4	4	-4
0	1	0	-1	-2	0	4	5	4	-4	-4
0	0	1	-1	6	0	-4	5	-4	-4	4
1	1	0	-7	4	4	0	11	-2	0	-8
1	0	1	17	-12	4	-8	-13	14	0	0
0	1	1	-7	4	4	0	11	-2	-8	0
1	1	1	11	-14	8	-4	-7	16	-4	-4

Table 15: The values of the  $b$  coefficients of Eq. (248) used to calculate the basic  $\mathcal{T}_{l_1 l_2 l_3 l_4 l_5}^{t_1 t_2 t_3}(1, j)$  terms of Eq. (256) with  $j = 1, 2$ .

In order to simplify the notation in the calculation of the energy, we rename the matrix elements in the isospin space:

$$\chi_{l_1 l_2 l_3 l_4 l_5}^{t_1 t_2 t_3}(i) = \mathcal{T}_{l_1 l_2 l_3 l_4 l_5}^{t_1 t_2 t_3}(i, i) \quad (257)$$

$$\eta_{l_1 l_2 l_3 l_4 l_5}^{t_1 t_2 t_3}(i) = \mathcal{T}_{l_1 L_2 l_3 L_4 l_5}^{t_1 t_2 t_3}(i, 3 - i) \quad (258)$$

In the above definitions, the limitations related to the SOC approximation in the possibilities of linking isospin exchange operators, have been considered by defining  $L_2 = \delta_{i1}l_2 + \delta_{i2}l_4$  and  $L_4 = \delta_{i1}l_4 + \delta_{i2}l_2$ . This implies that the isospin term of Eq. (246) with exponent  $l_2$  acts on the pair 13, and the term with exponent  $l_4$  on the pair 23.

## D The uncorrelated one-body densities

In this appendix we present the general expressions of the uncorrelated one-body densities involved in the calculation of the kinetic energy for systems not saturated in isospin. We use a set of single particle wave functions expressed as indicated by Eq. (88).

The one-body density  $\rho_{T1}^{t_1}$  is given by:

$$\begin{aligned}\rho_{T1}^{t_1}(\mathbf{r}_1) &= \sum_{nljm} \left( \phi_{nljm}^{t_1*}(\mathbf{r}_1) \nabla_1^2 \phi_{nljm}^{t_1}(\mathbf{r}_1) - \nabla_1 \phi_{nljm}^{t_1*}(\mathbf{r}_1) \cdot \nabla_1 \phi_{nljm}^{t_1}(\mathbf{r}_1) \right) \\ &= \frac{1}{4\pi} \sum_{nlj} (2j+1) \left[ R_{nlj}^{t_1}(r_1) \left( D_{nlj}^{t_1}(r_1) - \frac{l(l+1)}{r_1^2} R_{nlj}^{t_1}(r_1) \right) \right. \\ &\quad \left. - [R_{nlj}^{t_1'}(r_1)]^2 \right],\end{aligned}\tag{259}$$

where we have carried out the trace in the spin space and we have defined:

$$D_{nlj}^{t_1}(r_1) = R_{nlj}^{t_1''}(r_1) + \frac{2}{r_1} R_{nlj}^{t_1'}(r_1) - \frac{l(l+1)}{r_1^2} R_{nlj}^{t_1}(r_1).\tag{260}$$

For the one-body density matrices  $\rho_{T2}$  and  $\rho_{T2,j}$  we find:

$$\begin{aligned}\rho_{T2}^{t_1 t_2}(\mathbf{r}_1, \mathbf{r}_2) &= \rho_0^{t_1}(\mathbf{r}_1, \mathbf{r}_2) \nabla_1^2 \rho_0^{t_2}(\mathbf{r}_1, \mathbf{r}_2) - \nabla_1 \rho_0^{t_1}(\mathbf{r}_1, \mathbf{r}_2) \cdot \nabla_1 \rho_0^{t_2}(\mathbf{r}_1, \mathbf{r}_2) \\ &= \frac{1}{4(4\pi)^2} \sum_{nljn'l'j'} (2j+1)(2j'+1) R_{nlj}^{t_1}(r_2) R_{n'l'j'}^{t_2}(r_2) \left\{ \right. \\ &\quad \left[ R_{nlj}^{t_1}(r_1) D_{n'l'j'}^{t_2}(r_1) - R_{nlj}^{t_1'}(r_1) R_{n'l'j'}^{t_2'}(r_1) \right] P_l(\cos \theta) P_{l'}(\cos \theta) \\ &\quad \left. - \frac{\sin^2 \theta}{r_1^2} R_{nlj}^{t_1}(r_1) R_{n'l'j'}^{t_2}(r_1) P_l'(\cos \theta) P_{l'}'(\cos \theta) \right\},\end{aligned}\tag{261}$$

$$\begin{aligned}\rho_{T2,j}^{t_1 t_2}(\mathbf{r}_1, \mathbf{r}_2) &= \frac{1}{(4\pi)^2} \sum_{nljn'l'j'} (-1)^{j+j'-l-l'-1} R_{nlj}^{t_1}(r_2) R_{n'l'j'}^{t_2}(r_2) \left\{ \right. \\ &\quad \left[ R_{nlj}^{t_1}(r_1) D_{n'l'j'}^{t_2}(r_1) - R_{nlj}^{t_1'}(r_1) R_{n'l'j'}^{t_2'}(r_1) \right] Q_l(\cos \theta) Q_{l'}(\cos \theta) \\ &\quad \left. - \frac{\sin^2(\theta)}{r_1^2} R_{nlj}^{t_1}(r_1) R_{n'l'j'}^{t_2}(r_1) Q_l'(\cos \theta) Q_{l'}'(\cos \theta) \right\},\end{aligned}\tag{262}$$

where  $P_l$  are Legendre polynomials,  $\theta$  is the angle between the vectors  $\mathbf{r}_1$  and  $\mathbf{r}_2$  and we have defined:

$$\begin{aligned}Q_l(\cos \theta) &= \sin \theta P_l'(\cos \theta), \\ Q_l'(\cos \theta) &= \frac{1}{\sin \theta} \left( \cos \theta P_l'(\cos \theta) - l(l+1) P_l(\cos \theta) \right).\end{aligned}$$

For the  $\rho_{T3}$  densities we have:

$$\rho_{T3}^{t_1}(\mathbf{r}_1, \mathbf{r}_2) = 2 \nabla_1^2 \rho_0^{t_1}(\mathbf{r}_1, \mathbf{r}_2)$$

$$= \frac{1}{4\pi} \sum_{nlj} (2j+1) R_{nlj}^{t_1}(r_2) D_{nlj}^{t_1}(r_1) P_l(\cos \theta) , \quad (263)$$

$$\begin{aligned} \rho_{T3,j}^{t_1}(\mathbf{r}_1, \mathbf{r}_2) &= 2\nabla_1^2 \rho_{0j}^{t_1}(\mathbf{r}_1, \mathbf{r}_2) \\ &= \frac{1}{2\pi} \sum_{nlj} (-1)^{j-l-\frac{1}{2}} R_{nlj}^{t_1}(r_2) D_{nlj}^{t_1}(r_1) Q_l(\cos \theta) . \end{aligned} \quad (264)$$

The last density that appears in the calculation of the center of mass energy can be written as:

$$\begin{aligned} \rho_{T4}^{t_1}(\mathbf{r}_1, \mathbf{r}_2) &= \rho_{T6}^{t_1}(\mathbf{r}_1, \mathbf{r}_2) - \rho_0^{t_1}(\mathbf{r}_1, \mathbf{r}_2) \rho_{T5}^{t_1}(\mathbf{r}_1, \mathbf{r}_2) \\ &\quad - \rho_{0j}^{t_1}(\mathbf{r}_1, \mathbf{r}_2) \rho_{T5,j}^{t_1}(\mathbf{r}_1, \mathbf{r}_2) , \end{aligned} \quad (265)$$

where we have defined:

$$\begin{aligned} \rho_{T6}^{t_1}(\mathbf{r}_1, \mathbf{r}_2) &= 2 \left( \nabla_1 \rho_0^{t_1}(\mathbf{r}_1, \mathbf{r}_2) \cdot \nabla_2 \rho_0^{t_1}(\mathbf{r}_1, \mathbf{r}_2) + \right. \\ &\quad \left. \nabla_1 \rho_{0j}^{t_1}(\mathbf{r}_1, \mathbf{r}_2) \cdot \nabla_2 \rho_{0j}^{t_1}(\mathbf{r}_1, \mathbf{r}_2) \right) , \end{aligned} \quad (266)$$

$$\rho_{T5,(j)}^{t_1}(\mathbf{r}_1, \mathbf{r}_2) = 2 \nabla_1 \cdot \nabla_2 \rho_{0(j)}^{t_1}(\mathbf{r}_1, \mathbf{r}_2) . \quad (267)$$

The explicit expressions of the above defined quantities are:

$$\begin{aligned} \rho_{T5}^{t_1}(\mathbf{r}_1, \mathbf{r}_2) &= \frac{1}{4\pi} \sum_{nlj} (2j+1) \left[ R_{nlj}^{t_1'}(r_1) R_{nlj}^{t_1'}(r_2) \cos \theta P_l(\cos \theta) + \right. \\ &\quad \left( R_{nlj}^{t_1'}(r_2) \frac{R_{nlj}^{t_1}(r_1)}{r_1} + R_{nlj}^{t_1'}(r_1) \frac{R_{nlj}^{t_1}(r_2)}{r_2} \right) \sin^2 \theta P_l'(\cos \theta) + \\ &\quad \left. \frac{R_{nlj}^{t_1}(r_1) R_{nlj}^{t_1}(r_2)}{r_1 r_2} \left( \sin^2 \theta P_l'(\cos \theta) + l(l+1) \cos \theta P_l(\cos \theta) \right) \right] , \end{aligned} \quad (268)$$

$$\begin{aligned} \rho_{T5,j}^{t_1}(\mathbf{r}_1, \mathbf{r}_2) &= \frac{1}{2\pi} \sum_{nlj} (-1)^{j-l-1/2} \left[ R_{nlj}^{t_1'}(r_1) R_{nlj}^{t_1'}(r_2) \cos \theta Q_l(\cos \theta) + \right. \\ &\quad \left( R_{nlj}^{t_1'}(r_2) \frac{R_{nlj}^{t_1}(r_1)}{r_1} + R_{nlj}^{t_1'}(r_1) \frac{R_{nlj}^{t_1}(r_2)}{r_2} \right) \sin^2 \theta Q_l'(\cos \theta) + \\ &\quad \frac{R_{nlj}^{t_1}(r_1) R_{nlj}^{t_1}(r_2)}{r_1 r_2} \left\{ \sin^2 \theta Q_l'(\cos \theta) + \right. \\ &\quad \left. \left( l(l+1) - \frac{1}{\sin^2 \theta} \right) \cos \theta Q_l(\cos \theta) \right\} \left. \right] , \end{aligned} \quad (269)$$

$$\begin{aligned} \rho_{T6}^{t_1}(\mathbf{r}_1, \mathbf{r}_2) &= \frac{1}{2(4\pi)^2} \sum_{\substack{nlj \\ n'l'j'}} (2j+1)(2j'+1) R_{nlj}^{t_1}(r_2) R_{n'l'j'}^{t_1}(r_1) \\ &\quad \left\{ \cos \theta \left[ R_{nlj}^{t_1'}(r_2) R_{n'l'j'}^{t_1'}(r_1) P_l(\cos \theta) P_{l'}(\cos \theta) - \right. \right. \end{aligned} \quad (270)$$

$$\begin{aligned}
& \sin^2 \theta \frac{R_{nlj}^{t_1}(r_2) R_{n'l'j'}^{t_1}(r_1)}{r_1 r_2} P_l'(\cos \theta) P_{l'}'(\cos \theta) \Big] + \\
& \sin^2 \theta \left[ \frac{R_{nlj}^{t_1}(r_2)}{r_2} R_{n'l'j'}^{t_1}(r_1) P_l'(\cos \theta) P_{l'}'(\cos \theta) + \right. \\
& \left. R_{nlj}^{t_1}(r_2) \frac{R_{n'l'j'}^{t_1}(r_1)}{r_1} P_l(\cos \theta) P_{l'}'(\cos \theta) \right] \Big\} + \\
& \frac{1}{2(2\pi)^2} \sum_{\substack{nlj \\ n'l'j'}} (-1)^{j+j'-l-l'-1} R_{nlj}^{t_1}(r_2) R_{n'l'j'}^{t_1}(r_1) \\
& \left\{ \cos \theta \left[ R_{nlj}^{t_1}(r_2) R_{n'l'j'}^{t_1}(r_1) Q_l(\cos \theta) Q_{l'}(\cos \theta) - \right. \right. \\
& \left. \sin^2 \theta \frac{R_{nlj}^{t_1}(r_2) R_{n'l'j'}^{t_1}(r_1)}{r_1 r_2} Q_l'(\cos \theta) Q_{l'}'(\cos \theta) \right] + \\
& \left. \sin^2 \theta \left[ \frac{R_{nlj}^{t_1}(r_2)}{r_2} R_{n'l'j'}^{t_1}(r_1) Q_l'(\cos \theta) Q_{l'}'(\cos \theta) + \right. \right. \\
& \left. \left. R_{nlj}^{t_1}(r_2) \frac{R_{n'l'j'}^{t_1}(r_1)}{r_1} Q_l(\cos \theta) Q_{l'}'(\cos \theta) \right] \right\} .
\end{aligned}$$

## E The expressions of the energy expectation value

The *interaction energy* defined in Sect. 4 as  $T_F + V_2 \equiv W$ , can be expressed in terms of:

$$\begin{aligned}
H_{JF}^{p,q,r}(r_{12}) = & \frac{1}{f_1^2(r_{12})} \left\{ -\frac{\hbar^2}{2m} \delta_{q,1} \left[ f_p(r_{12}) \nabla^2 f_r(r_{12}) - \nabla f_p(r_{12}) \cdot \nabla f_r(r_{12}) \right. \right. \\
& - \frac{6}{r_{12}^2} f_p(r_{12}) f_r(r_{12}) (\delta_{r,5} + \delta_{r,6}) (1 + \delta_{p,5} + \delta_{p,6}) \Big] \\
& \left. + f_p(r_{12}) v^q(r_{12}) f_r(r_{12}) \right\}. \tag{271}
\end{aligned}$$

In the following, we shall use the separation of the spin and isospin operators as was done in Eqs. (51) and (105). We shall identify the various isospin independent operators by using the  $k$  and  $u$  indexes, which can assume the values 1,2, and 3. The  $l$  indexes can assume the values 0 and 1.

As in Sect. 4, the expectation value of the interaction energy is calculated in four parts, see Eq. (137) and Fig. 16. The first contribution, called  $W_0$ , is given by:

$$W_0 = \frac{1}{2} \int d\mathbf{r}_1 d\mathbf{r}_2 H_{JF}^{2k_1-1+l_1, 2k_2-1+l_2, 2k_3-1+l_3}(r_{12}) \left[ \tag{272}$$

$$\begin{aligned}
& I^{k_1 k_2 k_3} A^{k_3} \rho_{2,dir}^{t_1 t_2}(\mathbf{r}_1, \mathbf{r}_2) \chi_{l_1+l_2+l_3}^{t_1 t_2} \\
& + I^{k_4 k_1 k_5} I^{k_2 k_3 k_5} A^{k_5} \Delta^{k_4} \rho_{2,exc}^{t_1 t_2}(\mathbf{r}_1, \mathbf{r}_2) \chi_{l_1+l_2+l_3+l_4}^{t_1 t_2} \\
& + I^{k_4 k_1 k_5} I^{k_2 k_3 k_6} I^{k_5 k_6 2} \Delta^{k_4} \rho_{2,excj}^{t_1 t_2}(\mathbf{r}_1, \mathbf{r}_2) \chi_{l_1+l_2+l_3+l_4}^{t_1 t_2} \Big], \tag{273}
\end{aligned}$$

and corresponds to the case when  $p > 1$  operators act between the external particles only. These operators are associated to  $f_p$ ,  $v^q$  and  $f_r$  functions in Eq. (271) for the direct terms. In addition, we should recall that the exchange terms have additional spin and isospin dependent operators because of the presence of the exchange operator  $\Pi^{\sigma\tau}(1,2)$ , see Eq. (58). By definition, this operator may act on the bra or on the ket. In our conventions we make it act on the ket so it is always to the left of the rest of the operators. The sequence of the three operators we have mentioned above, plus the exchange operators, are present in all the terms we are going to analyze, therefore we shall always use the same set of indexes. Furthermore, we should point out that in Eq. (273) a sum on all the  $k, l$  and  $t$  indexes is understood. This convention will be used in all the equations of this appendix.

The expressions of the densities used in Eq. (273) are given in Eqs.(209-211) defined in Appendix B, and include only state-independent vertex corrections. In this way, the  $\rho$  functions consider all the direct and exchange central dressing linked to the external points. As discussed in Sect. 3,  $A^{k=1,2,3} = 1, 3, 6$  and  $\Delta^k = 1 - \delta_{k,3}$ . The values of  $I^{k_1 k_2 k_3}$  and  $J^{k_1 k_2 k_3}$  are given by Eqs. (110) and (114). The  $\chi_l^{t_1 t_2}$  functions give the isospin traces and their values are given by Eq. (121).

We now discuss the effects produced by one SOR linked to one of the interacting particles. This is the  $W_s$  diagram of Fig. 16. The operator structure that we must analyze, for the direct case, is:

$$\frac{1}{2} \{k_1, u_1\} k_2 \frac{1}{2} \{k_3, u_2\} =$$

$u_1 k_1 k_2 k_3 u_2$	$I^{k_1 k_2 k_3} A^{k_3} A^{u_1} \delta_{u_1 u_2}$
$u_1 k_1 k_2 u_2 k_3$	$I^{k_1 k_2 k_3} A^{k_3} (1 + D_{k_3 u_1}) A^{u_1} \delta_{u_1 u_2}$
$k_1 u_1 k_2 k_3 u_2$	$I^{k_1 k_2 k_3} A^{k_3} (1 + D_{k_1 u_1}) A^{u_1} \delta_{u_1 u_2}$
$k_1 u_1 k_2 u_2 k_3$	$I^{k_1 k_2 k_3} A^{k_3} (1 + D_{k_2 u_1}) A^{u_1} \delta_{u_1 u_2}$

Table 16: Spin traces of the operators in Eq. (274).

$$\frac{1}{4} (u_1 k_1 k_2 k_3 u_2 + u_1 k_1 k_2 u_2 k_3 + k_1 u_1 k_2 k_3 u_2 + k_1 u_1 k_2 u_2 k_3) , \quad (274)$$

In the above equation, the  $k$  and  $u$  indicate the operators  $P^k$  and  $P^u$ , Eq. (51). The  $k_1$ ,  $k_2$  and  $k_3$  operators act on the pair of particles 1 and 2. The  $u_1$  and  $u_2$  operators act, instead, on the particles pair 1 and 3, or 2 and 3. The symbol  $\{, \}$  indicates the anticommutator. The values of the traces of the various terms of Eq. (274), are given in Tab. 16.

$u_1 k_1 k_2 k_3 u_2$	$I^{k_4 k_1 k_5} I^{k_2 k_3 k_5} A^{k_5} (1 + D_{k_4 u_1}) A^{u_1} \delta_{u_1 u_2}$
$u_1 k_1 k_2 u_2 k_3$	$I^{k_4 k_1 k_5} I^{k_2 k_3 k_5} A^{k_5} (1 + D_{k_5 u_1}) A^{u_1} \delta_{u_1 u_2}$
$k_1 u_1 k_2 k_3 u_2$	$I^{k_4 k_1 k_5} I^{k_2 k_3 k_5} A^{k_5} (1 + D_{k_5 u_1}) A^{u_1} \delta_{u_1 u_2}$
$k_1 u_1 k_2 u_2 k_3$	$I^{k_4 k_1 k_5} I^{k_2 k_3 k_5} A^{k_5} (1 + D_{k_2 u_1}) A^{u_1} \delta_{u_1 u_2}$

Table 17: Spin traces for the parallel spins case of the operators of Eq. (274).

$k_4 u_1 k_1 k_2 k_3 u_2$	$I^{k_4 k_1 k_5} I^{k_2 k_3 k_6} I^{k_5 k_6^2} (1 + D_{k_4 u_1}) A^{u_1} \delta_{u_1 u_2}$
$k_4 u_1 k_1 k_2 u_2 k_3$	$I^{k_4 k_1 k_5} I^{k_2 k_3 k_6} I^{k_5 k_6^2} (1 + D_{k_5 u_1}) A^{u_1} \delta_{u_1 u_2}$
$k_4 k_1 u_1 k_2 k_3 u_2$	$I^{k_4 k_1 k_5} I^{k_2 k_3 k_6} I^{k_5 k_6^2} (1 + D_{k_5 u_1}) A^{u_1} \delta_{u_1 u_2}$
$k_4 k_1 u_1 k_2 u_2 k_3$	$I^{k_4 k_1 k_5} I^{k_2 k_3 k_6} I^{k_5 k_6^2} (1 + D_{k_2 u_1}) A^{u_1} \delta_{u_1 u_2}$

Table 18: Spin traces for the case of antiparallel spins between particles 1 and 2 in Eq. (274).

In the exchange case, an additional  $k_4$  operator must be included on the left hand side, following our conventions. Since we work with single particle wave functions expressed in a  $jj$  coupling scheme, antiparallel spin terms are usually contributing. For this reason in the exchange case, we have to distinguish the parallel and antiparallel spin situations. For the case of parallel spins between the interacting points, by following Ref. [21], we obtain results given in Tab. 17.

For the antiparallel spin term, we have to distinguish the case when the antiparallel spins are those of interacting points, whose results are given in Tab. 18, from the case when they are those of the 1 and 3 particles, or those of the 2 and 3 particles. In this last case  $u_1$  must be an exchange operator acting on the left hand side of the operator product. This produces the results given in Tab. 19.

In the Tabs. 17, 18, 19, we have used the following values of the  $D$  terms:

$$D_{k_1, k_2} = \begin{pmatrix} 0 & 0 & 0 \\ 0 & -4/3 & -4/3 \\ 0 & -4/3 & -4/3 \end{pmatrix} , \quad (275)$$

$u_1 k_1 k_2 k_3 u_2$	$I^{k_1 k_2 k_3} A^{k_3} I^{u_1 u_2 2}$
$u_1 k_1 k_2 u_2 k_3$	$I^{k_1 k_2 k_3} A^{k_3} I^{u_1 u_2 2} (1 + D_{k_3 u_1})$
$u_1 k_1 u_2 k_2 k_3$	$I^{k_1 k_2 k_3} A^{k_3} I^{u_1 u_2 2} (1 + D_{k_1 u_1})$
$u_1 u_2 k_1 k_2 k_3$	$I^{k_1 k_2 k_3} A^{k_3} I^{u_1 u_2 2}$

Table 19: Spin traces for the case of antiparallel spins between the particles in 1 and 3 or 2 and 3 in Eq. (274).

which corresponds to the odd values of  $E_{pq}$  defined in Tab. 13 of Appendix A.

All the isospin parts of the above operators can be written by using the  $\chi_{l_1 l_2 l_3 l_4 l_5}^{t_1 t_2 t_3}(i)$ , function defined in Eq. (257). The contribution of the SOR to the interaction energy is:

$$\begin{aligned}
W_s = & \frac{1}{8} \int d\mathbf{r}_1 d\mathbf{r}_2 H_{JF}^{2k_1-1+l_1, 2k_2-1+l_2, 2k_3-1+l_3}(r_{12}) \left( I^{k_1 k_2 k_3} A^{k_3} \right. \\
& \left\{ \rho_{2,dir}^{t_1 t_2}(\mathbf{r}_1, \mathbf{r}_2) \left[ M_{d,l_1,l_2,l_3}^{t_1 t_2 k_1 k_2 k_3}(\mathbf{r}_1) + M_{d,l_1,l_2,l_3}^{t_1 t_2 k_1 k_2 k_3}(\mathbf{r}_2) \right] \right. \\
& + \left[ g_{dd}^{t_1 t_2}(\mathbf{r}_1, \mathbf{r}_2) C_{22}^{t_2}(\mathbf{r}_2) + g_{de}^{t_1 t_2}(\mathbf{r}_1, \mathbf{r}_2) C_{d,22}^{t_2}(\mathbf{r}_2) \right] C_{d,22}^{t_1}(\mathbf{r}_1) M_{e,l_1,l_2,l_3}^{t_1 t_2 k_1 k_2 k_3}(\mathbf{r}_1) \\
& + \left[ g_{dd}^{t_1 t_2}(\mathbf{r}_1, \mathbf{r}_2) C_{22}^{t_1}(\mathbf{r}_1) + g_{ed}^{t_1 t_2}(\mathbf{r}_1, \mathbf{r}_2) C_{d,22}^{t_1}(\mathbf{r}_1) \right] C_{d,22}^{t_2}(\mathbf{r}_2) M_{e,l_1,l_2,l_3}^{t_1 t_2 k_1 k_2 k_3}(\mathbf{r}_2) \\
& + \left[ g_{dd}^{t_1 t_2}(\mathbf{r}_1, \mathbf{r}_2) C_{22}^{t_2}(\mathbf{r}_2) + g_{de}^{t_1 t_2}(\mathbf{r}_1, \mathbf{r}_2) C_{d,22}^{t_2}(\mathbf{r}_2) \right] C_{d,22}^{t_1}(\mathbf{r}_1) M_{ej,l_1,l_2,l_3}^{t_1 t_2 k_1 k_2 k_3}(\mathbf{r}_1) \\
& + \left. \left[ g_{dd}^{t_1 t_2}(\mathbf{r}_1, \mathbf{r}_2) C_{22}^{t_1}(\mathbf{r}_1) + g_{ed}^{t_1 t_2}(\mathbf{r}_1, \mathbf{r}_2) C_{d,22}^{t_1}(\mathbf{r}_1) \right] C_{d,22}^{t_2}(\mathbf{r}_2) M_{ej,l_1,l_2,l_3}^{t_1 t_2 k_1 k_2 k_3}(\mathbf{r}_2) \right\} \\
& + I^{k_4 k_1 k_5} I^{k_2 k_3 k_6} A^{k_5} \Delta^{k_4} \rho_{2,exc}^{t_1 t_2}(\mathbf{r}_1, \mathbf{r}_2) \left[ M_{d,l_1,l_2,l_3,l_4}^{t_1 t_2 k_2 k_4 k_5}(\mathbf{r}_1) + M_{d,l_1,l_2,l_3,l_4}^{t_1 t_2 k_2 k_4 k_5}(\mathbf{r}_2) \right] \\
& + I^{k_4 k_1 k_5} I^{k_2 k_3 k_6} I^{k_5 k_6 2} \Delta^{k_4} \rho_{2,excj}^{t_1 t_2}(\mathbf{r}_1, \mathbf{r}_2) \\
& \left. \left[ M_{d,l_1,l_2,l_3,l_4}^{t_1 t_2 k_2 k_4 k_5}(\mathbf{r}_1) + M_{d,l_1,l_2,l_3,l_4}^{t_1 t_2 k_2 k_4 k_5}(\mathbf{r}_2) \right] \right) , \tag{276}
\end{aligned}$$

where we have defined

$$\begin{aligned}
M_{m,l_1,l_2,l_3}^{t_1 t_2 k_1 k_2 k_3}(\mathbf{r}_i) = & M_{m,0,l_1+l_2+l_3,0}^{t_1 t_2 u_1}(\mathbf{r}_i) + (1 + D_{k_3 u_1}) M_{m,0,l_1+l_2,l_3}^{t_1 t_2 u_1}(\mathbf{r}_i) \\
& + (1 + D_{k_1 u_1}) M_{m,l_1,l_2+l_3,0}^{t_1 t_2 u_1}(\mathbf{r}_i) \\
& + (1 + D_{k_2 u_1}) M_{m,l_1,l_2,l_3}^{t_1 t_2 u_1}(\mathbf{r}_i) , \tag{277}
\end{aligned}$$

$$\begin{aligned}
M_{ej,l_1,l_2,l_3}^{t_1 t_2 k_1 k_2 k_3}(\mathbf{r}_i) = & M_{ej,0,0,l_1+l_2+l_3}^{t_1 t_2 u_1 u_2}(\mathbf{r}_i) + (1 + D_{k_3 u_1}) M_{ej,0,l_1+l_2,l_3}^{t_1 t_2 u_1 u_2}(\mathbf{r}_i) \\
& + (1 + D_{k_1 u_1}) M_{ej,0,l_1,l_2+l_3}^{t_1 t_2 u_1 u_2}(\mathbf{r}_i) + M_{ej,0,l_1+l_2+l_3,0}^{t_1 t_2 u_1 u_2}(\mathbf{r}_i) , \tag{278}
\end{aligned}$$

$$\begin{aligned}
M_{d,l_1,l_2,l_3,l_4}^{t_1 t_2 k_2 k_4 k_5}(\mathbf{r}_i) = & (1 + D_{k_5 u_1}) (M_{d,l_4+l_1,l_2+l_3,0}^{t_1 t_2 u_1}(\mathbf{r}_i) + M_{d,l_4,l_1+l_2,l_3}^{t_1 t_2 u_1}(\mathbf{r}_i)) \\
& + (1 + D_{k_4 u_1}) M_{d,l_4,l_1+l_2+l_3,0}^{t_1 t_2 u_1}(\mathbf{r}_i) \\
& + (1 + D_{k_2 u_1}) M_{d,l_4+l_1,l_2,l_3}^{t_1 t_2 u_1}(\mathbf{r}_i) , \tag{279}
\end{aligned}$$

$$M_{m,l_1,l_2,l_3}^{t_1 t_2 u_1}(\mathbf{r}_i) = A^{u_1} \left[ (1 - \delta_{u_1,1}) \chi_{l_1 0 l_2 0 l_3}^{t_1 t_2 t_3}(i) U_{m,2u_1-1,2u_1-1}^{\mu t_3}(\mathbf{r}_i) \right]$$

	Direct	Exchange
$u_1 k_1 k_2 k_3 u_2$	$I^{k_1 k_2 k_6} J^{k_3 k_5 k_6} A^{k_6}$	$I^{k_1 k_2 k_6} I^{k_6 k_3 k_7} J^{k_4 k_5 k_7}$
$u_1 k_1 k_2 u_2 k_3$	$I^{k_1 k_2 k_6} J^{k_3 k_5 k_6}$	$I^{k_1 k_2 k_6} I^{k_3 k_4 k_7} J^{k_7 k_5 k_6}$
$k_1 u_1 k_2 k_3 u_2$	$I^{k_2 k_3 k_6} J^{k_1 k_5 k_6}$	$I^{k_2 k_3 k_6} I^{k_4 k_1 k_7} J^{k_7 k_5 k_6}$
$k_1 u_1 k_2 u_2 k_3$	$I^{k_3 k_1 k_6} J^{k_2 k_5 k_6}$	$I^{k_3 k_4 k_6} I^{k_6 k_1 k_7} J^{k_2 k_5 k_7}$
$u_1 u_2 k_1 k_2 k_3$	$I^{k_1 k_2 k_6} J^{k_3 k_5 k_6} A^{k_6}$	$I^{k_4 k_5 k_6} I^{k_1 k_2 k_7} I^{k_6 k_7 k_3} A^{k_3}$
$k_1 u_1 u_2 k_2 k_3$	$I^{k_1 k_2 k_6} J^{k_3 k_5 k_6} A^{k_6}$	$I^{k_4 k_5 k_6} I^{k_1 k_2 k_7} I^{k_6 k_7 k_3} A^{k_3}$
$u_1 k_1 u_2 k_2 k_3$	$I^{k_2 k_3 k_6} J^{k_1 k_5 k_6}$	$I^{k_2 k_3 k_6} I^{k_6 k_4 k_7} J^{k_1 k_5 k_7}$
$k_1 k_2 k_3 u_1 u_2$	$I^{k_1 k_2 k_6} J^{k_3 k_5 k_6} A^{k_6}$	$I^{k_4 k_5 k_6} I^{k_1 k_2 k_7} I^{k_6 k_7 k_3} A^{k_3}$
$k_1 k_2 u_1 u_2 k_3$	$I^{k_1 k_2 k_6} J^{k_3 k_5 k_6} A^{k_6}$	$I^{k_4 k_5 k_6} I^{k_1 k_2 k_7} I^{k_6 k_7 k_3} A^{k_3}$
$k_1 k_2 u_1 k_3 u_2$	$I^{k_1 k_2 k_6} J^{k_3 k_5 k_6}$	$I^{k_4 k_1 k_6} I^{k_6 k_2 k_7} J^{k_3 k_5 k_7}$

Table 20: The traces obtained for the  $W_c(dd)$  term.

$$\begin{aligned}
& + \chi_{l_1 l_2 0 l_3}^{t_1 t_2 t_3}(i) U_{m, 2u_1, 2u_1-1}^{\mu t_3}(\mathbf{r}_i) + \chi_{l_1 0 l_2 1 l_3}^{t_1 t_2 t_3}(i) U_{m, 2u_1-1, 2u_1}^{\mu t_3}(\mathbf{r}_i) \\
& + \chi_{l_1 1 l_2 1 l_3}^{t_1 t_2 t_3}(i) U_{m, 2u_1, 2u_1}^{\mu t_3}(\mathbf{r}_i) \Big] , \tag{280}
\end{aligned}$$

$$\begin{aligned}
M_{ej, l_1, l_2, l_3}^{t_1 t_2 u_1 u_2}(\mathbf{r}_i) &= I^{u_1 u_2 2} \Big[ \chi_{l_1 0 l_2 0 l_3}^{t_1 t_2 t_3}(i) U_{ej, 2u_1-1, 2u_2-1}^{\mu t_3}(\mathbf{r}_i) + \chi_{l_1 1 l_2 0 l_3}^{t_1 t_2 t_3}(i) U_{ej, 2u_1, 2u_2-1}^{\mu t_3}(\mathbf{r}_i) \\
& + \chi_{l_1 0 l_2 1 l_3}^{t_1 t_2 t_3}(i) U_{ej, 2u_1-1, 2u_2}^{\mu t_3}(\mathbf{r}_i) + \chi_{l_1 1 l_2 1 l_3}^{t_1 t_2 t_3}(i) U_{ej, 2u_1, 2u_2}^{\mu t_3}(\mathbf{r}_i) \Big] , \tag{281}
\end{aligned}$$

In the above equations we have considered that  $i = 1, 2$ ,  $m = d, e$ , and  $\mu = t_1$  for  $i = 1$  and  $\mu = t_2$  for  $i = 2$ . The expressions of the  $U_{m, pq}^{t_1 t_2}(\mathbf{r}_i)$  and  $U_{ej, pq}^{t_1 t_2}(\mathbf{r}_i)$  functions are given by Eqs. (245).

The structure of the  $W_c$  term is more involved. We calculate separately the various terms according to the direct or exchange nature of the correlations reaching the external points.

$$W_c = W_c(dd) + W_c(ed) + W_c(de) + W_c(ee) + W_c(cc) . \tag{282}$$

The operator structure that we must analyze in the  $dd$  direct case is:

$$\begin{aligned}
& \frac{1}{4} \left[ \frac{1}{4} \{k_1, u_1\} k_2 \{k_3, u_2\} + \frac{1}{4} \{k_1, u_2\} k_2 \{k_3, u_1\} + \right. \\
& \frac{1}{6} \left( \{ \{u_1, u_2\}, k_1 \} + u_1 k_1 u_2 + u_2 k_1 u_1 \right) k_2 k_3 + \\
& \left. \frac{1}{6} k_1 k_2 \left( \{ \{u_1, u_2\}, k_3 \} + u_1 k_3 u_2 + u_2 k_3 u_1 \right) \right] , \tag{283}
\end{aligned}$$

where the various symbols have the same meaning as in Eq. (274).

We calculate the value of this term by using the result of Eq. (67), and the results are given in Tab. 20. In this table, the factors  $\zeta_{132}^{u_1 u_2 k_5}$  are not present, since they will be included in the expressions of the nodal diagrams terms  $N$  which we shall define in analogy to Eq. (71). The value of the spin traces are the same if we exchange  $u_1$  and  $u_2$ . For this reason, we have only



shown the results when  $u_1$  is on the left hand side of  $u_2$ . The isospin traces do not have this property and their values are given by the coefficients  $\eta_{l_1 l_2 l_3 l_4 l_5}^{t_1 t_2 t_3}(i)$  defined in Eq. (258). Since we have observed that the exchange contribution from antiparallel spins is much smaller than that from the parallel ones, we have neglected the contribution of the antiparallel spins in the SOC terms.

By using the above definitions we can write:

$$\begin{aligned}
W_c(dd) = & \frac{1}{24} \int d\mathbf{r}_1 d\mathbf{r}_2 H_{JF}^{2k_1-1+l_1, 2k_2-1+l_2, 2k_3-1+l_3}(r_{12}) \left( \rho_{2,dir}^{t_1 t_2}(\mathbf{r}_1, \mathbf{r}_2) \left[ \right. \right. \\
& I^{k_1 k_2 k_6} I^{k_3 k_5 k_6} A^{k_6} M_{1,dd,l_1,l_2,l_3}^{t_1 t_2 k_5}(\mathbf{r}_1, \mathbf{r}_2) \\
& + I^{k_1 k_2 k_6} J^{k_3 k_5 k_6} M_{2,dd,l_1,l_2,l_3}^{t_1 t_2 k_5}(\mathbf{r}_1, \mathbf{r}_2) \\
& + I^{k_2 k_3 k_6} J^{k_1 k_5 k_6} M_{3,dd,l_1,l_2,l_3}^{t_1 t_2 k_5}(\mathbf{r}_1, \mathbf{r}_2) + \frac{3}{2} I^{k_3 k_1 k_6} J^{k_2 k_5 k_6} M_{dd,l_1,l_2,l_3}^{t_1 t_2 k_5}(\mathbf{r}_1, \mathbf{r}_2) \left. \right] \\
& + \Delta^{k_4} \rho_{2,exc}^{t_1 t_2}(\mathbf{r}_1, \mathbf{r}_2) \left\{ \frac{3}{2} \left[ I^{k_1 k_2 k_6} I^{k_6 k_3 k_7} J^{k_4 k_5 k_7} M_{dd,l_4,l_1+l_2+l_3,0}^{t_1 t_2 k_5}(\mathbf{r}_1, \mathbf{r}_2) \right. \right. \\
& + I^{k_1 k_2 k_6} I^{k_3 k_4 k_7} J^{k_7 k_5 k_6} M_{dd,l_4,l_1+l_2,l_3}^{t_1 t_2 k_5}(\mathbf{r}_1, \mathbf{r}_2) \\
& + I^{k_2 k_3 k_6} I^{k_4 k_1 k_7} J^{k_7 k_5 k_6} M_{dd,l_4+l_1,l_2+l_3,0}^{t_1 t_2 k_5}(\mathbf{r}_1, \mathbf{r}_2) \\
& + I^{k_3 k_4 k_6} I^{k_6 k_1 k_7} J^{k_2 k_5 k_7} M_{dd,l_4+l_1,l_2,l_3}^{t_1 t_2 k_5}(\mathbf{r}_1, \mathbf{r}_2) \left. \right] \\
& + I^{k_4 k_5 k_6} I^{k_1 k_2 k_7} I^{k_6 k_7 k_3} A^{k_3} M_{4,dd,l_1,l_2,l_3,l_4}^{t_1 t_2 k_5}(\mathbf{r}_1, \mathbf{r}_2) \\
& + I^{k_2 k_3 k_6} I^{k_6 k_4 k_7} J^{k_1 k_5 k_7} M_{dd,l_4,l_1,l_2+l_3}^{t_1 t_2 k_5}(\mathbf{r}_1, \mathbf{r}_2) \\
& + I^{k_4 k_1 k_6} I^{k_6 k_2 k_7} J^{k_3 k_5 k_7} M_{dd,l_4+l_1+l_2,l_3,0}^{t_1 t_2 k_5}(\mathbf{r}_1, \mathbf{r}_2) \left. \right\} \Bigg) , \tag{284}
\end{aligned}$$

where we have defined

$$M_{dd,l_1,l_2,l_3}^{t_1 t_2 k_5}(\mathbf{r}_1, \mathbf{r}_2) = \frac{1}{2} \left[ M_{dd,l_1,l_2,l_3}^{t_1 t_2 k_5}(\mathbf{r}_1, \mathbf{r}_2; 1) + M_{dd,l_1,l_2,l_3}^{t_1 t_2 k_5}(\mathbf{r}_1, \mathbf{r}_2; 2) \right], \tag{285}$$

$$\begin{aligned}
M_{1,dd,l_1,l_2,l_3}^{t_1 t_2 k_5}(\mathbf{r}_1, \mathbf{r}_2) = & \frac{3}{2} M_{dd,0,l_1+l_2+l_3,0}^{t_1 t_2 k_5}(\mathbf{r}_1, \mathbf{r}_2) + M_{dd,0,0,l_1+l_2+l_3}^{t_1 t_2 k_5}(\mathbf{r}_1, \mathbf{r}_2) + \\
& M_{dd,l_1,0,l_2+l_3}^{t_1 t_2 k_5}(\mathbf{r}_1, \mathbf{r}_2) + M_{dd,l_1+l_2+l_3,0,0}^{t_1 t_2 k_5}(\mathbf{r}_1, \mathbf{r}_2) + \\
& M_{dd,l_1+l_2,0,l_3}^{t_1 t_2 k_5}(\mathbf{r}_1, \mathbf{r}_2), \tag{286}
\end{aligned}$$

$$M_{2,dd,l_1,l_2,l_3}^{t_1 t_2 k_5}(\mathbf{r}_1, \mathbf{r}_2) = \frac{3}{2} M_{dd,0,l_1+l_2,l_3}^{t_1 t_2 k_5}(\mathbf{r}_1, \mathbf{r}_2) + M_{dd,l_1+l_2,l_3,0}^{t_1 t_2 k_5}(\mathbf{r}_1, \mathbf{r}_2), \tag{287}$$

$$M_{3,dd,l_1,l_2,l_3}^{t_1 t_2 k_5}(\mathbf{r}_1, \mathbf{r}_2) = \frac{3}{2} M_{dd,l_1,l_2+l_3,0}^{t_1 t_2 k_5}(\mathbf{r}_1, \mathbf{r}_2) + M_{dd,0,l_1,l_2+l_3}^{t_1 t_2 k_5}(\mathbf{r}_1, \mathbf{r}_2), \tag{288}$$

$$\begin{aligned}
M_{4,dd,l_1,l_2,l_3,l_4}^{t_1 t_2 k_5}(\mathbf{r}_1, \mathbf{r}_2) = & M_{dd,l_4,0,l_1+l_2+l_3}^{t_1 t_2 k_5}(\mathbf{r}_1, \mathbf{r}_2) + M_{dd,l_4+l_1,0,l_2+l_3}^{t_1 t_2 k_5}(\mathbf{r}_1, \mathbf{r}_2) + \\
& M_{dd,l_4+l_1+l_2+l_3,0,0}^{t_1 t_2 k_5}(\mathbf{r}_1, \mathbf{r}_2) + M_{dd,l_4+l_1+l_2,0,l_3}^{t_1 t_2 k_5}(\mathbf{r}_1, \mathbf{r}_2), \tag{289}
\end{aligned}$$

and

$$M_{mn,l_1,l_2,l_3}^{t_1 t_2 k_5}(\mathbf{r}_1, \mathbf{r}_2; i) = \sum_{u_1, u_2=1}^3 \sum_{t_3=p,n} \left[ \eta_{l_1,1,l_2,1,l_3}^{t_1 t_2 t_3}(i) N_{mn,2k_5,2u_1,2u_2}^{t_1 t_2 t_3}(\mathbf{r}_1, \mathbf{r}_2) \right]$$

$$\begin{aligned}
& + \eta_{l_1,1,l_2,0,l_3}^{t_1 t_2 t_3}(i) N_{mn,2k_5-1,2u_1,2u_2-1}^{t_1 t_2 t_3}(\mathbf{r}_1, \mathbf{r}_2) \\
& + \eta_{l_1,0,l_2,1,l_3}^{t_1 t_2 t_3}(i) N_{mn,2k_5-1,2u_1-1,2u_2}^{t_1 t_2 t_3}(\mathbf{r}_1, \mathbf{r}_2) \\
& + (1 - \delta_{k_5 1}) \eta_{l_1,0,l_2,0,l_3}^{t_1 t_2 t_3}(i) N_{mn,2k_5-1,2u_1-1,2u_2-1}^{t_1 t_2 t_3}(\mathbf{r}_1, \mathbf{r}_2) \Big] , \quad (290)
\end{aligned}$$

The  $mn$  labels indicate that this last equation is valid not only for the  $dd$  case but also for the  $ed$ ,  $de$  and  $ee$  ones.

So far, we have calculated diagrams where only dynamical correlations reach the external points 1 and 2. The statistical correlations, labeled with  $e$ , are treated by using the spin-isospin exchange operator. In the  $ed$  part, the operator structure is:

$$\frac{1}{2} u_1 \left[ \frac{1}{2} k_1 k_2 \{k_3, u_2\} + \frac{1}{2} \{k_1, u_2\} k_2 k_3 \right] , \quad (291)$$

since  $u_1$  is the spin-isospin exchange operator acting always on the left hand side. The various terms have already been calculated in the evaluation of the  $dd$  part (see Tab. 20). We obtain:

$$\begin{aligned}
W_c(ed) &= \frac{1}{8} \int d\mathbf{r}_1 d\mathbf{r}_2 H_{JF}^{2k_1-1+l_1, 2k_2-1+l_2, 2k_3-1+l_3}(r_{12}) \cdot \\
& (g_{dd}^{t_1 t_2}(\mathbf{r}_1, \mathbf{r}_2) C_{22}^{t_2}(\mathbf{r}_2) + g_{de}^{t_1 t_2}(\mathbf{r}_1, \mathbf{r}_2) C_{d,22}^{t_2}(\mathbf{r}_2)) C_{d,22}^{t_1}(\mathbf{r}_1) \\
& \left\{ I^{k_1 k_2 k_6} J^{k_3 k_5 k_6} A^{k_6} \left[ M_{ed,0,l_1+l_2+l_3,0}^{t_1 t_2 k_5}(\mathbf{r}_1, \mathbf{r}_2; 1) + M_{ed,0,0,l_1+l_2+l_3}^{t_1 t_2 k_5}(\mathbf{r}_1, \mathbf{r}_2; 1) \right] \right. \\
& + I^{k_1 k_2 k_6} J^{k_3 k_5 k_6} M_{ed,0,l_1+l_2,l_3}^{t_1 t_2 k_5}(\mathbf{r}_1, \mathbf{r}_2; 1) \\
& \left. + I^{k_2 k_3 k_6} J^{k_1 k_5 k_6} M_{ed,0,l_1,l_2+l_3}^{t_1 t_2 k_5}(\mathbf{r}_1, \mathbf{r}_2; 1) \right\} . \quad (292)
\end{aligned}$$

The  $de$  term of Eq. (282) has the same operator structure as the  $ed$  term when  $u_1$  and  $u_2$  are interchanged. This does not change the spin traces, therefore the result is:

$$\begin{aligned}
W_c(de) &= \frac{1}{8} \int d\mathbf{r}_1 d\mathbf{r}_2 H_{JF}^{2k_1-1+l_1, 2k_2-1+l_2, 2k_3-1+l_3}(r_{12}) \\
& \left[ g_{dd}^{t_1 t_2}(\mathbf{r}_1, \mathbf{r}_2) C_{22}^{t_1}(\mathbf{r}_1) + g_{ed}^{t_1 t_2}(\mathbf{r}_1, \mathbf{r}_2) C_{d,22}^{t_1}(\mathbf{r}_1) \right] C_{d,22}^{t_2}(\mathbf{r}_2) \\
& \left\{ I^{k_1 k_2 k_6} J^{k_3 k_5 k_6} A^{k_6} \left[ M_{de,0,l_1+l_2+l_3,0}^{t_1 t_2 k_5}(\mathbf{r}_1, \mathbf{r}_2; 2) + M_{de,0,0,l_1+l_2+l_3}^{t_1 t_2 k_5}(\mathbf{r}_1, \mathbf{r}_2; 2) \right] \right. \\
& + I^{k_1 k_2 k_6} J^{k_3 k_5 k_6} M_{de,0,l_1+l_2,l_3}^{t_1 t_2 k_5}(\mathbf{r}_1, \mathbf{r}_2; 2) \\
& \left. + I^{k_2 k_3 k_6} J^{k_1 k_5 k_6} M_{de,0,l_1,l_2+l_3}^{t_1 t_2 k_5}(\mathbf{r}_1, \mathbf{r}_2; 2) \right\} . \quad (293)
\end{aligned}$$

Since  $u_1$  and  $u_2$  are spin-isospin exchange operators, in the  $ee$  term, the only possible ordering of operators is  $1/2\{u_1, u_2\}k_1 k_2 k_3$ . We obtain:

$$\begin{aligned}
W_c(ee) &= \frac{1}{2} \int d\mathbf{r}_1 d\mathbf{r}_2 H_{JF}^{2k_1-1+l_1, 2k_2-1+l_2, 2k_3-1+l_3}(r_{12}) \\
& C_{d,22}^{t_1}(\mathbf{r}_1) g_{dd}^{t_1 t_2}(\mathbf{r}_1, \mathbf{r}_2) C_{d,22}^{t_2}(\mathbf{r}_2) I^{k_1 k_2 k_6} J^{k_3 k_5 k_6} A^{k_6} \\
& \frac{1}{2} \left[ M_{ee,l_1 l_2 l_3}^{t_1 t_2 k_5}(\mathbf{r}_1, \mathbf{r}_2; 1) + M_{ee,0,0,l_1+l_2+l_3}^{t_1 t_2 k_5}(\mathbf{r}_1, \mathbf{r}_2; 2) \right] . \quad (294)
\end{aligned}$$

To calculate the  $W_c(cc)$  term of the eq. (282) we found it useful to consider separately the situations where the  $p > 1$  operators appear on the left, or on the right hand sides of the folding integrals. Specifically we define non-nodal diagrams as:

$$X_{cc,p}^{Zt_1}(\mathbf{r}_1, \mathbf{r}_2) = \left[ 2f_1(r_{12})f_p(r_{12}) + N_{dd,p}^{t_1t_1}(\mathbf{r}_1, \mathbf{r}_2) \right] g_{cc}^{t_1}(\mathbf{r}_1, \mathbf{r}_2) + [g_{dd}^{t_1t_1}(\mathbf{r}_1, \mathbf{r}_2) - 1] N_{cc,p}^{Zt_1}(\mathbf{r}_1, \mathbf{r}_2), \quad (295)$$

where the label  $Z$  can be  $L$  (for left) and  $R$  (for right). By using Eqs. (219) and (220) we define the left and right nodal diagrams as:

$$N_{cc,pqr}^{Lt_1t_3}(\mathbf{r}_1, \mathbf{r}_2) = \left( X_{cc,q}^{Lt_1}(1, 3) \zeta_{132}^{k_2k_3k_1} C_{d,q}^{t_3}(3) \frac{\Delta^{k_3}}{2} \left| X_{cc}^{t_3}(3, 2) + N_{cc}^{t_3}(3, 2) - \rho_0^{t_3}(3, 2) \right| \right), \quad (296)$$

$$N_{cc,pqr}^{Rt_1t_3}(\mathbf{r}_1, \mathbf{r}_2) = \left( X_{cc}^{t_1}(1, 3) \frac{\Delta^{k_2}}{2} \zeta_{132}^{k_2k_3k_1} C_{d,q}^{t_3}(3) \left| X_{cc,r}^{Rt_3}(3, 2) + N_{cc,r}^{Rt_3}(3, 2) \right| \right). \quad (297)$$

The above equations (295), (296), (297) form a set of hypernetted equations which can be solved iteratively. For example, one may start by setting the nodal diagrams equal to zero in Eq. (295). The  $(cc)$  nodal diagrams to be used in the evaluation of  $W_c(cc)$  are those where the left and right nodal diagrams are subtracted:

$$N_{cc,p}^{int,t_1}(\mathbf{r}_1, \mathbf{r}_2) = N_{cc,p}^{t_1}(\mathbf{r}_1, \mathbf{r}_2) - N_{cc,p}^{Rt_1}(\mathbf{r}_1, \mathbf{r}_2) - N_{cc,p}^{Lt_1}(\mathbf{r}_1, \mathbf{r}_2). \quad (298)$$

The operator structure of the spin-tensor terms of the  $R$  diagrams is:

$$\frac{1}{4} \{k_4, u_1\} \left[ \frac{1}{2} \{k_1, u_2\} k_2 k_3 + \frac{1}{2} k_1 k_2 \{k_3, u_2\} \right]. \quad (299)$$

The terms related to the diagrams  $L$  are obtained by exchanging  $u_1$  and  $u_2$ . The various possibilities are given in Tab. 21.

	Traces
$k_4 u_1 u_2 k_1 k_2 k_3$	$I^{k_2 k_3 k_6} I^{k_6 k_4 k_7} I^{k_1 k_7 k_5} A^{k_5}$
$k_4 u_1 k_1 u_2 k_2 k_3$	$I^{k_2 k_3 k_6} I^{k_6 k_4 k_7} J^{k_1 k_7 k_5}$
$k_4 u_1 k_1 k_2 u_2 k_3$	$I^{k_1 k_2 k_6} I^{k_3 k_4 k_7} J^{k_7 k_6 k_5}$
$k_4 u_1 k_1 k_2 k_3 u_2$	$I^{k_2 k_3 k_6} I^{k_1 k_6 k_7} J^{k_4 k_7 k_5}$
$u_1 k_4 u_2 k_1 k_2 k_3$	$I^{k_2 k_3 k_6} I^{k_1 k_6 k_7} J^{k_4 k_7 k_5}$
$u_1 k_4 k_1 u_2 k_2 k_3$	$I^{k_2 k_3 k_6} I^{k_4 k_1 k_7} J^{k_6 k_7 k_5}$
$u_1 k_4 k_1 k_2 u_2 k_3$	$I^{k_1 k_2 k_6} I^{k_4 k_6 k_7} J^{k_7 k_3 k_5}$
$u_1 k_4 k_1 k_2 k_3 u_2$	$I^{k_2 k_3 k_6} I^{k_4 k_1 k_7} I^{k_6 k_7 k_5} A^{k_5}$

Table 21: Tensor-spin traces for the Eq. (299).

By putting together the various terms we obtain

$$W_c(cc) = -\frac{1}{8} \int d\mathbf{r}_1 d\mathbf{r}_2 H_{JF}^{2k_1-1+l_1, 2k_2-1+l_2, 2k_3-1+l_3}(r_{12})$$

$$\begin{aligned}
& C_{d,22}^{t_1}(\mathbf{r}_1) g_{cc}^{t_1}(\mathbf{r}_1, \mathbf{r}_2) C_{d,22}^{t_2}(\mathbf{r}_2) \Delta^{k_4} \\
& \left[ \begin{aligned}
& 8 I^{k_2 k_3 k_6} I^{k_1 k_6 k_7} J^{k_7 k_4 k_5} \chi_{l_1+l_2+l_3+l_4} N_{cc,2k_5-1+l_5}^{int,t_2}(\mathbf{r}_1, \mathbf{r}_2) \\
& + I^{k_2 k_3 k_6} I^{k_6 k_4 k_7} I^{k_1 k_7 k_5} A^{k_5} M_{cc,l_4,0,l_1+l_2+l_3}^{t_2 k_5}(\mathbf{r}_1, \mathbf{r}_2) \\
& + I^{k_2 k_3 k_6} I^{k_6 k_4 k_7} J^{k_1 k_7 k_5} M_{cc,l_4,l_1,l_2+l_3}^{t_2 k_5}(\mathbf{r}_1, \mathbf{r}_2) \\
& + I^{k_1 k_2 k_6} I^{k_3 k_4 k_7} J^{k_7 k_6 k_5} M_{cc,l_4,l_1+l_2,l_3}^{t_2 k_5}(\mathbf{r}_1, \mathbf{r}_2) \\
& + I^{k_2 k_3 k_6} I^{k_1 k_6 k_7} J^{k_4 k_7 k_5} M_{cc,0,l_4,l_1+l_2+l_3}^{t_2 k_5}(\mathbf{r}_1, \mathbf{r}_2) \\
& + I^{k_2 k_3 k_6} I^{k_1 k_6 k_7} J^{k_4 k_7 k_5} M_{cc,l_4,l_1+l_2+l_3,0}^{t_2 k_5}(\mathbf{r}_1, \mathbf{r}_2) \\
& + I^{k_2 k_3 k_6} I^{k_4 k_1 k_7} J^{k_6 k_7 k_5} M_{cc,0,l_4+l_1,l_2+l_3}^{t_2 k_5}(\mathbf{r}_1, \mathbf{r}_2) \\
& + I^{k_1 k_2 k_6} I^{k_4 k_6 k_7} J^{k_7 k_3 k_5} M_{cc,0,l_4+l_1+l_2,l_3}^{t_2 k_5}(\mathbf{r}_1, \mathbf{r}_2) \\
& + I^{k_2 k_3 k_6} I^{k_4 k_1 k_7} I^{k_6 k_7 k_5} A^{k_5} M_{cc,0,l_4+l_1+l_2+l_3,0}^{t_2 k_5}(\mathbf{r}_1, \mathbf{r}_2)
\end{aligned} \right], \quad (300)
\end{aligned}$$

with

$$M_{cc,l_1,l_2,l_3}^{t_1k_5}(\mathbf{r}_1, \mathbf{r}_2) = \frac{1}{2} \left[ M_{cc,l_1,l_2,l_3}^{Rt_1k_5}(\mathbf{r}_1, \mathbf{r}_2; 1) + M_{cc,l_1,l_2,l_3}^{Lt_1k_5}(\mathbf{r}_1, \mathbf{r}_2; 2) \right]. \quad (301)$$

In the above equation the  $R$  and  $L$  functions are defined as in Eq. (290) by substituting the nodal diagrams  $N$  with the left and right nodal diagrams of Eqs. (296) and (297).

We give now the expression of the kinetic energy terms. For the  $T_\phi^{(1)}$  term we obtain:

$$T_{\phi}^{(1)} = -\frac{\hbar^2}{4m} \int d\mathbf{r}_1 \rho_{T_1}^{t_1}(\mathbf{r}_1) C_{d,11}^{t_1}(\mathbf{r}_1), \quad (302)$$

where  $\rho_{T1}^{t_1}(\mathbf{r}_1)$  has been defined in Eq. (132) and a sum on  $t_1$  is understood.

As indicated in Sect. 4.1, we separate the remaining terms in three parts:

$$T_\phi^{(n)} = T_{\phi,0}^{(n)} + T_{\phi,s}^{(n)} + T_{\phi,c}^{(n)} \quad n = 2, 3. \quad (303)$$

In order to express the above quantity in a closed form, we define the function:

$$h_{p,r}^{t_1 t_2}(\mathbf{r}_1, \mathbf{r}_2) = \left[ \frac{f_p(r_{12}) f_r(r_{12})}{f_1^2(r_{12})} g_{dd}^{t_1 t_2}(\mathbf{r}_1, \mathbf{r}_2) - \delta_{p,1} \delta_{r,1} \right] C_{d,22}^{t_1}(\mathbf{r}_1) C_{d,22}^{t_2}(\mathbf{r}_2) , \quad (304)$$

where we have included the scalar dressing of the correlation operator acting on the external particles. We can see an analogy with the kinetic energy part in Eq. (271). In addition, we have to consider a spin-isospin exchange operator acting on the external particles. By associating the indexes  $k_1$  and  $l_1$  to  $p$ ,  $k_3$  and  $l_3$  to  $r$  and  $k_4$  and  $l_4$  to the exchange operator, we can use the results obtained for the traces of the interaction energy in the case  $q = 1$ , corresponding to  $k_2 = 1$  and  $l_2 = 0$ .

Consequently, for  $T_{\phi,0}^{(n)}$  we get:

$$T_{\phi,0}^{(2)} = \frac{\hbar^2}{4m} \int d\mathbf{r}_1 d\mathbf{r}_2 \left\{ h_{2k_1-1+l_1, 2k_3-1+l_3}^{t_1 t_2}(\mathbf{r}_1, \mathbf{r}_2) \Delta^{k_4} \chi_{l_1+l_3+l_4}^{t_1 t_2} \right. \\ \left. \left[ I^{k_4 k_1 k_3} A^{k_3} \rho_{T_2}^{t_1 t_2}(\mathbf{r}_1, \mathbf{r}_2) + I^{k_4 k_1 k_5} I^{k_5 k_3 2} \rho_{T_2, j}^{t_1 t_2}(\mathbf{r}_1, \mathbf{r}_2) \right] + \right. \quad (305)$$

$$\begin{aligned}
& 2\delta_{t_1 t_2} \left[ \rho_{T2}^{t_1 t_2}(\mathbf{r}_1, \mathbf{r}_2) + \rho_{T2,j}^{t_1 t_2}(\mathbf{r}_1, \mathbf{r}_2) \right] C_{d,22}^{t_1}(\mathbf{r}_1) \left[ C_{d,22}^{t_2}(\mathbf{r}_2) - 1 \right] \Big\} , \\
T_{\phi,0}^{(3)} = & -\frac{\hbar^2}{2m} \int d\mathbf{r}_1 d\mathbf{r}_2 \left( h_{2k_1-1+l_1, 2k_3-1+l_3}^{t_1 t_2}(\mathbf{r}_1, \mathbf{r}_2) \Delta^{k_4} \chi_{l_1+l_3+l_4}^{t_1 t_2} \right. \\
& \left[ I^{k_4 k_1 k_3} A^{k_3} \rho_{T3}^{t_1 t_2}(\mathbf{r}_1, \mathbf{r}_2) N_{cc}^{t_2}(\mathbf{r}_1, \mathbf{r}_2) + \right. \\
& \left. I^{k_4 k_1 k_5} I^{k_5 k_3 2} \rho_{T3,j}^{t_1 t_2}(\mathbf{r}_1, \mathbf{r}_2) N_{ccj}^{t_2}(\mathbf{r}_1, \mathbf{r}_2) \right] + 2\delta_{t_1 t_2} C_{d,22}^{t_1}(\mathbf{r}_1) \Big\{ \\
& \left[ \rho_{T3}^{t_1 t_2}(\mathbf{r}_1, \mathbf{r}_2) N_{cc}^{(x)t_2}(\mathbf{r}_2, \mathbf{r}_1) + \rho_{T3,j}^{t_1 t_2}(\mathbf{r}_1, \mathbf{r}_2) N_{ccj}^{(x)t_2}(\mathbf{r}_2, \mathbf{r}_1) \right] C_{d,22}^{t_2}(\mathbf{r}_2) + \\
& \left[ \rho_{T3}^{t_1 t_2}(\mathbf{r}_1, \mathbf{r}_2) N_{cc}^{(\rho)t_2}(\mathbf{r}_2, \mathbf{r}_1) + \rho_{T3,j}^{t_1 t_2}(\mathbf{r}_1, \mathbf{r}_2) N_{ccj}^{(\rho)t_2}(\mathbf{r}_2, \mathbf{r}_1) \right] \\
& \left. \left[ C_{d,22}^{t_2}(\mathbf{r}_2) - 1 \right] \right\} \Big) , \tag{306}
\end{aligned}$$

where the one-body densities  $\rho_{T2}$ ,  $\rho_{T2,j}$ ,  $\rho_{T3}$  and  $\rho_{T3,j}$  have been defined in Appendix D. A comparison with Eq. (273) shows that we have only the exchange terms. We have substituted  $\rho_{2,exc(j)}$  with  $\rho_{Tn,(j)}$  and we have used  $I^{1k_3 k_5} = \delta_{k_3 k_5}$ . The term without operators that appears in the above equations is caused by the different vertex correction that must be used when no dynamical correlations reach the particle 2.

Using the property mentioned above for the  $I$  matrices, we get the following expressions for the SOR contributions:

$$\begin{aligned}
T_{\phi,s}^{(2)} = & \frac{\hbar^2}{4m} \int d\mathbf{r}_1 d\mathbf{r}_2 \left\{ \frac{1}{4} h_{2k_1-1+l_1, 2k_3-1+l_3}^{t_1 t_2}(\mathbf{r}_1, \mathbf{r}_2) \Delta^{k_4} \right. \\
& \left[ I^{k_4 k_1 k_3} A^{k_3} \rho_{T2}^{t_1 t_2}(\mathbf{r}_1, \mathbf{r}_2) + I^{k_4 k_1 k_5} I^{k_5 k_3 2} \rho_{T2,j}^{t_1 t_2}(\mathbf{r}_1, \mathbf{r}_2) \right] \\
& \left[ M_{d,l_1,0,l_3,l_4}^{t_1 t_2 1k_4 k_3}(\mathbf{r}_1) + M_{d,l_1,0,l_3,l_4}^{t_1 t_2 1k_4 k_3}(\mathbf{r}_2) \right] + \\
& 2\delta_{t_1 t_2} \left[ \rho_{T2}^{t_1 t_2}(\mathbf{r}_1, \mathbf{r}_2) + \rho_{T2,j}^{t_1 t_2}(\mathbf{r}_1, \mathbf{r}_2) \right] C_{d,22}^{t_1}(\mathbf{r}_1) \\
& \left. \left[ U_{d,SOC}^{t_1}(\mathbf{r}_1) \left[ C_{d,22}^{t_2}(\mathbf{r}_2) - 1 \right] + C_{d,22}^{t_2}(\mathbf{r}_2) U_{d,SOC}^{t_2}(\mathbf{r}_2) \right] \right\} , \tag{307}
\end{aligned}$$

$$\begin{aligned}
T_{\phi,s}^{(3)} = & -\frac{\hbar^2}{2m} \int d\mathbf{r}_1 d\mathbf{r}_2 \left[ \frac{1}{4} h_{2k_1-1+l_1, 2k_3-1+l_3}^{t_1 t_2}(\mathbf{r}_1, \mathbf{r}_2) \Delta^{k_4} \right. \\
& \left[ I^{k_4 k_1 k_3} A^{k_3} \rho_{T3}^{t_1 t_2}(\mathbf{r}_1, \mathbf{r}_2) N_{cc}^{t_2}(\mathbf{r}_1, \mathbf{r}_2) + \right. \\
& \left. I^{k_4 k_1 k_5} I^{k_5 k_3 2} \rho_{T3,j}^{t_1 t_2}(\mathbf{r}_1, \mathbf{r}_2) N_{ccj}^{t_2}(\mathbf{r}_1, \mathbf{r}_2) \right] \\
& \left[ M_{d,l_1,0,l_3,l_4}^{t_1 t_2 1k_4 k_3}(\mathbf{r}_1) + M_{d,l_1,0,l_3,l_4}^{t_1 t_2 1k_4 k_3}(\mathbf{r}_2) \right] + 2\delta_{t_1 t_2} C_{d,22}^{t_1}(\mathbf{r}_1) \Big( \\
& \left[ \rho_{T3}^{t_1 t_2}(\mathbf{r}_1, \mathbf{r}_2) N_{cc}^{t_2}(\mathbf{r}_1, \mathbf{r}_2) + \rho_{T3,j}^{t_1 t_2}(\mathbf{r}_1, \mathbf{r}_2) N_{ccj}^{t_2}(\mathbf{r}_1, \mathbf{r}_2) \right] \\
& C_{d,22}^{t_2}(\mathbf{r}_2) U_{d,SOC}^{t_2}(\mathbf{r}_2) + U_{d,SOC}^{t_1}(\mathbf{r}_1) \Big\{ \\
& \left[ \rho_{T3}^{t_1 t_2}(\mathbf{r}_1, \mathbf{r}_2) N_{cc}^{(x)t_2}(\mathbf{r}_2, \mathbf{r}_1) + \rho_{T3,j}^{t_1 t_2}(\mathbf{r}_1, \mathbf{r}_2) N_{ccj}^{(x)t_2}(\mathbf{r}_2, \mathbf{r}_1) \right] C_{d,22}^{t_2}(\mathbf{r}_2) + \tag{308}
\end{aligned}$$

$$\left[ \rho_{T3}^{t_1 t_2}(\mathbf{r}_1, \mathbf{r}_2) N_{cc}^{(\rho) t_2}(\mathbf{r}_2, \mathbf{r}_1) + \rho_{T3,j}^{t_1 t_2}(\mathbf{r}_1, \mathbf{r}_2) N_{ccj}^{(\rho) t_2}(\mathbf{r}_2, \mathbf{r}_1) \right] \left[ C_{d,22}^{t_2}(\mathbf{r}_2) - 1 \right] \Bigg\} \Bigg] .$$

In the evaluation of the  $T_{\phi,c}$  terms we neglect  $T_{\phi,c}^{(3)}$ . This approximation is justified by the fact that the contribution of the  $T_{\phi,0,s}^{(3)}$  terms are much smaller than those of the  $T_{\phi,0,s}^{(2)}$  terms. The structure of the  $T_{\phi,c}^{(2)}$  term is analogous to that of the exchange case of  $W_c(dd)$  when  $k_2 = 1$  and  $l_2 = 0$ . In this case, we use  $J^{1k_5 k_7} = A^{k_5} \delta_{k_5 k_7}$ , and obtain the expression:

$$\begin{aligned} T_{\phi,c}^{(2)} = & -\frac{\hbar^2}{48m} \int d\mathbf{r}_1 d\mathbf{r}_2 \rho_{T2}^{t_1 t_2}(\mathbf{r}_1, \mathbf{r}_2) f_{2k_1-1+l_1}(r_{12}) f_{2k_3-1+l_3}(r_{12}) \cdot \\ & \Delta^{k_4} C_{d,22}^{t_1}(\mathbf{r}_1) C_{d,22}^{t_2}(\mathbf{r}_2) g_{dd}^{t_1 t_2}(\mathbf{r}_1, \mathbf{r}_2) \left\{ \frac{3}{2} \left[ I^{k_1 k_3 k_6} J^{k_4 k_5 k_6} M_{dd,l_4,l_1+l_3,0}^{t_1 t_2 k_5}(\mathbf{r}_1, \mathbf{r}_2) \right. \right. \\ & + I^{k_3 k_4 k_6} J^{k_6 k_5 k_1} M_{dd,l_4,l_1,l_3}^{t_1 t_2 k_5}(\mathbf{r}_1, \mathbf{r}_2) + I^{k_4 k_1 k_6} J^{k_6 k_5 k_3} M_{dd,l_4+l_1,l_3,0}^{t_1 t_2 k_5}(\mathbf{r}_1, \mathbf{r}_2) \\ & + I^{k_4 k_3 k_6} I^{k_6 k_1 k_5} A^{k_5} M_{dd,l_4+l_1,0,l_3}^{t_1 t_2 k_5}(\mathbf{r}_1, \mathbf{r}_2) \Big] + I^{k_3 k_4 k_6} J^{k_1 k_5 k_6} M_{dd,l_4,l_1,l_3}^{t_1 t_2 k_5}(\mathbf{r}_1, \mathbf{r}_2) \\ & + I^{k_4 k_5 k_6} I^{k_6 k_1 k_3} A^{k_3} M_{4,dd,l_1,0,l_3,l_4}^{t_1 t_2 k_5}(\mathbf{r}_1, \mathbf{r}_2) \\ & \left. + I^{k_4 k_1 k_6} J^{k_3 k_5 k_6} M_{dd,l_4+l_1,l_3,0}^{t_1 t_2 k_5}(\mathbf{r}_1, \mathbf{r}_2) \right\} . \end{aligned} \quad (309)$$

We present now the contribution of the spin-orbit terms. In our calculations we use correlations up to the tensor channels, therefore the presence of spin-orbit operators is only due to the interaction. We consider only the case of spin-orbit operators acting on the external particles. In this case we write:

$$\begin{aligned} \langle v^{7+l_2} \rangle_0 = & -9 \int d\mathbf{r}_1 d\mathbf{r}_2 \frac{f_{5+l_1}(r_{12}) v^{7+l_2}(r_{12}) f_{5+l_3}(r_{12})}{f_1^2(r_{12})} \\ & \left\{ \rho_{2,dir}^{t_1 t_2}(\mathbf{r}_1, \mathbf{r}_2) \chi_{l_1+l_2+l_3}^{t_1 t_2} + \right. \\ & \left. 2 \left[ \rho_{2,exc}^{t_1 t_2}(\mathbf{r}_1, \mathbf{r}_2) + \frac{1}{3} \rho_{2,excj}^{t_1 t_2}(\mathbf{r}_1, \mathbf{r}_2) \right] \left[ \chi_{l_1+l_2+l_3}^{t_1 t_2} + \chi_{l_1+l_2+l_3+1}^{t_1 t_2} \right] \right\} , \end{aligned} \quad (310)$$

where we have used the relation:

$$C \left[ P_{12}^{k_1}(\mathbf{L} \cdot \mathbf{S})_{12} P_{12}^{k_3} \right] = -18 \delta_{k_1 3} \delta_{k_3 3} . \quad (311)$$

Finally, we analyze the expressions used to calculate the contribution to the energy of the three-body potential, Eq.(141). The diagrams we consider in this calculation have been presented in Fig. 19. We start by considering the  $v_{123}^R$  term of the three-body force, Eq. (143), which is a scalar function. The diagram (3.1) of Fig. 19, is the leading term, and its contribution can be expressed as:

$$\langle v_{123}^R \rangle_{3.1} = \frac{1}{6} \int d\mathbf{r}_1 d\mathbf{r}_2 d\mathbf{r}_3 v_{123}^R \rho_3^{t_1 t_2 t_3}(\mathbf{r}_1, \mathbf{r}_2, \mathbf{r}_3) , \quad (312)$$

where a sum on the  $t$  indexes is understood,  $\rho_3$  is the three-body density that can be written as:

$$\begin{aligned} \rho_3^{t_1 t_2 t_3}(\mathbf{r}_1, \mathbf{r}_2, \mathbf{r}_3) &= \rho_{3,dir}^{t_1 t_2 t_3}(\mathbf{r}_1, \mathbf{r}_2, \mathbf{r}_3) + \delta_{t_1 t_2} \delta_{t_1 t_3} \rho_{3,exc}^{t_1 t_2 t_3}(\mathbf{r}_1, \mathbf{r}_2, \mathbf{r}_3) \\ &= \sum_{mm', nn', ll'=dd, de, ed} g_{ml'}^{t_1 t_3}(\mathbf{r}_1, \mathbf{r}_3) V_{ll'}^{t_3}(\mathbf{r}_3) g_{ln'}^{t_3 t_2}(\mathbf{r}_3, \mathbf{r}_2) V_{nn'}^{t_2}(\mathbf{r}_2) g_{lm'}^{t_2 t_1}(\mathbf{r}_2, \mathbf{r}_1) V_{mm'}^{t_1}(\mathbf{r}_1) \\ &\quad + 2\delta_{t_1 t_2} \delta_{t_1 t_3} g_{cc}^{t_3}(\mathbf{r}_1, \mathbf{r}_3) V_{cc}^{t_3}(\mathbf{r}_3) g_{cc}^{t_2}(\mathbf{r}_3, \mathbf{r}_2) V_{cc}^{t_2}(\mathbf{r}_2) g_{cc}^{t_1}(\mathbf{r}_2, \mathbf{r}_1) V_{cc}^{t_1}(\mathbf{r}_1), \end{aligned} \quad (313)$$

where  $V_{mn}^{t_i}(\mathbf{r}_i)$  has been defined in Eq. (198). We have separated the direct and the exchange parts of the three-body density, and we have neglected the contribution of the Abe diagrams [95]. These Abe diagrams are simple non-nodal ones with three external points that play the same role as elementary diagrams in the TBDF.

The expressions of the diagram (3.2) is:

$$\begin{aligned} < v_{123}^R >_{3.2} = \frac{1}{2} \int d\mathbf{r}_1 d\mathbf{r}_2 d\mathbf{r}_3 \frac{f_{2k_1-1+l_1}(r_{12}) f_{2k_2-1+l_2}(r_{12})}{[f_1(r_{12})]^2} \\ &\quad \left[ A^{k_1} \delta_{k_1, k_2} \chi_{l_1+l_2}^{t_1 t_2} \rho_{3,dir}^{t_1 t_2 t_3}(\mathbf{r}_1, \mathbf{r}_2, \mathbf{r}_3) + \right. \\ &\quad \left. \Delta^{k_3} I^{k_3 k_1 k_2} A^{k_2} \chi_{l_1+l_2+l_3}^{t_1 t_2} \rho_{3,exc}^{t_1 t_2 t_3}(\mathbf{r}_1, \mathbf{r}_2, \mathbf{r}_3) \right]. \end{aligned} \quad (314)$$

where, as in all the previous equations, a sum on the operator channels, here indicated by the indexes  $k$  and  $l$ , is understood. As indicated in diagram (3.2) of Fig. 19, the various operators act between the 1 and 2 particles. In this respect, we should point out that the scalar operator term, i. e. the case  $k_1 = k_2 = 1$  and  $l_1 = l_2 = 0$ , is not considered in Eq. (314), since this would produce a double counting with the contribution of the (3.1) diagram, Eq. (313).

We consider now the contribution of the  $v_{123}^{2\pi}$  term of the three-body force, Eq. (142). We define first two effective potentials:

$$\begin{aligned} v_{eff,mn}^{k_3, t_1 t_2}(\mathbf{r}_1, \mathbf{r}_2) &= \sum_{k_1, k_2=2}^3 \sum_{t_3} 4A_{2\pi} \int d\mathbf{r}_3 \left[ g_{md}^{t_1 t_3}(\mathbf{r}_1, \mathbf{r}_3) C_{22}^{t_3}(\mathbf{r}_3) g_{dn}^{t_3 t_2}(\mathbf{r}_3, \mathbf{r}_2) \right. \\ &\quad + g_{md}^{t_1 t_3}(\mathbf{r}_1, \mathbf{r}_3) C_{d,22}^{t_3}(\mathbf{r}_3) g_{en}^{t_3 t_2}(\mathbf{r}_3, \mathbf{r}_2) \\ &\quad \left. + g_{me}^{t_1 t_3}(\mathbf{r}_1, \mathbf{r}_3) C_{d,22}^{t_3}(\mathbf{r}_3) g_{dn}^{t_3 t_2}(\mathbf{r}_3, \mathbf{r}_2) \right] \\ &\quad \zeta_{132}^{k_1 k_2 k_3} X^{k_1}(r_{13}) X^{k_2}(r_{32}) \end{aligned} \quad (315)$$

$$\begin{aligned} v_{eff,cc}^{k_3, t_1}(\mathbf{r}_1, \mathbf{r}_2) &= \sum_{k_1, k_2=2}^3 \sum_{t_3} 4A_{2\pi} \int d\mathbf{r}_3 g_{cc}^{t_1}(\mathbf{r}_1, \mathbf{r}_3) C_{d,22}^{t_3}(\mathbf{r}_3) g_{cc}^{t_3}(\mathbf{r}_3, \mathbf{r}_2) \\ &\quad \zeta_{132}^{k_1 k_2 k_3} X^{k_1}(r_{13}) X^{k_2}(r_{32}) \end{aligned} \quad (316)$$

with  $m, n = d, e$  and  $X^k(r)$  defined in Eq. (145). With the help of the above defined quantities we express the contribution of  $v_{123}^{2\pi}$ , related to the (2.1) diagram of Fig. 19, as:

$$\begin{aligned} < v_{123}^{2\pi} >_{2.1} &= \frac{1}{2} \sum_{t_1 t_2} \int d\mathbf{r}_1 \int d\mathbf{r}_2 \frac{f_{2k_1-1+l_1}(r_{12}) f_{2k_2-1+l_2}(r_{12})}{f_1^2(r_{12})} \\ &\quad \cdot I^{k_1 k_3 k_2} A^{k_2} \chi_{l_1+l_2+1}^{t_1 t_2} \left\{ \right. \end{aligned}$$

$$\begin{aligned}
& v_{eff,dd}^{k_3,t_1t_2}(\mathbf{r}_1, \mathbf{r}_2) \left[ g_{dd}^{t_1t_2}(\mathbf{r}_1, \mathbf{r}_2) C_{22}^{t_1}(\mathbf{r}_1) C_{22}^{t_2}(\mathbf{r}_2) \right. \\
& + g_{de}^{t_1t_2}(\mathbf{r}_1, \mathbf{r}_2) C_{22}^{t_1}(\mathbf{r}_1) C_{d,22}^{t_2}(\mathbf{r}_2) + g_{ed}^{t_1t_2}(\mathbf{r}_1, \mathbf{r}_2) C_{d,22}^{t_1}(\mathbf{r}_1) C_{22}^{t_2}(\mathbf{r}_2) \\
& + g_{ee}^{t_1t_2}(\mathbf{r}_1, \mathbf{r}_2) C_{d,22}^{t_1}(\mathbf{r}_1) C_{d,22}^{t_2}(\mathbf{r}_2) \left. \right] \\
& + v_{eff,de}^{k_3,t_1t_2}(\mathbf{r}_1, \mathbf{r}_2) C_{d,22}^{t_2}(\mathbf{r}_2) \left[ g_{dd}^{t_1t_2}(\mathbf{r}_1, \mathbf{r}_2) C_{22}^{t_1}(\mathbf{r}_1) \right. \\
& + g_{ed}^{t_1t_2}(\mathbf{r}_1, \mathbf{r}_2) C_{d,22}^{t_1}(\mathbf{r}_1) \left. \right] \\
& + v_{eff,ed}^{k_3,t_1t_2}(\mathbf{r}_1, \mathbf{r}_2) C_{d,22}^{t_1}(\mathbf{r}_1) \left[ g_{dd}^{t_1t_2}(\mathbf{r}_1, \mathbf{r}_2) C_{22}^{t_2}(\mathbf{r}_2) \right. \\
& + g_{de}^{t_1t_2}(\mathbf{r}_1, \mathbf{r}_2) C_{d,22}^{t_2}(\mathbf{r}_2) \left. \right] \\
& + v_{eff,ee}^{k_3,t_1t_2}(\mathbf{r}_1, \mathbf{r}_2) g_{dd}^{t_1t_2}(\mathbf{r}_1, \mathbf{r}_2) C_{d,22}^{t_1}(\mathbf{r}_1) C_{d,22}^{t_2}(\mathbf{r}_2) \left. \right\} \\
& - \frac{1}{2} \int d\mathbf{r}_1 \int d\mathbf{r}_2 f_{2k_1-1+l_1}(r_{12}) f_{2k_2-1+l_2}(r_{12}) g_{dd}^{t_1t_2}(\mathbf{r}_1, \mathbf{r}_2) \\
& \cdot C_{d,22}^{t_1}(\mathbf{r}_1) C_{d,22}^{t_2}(\mathbf{r}_2) I^{k_1k_3k_4} I^{k_4k_2k_5} A^{k_5} (\chi_{l_1+l_2+1}^{t_1t_2} + \chi_{l_1+l_2+2}^{t_1t_2}) \Delta^{k_5} \\
& \left\{ v_{eff,dd}^{k_3,t_1t_2}(\mathbf{r}_1, \mathbf{r}_2) \left[ N_{cc}^{t_1}(\mathbf{r}_1, \mathbf{r}_2) - \rho_0^{t_1}(\mathbf{r}_1, \mathbf{r}_2) \right] \right. \\
& \left[ N_{cc}^{t_2}(\mathbf{r}_1, \mathbf{r}_2) - \rho_0^{t_2}(\mathbf{r}_1, \mathbf{r}_2) \right] \\
& + 2v_{eff,cc}^{k_3,t_1}(\mathbf{r}_1, \mathbf{r}_2) \left[ N_{cc}^{t_2}(\mathbf{r}_1, \mathbf{r}_2) - \rho_0^{t_2}(\mathbf{r}_1, \mathbf{r}_2) \right] \left. \right\}, \tag{317}
\end{aligned}$$

In the above expression, we have considered only the contribution of the anticommutator term.

In the (2.2) diagram of Fig. 19, the operators act on the 13 and 23 particle pairs. In this case, the operator structure is:

$$\begin{aligned}
& \frac{1}{4} \left[ \frac{1}{2} \{O_{13}^p, O_{23}^{s_1}\} (O_{13}^q O_{23}^{s_2})_{\pm} + \frac{1}{2} (O_{13}^q, O_{23}^{s_2})_{\pm} \{O_{13}^p, O_{23}^{s_1}\} \right. \\
& \left. + O_{13}^p (O_{13}^q, O_{23}^{s_2})_{\pm} O_{23}^{s_1} + O_{23}^{s_1} (O_{13}^q, O_{23}^{s_2})_{\pm} O_{13}^p \right] \tag{318}
\end{aligned}$$

where we have defined:

$$(O_{13}^q, O_{23}^{s_2})_{\pm} = O_{13}^q O_{23}^{s_2} \pm O_{23}^{s_2} O_{13}^q$$

The contributions of Eq. (318), with  $p = 2k_3 - 1 + l_1$ ,  $q = 2k_1$ ,  $s_1 = 2k_4 - 1 + l_2$  and  $s_2 = 2k_2$ , are given in Tab. 22, where we used the matrix  $R^{k_1k_2k_3k_4}$  defined as [96]:

$$\begin{aligned}
R^{k_1k_2k_3k_4} &= C(P_{13}^{k_1} P_{23}^{k_2} P_{13}^{k_3} P_{23}^{k_4}) \tag{319} \\
&= A^{k_1} \delta_{k_1k_3} A^{k_2} \delta_{k_2k_4} \left( 1 + D_{k_2k_3} \right) + 12P_2(\hat{r}_{13} \cdot \hat{r}_{23}) \times \\
&\quad \left[ 1 - (1 - \delta_{k_13})(1 - \delta_{k_33}) \right] \left[ 1 - (1 - \delta_{k_23})(1 - \delta_{k_43}) \right].
\end{aligned}$$

The plus signs in the table correspond to the anticommutator terms and the minus signs to the commutator ones.



	Traces
$k_3 k_4 (k_1, k_2) \pm$	$R^{k_3 k_4 k_1 k_2} \pm A^{k_3} \delta_{k_3 k_1} A^{k_4} \delta_{k_2 k_4}$
$k_4 k_3 (k_1, k_2) \pm$	$A^{k_3} \delta_{k_3 k_1} A^{k_4} \delta_{k_2 k_4} \pm R^{k_4 k_3 k_2 k_1}$
$(k_1, k_2) \pm k_3 k_4$	$R^{k_1 k_2 k_3 k_4} \pm A^{k_3} \delta_{k_3 k_1} A^{k_4} \delta_{k_2 k_4}$
$(k_1, k_2) \pm k_4 k_3$	$A^{k_3} \delta_{k_3 k_1} A^{k_4} \delta_{k_2 k_4} \pm R^{k_1 k_2 k_3 k_4}$
$k_3 (k_1, k_2) \pm k_4$	$A^{k_3} \delta_{k_3 k_1} A^{k_4} \delta_{k_2 k_4} \pm R^{k_3 k_2 k_1 k_4}$
$k_4 (k_1, k_2) \pm k_3$	$R^{k_4 k_1 k_2 k_3} \pm A^{k_3} \delta_{k_3 k_1} A^{k_4} \delta_{k_2 k_4}$

Table 22: Tensor-spin traces of the operator of Eq. (318).

When the isospin traces are included we obtain:

$$\begin{aligned}
\Omega_{k_1 k_2 k_3 k_4, l_1 l_2}^{t_1 t_2 t_3 \pm} &= \frac{1}{8} \left( R^{k_3 k_4 k_1 k_2} \pm A^{k_3} \delta_{k_3 k_1} A^{k_4} \delta_{k_2 k_4} \right) \\
&\quad \left[ \chi_{l_1 l_2 110}^{t_1 t_3 t_2} (2) \pm \chi_{l_1 l_2 011}^{t_1 t_3 t_2} (2) \pm \chi_{0 l_2 l_1 + 110}^{t_1 t_3 t_2} (2) \right. \\
&\quad + \chi_{0 l_2 l_1 11}^{t_1 t_3 t_2} (2) + \chi_{11 l_1 l_2 0}^{t_1 t_3 t_2} (2) \pm \chi_{01 l_1 + 1 l_2 0}^{t_1 t_3 t_2} (2) \pm \chi_{110 l_2 l_1}^{t_1 t_3 t_2} (2) \\
&\quad + \chi_{011 l_2 l_1}^{t_1 t_3 t_2} (2) \pm 2 \chi_{l_1 + 110 l_2 0}^{t_1 t_3 t_2} (2) + 2 \chi_{l_1 11 l_2 0}^{t_1 t_3 t_2} (2) + 2 \chi_{0 l_2 11 l_1}^{t_1 t_3 t_2} (2) \\
&\quad \left. \pm 2 \chi_{0 l_2 01 l_1 + 1}^{t_1 t_3 t_2} (2) \right] \quad (320)
\end{aligned}$$

where we have defined the  $\Omega_{k_1 k_2 k_3 k_4, l_1 l_2}^{t_1 t_2 t_3 \pm}$  symbols which allows us to express the contribution of diagram (2.2) of Fig. 19 as:

$$\begin{aligned}
\langle v_{123}^{2\pi} \rangle_{2.2} &= A_{2\pi} \int d\mathbf{r}_1 d\mathbf{r}_2 d\mathbf{r}_3 \frac{f_{2k_3-1+l_1}(r_{13})}{f_1(r_{13})} X^{k_1}(r_{13}) \frac{f_{2k_4-1+l_2}(r_{23})}{f_1(r_{23})} X^{k_2}(r_{32}) \\
&\quad \rho_3^{t_1 t_2 t_3}(\mathbf{r}_1, \mathbf{r}_2, \mathbf{r}_3) \left( \Omega_{k_1 k_2 k_3 k_4, l_1 l_2}^{t_1 t_2 t_3 +} + \frac{1}{4} \Omega_{k_1 k_2 k_3 k_4, l_1 l_2}^{t_1 t_2 t_3 -} \right), \quad (321)
\end{aligned}$$

where the sum over all the  $k$ ,  $l$  and  $t$  indexes is understood.

In the diagram (2.3) of Fig. 19, the operator dependent correlations act on the 1,2 and 1,3 particle pairs. This implies that the only contribution comes from the commutator term of Eq. (142). In this case, the operator structure is:

$$\begin{aligned}
&\frac{1}{4} \left( \frac{1}{2} \{ O_{13}^p, O_{12}^{s_1} \} [O_{13}^q, O_{23}^{s_2}] + \frac{1}{2} [O_{13}^q, O_{23}^{s_2}] \{ O_{13}^p, O_{12}^{s_1} \} \right. \\
&\quad \left. + O_{13}^p [O_{13}^q, O_{23}^{s_2}] O_{12}^{s_1} + O_{12}^{s_1} [O_{13}^q, O_{23}^{s_2}] O_{13}^p \right) \quad (322)
\end{aligned}$$

The spin and tensor traces of this set of operators are given in Tab. 23, where we have not written a function  $\zeta_{123}^{k_4 k_2 k_5}$  that is present in all the traces.

After considering the isospin traces we obtain the expression:

$$\begin{aligned}
&\frac{1}{8} (J^{k_3 k_1 k_5} - I^{k_3 k_1 k_5} A^{k_5}) \left[ \eta_{l_1 l_2 110}^{t_1 t_3 t_2} (1) - \eta_{l_1 l_2 011}^{t_1 t_3 t_2} (1) - \eta_{0 l_2 l_1 + 110}^{t_1 t_3 t_2} (1) \right. \\
&\quad + \eta_{0 l_2 l_1 11}^{t_1 t_3 t_2} (1) + \eta_{1 l_2 l_1 10}^{t_1 t_3 t_2} (2) - \eta_{1 l_2 01 l_1}^{t_1 t_3 t_2} (2) - \eta_{0 l_2 l_1 + 110}^{t_1 t_3 t_2} (2) \\
&\quad + \eta_{0 l_2 11 l_1}^{t_1 t_3 t_2} (2) - 2 \eta_{l_1 + 11 l_2 010}^{t_1 t_3 t_2} (2) + 2 \eta_{l_1 l_2 110}^{t_1 t_3 t_2} (2) + 2 \eta_{0 l_2 11 l_1}^{t_1 t_3 t_2} (1) \\
&\quad \left. - 2 \eta_{0 l_2 01 l_1 + 1}^{t_1 t_3 t_2} (1) \right] \quad (323)
\end{aligned}$$

	Traces
$k_3 k_4 [k_1, k_2]$	$J^{k_3 k_1 k_5} - I^{k_3 k_1 k_5} A^{k_5}$
$k_4 k_3 [k_1, k_2]$	$-J^{k_3 k_1 k_5} + I^{k_3 k_1 k_5} A^{k_5}$
$[k_1, k_2] k_3 k_4$	$J^{k_3 k_1 k_5} - I^{k_3 k_1 k_5} A^{k_5}$
$[k_1, k_2] k_4 k_3$	$-J^{k_3 k_1 k_5} + I^{k_3 k_1 k_5} A^{k_5}$
$k_3 [k_1, k_2] k_4$	$-J^{k_3 k_1 k_5} + I^{k_3 k_1 k_5} A^{k_5}$
$k_4 [k_1, k_2] k_3$	$J^{k_3 k_1 k_5} - I^{k_3 k_1 k_5} A^{k_5}$

Table 23: Tensor-spin traces of the operators of Eq. (322).

Calling  $\Xi_{k_1 k_3 k_5, l_1 l_2}^{t_1 t_2 t_3}$  the above trace, we can write:

$$\begin{aligned}
\langle v_{123}^{2\pi} \rangle_{2.3} &= \frac{A_{2\pi}}{4} \int d\mathbf{r}_1 d\mathbf{r}_2 d\mathbf{r}_3 \frac{f_{2k_3-1+l_1}(r_{13})}{f_1(r_{13})} X^{k_1}(r_{13}) \frac{f_{2k_4-1+l_2}(r_{12})}{f_1(r_{12})} \\
&\quad X^{k_2}(r_{32}) \zeta_{123}^{k_4 k_2 k_5} \rho_3^{t_1 t_2 t_3}(\mathbf{r}_1, \mathbf{r}_2, \mathbf{r}_3) \Xi_{k_1 k_3 k_5, l_1 l_2}^{t_1 t_2 t_3}
\end{aligned} \tag{324}$$

## F The Euler procedure

In this Appendix we present the method used to fix the correlation function. We have named this method *Euler procedure*. The starting point is the calculation of the hamiltonian mean value, considering only cluster terms up to the second order. In this case, the contribution to the  $W$  terms of Eq. (137) is given only by the  $W_0$  term, since the other terms are produced by clusters of higher order. In analogy, only the terms  $T_{\Phi}^{(1,2)}$  contribute to the  $T_{\Phi}$  term of Eq. (128). Therefore, the total energy in the two-body cluster approximation is given by:

$$E_2 = W_2 + T_{\Phi,2}^{(1)} + T_{\Phi,2}^{(2)}, \quad (325)$$

where the expression of the various terms are:

$$\begin{aligned} W_2 = & \frac{1}{2} \int d\mathbf{r}_1 d\mathbf{r}_2 H_{JF}^{2k_1-1+l_1, 2k_2-1+l_2, 2k_3-1+l_3}(r_{12}) \\ & \left\{ \rho_0^{s_1 s_2 t_1}(\mathbf{r}_1, \mathbf{r}_1) \rho_0^{s_3 s_4 t_2}(\mathbf{r}_2, \mathbf{r}_2) \chi_{s_1}^+(1) \chi_{s_3}^+(2) P_{12}^{k_1} P_{12}^{k_2} P_{12}^{k_3} \chi_{s_2}(1) \chi_{s_4}(2) \right. \\ & \chi_{t_1}^+(1) \chi_{t_2}^+(2) (\boldsymbol{\tau}_1 \cdot \boldsymbol{\tau}_2)^{l_1+l_2+l_3} \chi_{t_1}(1) \chi_{t_2}(2) \\ & - \rho_0^{s_1 s_2 t_1}(\mathbf{r}_1, \mathbf{r}_2) \rho_0^{s_3 s_4 t_2}(\mathbf{r}_2, \mathbf{r}_1) \chi_{s_1}^+(1) \chi_{s_3}^+(2) P_{12}^{k_1} P_{12}^{k_2} P_{12}^{k_3} \chi_{s_4}(1) \chi_{s_2}(2) \\ & \left. \chi_{t_1}^+(1) \chi_{t_2}^+(2) (\boldsymbol{\tau}_1 \cdot \boldsymbol{\tau}_2)^{l_1+l_2+l_3} \chi_{t_2}(1) \chi_{t_1}(2) \right\}, \quad (326) \end{aligned}$$

$$\begin{aligned} T_{\Phi,2}^{(1)} = & -\frac{\hbar^2}{4m} \int d\mathbf{r}_1 \rho_{T1}^{s_1 s_2 t_1}(\mathbf{r}_1, \mathbf{r}_1) \int d\mathbf{r}_2 \rho_0^{s_3 s_4 t_2}(\mathbf{r}_2, \mathbf{r}_2) \\ & \left( f_{2k_1-1+l_1}(r_{12}) f_{2k_2-1+l_2}(r_{12}) - \delta_{2k_1-1+l_1,1} \delta_{2k_2-1+l_2,1} \right) \\ & \chi_{s_1}^+(1) \chi_{s_3}^+(2) P_{12}^{k_1} P_{12}^{k_2} \chi_{s_2}(1) \chi_{s_4}(2) \\ & \chi_{t_1}^+(1) \chi_{t_2}^+(2) (\boldsymbol{\tau}_1 \cdot \boldsymbol{\tau}_2)^{l_1+l_2} \chi_{t_1}(1) \chi_{t_2}(2), \quad (327) \end{aligned}$$

$$\begin{aligned} T_{\Phi,2}^{(2)} = & \frac{\hbar^2}{4m} \int d\mathbf{r}_1 d\mathbf{r}_2 \rho_{T2}^{s_1 s_2 s_3 s_4 t_1 t_2}(\mathbf{r}_1, \mathbf{r}_2) \\ & \left( f_{2k_1-1+l_1}(r_{12}) f_{2k_2-1+l_2}(r_{12}) - \delta_{2k_1-1+l_1,1} \delta_{2k_2-1+l_2,1} \right) \\ & \chi_{s_1}^+(1) \chi_{s_3}^+(2) P_{12}^{k_1} P_{12}^{k_2} \chi_{s_4}(1) \chi_{s_2}(2) \\ & \chi_{t_1}^+(1) \chi_{t_2}^+(2) (\boldsymbol{\tau}_1 \cdot \boldsymbol{\tau}_2)^{l_1+l_2} \chi_{t_2}(1) \chi_{t_1}(2). \quad (328) \end{aligned}$$

As in the calculation of the energy expectation values, the  $k$  indexes can assume the values 1, 2 and 3, and the  $l$  indexes the values 0 and 1. The  $s = \pm 1/2$  indexes indicate the spin third component and the  $t = \pm 1/2$  the isospin third component. A sum on all the third components of spin and isospin and on the repeated indexes is understood in the above equations, and in the following ones.

The other quantities of the above equations are the two-body correlation functions  $f_p$ ,  $H_{JF}^{pqr}$  defined in Eq. (271) and the isospin independent  $P_{12}^k$  operators, see Eq. (49). We use the expressions of the one-body densities (132) and (133) where the spin dependence is explicit:

$$\rho_{T1}^{t_1}(\mathbf{r}_1) = \sum_{s_1, s_2} \rho_{T1}^{s_1 s_2 t_1}(\mathbf{r}_1, \mathbf{r}_1) \chi_{s_1}^*(1) \chi_{s_2}(1), \quad (329)$$

$$\begin{aligned} \rho_{T2}^{s_1 s_2 s_3 s_4 t_1 t_2}(\mathbf{r}_1, \mathbf{r}_2) &= \rho_0^{s_1 s_2 t_1}(\mathbf{r}_1, \mathbf{r}_2) \nabla_1^2 \rho_0^{s_3 s_4 t_2}(\mathbf{r}_2, \mathbf{r}_1) \\ &\quad - \nabla_1 \rho_0^{s_1 s_2 t_1}(\mathbf{r}_1, \mathbf{r}_2) \cdot \nabla_1 \rho_0^{s_3 s_4 t_2}(\mathbf{r}_2, \mathbf{r}_1) . \end{aligned} \quad (330)$$

We obtain the optimal correlation functions  $f_p$  by solving the Euler-Lagrange equation:

$$\frac{\delta(E_2 - C_2)}{\delta f_p} = 0 , \quad (331)$$

where we have indicated with  $C_2$  the contributions of the constraints. The expression of  $C_2$  is analogous to that of  $W_2$  after substituting  $H_{JF}^{pqr}$  with  $f_p \lambda_q f_r$ ,  $\lambda_q$  being the Lagrange multipliers. The values of these multipliers, are fixed by imposing the conditions that the various terms of the two-body correlation function assume their asymptotic values after a certain internucleon distance  $d_p$ , called healing distance:

$$f_1(r \geq d_1) = 1 , \quad (332)$$

$$f_{p>1}(r \geq d_p) = 0 , \quad (333)$$

In addition we impose the condition:

$$\left. \frac{\partial f_p}{\partial r} \right|_{r=d_p} = 0 . \quad (334)$$

Since we use correlation functions composed by six operator channels, the minimization procedure (331) should be applied to fix the values of six healing distances  $d_p$ . This produces a system of six interconnected differential equations. It is possible to separate these equations by using a representation of the Euler equations in terms of the total spin and isospin  $S$  and  $T$  of the correlated nucleon pair. We use the projection operators:

$$\Pi_{12}^S = \frac{1}{4}[2S + 1 + (-1)^{S+1} \boldsymbol{\sigma}_1 \cdot \boldsymbol{\sigma}_2] , \quad (335)$$

$$\Pi_{12}^T = \frac{1}{4}[2T + 1 + (-1)^{T+1} \boldsymbol{\tau}_1 \cdot \boldsymbol{\tau}_2] , \quad (336)$$

with  $S, T = 0, 1$ . In the  $(T, S)$  representation we can write:

$$\sum_{p=1}^6 x_p O_{12}^p = \sum_{S,T=0,1} (x_{TS} + \delta_{S,1} x_{Tt} S_{12}) \Pi_{12}^T \Pi_{12}^S , \quad (337)$$

where  $x_p$  can be the scalar part of the correlation,  $f_p$ , that of the interaction  $v^p$ , or the Langrange multiplier  $\lambda_p$ . The relation between the expressions of these quantities in the two representations is:

$$x_{ST} = x_1 + (4T - 3)x_2 + (4S - 3)x_3 + (4T - 3)(4S - 3)x_4 , \quad (338)$$

$$x_{tT} = x_5 + (4T - 3)x_6 . \quad (339)$$

As discussed in Sect. 5.3, in our calculations we have used only two healing distances, one for the four central channels,  $d_{p=1,2,3,4} = d_c$ , and the other one for the two tensor channels,  $d_{p=5,6} = d_t$ . In terms of these quantities, we can rewrite the boundary conditions as:

$$f_{ST}(r \geq d_c) = 1 \quad \left. \frac{\partial f_{ST}}{\partial r} \right|_{r=d_c} = 0 , \quad (340)$$

$$f_{Tt}(r \geq d_t) = 0 \quad \left. \frac{\partial f_{Tt}}{\partial r} \right|_{r=d_t} = 0 . \quad (341)$$

After some algebra, and by using the properties of the Pauli matrices, we obtain for  $E_2$  the following expression:

$$\begin{aligned}
E_2 = & \sum_{s_1 s_2 s_3 s_4 t_1 t_2} \left\{ \int d\mathbf{r}_1 d\mathbf{r}_2 \left[ \frac{1}{2} v_{TS}(r_{12}) f_{TS}^2(r_{12}) \right. \right. \\
& - \frac{\hbar^2}{4m} \left( f_{TS}(r_{12}) \nabla^2 f_{TS}(r_{12}) - (\nabla f_{TS}(r_{12}))^2 \right) \\
& + 8\delta_{S,1} \left( \left( \frac{1}{2} v_{T1}(r_{12}) - v_{Tt}(r_{12}) \right) f_{Tt}^2(r_{12}) + v_{Tt}(r_{12}) f_{T1}(r_{12}) f_{Tt}(r_{12}) \right. \\
& \left. \left. - \frac{\hbar^2}{4m} \left( f_{Tt}(r_{12}) \left( \nabla^2 f_{Tt}(r_{12}) - \frac{12}{r_{12}^2} f_{Tt}(r_{12}) \right) - (\nabla f_{Tt}(r_{12}))^2 \right) \right) \right] \\
& \left[ \rho_0^{s_1 s_2 t_1}(\mathbf{r}_1, \mathbf{r}_1) \rho_0^{s_3 s_4 t_2}(\mathbf{r}_2, \mathbf{r}_2) - (-1)^{T+S} \rho_0^{s_1 s_2 t_1}(\mathbf{r}_1, \mathbf{r}_2) \rho_0^{s_3 s_4 t_2}(\mathbf{r}_1, \mathbf{r}_2) \right] \\
& - \frac{\hbar^2}{4m} \int d\mathbf{r}_1 \int d\mathbf{r}_2 \left( f_{TS}^2(r_{12}) + 8\delta_{S,1} f_{Tt}^2(r_{12}) - 1 \right) \\
& \left[ \rho_{T1}^{s_1 s_2 t_1}(\mathbf{r}_1, \mathbf{r}_1) \rho_0^{s_3 s_4 t_2}(\mathbf{r}_2, \mathbf{r}_2) - (-1)^{T+S} \rho_{T2}^{s_1 s_2 s_3 s_4 t_1 t_2}(\mathbf{r}_1, \mathbf{r}_2) \right] \Big\} \\
& \frac{1}{2} \left( \delta_{s_1 s_2} \delta_{s_3 s_4} + (-1)^{S+1} \delta_{s_1 s_4} \delta_{s_2 s_3} \right) \frac{1}{2} \left( 1 + (-1)^{T+1} \delta_{t_1 t_2} \right). \tag{342}
\end{aligned}$$

In order to make the variation on  $E_2$ , we found convenient to rewrite the above expression as a function of two new quantities  $P_{TS}(\mathbf{r}_1, \mathbf{r}_2)$  and  $Q_{TS}(\mathbf{r}_1, \mathbf{r}_2)$ , defined as:

$$\begin{aligned}
P_{TS}(\mathbf{r}_1, \mathbf{r}_2) = & \frac{4}{2T+1} \left[ \delta_{T1} \left[ \rho_0^p(\mathbf{r}_1) \rho_0^p(\mathbf{r}_2) + \rho_0^n(\mathbf{r}_1) \rho_0^n(\mathbf{r}_2) \right. \right. \\
& + (-1)^S 4 \left( \rho_0^p(\mathbf{r}_1, \mathbf{r}_2) \rho_0^p(\mathbf{r}_1, \mathbf{r}_2) + \rho_0^n(\mathbf{r}_1, \mathbf{r}_2) \rho_0^n(\mathbf{r}_1, \mathbf{r}_2) \right) \Big] \\
& + \frac{1}{2} \left[ \rho_0^p(\mathbf{r}_1) \rho_0^n(\mathbf{r}_2) + \rho_0^n(\mathbf{r}_1) \rho_0^p(\mathbf{r}_2) \right. \\
& \left. \left. - (-1)^{T+S} 4 \left( \rho_0^p(\mathbf{r}_1, \mathbf{r}_2) \rho_0^n(\mathbf{r}_1, \mathbf{r}_2) + \rho_0^n(\mathbf{r}_1, \mathbf{r}_2) \rho_0^p(\mathbf{r}_1, \mathbf{r}_2) \right) \right] \right] \\
& + \frac{16(-1)^T}{(2S+1)(2T+1)} \left[ \right. \\
& \delta_{T1} \left( \rho_{0j}^p(\mathbf{r}_1, \mathbf{r}_2) \rho_{0j}^n(\mathbf{r}_2, \mathbf{r}_1) + \rho_{0j}^n(\mathbf{r}_1, \mathbf{r}_2) \rho_{0j}^p(\mathbf{r}_2, \mathbf{r}_1) \right) \\
& \left. + \frac{1}{2} \left( \rho_{0j}^p(\mathbf{r}_1, \mathbf{r}_2) \rho_{0j}^n(\mathbf{r}_2, \mathbf{r}_1) + \rho_{0j}^n(\mathbf{r}_1, \mathbf{r}_2) \rho_{0j}^p(\mathbf{r}_2, \mathbf{r}_1) \right) \right], \tag{343} \\
Q_{TS}(\mathbf{r}_1, \mathbf{r}_2) = & - \frac{\hbar^2}{4m} \sum_{t_1 t_2 = p, n} \frac{1}{2} \left( 1 + (-1)^{T+1} \delta_{t_1, t_2} \right) \\
& \left[ \frac{4}{2T+1} \left( \rho_{T1}^{t_1}(\mathbf{r}_1) \rho_0^{t_2}(\mathbf{r}_2) - 4(-1)^{T+S} \left( \rho_0^{t_1}(\mathbf{r}_1, \mathbf{r}_2) \nabla_1^2 \rho_0^{t_2}(\mathbf{r}_2, \mathbf{r}_1) \right. \right. \right. \\
& \left. \left. \left. - \nabla_1 \rho_0^{t_1}(\mathbf{r}_1, \mathbf{r}_2) \cdot \nabla_1 \rho_0^{t_2}(\mathbf{r}_2, \mathbf{r}_1) \right) \right) \right]
\end{aligned}$$

$$\begin{aligned}
& + \frac{16(-1)^T}{(2S+1)(2T+1)} \left( \rho_{0j}^{t_1}(\mathbf{r}_1, \mathbf{r}_2) \nabla_1^2 \rho_{0j}^{t_2}(\mathbf{r}_2, \mathbf{r}_1) \right. \\
& \left. - \nabla_1 \rho_{0j}^{t_1}(\mathbf{r}_1, \mathbf{r}_2) \cdot \nabla_1 \rho_{0j}^{t_2}(\mathbf{r}_2, \mathbf{r}_1) \right) \Bigg] + \frac{1}{2} P_{TS}(\mathbf{r}_1, \mathbf{r}_2) v_{TS}(r_{12}), \tag{344}
\end{aligned}$$

where we have explicitly written the sum over the spin and the isospin. In order to obtain a quantity depending only on the relative distance  $r_{12}$  between the particles 1 and 2 we integrate Eq. (342) over  $r_1$  and  $r_2$  by keeping fixed the value of  $r_{12}$ . We define the quantity:

$$\tilde{P}_{TS} = \int d\mathbf{r}_2 P_{TS}(\mathbf{r}_1, \mathbf{r}_2) = \frac{2\pi}{r_{12}} \int_0^\infty r_2 dr_2 \int_{|r_2-r_{12}|}^{|r_2+r_{12}|} r_1 dr_1 P_{TS}(\mathbf{r}_1, \mathbf{r}_2) \tag{345}$$

and an analogous expression for  $\tilde{Q}_{TS}$ , therefore we write  $E_2$  as:

$$\begin{aligned}
E_2 = & \int d\mathbf{r}_{12} \left[ \tilde{Q}_{TS} f_{TS}^2 - \frac{\hbar^2}{4m} \tilde{P}_{TS} \left( f_{TS} \nabla^2 f_{TS} - (\nabla f_{TS})^2 \right) \right. \\
& + 8\delta_{S,1} \left( \left( \tilde{Q}_{T1} - \tilde{P}_{T1} v_{Tt} + \frac{3\hbar^2}{mr_{12}^2} \tilde{P}_{T1} \right) f_{Tt}^2 + \tilde{P}_{T1} v_{Tt} f_{T1} f_{Tt} \right. \\
& \left. \left. - \frac{\hbar^2}{4m} \tilde{P}_{T1} \left( f_{Tt} \nabla^2 f_{Tt} - (\nabla f_{Tt})^2 \right) \right) + \tilde{Q}_{TS} + \frac{1}{2} \tilde{P}_{TS} v_{TS} \right]. \tag{346}
\end{aligned}$$

where we must understand that all the functions and the operators act on the  $\mathbf{r}_{12}$  coordinate. The expression of the variation of  $E_2$  with respect to  $f_{TS}$  and  $f_{Tt}$  is:

$$\begin{aligned}
\delta(E_2 - C_2) = & \int d\mathbf{r}_{12} \left[ \delta f_{TS} P_{TS}^{1/2} \left\{ -\frac{\hbar^2}{m} \nabla^2 F_{TS} + \left( \tilde{V}_{TS} - \lambda_{TS} \right) F_{TS} \right. \right. \\
& + \delta_{S,1} (v_{Tt} - \lambda_{Tt}) F_{Tt} \left. \right\} + 8\delta_{S,1} \delta f_{Tt} P_{T1}^{1/2} \left\{ -\frac{\hbar^2}{m} \nabla^2 F_{Tt} + \right. \\
& \left( \tilde{V}_{T1} - \lambda_{T1} - 2v_{Tt} + 2\lambda_{Tt} + \frac{6\hbar^2}{mr_{12}^2} \right) F_{Tt} + \\
& \left. \left. (v_{T1} - \lambda_{T1}) F_{T1} \right\} \right] = 0, \tag{347}
\end{aligned}$$

where we have defined

$$F_{TS} = f_{TS} \tilde{P}_{TS}^{1/2}, \tag{348}$$

$$F_{Tt} = f_{Tt} \tilde{P}_{T1}^{1/2}, \tag{349}$$

$$\tilde{V}_{TS} = \frac{1}{\tilde{P}_{TS}} \left[ 2\tilde{Q}_{TS} + \frac{\hbar^2}{4m} \left( \nabla^2 \tilde{P}_{TS} - \frac{(\nabla \tilde{P}_{TS})^2}{\tilde{P}_{TS}} \right) \right]. \tag{350}$$

The fact that Eq. (347) has to be valid for every variation of  $f_{TS}$  or  $f_{Tt}$ , implies that both expressions included in the braces has to be zero. By imposing this condition we obtain the Euler-Lagrange equations:

$$-\frac{\hbar^2}{m} \nabla^2 F_{TS} + \left( \tilde{V}_{TS} - \lambda_{TS} \right) F_{TS} + \delta_{S,1} (v_{Tt} - \lambda_{Tt}) F_{Tt} = 0,$$

$$\begin{aligned}
-\frac{\hbar^2}{m}\nabla^2 F_{Tt} &+ \left( \tilde{V}_{T1} - \lambda_{T1} - 2v_{Tt} + 2\lambda_{Tt} + \frac{6\hbar^2}{mr_{12}^2} \right) F_{Tt} \\
&+ (v_{T1} - \lambda_{T1}) F_{T1} = 0 .
\end{aligned} \tag{351}$$

The expressions (351) represent a system of differential equations, the two equations corresponding to  $S = 0$  are not coupled, while the other equations are coupled. The solution of the above equations gives the optimal value for  $f_{TS}$  and  $f_{Tt}$  and by using Eq. (337) we obtain the correlation functions  $f_p$ , in the representation used in the FHNC calculations.

In the case of infinite systems, nuclear and neutron matter, these equations have been generalized to include the spin-orbit channels in the correlation with  $v_8$  [21] and  $v_{14}$  [97] potentials.

## G Acronyms

AFDMC	Auxiliary Field Diffusion Monte Carlo
AV8'	Argonne $v'_8$ nucleon-nucleon potential
AV18	Argonne $v_{18}$ nucleon-nucleon potential
CBF	Correlated Basis Function
FHNC	Fermi HyperNetted Chain
FHNC/SOC	Fermi HyperNetted Chain/Single Operator Chain
GFMC	Green's Function Monte Carlo
HF	Hartree-Fock
HNC	HyperNetted Chain
IPM	Independent Particle Model
MBCF	Many-Body Correlation Function
MF	Mean Field
NN	Nucleon-Nucleon
OBDF	One-Body Distribution Function
OBDM	One-Body Density Matrix
RFHNC	Renormalized Fermi HyperNetted Chain
QCD	Quantum ChromoDynamics
SOC	Single Operator Chain
SOR	Single Operator Ring
SRC	Short Range Correlations
TBCF	Two-Body Correlation Function
TBDF	Two-Body Distribution Function
TBDM	Two-Body Density Matrix
U14	Urbana $v_{14}$ nucleon-nucleon potential
UVII	Urbana VII three-nucleon interaction
UIX	Urbana IX three-nucleon interaction



## H Symbols

Symbol	Meaning	Note
$\left(\left \right.\right)$	folding product	Eq. (24)
$<   >$	Clebsch-Gordan coefficient	
$A$	number of particles	
$A^k$	$B^{2k-1}$	
$a_0^\alpha, a_{ls}^\alpha$	parameters of the WS potential	Eq. (86)
$B^p$	$C$ -trace of two operators	Tab. 10
$C(r_{12})$	sum of the composite diagrams	Eq. (20)
$C(O_{12}^p)$	$C$ -trace	Sect. 2.3.1
$C_m^t(1)$	vertex corrections	Eq. (203-204)
$C_{m,pq}^t(1)$	vertex corrections	Eq. (238-239)
$cc$	sub-index for cyclic-cyclic	Sect. 2.2
$D_{k_1 k_2}$	$E_{2k_1-1, 2k_2-1}$	
$D_{nlj}^t(r)$		Eq. (260)
$dd$	sub-index for dynamical-dynamical	Sect. 2.2
$de$	sub-index for dynamical-exchange	Sect. 2.2
$E(r_{12})$	contribution of elementary diagrams	
$E_{pq}$	matrix used in SOC calculations	Tab. 13
$ee$	sub-index for exchange-exchange	Sect. 2.2
$F(x_1, \dots, x_A)$	many-body correlation function	Eq. (2)
$\mathcal{F}(1 \dots A)$	operator dependent correlation function	Eq. (57)
$f(r)$	two-body correlation function	Eq. (3)
$f_p(r)$	state dependent correlation function	Eq. (48)
$g(x_1, x_2)$	two-body distribution function	Eq. (10)
$g_p^{t_1 t_2}(1, 2)$	State dependent TBDF	Eq. (53)
$H_{ij}$	state dependent part of the TBCF	Eq. (56)
$H_{JF}^{pqr}(r_{12})$		Eq. (271)

$h(r)$	two-body h-function	Eq. (14)
$h_c(r)$	used in SOC Eqs.	Eq. (77)
$h_p(r)$	used in SOC Eqs.	Eq. (76)
$I^{ijk}$	spin part of $K^{pqr}$	Eq. (110)
$J^{ijk}$	spin part of $L^{pqr}$	Eq. (114)
$K^{pqr}$	used in the product of two operators	Tab. 11
$L(r_{12})$	used in SOC Eqs.	Eq. (78)
$L^{pqr}$	used in the product of four operators	Tab. 12
$\ell(x)$	Slater function	Eq. (36)
$M_{x,l_1,l_2,l_3}^{t_1t_2k_1k_2k_3}(i)$		Eq. (277-281)
$m_\pi$	pion mass	Eq. (86)
$N$	number of neutrons	
$N(r_{12})$	contribution of nodal diagrams	
$N_{cc}^{xx}$ , $N_{cc}^{x\rho}$ , $N_{cc}^{\rho\rho}$		Eq. (219-224)
$\mathcal{N}_{nljm}^t(r)$	used in the quasi-hole wave function	Eq.(172)
$n^t(k)$	momentum distribution	Eq.(155)
$O_{ij}^p$	interaction and correlation operators	Eq. (49)
$P_l(\cos\theta)$	Legendre polynomials	
$P_1^t$	proton / neutron projector operator	Eq. (100)
$P_{ij}^k$	$O_{ij}^{2k-1}$	Eq. (51)
$R_0^t$ , $R_{ls}^t$ , $R_C$	parameters of the WS potential	Eqs. (86, 87)
$R_{nlj}^t(r)$	radial part of $\phi(x)$	Eq. (88)
$R^{k_1k_2k_3k_4}$	spin $C$ -traces	Eq. (320)
$\mathbf{r}_i$	spatial coordinate of the particle $i$	
$S(r_{12})$		Eq. (205)
$S_{ij}$	tensor operator	Eq. (50)
$S_1^{p,n}$	one-body sum rule	Eq. (147)
$S_2^{pp,pn,nn}$	two-body sum rule	Eqs. (148)
$S_{2,\sigma}$	spin sum rule	Eq. (149)

$S_{nlj}^t$	spectroscopic factor	Eq. (180)
$S$	symmetrizer operator	
$T_{\phi}^{(i)}, T_F, T_{c.m.}$	kinetic energy terms	Eqs. (128-130)
$T_{l_1 l_2}^{t_1 t_2 t_3}(i)$	used in the isospin traces	Eq. (251)
$\mathcal{T}_{l_1 l_2 l_3 l_4 l_5}^{t_1 t_2 t_3}(i)$	used in the isospin traces	Eq. (246)
$U^t(r)$	mean-field potential	Eqs. (85,86)
$U_x^t(1)$		Eqs. (206-207)
$U_{m,pq}^{t_1 t_2}(1)$		Eqs. (240-245)
$V$	volume of the system	
$V_0^t, V_{ls}^t$	parameter of the WS potential	Eq. (86)
$v^p(r_{12})$	scalar parts of the interaction	
$v_{123}^{2\pi}$	part of the three-body force	Eq. (142)
$v_{123}^R$	part of the three-body force	Eq. (143)
$X(r_{12})$	contribution of non-nodal diagrams	Eq. (23)
$X_{ij}$		Eq. (145)
$\mathcal{X}_{nljm}^t$	used in the quasi-hole states	
$x_i$	generalized coordinate of particle $i$	
$Y_{l\mu}(\Omega_i)$	spherical harmonics	
$\mathbf{Y}_{lj}^m$	spin spherical harmonics	Eq. (88)
$W_0 \ W_s \ W_c \ W_{cs}$	interaction energy terms	Eq. (137)
$Z$	number of protons	
$\Delta^k$	$\Gamma^{2k-1}$	
$\Delta_p(1, \dots, p)$	sub-determinant	Eq. (31)
$\eta_{l_1 l_2 l_3 l_4 l_5}^{t_1 t_2 t_3}(i)$	used in the isospin traces	Eq. (258)
$\Gamma^p$	matrix used in SOC Eqs.	Tab. 9
$\nu$	spin-isospin degeneracy	Eq. (27)
$\zeta_{123}^{pqr}$	function used to calculate SOR	Eq. (65)
$\Xi_{k_1 k_2 k_3, l_1 l_2}^{t_1 t_2 t_3}$		Eq. (323)
$\zeta_{123}^{k_1 k_2 k_3}$	spin part of $\zeta_{123}^{pqr}$	Eq. (65)

$\Pi^{\sigma,\tau}$	spin-isospin exchange operator	Eq. (58)
$\rho$	particle density	
$\rho_{T1,...,T4}$	kinetic energy densities	Eqs. (132-135)
$\rho_{T5,T6}$	kinetic energy densities	Eqs. (266, 267)
$\rho^t(\mathbf{r}_1)$	OBDF	Eq. (100)
$\rho_0^t$	parallel spin OBDM	Eqs. (91,93)
$\rho_{0j}^t$	antiparallel spin OBDM	Eqs. (92,93)
$\rho_2^{q,t_1t_2}(1,2)$	operator dependent TBDF	Eq. (101)
$\rho_{2,dir,exc,exc}^{q,t_1t_2}(1,2)$		Eq. (209 - 211)
$\rho^{s,s';t}(\mathbf{r}_1, \mathbf{r}_2)$	OBDM	Eq. (151)
$\Phi(1, ..., A)$	independent particle wave function	
$\phi(x)$	single particle wave function	
$\phi_{nlj}^{t,NO}(x)$	natural orbit	Eq. (158)
$\chi_{s,t}$	Pauli spinors	Eq. (27)
$\chi_n^{t_1t_2}$	used in the isospin traces	Eq. (121)
$\Psi(1, ..., A)$	correlated many-body wave function	
$\psi_{nljm}^t(x)$	quasi-hole wave function	Eq. (168)
$\Omega_i$	the polar angles $\theta_i$ and $\phi_i$	
$\Omega_{k_1k_2k_3k_4,l_1l_2}^{t_1t_2t_3\pm}$		Eq. (320)

## References

- [1] R. Machleidt, K. Holinde, C. Elster, Phys. Rep. 149 (1987) 1.
- [2] R. Machleidt, Adv. Nucl. Phys. 19 (1989) 189.
- [3] V. G. J. Stoks, R. A. M. Klomp, M. C. M. Rentmeester, J. de Swart, Phys. Rev. C 48 (1993) 792.
- [4] V. G. J. Stoks, R. A. M. Klomp, C. P. F. Terheggen, J. J. de Swart, Phys. Rev. C 49 (1994) 2950.
- [5] R. B. Wiringa, V. G. J. Stoks, R. Schiavilla, Phys. Rev. C 51 (1995) 38.
- [6] B. S. Pudliner, V. R. Pandharipande, J. Carlson, R. B. Wiringa, Phys. Rev. Lett. 74 (1995) 4396.
- [7] B. S. Pudliner, V. R. Pandharipande, J. Carlson, S. C. Pieper, R. B. Wiringa, Phys. Rev. C 56 (1997) 1720.
- [8] S. C. Pieper, R. B. Wiringa, Ann. Rev. Nucl. Part. Sc. 51 (2001) 53.
- [9] S. C. Pieper, Nucl. Phys. A 751 (2005) 516.
- [10] H. Kamada, et al., Phys. Rev. C 64 (2001) 044001.
- [11] S. Gandolfi, F. Pederiva, S. Fantoni, K. E. Schmidt, Phys. Rev. C 73 (2006) 044304.
- [12] H. Mütter, A. Polls, Phys. Rev. C 61 (2000) 014304.
- [13] E. Krotcheck, Introduction to modern methods of quantum many-body theory and their applications, A. Fabrocini, S. Fantoni and E. Krotscheck eds., World Scientific, Singapore, 2002.
- [14] R. Jastrow, Phys. Rev. 98 (1955) 1479.
- [15] J. E. Mayer, M. G. Mayer, Statistical Mechanics, Wiley, New York, 1940.
- [16] J. M. J. van Leeuwen, Groeneveld, J. de Boer, Physica 25 (1959) 792.
- [17] M. Gaudin, J. Gillespie, G. Ripka, Nucl. Phys. A 176 (1971) 273.
- [18] S. Fantoni, S. Rosati, Nuovo Cimento A 20 (1974) 179.
- [19] S. Fantoni, S. Rosati, Nuovo Cimento A 25 (1975) 593.
- [20] S. Fantoni, S. Rosati, Nuov. Cim. A 43 (1978) 413.
- [21] V. R. Pandharipande, R. B. Wiringa, Rev. Mod. Phys. 51 (1979) 821.
- [22] S. Fantoni, V. R. Pandharipande, Nucl. Phys. A 427 (1984) 473.
- [23] S. Fantoni, V. R. Pandharipande, Nucl. Phys. A 473 (1987) 234.

- [24] R. B. Wiringa, V. Fiks, A. Fabrocini, Phys. Rev. C 38 (1988) 1010.
- [25] A. Akmal, V. R. Pandharipande, D. G. Ravenhall, Phys. Rev. C 58 (1998) 1804.
- [26] S. Fantoni, S. Rosati, Nucl. Phys. A 328 (1979) 478.
- [27] G. Co', A. Fabrocini, S. Fantoni, I. E. Lagaris, Nucl. Phys. A 549 (1992) 439.
- [28] G. Co', A. Fabrocini, S. Fantoni, Nucl. Phys. A 568 (1994) 73.
- [29] F. A. de Saavedra, G. Co', A. Fabrocini, S. Fantoni, Nucl. Phys. A 605 (1996) 359.
- [30] A. Fabrocini, F. A. de Saavedra, G. Co', P. Folgarait, Phys. Rev. C 57 (1998) 1668.
- [31] A. Fabrocini, F. A. de Saavedra, G. Co', Phys. Rev. C 61 (2000) 044302.
- [32] A. Fabrocini, G. Co', Phys. Rev. C 63 (2001) 044319.
- [33] C. Bisconti, F. A. de Saavedra, G. Co', A. Fabrocini, Phys. Rev. C 73 (2006) 054304.
- [34] J. W. Clark, Prog. Part. Nucl. Phys. 2 (1979) 89.
- [35] S. Rosati, From nuclei to particles: Proc. Int. School E. Fermi, course LXXIX, A. Molinari ed., North-Holland, Amsterdam, 1982.
- [36] A. Fabrocini, S. Fantoni, First international course on condensed matter, D. Prosperi, S. Rosati and G. Violini eds., World Scientific, Singapore, 1987.
- [37] A. Polls, F. Mazzanti, Introduction to modern methods of quantum many-body theory and their applications, A. Fabrocini, S. Fantoni and E. Krotscheck eds., World Scientific, Singapore, 2002.
- [38] R. B. Dingle, Phil. Mag. 40 (1949) 573.
- [39] S. Fantoni, S. Rosati, Phys. Lett. B 84 (1979) 23.
- [40] A. Akmal, V. R. Pandharipande, Phys. Rev. C 56 (1997) 2261.
- [41] S. C. Pieper, R. B. Wiringa, V. R. Pandharipande, Phys. Rev. C 46 (1992) 1741.
- [42] A. R. Edmonds, Angular momentum in quantum mechanics, Princeton University Press, Princeton, 1957.
- [43] S. Fantoni, Nuov. Cim. A 44 (1978) 191.
- [44] H. W. Jackson, E. Feenberg, Ann. Phys. (NY) 15 (1961) 266.
- [45] H. W. Jackson, E. Feenberg, Rev. Mod. Phys. 34 (1962) 686.
- [46] J. Carlson, V. R. Pandharipande, R. B. Wiringa, Nucl. Phys. A 401 (1983) 59.
- [47] J. Fujita, H. Miyazawa, Prog. Theor. Phys. 17 (1957) 360.
- [48] R. A. Arndt, L. D. Roper, R. L. Workman, M. W. McNaughton, Phys. Rev. D 45 (1992) 3995.

- [49] I. Lagaris, V. R. Pandharipande, Nucl. Phys. A 359 (1981) 331.
- [50] S. C. Pieper, V. R. Pandharipande, R. B. Wiringa, J. Carlson, Phys. Rev. C 64 (2001) 014001.
- [51] R. Schiavilla, V. R. Pandharipande, R. B. Wiringa, Nucl. Phys. A 449 (1986) 219.
- [52] G. Audi, A. H. Wapstra, Nucl. Phys. A 565 (1993) 1.
- [53] C. Bisconti, The cbf theory for medium-heavy nuclei, Ph.D. thesis, Università di Lecce (Italy), unpublished (2006).
- [54] C. W. D. Jager, C. D. Vries, At. Data Nucl. Data Tables 36 (1987) 495.
- [55] F. A. de Saavedra, G. Co', M. M. Renis, Phys. Rev. C 55 (1997) 673.
- [56] R. Anni, G. Co', P. Pellegrino, Nucl. Phys. A 584 (1995) 35.
- [57] R. Anni, G. Co', Nucl. Phys. A 588 (1995) 463.
- [58] J. M. Cavedon, Ph.D. thesis, Université de Paris-Sud (France), unpublished (1980).
- [59] I. Sick, private communication.
- [60] C. Bisconti, F. A. de Saavedra, G. Co', Phys. Rev. C 75 (2007) 054302.
- [61] P. Božek, Phys. Lett. B 586 (2004) 239.
- [62] T. Frick, H. Mütter, A. Rios, A. Polls, A. Ramos, Phys. Rev. C 71 (2005) 014313.
- [63] A. N. Antonov, P. E. Hodgson, I. Z. Petkov, Nucleon momentum and density distributions, Clarendon, Oxford, 1988.
- [64] D. S. Lewart, V. R. Pandharipande, S. Pieper, Phys. Rev. B 37 (1988) 4950.
- [65] A. Polls, H. Mütter, W. H. Dickhoff, Nucl. Phys. A 594 (1995) 117.
- [66] O. Benhar, V. R. Pandharipande, S. C. Pieper, Rev. Mod. Phys. 65 (1993) 817.
- [67] J. M. Cavedon, et al., Phys. Rev. Lett. 49 (1982) 978.
- [68] L. Zamick, V. Klemmt, J. Speth, Nucl. Phys. 245 (1975) 365.
- [69] V. Klemmt, J. Speth, Z. Phys. A 278 (1976) 59.
- [70] G. Co', J. Speth, Z. Phys. A 326 (1987) 361.
- [71] M. Anguiano, G. Co', Jour. Phys. G 27 (2001) 2109.
- [72] A. Fabrocini, S. Fantoni, Nucl. Phys. A 435 (1985) 448.
- [73] O. Benhar, A. Fabrocini, S. Fantoni, Nucl. Phys. A 505 (1989) 267.
- [74] A. Fabrocini, S. Fantoni, Nucl. Phys. A 503 (1987) 375.

- [75] A. Fabrocini, Phys. Rev. C 55 (1997) 338.
- [76] A. L. Fetter, J. D. Walecka, Quantum theory of many-particle systems, McGraw-Hill, S. Francisco, 1971.
- [77] A. Fabrocini, A. Polls, Phys. Rev. B 25 (1982) 4533.
- [78] J. Boronat, F. A. de Saavedra, E. Buendía, A. Polls, J. Low Temp. Phys. 94 (1994) 325.
- [79] F. A. de Saavedra, G. Co', A. Fabrocini, Phys. Rev. C 63 (2001) 064308.
- [80] P. H. Pile, et al., Phys. Rev. Lett. 66 (1991) 4343.
- [81] T. Hasegawa, et al., Phys. Rev. C 53 (1996) 1210.
- [82] J. W. Clark, P. Westhaus, Phys. Rev. 141 (1966) 833.
- [83] J. W. Clark, P. Westhaus, Phys. Rev. 149 (1966) 990.
- [84] E. Feenberg, Theory of Quantum Fluids, Academic Press, New York, 1969.
- [85] S. Fantoni, B. L. Friman, V. R. Pandharipande, Nucl. Phys. A 399 (1983) 51.
- [86] O. Benhar, A. Fabrocini, S. Fantoni, Phys. Rev. C 41 (1990) R24.
- [87] S. Fantoni, B. L. Friman, V. R. Pandharipande, Nucl. Phys. A 386 (1982) 1.
- [88] J. W. Clark, The many body problem, Jastrow vs Brueckner theory, R. Guardiola and J. Ros eds., Lectures Notes in Physics, 138, Berlin, 1981.
- [89] E. Krotscheck, Phys. Rev. A 26 (1996) 3536.
- [90] A. de Florio, Sviluppo di una teoria a molticorpi per la descrizione di stati eccitati in base correlata, Master's thesis, Università di Lecce (Italy), unpublished (1998).
- [91] E. Buendía, F. J. Gálvez, J. Praena, A. Sarsa, Nucl. Phys. A 710 (2002) 29.
- [92] J. Praena, E. Buendía, F. J. Gálvez, A. Sarsa, Phys. Rev. C 67 (2003) 044301.
- [93] R. B. Wiringa, S. C. Pieper, J. Carlson, V. R. Pandharipande, Phys. Rev. C 62 (2000) 014001.
- [94] D. M. Brink, E. Boeker, Nucl. Phys. A 91 (1967) 1.
- [95] R. Abe, Progr. Theo. Phys. 21 (1959) 421.
- [96] R. B. Wiringa, Nucl. Phys. A 338 (1980) 57.
- [97] I. Lagaris, V. R. Pandharipande, Nucl. Phys. A 359 (1981) 349.